

FINAL REPORT

(NASA-CR-122451) OSO-6 ORBITING SOLAR
OBSERVATORY Final Report (Ball Bros.
Research Corp.) 12 Jan. 1972 422 p CSCL

N72-30900

22B

G3/31

Unclas
39476



OSO-6

orbiting solar observatory

Prepared for
NATIONAL AERONAUTICS AND SPACE ADMINISTRATION
GODDARD SPACE FLIGHT CENTER
GREENBELT, MARYLAND



BALL BROTHERS RESEARCH CORPORATION
SUBSIDIARY OF BALL CORPORATION
BOULDER, COLORADO

2-10
m1 x



BALL BROTHERS RESEARCH CORPORATION

NASA CR- BOULDER, COLORADO
122451

FINAL REPORT
OSO-6
ORBITING SOLAR OBSERVATORY

F70-03

12 Jan 1972

Prepared for
GODDARD SPACE FLIGHT CENTER
NATIONAL AERONAUTICS AND SPACE ADMINISTRATION
Contract NAS5-9300

PREPARED

OSO Project Staff

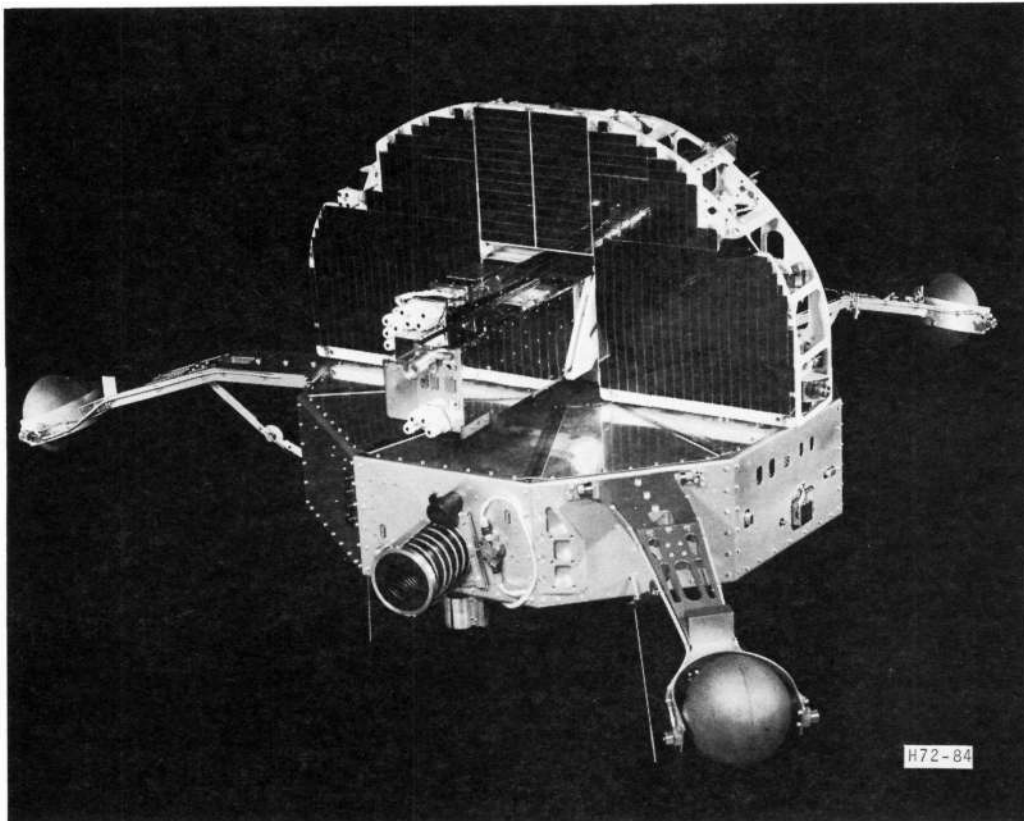
APPROVED

J. O. Simpson
J. O. Simpson
Director,
OSO Programs

Details of illustrations in
this document may be better
studied on microfiche



F70-03



OSO-6 ORBITING SOLAR OBSERVATORY

ii



BALL BROTHERS RESEARCH CORPORATION

SUBSIDIARY OF BALL BROTHERS COMPANY INCORPORATED

BOULDER, COLORADO

Doc. No.

F70-03

Chg. No. _____

LIST OF EFFECTIVE PAGES

NOTE: The portion of the text affected by the latest change or revision is indicated by a vertical line in the outer margins of the page.

THE TOTAL NUMBER OF PAGES IN THIS PUBLICATION IS 422,
CONSISTING OF THE FOLLOWING:

Page No.	Issue	Change No.
Title	Original	
Frontispiece	Original	
A	Original	
iv thru xx	Original	
1-1 thru 1-42	Original	
2-1 thru 2-26	Original	
3-1 thru 3-52	Original	
4-1 thru 4-16	Original	
5-1 thru 5-20	Original	
6-1 thru 6-24	Original	
7-1 thru 7-68	Original	
8-1 thru 8-18	Original	
9-1 thru 9-54	Original	
10-1 thru 10-14	Original	
11-1 thru 11-20	Original	
A-1 thru A-6	Original	
B-1 thru B-6	Original	
C-1 thru C-8	Original	
D-1 thru D-28	Original	

...



PRECEDING PAGE BLANK NOT FILMED

FOREWORD

The greatest obstacle in measuring solar and celestial radiation is the earth's atmosphere which acts as a shield and thus prevents earthbound observers from observing such phenomena. The Orbiting Solar Observatory (OSO) was conceived as a means of overcoming both this obstacle and the endurance limitations of earlier balloon-borne and rocket-borne experiments.

In 1958, Ball Brothers Research Corporation (BBRC) was awarded a feasibility-study contract by the Goddard Space Flight Center (GSFC) of the National Aeronautics and Space Administration (NASA) to investigate problems associated with designing and building such a satellite. The satellite would need to survive the rigors of launching and long-term space environment and to provide a stable platform from which scientific instruments could detect and measure cosmic phenomena.

Furthermore, it was necessary that the experiment capacity of the basic spacecraft be a flexible design to accommodate scientific experiments with differing configurations as governed by their mission objectives. Therefore, the OSO configuration differs slightly from model to model to accommodate different experiments and to reflect spacecraft design changes.

The OSO-1 observatory, launched 7 March 1962, from Cape Canaveral (now Cape Kennedy), Florida, was the outgrowth of the feasibility studies. This first OSO proved very successful and the OSO program was subsequently expanded to include a series of observatories.



The second OSO flight model (designated OSO-B) was built and delivered to the Eastern Test Range (ETR) facilities at Cape Kennedy in March, 1964. In April, accidental ignition of the third-stage motor resulted in extensive damage to the observatory. An accelerated refurbishing program was begun and OSO-B2 was built using some of the components salvaged from OSO-B1 and other available hardware.

OSO-B2 was successfully launched as OSO-2 from ETR on 3 February 1965. OSO-2 operated very successfully for nine months, at which time the mission was ended due to the depletion of its pitch-control gas.

OSO-C was delivered to ETR in July, 1965, and was launched on 25 August 1965. Due to the premature ignition of the Delta third-stage motor, however, the observatory was not placed into a successful orbit. In September of 1965, it was decided to modify the OSO-E spacecraft, then in production, to accommodate the OSO-C flight-spare experiments.

The modified OSO-E, renamed OSO-E1, was developed under an accelerated program, much like OSO-B2, and was delivered to ETR in February, 1967. This observatory was successfully launched on 8 March 1967, and was redesignated OSO-3. The OSO-3 performed nearly flawlessly for more than 3 years. The only spacecraft system problems during that period were the failure of the two tape recorders during the 3rd and 15th month of operation. OSO-3 continued to provide valuable scientific data on a realtime basis after the tape recorders failed.

OSO-D was successfully placed into orbit on 18 October 1967 and was redesignated OSO-4. It has also performed nearly perfectly except for the failure of its two tape recorders.



during the fourth and sixth months of operation. At the time of writing, OSO-4 continues to provide valuable scientific data on a realtime basis.

OSO-F was successfully placed into orbit on 22 January 1969 and was redesignated OSO-5. At the time of this writing, OSO-5 has had no failures and continues to provide valuable scientific data.

OSO-G was successfully placed into orbit on 9 August 1969 and redesignated OSO-6. This report describes this observatory, its development history, and its orbital performance.



SUMMARY

This document is the final project report containing the description, development history, test history, and orbital performance analysis of the OSO-6 Orbiting Solar Observatory. The spacecraft contractor was Ball Brothers Research Corporation, Boulder, Colorado. The project was sponsored and directed by the Goddard Space Flight Center (GSFC) division of the National Aeronautics and Space Administration (NASA). The work was performed under contract number NAS5-9300.

The OSO-6 Orbiting Solar Observatory was the sixth flight model of a series of scientific spacecraft designed to provide a stable platform for experiments engaged in the collection of solar and celestial radiation data. The design objective was 180 days of orbital operation.

The OSO-6 contained seven primary scientific experiments furnished by the following organizations: University of New Mexico, Los Alamos Scientific Laboratory, Harvard College Observatory, Rutgers State University of New Jersey, University of Bologna, University College of London, and the Naval Research Laboratory.

This observatory was successfully launched into a near-earth orbit on 9 August 1969 from the Eastern Test Range (ETR) facilities at Cape Kennedy, Florida. The launch vehicle was a McDonnell/Douglas Astronautics Company two-stage Delta DSV-3N.

OSO-6 has telemetered an enormous amount of very useful experiment and housekeeping data to GSFC ground stations. Observatory operation during the two-year reporting period was very successful except for some experiment instrument problems.



The in-orbit performance history and the development history are presented in Sections 2 and 3, respectively, of this report. A brief summary of the first year of spacecraft operation and experiment operation is presented in the two tables below and in Section 1.



OSO-6 EXPERIMENT AND INTERFACE ONE-YEAR OPERATIONAL SUMMARY

Instrument	Operation Status	SPACECRAFT/EXPERIMENT INTERFACE											
		Telemetry				Command				Thermal			
		Failed	Poor	Adequate	Excellent	Failed	Poor	Adequate	Excellent	Failed	Poor	Adequate	Excellent
<u>Pointed Instruments</u>													
NRL X-Ray	Sensitivity Problem in burst detector. Data collected.				X				X				X
HCO UV	Sensitivity degraded with time. Usable data collected.				X				X				X
<u>Wheel Instruments</u>													
UCL X-Ray	Two Ion Chambers have failed, other nine chambers satisfactory.				X				X				X
Bologna X-Ray	No Problems				X				X				X
Rutgers Zodiacal	Occasional logic circuit problems. Data satisfactory.				X				X				X
New Mex. Neutron	Occasional problems with one detector. Data Satisfactory.				X				X				X
LASL X-Ray	No Problems.				X				X				X



OSO-6 SPACECRAFT SYSTEMS ONE-YEAR PERFORMANCE SUMMARY

System or Subsystem	Operation Status	Performance Quality			
		Failed	Poor	Adequate	Excellent
Telemetry					
Dig. Mult/Encoder #1	Continuous				X
Dig. Mult/Encoder #2	Operated when selected				X
Tape Recorder #1	Operated when selected				X
Tape Recorder #2	Operated when selected				X
Transmitter #1	Continuous				X
Transmitter #2	Operated when selected				X
Command					
Receiver #1	Continuous				X
Receiver #2	Continuous				X
Wheel Decoder #1	Continuous				X
Wheel Decoder #2	Continuous				X
Sail Decoder #1	Continuous				X
Sail Decoder #2	Continuous				X
Pointing Control	Continuous				X
Pitch Control	Continuous				X
Spin Control	Continuous				X
Aspect Measuring	Continuous				X
Nutation Control	Continuous				X
Launch Sequence	Operated during orbit "0"				X
Mass Balance	----			X*	
Thermal Control	----				X
Power Supply	Continuous				X

LEGEND:

- Excellent = Significantly surpassed design specifications
- Adequate = Performed near design specifications
- Poor = Did not meet design specifications
- Failed = Stopped functioning completely

*An apparent mass unbalance condition (wobble) was observed in the pitch data received from OSO-6. The wobble amounted to about 0.2 deg P-P but did not adversely effect the operation of either the spacecraft systems or the experiment instruments.



CONTENTS

Section		Page
	LIST OF EFFECTIVE PAGES	A
	FOREWORD	iv
	SUMMARY	vii
1	PROJECT HIGHLIGHTS	1-1
	1.1 Introduction	1-1
	1.2 Mission Description	1-1
	1.3 Schedule Highlights	1-5
	1.4 Observatory In-Orbit Performance Summary	1-5
	1.5 Launch Vehicle Description and Launch Summary	1-11
	1.6 Spacecraft Description	1-19
2	OSO-6 FLIGHT PERFORMANCE	2-1
	2.1 Introduction	2-1
	2.2 Performance in the Launch Phase	2-1
	2.3 Pointing Control System in Orbit	2-2
	2.4 Attitude and Spin Controls and Monitors	2-11
	2.5 Telemetry System in Orbit	2-14
	2.6 Command System in Orbit	2-16
	2.7 Power System in Orbit	2-17
	2.8 Structures and Temperature in Orbit	2-18
	2.9 Experiment Interfaces in Orbit	2-19
	2.10 In-Orbit One-Year Performance Summary	2-22
3	OSO-6 DEVELOPMENT AND SUPPORT HISTORY	3-1
	3.1 Introduction	3-1
	3.2 Management	3-1
	3.3 Schedule	3-2
	3.4 Design Review and Hardware Selection	3-2
	3.5 Component Fabrication and Test	3-4
	3.6 Spacecraft Integration and Test	3-11
	3.7 Experiment Accommodation	3-12
	3.8 Observatory Integration and Test	3-22
	3.9 Launch Activities	3-44



CONTENTS (continuation)

Section		Page
	3.10 Post-Launch Activities	3-50
4	DATA REDUCTION COMPUTER PROGRAMS	4-1
	4.1 Experiment Print Routines	4-1
	4.2 Observatory Automatic Testing System (OATS)	4-10
	4.3 Flight Data Plotting Programs	4-14
5	ASPECT MEASURING SYSTEM	5-1
	5.1 General Description	5-1
	5.2 Aspect Geometry	5-3
	5.3 Aspect System Electronics	5-9
	5.4 Aspect Computation	5-17
6	DYNAMICS	6-1
	6.1 Introduction	6-1
	6.2 Rotational Dynamics of OSO	6-1
7	CONTROL SYSTEMS FUNCTIONAL DESCRIPTION	7-1
	7.1 Introduction	7-1
	7.2 Control Systems Interaction	7-2
	7.3 Control Systems Operation in the Launch Phase	7-5
	7.4 Control Systems In-Orbit Operation	7-8
	7.5 Pitch Control System Functional Description	7-10
	7.6 Spin Control System Functional Description	7-17
	7.7 Offset Pointing Control Functional Description	7-29
	7.8 Coarse Servo Functional Description	7-36
	7.9 Fine Azimuth and Elevation Servo Loops	7-50
	7.10 Pointing Control Interaction with Other Systems	7-55
	7.11 Pointing Parameters and Monitors	7-56
	7.12 Launch Sequence System Functional Description	7-58



CONTENTS (continuation)

Section		Page
	7.13 Nutation Control System Functional Description	7-65
8	POWER AND DISTRIBUTION DESCRIPTION	8-1
	8.1 Introduction	8-1
	8.2 Power Supply	8-1
	8.3 Power Control and Distribution	8-9
	8.4 Solar Array Output and Observatory Power Budget	8-12
	8.5 Power System Differences	8-17
9	TELEMETRY SYSTEM DESCRIPTION	9-1
	9.1 Introduction	9-1
	9.2 Data Handling Subsystem	9-1
	9.3 RF Subsystem	9-38
	9.4 Spacecraft Housekeeping Data Acquisition	9-51
	9.5 Telemetry System Performance Requirements	9-52
10	COMMAND SYSTEM DESCRIPTION	10-1
	10.1 Introduction	10-1
	10.2 Command Format	10-1
	10.3 Command Receivers	10-6
	10.4 Command Decoders	10-9
	10.5 System Performance Requirements	10-11
11	STRUCTURES, THERMAL CONTROL, PNEUMATICS, AND HYDRAULICS	11-1
	11.1 Spacecraft Structures	11-1
	11.2 Thermal Control	11-7
	11.3 Hydraulic Systems	11-14
	11.4 Pneumatic Systems	11-16
Appendix		Page
A	ABBREVIATIONS USED IN THIS REPORT	A-1
B	BIBLIOGRAPHY	B-1
C	OSO-6 SYSTEMS AND COMPONENTS DESCRIPTION	C-1
D	OSO-G MODEL SPECIFICATION	D-1



ILLUSTRATIONS

Figure		Page
	OSO-6 Orbiting Solar Observatory (Frontispiece)	
1-1	OSO-6 Experiment Windows	1-6
1-2	OSO-6 Mission Description	1-7
1-3	NRL X-Ray Pointed Instrument	1-7
1-4	HCO Ultraviolet Pointed Instrument	1-8
1-5	UCL Ultraviolet Wheel Instrument	1-8
1-6	Rutgers Zodiacal Light Wheel Instrument	1-9
1-7	Bologna X-Ray Wheel Instrument	1-9
1-8	UNM Neutron Wheel Instrument	1-10
1-9	LASL X-Ray Wheel Instrument	1-10
1-10	Delta-N Launch Vehicle	1-13
1-11	Delta-N Separation Mechanisms	1-15
1-12	OSO-6 Launch	1-17
1-13	OSO Subsatellite Plot	1-20
1-14	Main Features of OSO Structure	1-22
1-15	Wheel Electronics Systems	1-23
1-16	Hub and Azimuth Shaft Assembly	1-23
1-17	Sail Electronics	1-25
1-18	Control Systems	1-25
1-19	Gas Control Systems	1-26
1-20	OSO Overall Dimensions	1-26
1-21	Pointing Modes	1-31
1-22	OSO-6 Launch Sequence	1-34
2-1	OSO-6 Typical Orbit Profile--Sun-Centered Point	2-3
2-2	OSO-6 Typical Orbit Profile--Large Raster	2-5
2-3	OSO-6 Typical Orbit Profile--Small Raster	2-6
2-4	OSO-6 Typical Orbit Profile--Offset Point	2-7
2-5	Point Mode Performance--First 100 Days	2-9
2-6	OSO-6 Attitude History	2-12
2-7	OSO-6 Typical Orbit Profile--Frame Count	2-15



ILLUSTRATIONS (continuation)

Figure		Page
3-1	OSO-G Wheel Pre-Mate I and T Activity	3-13
3-2	OSO-G Sail Pre-Mate I and T Activity	3-14
3-3	OSO-G Spacecraft Integration and Test	3-15
3-4	OSO Spacecraft Simulator	3-20
3-5	OSO-6 (OSO-G) Integration and Test History	3-24
3-6	Thermal-Vacuum Chamber	3-28
3-7	OSO Axes of Vibration	3-33
3-8	OSO-6 Z-Axis Vibration	3-33
3-9	OSO-6 X-Axis Vibration	3-33
3-10	OSO-6 Y-Axis Vibration	3-33
3-11	OSO-2 on Balance Machine	3-37
3-12	Spin MOI Test Setup	3-37
3-13	CG/MOI Test Fixture	3-37
3-14	OSO on Weighing Scale	3-40
3-15	Observatory Demagnetizer	3-43
3-16	OSO on Magnetotropometer	3-45
3-17	OSO Shipping Container	3-46
3-18	OSO Protective Cover	3-48
3-19	OSO Ground Station During Launch	3-51
4-1	Data Processing System Interfaces	4-2
4-2	Data Processing System	4-5
4-3	Main Frame Print Format	4-8
4-4	Typical Experiment Print Format	4-9
4-5	Sample Page of OATS Procedure	4-11
5-1	OSO Aspect Coordinate Systems	5-4
5-2	Geometry of SORE Count Angles	5-7
5-3	Flux Gate Magnetometer	5-9
5-4	Diagram of Pitch Readout Sensor	5-11
5-5	Pitch Readout Sensor Output Curve	5-12
5-6	Aspect Detector	5-13
5-7	SORE Block Diagram	5-14
5-8	SORE Timing Diagram	5-15



ILLUSTRATIONS (continuation)

Figure		Page
6-1	Motion of \bar{H} and \bar{S} During Pitch Precession	6-5
6-2	Effect of Pitch Precession Torque	6-7
6-3	Residual Nutation of \bar{S} After Constant Torquing Stops	6-11
6-4	Interaction of Elevation Servo with Nutation	6-15
6-5	Nutation Generated during Normal Solar Acquisition	6-16
6-6	Nutation Generated during Solar Acquisition when the PIA Strikes the Stops	6-20
7-1	Control Systems Components	7-11
7-2	Pneumatic Pitch Control System Block Diagram	7-12
7-3	Spin Control System Block Diagram	7-18
7-4	Spin-Down Loop Timing Diagram	7-22
7-5	Spin-Up Loop Timing Diagram	7-25
7-6	Day Power Turn-On Circuits	7-27
7-7	OSO-6 Raster Patterns	7-31
7-8	Elevation Offset Channel	7-34
7-9	Azimuth Offset Channel	7-35
7-10	OSO-6 Pointing Control Block Diagram	7-38
7-11	Coarse Sensor Assemblies	7-40
7-12	Coarse Sensor Signal	7-41
7-13	Rate Signal Compensation	7-44
7-14	Typical Coarse Azimuth Preamp/AC Amp Response	7-46
7-15	Typical PWM/Power Switch Response	7-48
7-16	Typical Fine-Eye Response	7-52
7-17	Overall Fine Servo Gain Showing Dead Zone	7-54
7-18	Launch Sequence System Block Diagram	7-59
7-19	Launch Sequence Timer Schematic Diagram	7-61
7-20	Typical Squib Firing Circuit	7-64
7-21	Nutation Damper	7-67
8-1	OSO-6 Power Distribution Diagram	8-2
8-2	Main Battery and Solar-Cell Array	8-3



ILLUSTRATIONS (continuation)

Figure		Page
8-3	N-P Silicon Solar Cell	8-5
8-4	Solar-Cell Response	8-5
8-5	Solar Array Power	8-8
9-1	OSO-6 Telemetry System Block Diagram	9-2
9-2	OSO-6 Telemetry Format	9-5
9-3	Data-Handling System Functional Diagram	9-7
9-4	Digital Multiplexer and Encoder Logic Diagram	9-8
9-5	DME Timing Chart	9-10
9-6	Analog Subcommutator Functional Block Diagram	9-16
9-7	Analog Subcommutator Logic Diagram	9-17
9-8	ASC Timing Chart	9-18
9-9	Analog Sub-Subcommutator Block Diagram	9-21
9-10	PCM J-Box Functional Diagram	9-22
9-11	Frame Counter and Digital Submultiplexer Functional Block Diagram	9-25
9-12	Tape Recorder Block Diagram	9-28
9-13	Word Gate Generator Interface Diagram	9-33
9-14	Word Gate Generator Functional Diagram	9-35
9-15	Telemetry Transmitter (PSK-600A) Block Diagram	9-40
9-16	OSO-6 Transmitter Antenna Pattern ($E\theta$ Polarization)	9-45
9-17	OSO-6 Transmitter Antenna Pattern ($E\phi$ Polarization)	9-46
9-18	Coordinate System for Radiation Pattern	9-47
9-19	Orientation of OSO Relative to Contour Plots	9-48
9-20	Receiver Antenna Pattern, Right-Circular Polarization	9-49
9-21	Antenna and Support Bracket Details	9-50
10-1	Command System Block Diagram	10-2
10-2	OSO Command Format	10-4
10-3	VHF Command Receiver Block Diagram	10-7
10-4	Command Decoder Functional Diagram	10-10



ILLUSTRATIONS (continuation)

Figure		Page
10-5	OSO-6 Command Logic Diagram	10-13/14
11-1	OSO-6 Surface Finishes	11-9
11-2	Arm Damper System	11-15
11-3	Gas System Block Diagram	11-17
D-1	OSO Coordinate System	D-25



TABLES

<u>Table</u>		<u>Page</u>
	OSO-6 Experiment and Interface One-Year Operational Summary	ix
	OSO-6 Spacecraft Systems One-Year Performance Summary	x
1-1	Sun's Emissions	1-3
1-2	OSO-6 Milestone Dates	1-11
1-3	Significant Launch Events	1-18
1-4	OSO-6 Important Mass Properties	1-27
2-1	OSO-6 Experiment Initial Turn-On History	2-20
2-2	Summary of Spacecraft Systems Performance vs. Model Specification for First Year of Operation	2-23
3-1	OSO-6 Spacecraft Subassembly Identification	3-5
3-2	OSO-6 Experiment Power, Command, Telemetry, Weight	3-19
3-3	OSO-6 Experiment Support Documentation	3-23
3-4	OSO-6 Vibration Acceptance Test Levels	3-32
3-5	OSO-6 Weight, CG, and MOI	3-38
3-6	OSO-6 Magnetic Dipole Moments	3-40
3-7	OSO-6 ETR Prelaunch Milestones	3-49
8-1	OSO-6 Predicted Solar Array Output	8-13
8-2	OSO-6 Spacecraft Power Summary	8-15
8-3	OSO-6 Flight Instruments Actual Power Budget	8-16
9-1	Specifications for the PSK-600A Telemetry Transmitter	9-41
9-2	OSO-6 Telemetry Link Gain Margin at 14,400 bps	9-53/54
10-1	OSO-6 Command Allocations	10-5
10-2	Receiver Electrical Characteristics	10-8
10-3	Command Link Gain Margins	10-13
A-1	Abbreviations Used in This Report	A-2
B-1	Bibliography	B-2
C-1	Functional Description of OSO-6 Spacecraft Systems	C-2
C-2	Functional Description of OSO-6 Major Spacecraft Components	C-3
D-1	Offset Mode Characteristics	D-11
D-2	Offset Mode Performance	D-15



Section 1 PROJECT HIGHLIGHTS

1.1 INTRODUCTION

Brief descriptions of the OSO-6 mission objectives, development history, in-orbit performance, spacecraft and scientific instrument systems, and the Delta launch vehicle are presented in this section. Detailed descriptions of these topics are presented in other sections of this final report. Also, material of a detailed nature, related to but not included in this report, is appropriately referenced.

In this report, the term "observatory" refers to the entire payload which includes the basic spacecraft and experiment complement. The term "spacecraft" refers only to the basic spacecraft portion and its systems excluding the scientific experiments. A list of the abbreviations used in this report is presented in Appendix A. A bibliography of source material and related documents is presented in Appendix B. A concise listing of the spacecraft systems and major components (including their functions) is given in Appendix C.

1.2 MISSION DESCRIPTION

1.2.1 Why OSO is Needed

The sun continually emits electromagnetic radiation of greatly varying intensities across a broad spectrum. The earth's atmosphere acts as a shield and absorbs the major portion of this energy, making it difficult, and in some cases impossible, for ground-based observers to evaluate the detailed characteristics of solar radiation. Thus, the primary objective of the Orbiting Solar Observatory is to gather such data from its vantage



point above the earth's atmosphere, and telemeter this information to earth ground stations. OSO-1 through OSO-5 have contributed significantly to our knowledge of solar and celestial emissions. OSO-6 continued these objectives by providing the participating experimenters with additional data.

1.2.2 Why the Cosmic Radiation Region is Studied

Although the sun's total energy output (of which over 99 percent is in the visible, UV, and IR light regions¹) varies less than one percent, the energy of the low-frequency (radio frequency), particulate, and the extremely high-frequency (cosmic) radiation is known to vary enormously (see Table 1-1). These regions of highly variable but of relatively low energy emissions seem to have the greatest influence on earth's geophysical nature. The low frequency RF emissions have been extensively investigated by ground-based radio telescopes. However, the extremely high frequency emissions consisting of ultraviolet, X-rays, and gamma rays are almost entirely blocked by the earth's ionosphere and atmosphere and, therefore, cannot be observed from the ground. Furthermore, it is believed that these extremely high frequency emissions hold important secrets of the sun's processes.

To summarize, there are two primary reasons for studying the sun's processes: (1) that a greater knowledge of these processes will help in understanding the sun-earth relationship, i.e., the effect the sun has on geophysical processes such as weather, geomagnetic storms, and radiowave propagation; and (2) that by understanding the sun's natural processes, we may find the answers to other celestial processes and phenomena.

¹The spectrum in these regions is very much like the spectrum of a 6000°K "black body".



Table 1-1
SUN'S EMISSIONS

<u>Emission</u>	<u>Wavelength*</u>	<u>Energy at Earth in ergs/cm²-sec</u>	<u>Magnitude of Variations</u>
RF Waves	10 ⁴ m - 1 mm	3 x 10 ⁻⁷	x 10 ³
Infrared	1 mm - 9000 Å	3 x 10 ⁴	very small
Photographic	9000 to 3000 Å	1.4 x 10 ⁶	very small
UV	3000 to 1500 Å	2 x 10 ⁴	very small
Lyman-Alpha UV	1216 Å	5 to 10	x 3
EUV	1500 to 300 Å	1	x 100
XUV	1500 to 1 Å		
X-rays	300 Å - 1 Å	10 ⁻³ to 10 ⁻⁴	x 10 ³
High Energy Spectrum	<1 Å, >10 Kev	uncertain	x 10 ⁶

* These bandwidths can not be precisely defined and there is generally considerable overlap.

1.2.3 Mission Objectives

The primary¹ objective of the OSO-6 mission was to launch and place into orbit a spacecraft carrying solar physics experiments. These experiments were to detect and measure electro-magnetic

¹A secondary objective for the launch vehicle was to place an experimental Packaged Attitude Control (PAC) into orbit. The purpose of the PAC mission was to flight test an earth stabilized control system which might be used in the future for adapting the Delta second stage for a wide variety of piggyback payloads.



radiation in selected areas of the spectrum, from the sun and other sources.

Specific mission objectives were:

- To study solar radiation in the spectral range of 300 to 1300 Å from localized regions
- To perform spectral, burst, and mapping measurements of solar X-rays within the range of 0.2 to 28 Å
- To monitor photon flux in six selected spectral lines within the range of 16 to 40 Å
- To measure the ellipticity, brightness, and polarization of zodiacal light
- To monitor solar X-rays, celestial X-rays, and the terrestrial X-ray albedo within the range of 20 to 200 keV
- To determine the energy spectrum and angular distribution of high-energy neutron flux within the range of 20 to 130 MeV
- To study solar resonance lines and optically thin lines of helium I, helium II, iron XI, oxygen, and nitrogen
- To study F-layer ionization and flares

In Fig. 1-1, we have superimposed the individual experiment "windows" on the sun's electromagnetic spectrum to show the areas investigated by the OSO-6 experiments. Summary descriptions of the spacecraft and its experiments are given in Figs. 1-2



through 1-9. Note that the NRL X-Ray Spectroheliograph and the HCO Ultraviolet Spectroheliograph instruments were located in the solar-oriented part of the observatory and were concerned only with solar phenomena. The other instruments (the "wheel" experiments) were located in the rotating section of the observatory. These instruments swept the celestial sphere and viewed its components (including earth and sun).

Detailed descriptions of the experiments are presented in BBRC Document TN69-04, OSO-G Experiment Payload Description, issued 16 June 1969.

1.3 SCHEDULE HIGHLIGHTS

Milestone dates for the OSO-G/OSO-6 program are listed in Table 1-2.

1.4 OBSERVATORY IN-ORBIT PERFORMANCE SUMMARY

The OSO-6 Orbiting Solar Observatory has, at the time of this writing, operated continuously for more than two years, making over 12,000 revolutions of the earth. During this time, every mission requirement has been met or exceeded, with the exception of some scientific experiment malfunctions which reduced the ability of the observatory to completely fulfill its scientific objectives.

Spacecraft systems performance is presented in some detail in Section 2 of this report. Comparison of performance data with the criteria defined in the OSO-G Model Specification, BBRC Document 26493 (See Appendix D), shows that OSO-6 greatly exceeded the 6-month minimum performance requirements during the first two years of in-orbit operation.

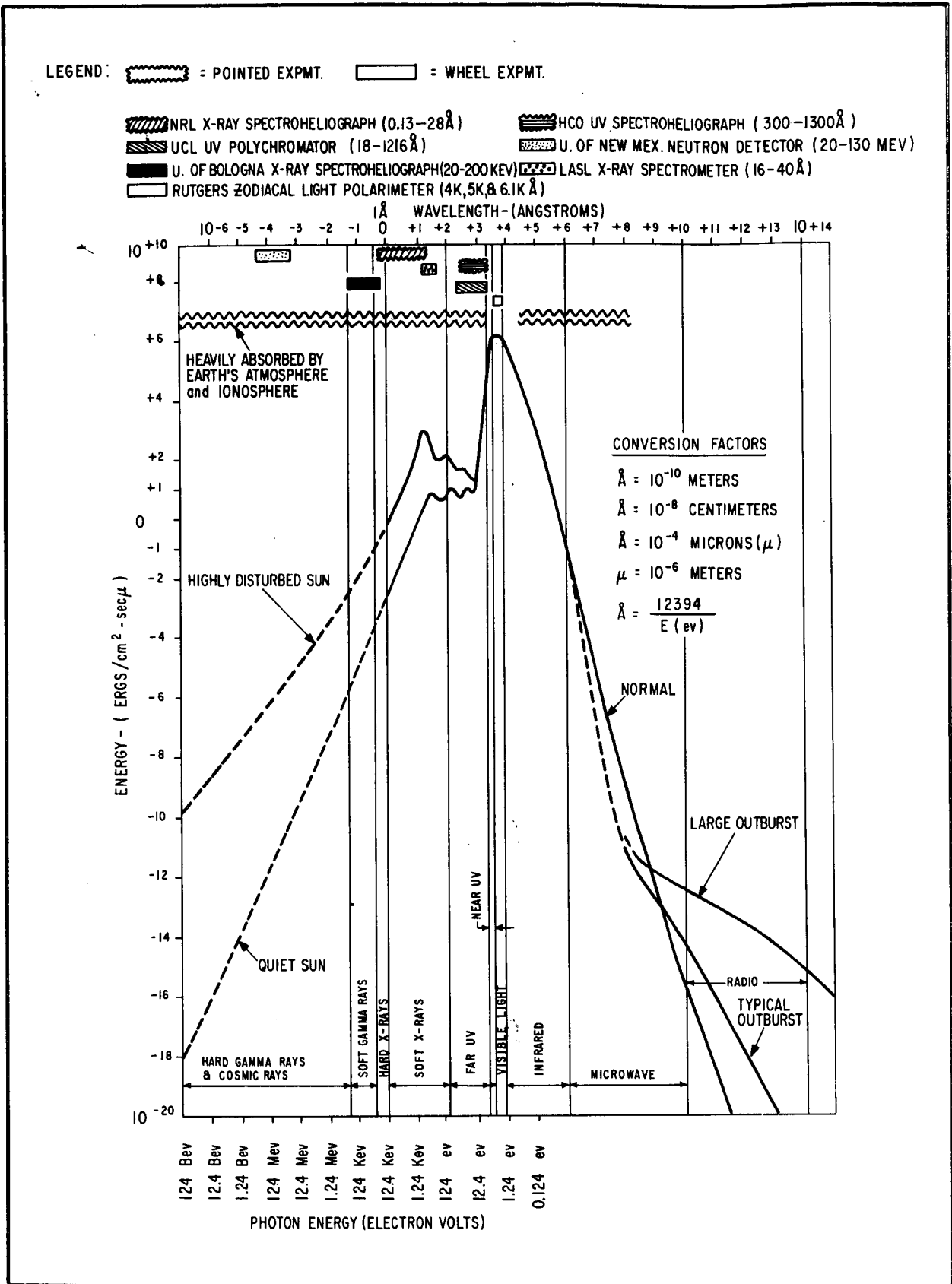
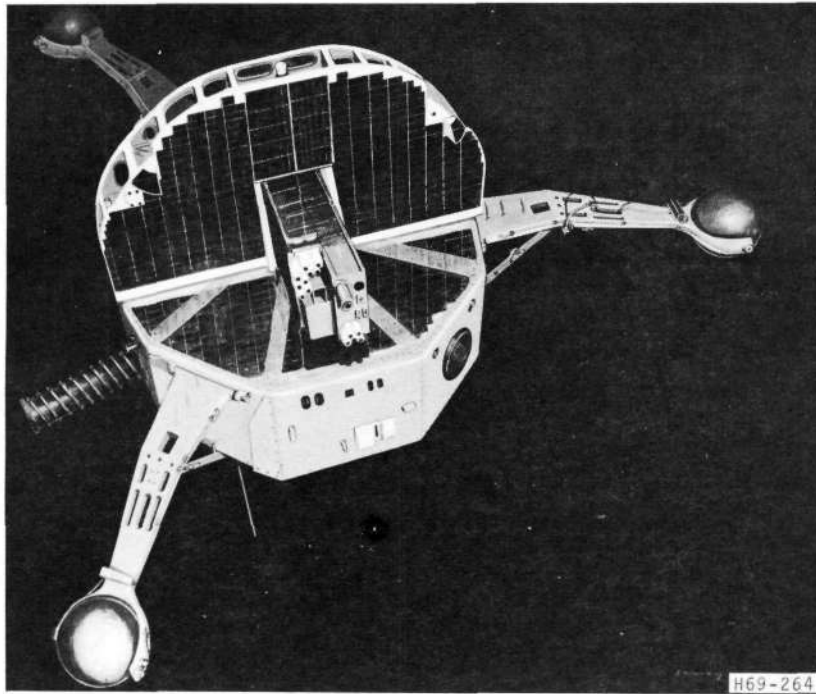


Fig. 1-1 OSO-6 Experiment Windows



PROGRAM SUMMARY

PROJECT ORBITING SOLAR OBSERVATORY (OSO-6)
PROJECT DIRECTION NASA / GSFC
PRIME CONTRACTOR BALL BROTHERS RESEARCH CORP.
EXPERIMENT ORGANIZATIONS U.S. NAVAL RESEARCH LABORATORY, UNIVERSITY COLLEGE LONDON, HARVARD COLLEGE OBSERVATORY, UNIVERSITY OF BELGIUM, LOS ALAMOS SCIENTIFIC LABORATORY, UNIVERSITY OF NEW MEXICO, RUTGERS STATE UNIVERSITY
MAJOR OBJECTIVES THE OSO-6 RESEARCH SPACECRAFT DESIGNED FOR MEASUREMENT OF SOLAR PHENOMENA AND SOLAR EFFECTS THE VARIATION IN ATTITUDE OF THE OBSERVATORY DURING ITS LIFETIME WILL ALSO PERMIT OBSERVATION OF THE ENTIRE CELESTIAL SPHERE AND PORTIONS OF THE EARTH'S SURFACE
LIFETIME ESTIMATED SIX MONTHS
LAUNCH VEHICLE DELTA N
CIRCULAR ORBIT 301 ± 30 NAUTICAL MILES
INCLINATION 33 ± 3 DEGREES
NOMINAL PERIOD NIGHT 36 MIN - DAY 80 MIN TOTAL 96 MIN
TOTAL OBSERVATORY WEIGHT ESTIMATED 290 KG (639.9 LB.)
POINTING ACCURACY NOT MORE THAN ONE MINUTE OF ARC
POINT MODE STATIONARY POINTING AT CENTER OF SOLAR DISC
LARGE RASTER MODE 46 BY 90 MINUTES OF ARC
SMALL RASTER MODE 7 BY 75 MINUTES OF ARC
OFFSET POINT MODE 16384 POINTS WITHIN 46 BY 46 ARC MINUTE PATTERN

H69-264

Fig. 1-2 OSO-6 Mission Description

Naval Research Laboratory- X-Ray Spectroheliograph
Principal Investigators: Dr. T. Chubb and Mr. R.W. Kreplin

Objectives: Measure the solar x-ray energy and spatial distribution in the spectral region of 0.13 to 28 Å

Description: Consists of four individual experiments: (1) pulse height analyzer, (2) Bragg spectrometer, (3) raster experiment, and (4) burst experiment.

The pulse height analyzer uses a sodium iodide scintillator and a proportional counter to monitor rapid energy changes in the 2 to 90 keV (0.14 to 6 Å) region. The scintillator covers the high energy region of 20 to 90 keV and the PC covers the low energy region of 2 to 20 keV.

The Bragg spectrometer uses three crystal spectrometers to provide fine spectral resolution through the soft x-ray region of 0.6 to 25 Å. The ranges of the spectrometers are: 0.6 to 4 Å, 14 to 8.4 Å, and 18 to 25 Å. The photon flux passed by each crystal is measured by a geiger counter.

The raster experiment consists of three geiger counter detectors. One determines the photon spatial distribution in the 8 to 20 Å region. The second pinpoints hot spots in the 1 to 8 Å region. The third detects and measures the lateral velocity of flares in the 8 to 20 Å region.

The burst experiment uses two geiger counter detectors to monitor the solar disc for very short duration bursts in the 18 to 25 Å region and to detect cosmic background radiation in the 2 to 8 Å region.

H72-85

Fig. 1-3 NRL X-Ray Pointed Instrument

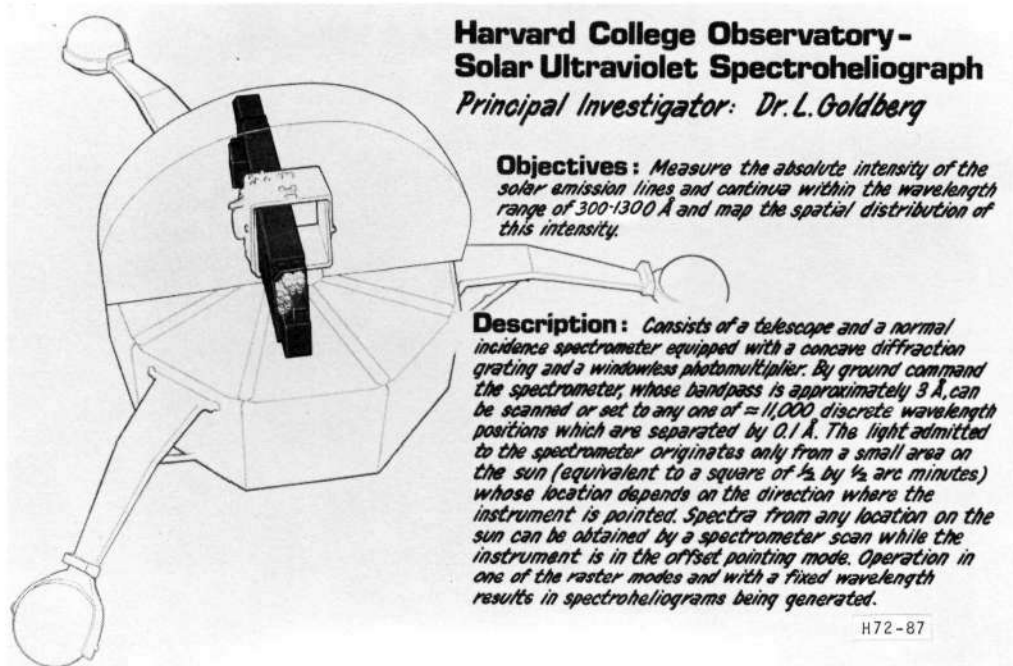


Fig. 1-4 HCO Ultraviolet Pointed Instrument

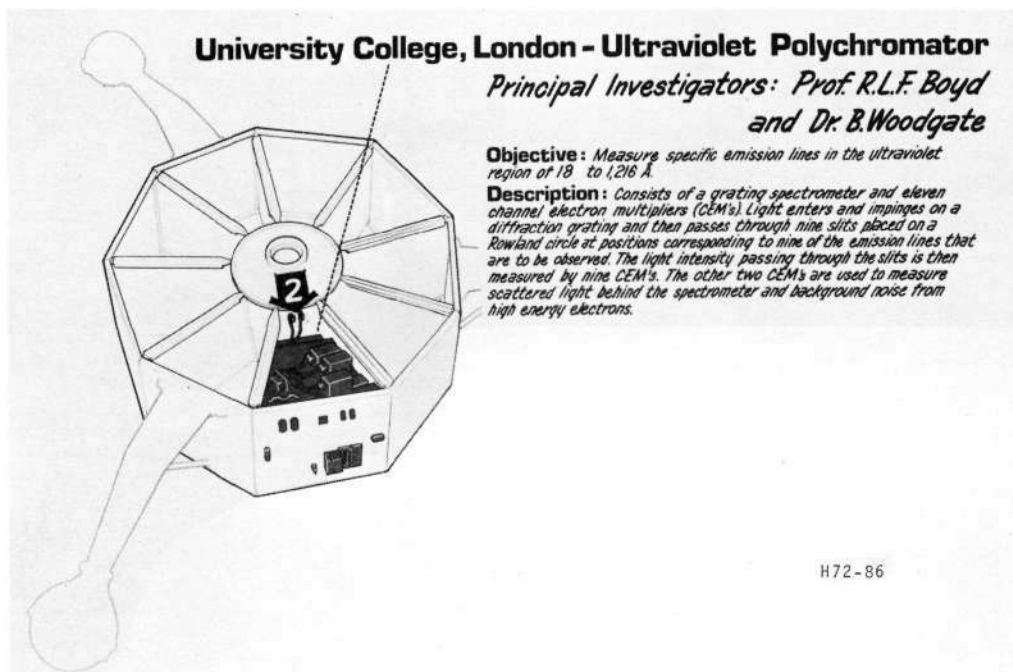


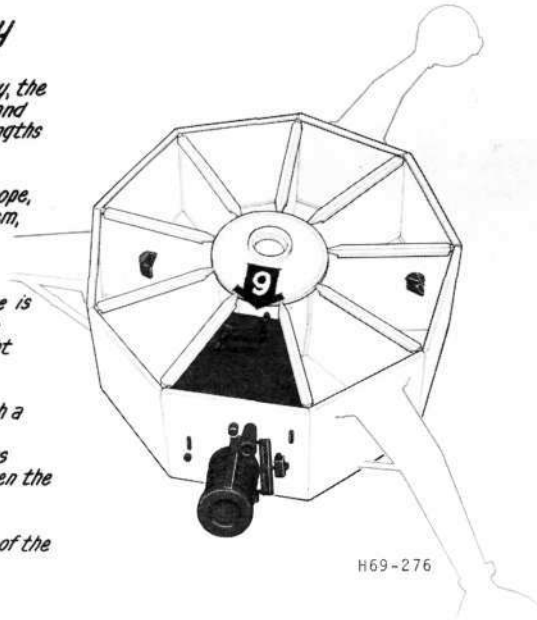
Fig. 1-5 UCL Ultraviolet Wheel Instrument

Rutgers State University- Zodiacal Light Polarimeter

Principal Investigator: Dr. A.L. Rouy

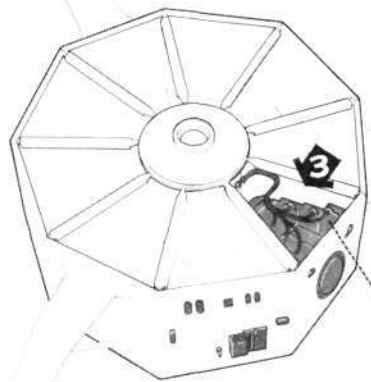
Objectives: Measure Zodiacal light intensity, the degree and axis of polarization and the amount and nature of any elliptically polarized light at wavelengths of 4,000, 5,000 and 6,100 Å.

Description: Consists of a collimating telescope, quartz rotators, retardation plates, polarizing prism, monochromating filters and photomultiplier. Zodiacal light (which is polarized) is first collected and collimated by the telescope with a look-angle of less than two degrees. The telescope is protected from stray and scattered light by a sun shield that extends out from the rim panel. The light passes through an optical system in which the polarization axis of the light is rotated in increments of 45°. The light then passes through a Rouy prism and the resulting intensities are measured by the photomultiplier at the various angles. Additional measurements are made when the light in one axis is retarded in phase by the retardation plate. This data is then used to calculate the degree and angle of polarization of the zodiacal light.



H69-276

Fig. 1-6 Rutgers Zodiacal Light Wheel Instrument



University of Bologna Solar X-Ray Spectroheliograph

Principal Investigator: Prof. D. Brini

Objectives: Measure the solar hard x-ray energy, celestial spatial distribution, and earth albedo in the spectral region of 20 to 200 keV.

Description: Consists of a sodium iodide scintillator detector and a photomultiplier. The scintillator converts entering x-ray photons into light pulses. The photomultiplier and logic circuits then convert these light pulses into electrical pulses in four ranges corresponding to photon energy ranges of 20 to 40, 40 to 70, 70 to 110 and 110 to 200 keV.

H69-259

Fig. 1-7 Bologna X-Ray Wheel Instrument

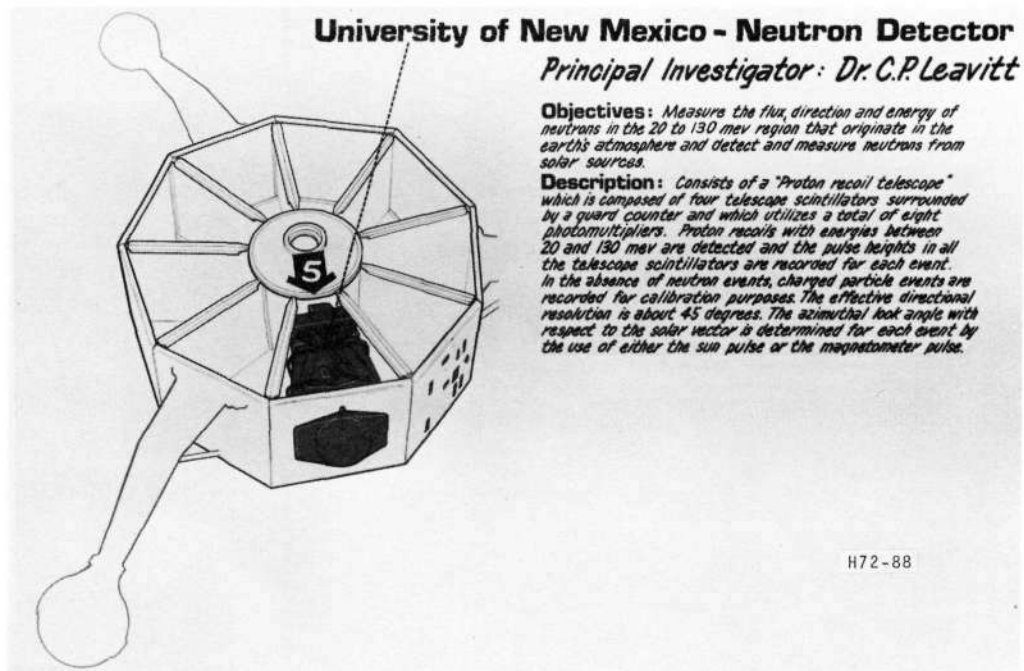


Fig. 1-8 UNM Neutron Wheel Instrument

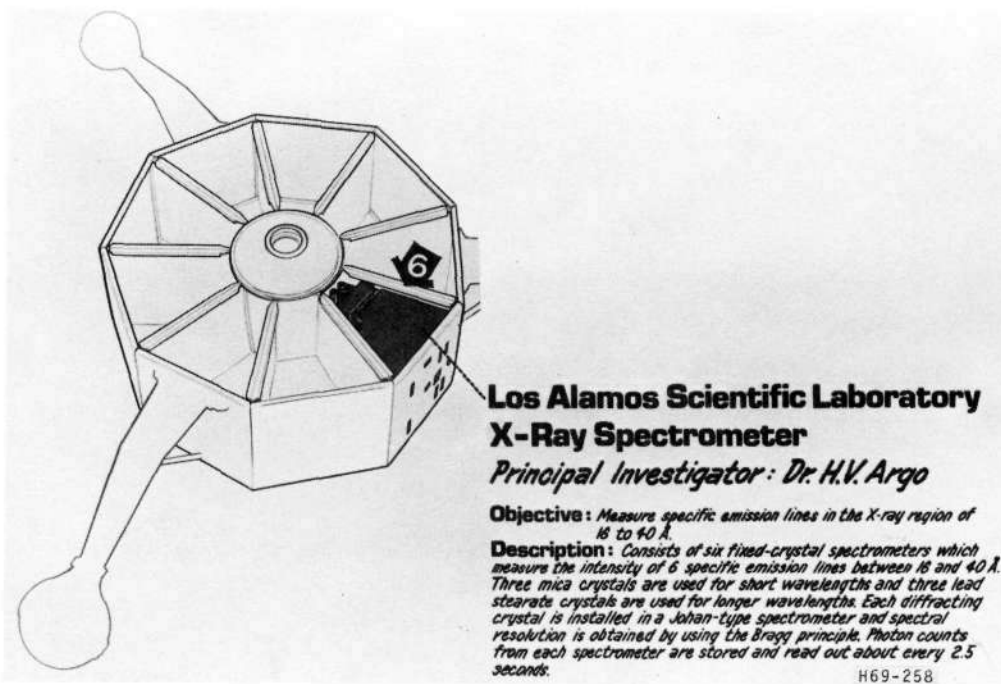


Fig. 1-9 LASL X-Ray Wheel Instrument



Table 1-2
OSO-6 MILESTONE DATES

Date	Milestone Event
7 Oct 65	Initial Experimenters' Meeting
31 Oct 66	Begin Design Review and Production Activities
26 Jun 68	Wheel Section Delivered from Production to Integration and Test Facility
26 Jul 68	Sail Section Delivered from Production to Integration and Test Facility
5 Oct 68	Mate Sail Section to Wheel Section
29 Nov 68	Spacecraft 90-percent Acceptance
23 Mar 69	Final 10-percent Spacecraft Acceptance
9 Apr 69	Experiment Instrument Integration Starts
24 May 69	Observatory Vibration Testing Starts
4 Jun 69	Observatory Thermal-Vacuum Testing Starts
17 Jul 69	Observatory Acceptance/Shipment to ETR
9 Aug 69	Launch

Throughout the observatory lifetime, hundreds of outbursts of solar activity were monitored by OSO-6's scientific instruments. A great amount of information on solar and nonsolar gamma radiation, ultraviolet radiation, and X-ray radiation sources and intensities and charged-particle spectra has been obtained. This data included the solar eclipse of 7 March 1970.

Rigorous treatment of experiment performance, which involves experimenter proprietary information, is left to the prerogative of the particular scientists involved.

1.5 LAUNCH VEHICLE DESCRIPTION AND LAUNCH SUMMARY



1.5.1 Launch Vehicle Description

The OSO-6 spacecraft was launched from Cape Kennedy, Florida, by a launch vehicle designated Delta-72.

Delta-72 was a two-stage DSV-3N launch vehicle (Fig. 1-10) for which the McDonnell Douglas Astronautics Company (MDAC) is prime contractor. The first stage (S/N 20012) was a modified (long tank), liquid propellant Thor booster powered by an MB-3 Block III Rocketdyne engine system rated at 172,000 pounds of thrust at sea level. This stage used RJ-1 as the fuel and liquid oxygen (LOX) as the oxidizer. It burned to propellant depletion in about 220 seconds. Pitch and yaw control was provided by gimbaling the main engine in response to signals from an inertial reference package. Two small vernier engines provided roll control.

The first stage was thrust-augmented by three strapped-on Thiokol TX354-5 solid propellant motors (S/Ns 93, 143, and 162) each rated at about 52,000 pounds of thrust and having a nominal burn time of 37 seconds. These motors burned to completion and were jettisoned 70 seconds after liftoff. This combination of the main engine and solids plus two vernier engines provided a liftoff thrust of about 330,000 pounds.

The second stage (S/N 20239) was an Aerojet General AJ10-118E liquid propellant engine system rated at 7,800 pounds average thrust in a vacuum. This engine used unsymmetrical dimethylhydrazine (UDMH) as the fuel and inhibited red nitric acid (IRFNA) as the oxidizer. It's burn time was controlled from the ground and was about 600 seconds. Attitude control during the powered portion of the second-stage flight was accomplished in the same manner as the first stage except that the thrust for roll correction was provided by cold-gas thrusters. The second-stage guidance compartment housed the flight control

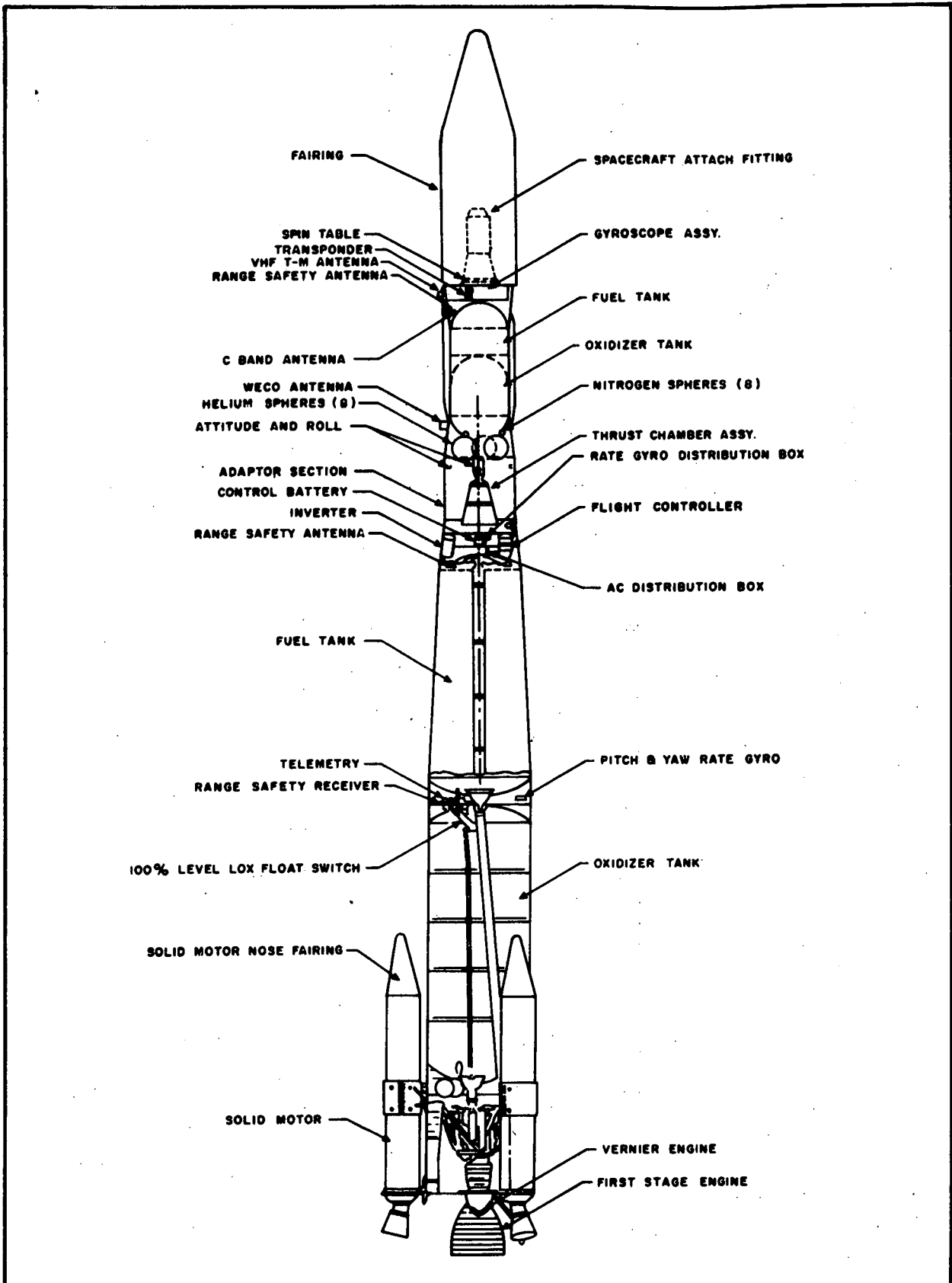


Fig. 1-10 Delta-N Launch Vehicle



system, the radio guidance system, the velocity cut-off system instrumentation, the radio destruct system, and tracking and power systems.

The OSO was attached to the second stage by an interstage structure which included a spin table (Fig. 1-11). The purpose of the spin table was to spin-stabilize the OSO (at about 100 rpm) just before it was separated from the launch vehicle. Spinup was provided by several small rockets located around the perimeter of the spin table. Separation was accomplished by the vehicle timer which fired bolt-cutting squibs which released the retaining bands that attached OSO to the adapter. A small velocity increment was imparted to OSO by a helical spring that was compressed between the OSO attach fitting and the third-stage adapter. At separation OSO's separation switches closed and power was applied to the OSO launch sequence timers (see Paragraph 1.6.6).

The first and second stages were guided by two separate pre-programmed autopilot systems. The Western Electric Company (WECO) provided a ground-based radio guidance system to make any necessary trajectory changes during first and second stage powered flight. The communications system of the launch vehicle monitored functional and environmental conditions of the vehicle. The data was transmitted to the ETR ground stations through VHF FM/FM telemetry equipment. Tracking was accomplished through a C-band transponder which responds to interrogation from ground radar sites.

1.5.2 Launch Summary

The Delta-72 vehicle and OSO-6 spacecraft were launched from Pad 17A, Cape Kennedy Air Force Station, Florida, at the scheduled time of 0352:00.1 EDT on 9 August 1969 (Fig. 1-12).

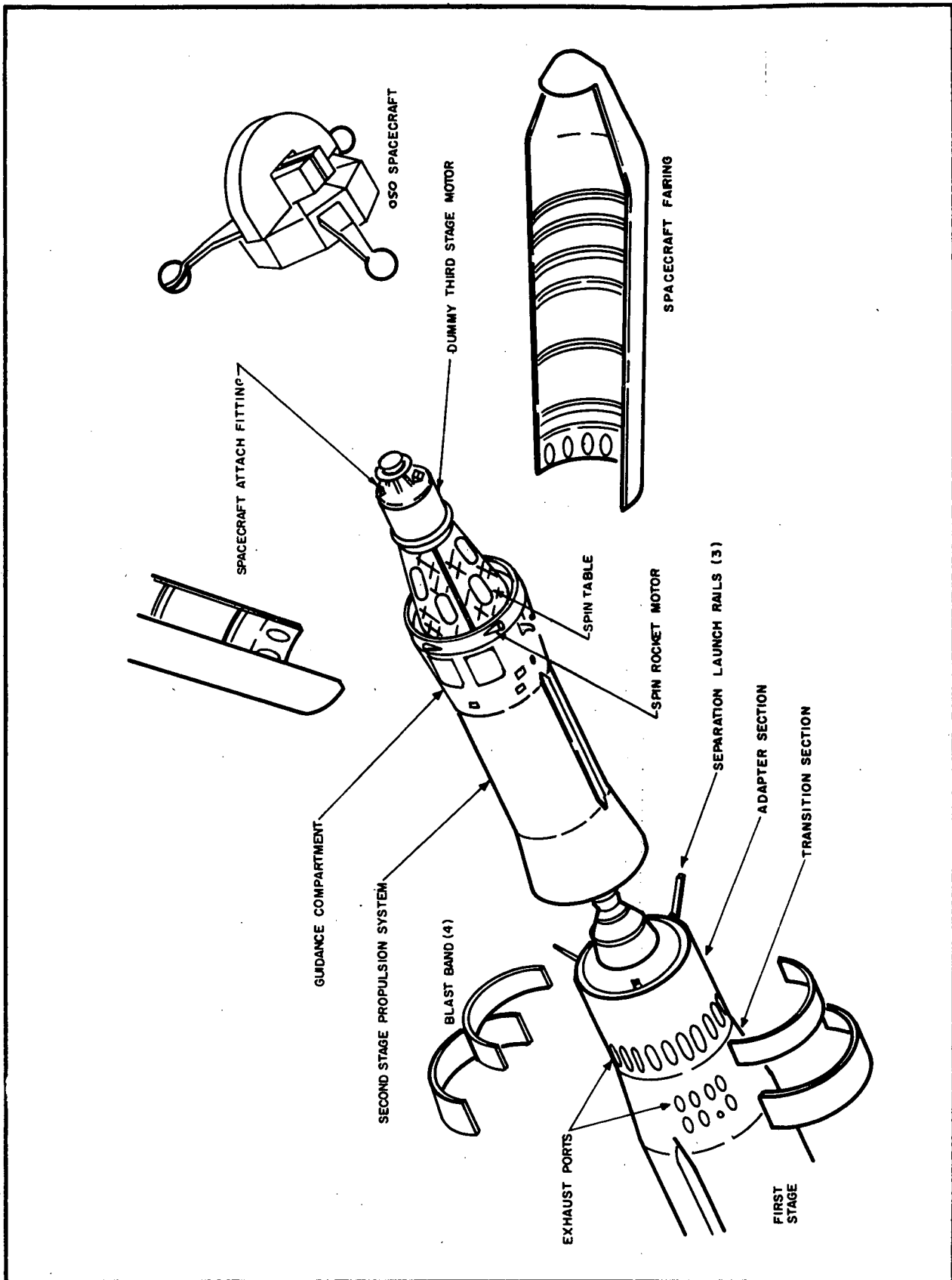


Fig. 1-11 Delta-N Separation Mechanisms



There were no major problems or unscheduled holds during the final F-0 Day countdown. The weather on F-0 Day was very good and caused no problems. There was no major pad damage.

Guidance, control, electrical, and propulsion systems on both vehicle stages were generally nominal. Telemetry performance and data acquisition were excellent. Radar and optics support were good except for the loss of one camera.

Launch Vehicle Operation. The Delta-72 vehicle was launched on a flight azimuth of 108 degrees true. Initial plots of the early portion of the flight showed the vehicle to be right and high of the nominal predicted. (The position plots were about 2 nm higher than nominal XZ until MECO.) The balance of the flight was nominal or near nominal. The angle between the OSO wheel plane and the sun was 2.7 degrees at orbit injection.

The Instantaneous Impact Chart plots were slightly right of nominal until WECO guidance brought them back to nominal at about T+150 seconds. These plots remained nominal for the rest of the flight.

MECO occurred as predicted and SECO appeared to have occurred as expected. The rest of the flight was on time. The major flight events and their nominal and actual times of occurrence are shown in Table 1-3.



Fig. 1-12 OSO-6 Launch



Table 1-3
SIGNIFICANT LAUNCH EVENTS

Event	Times After Liftoff (sec)	
	Nominal	Actual
Liftoff	0352:00 EDT	0352:00.1 EDT
Main engine cutoff	220.8	217.6
Stage-II ignition and Stage-I/II separation	224.8	221.6
Fairing jettison	229.8	226.6
Second-stage engine cutoff	605.6	591.6
Terminal pitch maneuver started	631.88	Unknown
Pitch maneuver ended	718.83	Unknown
Spin Table spinup	738.8	735.6
OSO separation	740.8	737.6

OSO Spacecraft. Spacecraft functions occurred normally during powered flight. At T+735.6 seconds the spacecraft was spun up to 97.87 rpm. Realtime data from Antigua verified spacecraft separation, initiation of the spacecraft timer, and deployment of the spacecraft arms. Realtime data from Ascension Island indicated the spacecraft was despun, the sun was acquired, nutation damper was uncaged, pointed experiments elevation unlocked, and the auto pitch and spin limiters were enabled.

The elevation drive motor current was higher than expected when in the pitch up position due to slight loading by the flex cables. This anomaly did not degrade spacecraft operation.

The early OSO-6 orbital parameters from Tracking and Data System were:



	<u>Nominal</u>	<u>Actual</u>
Apogee (kilometers)	552.6	560.3 (302.4 nm)
Perigee (kilometers)	540.0	494.6 (266.9 nm)
Inclination (degrees)	32.9	32.964
Period (minutes)	95.68	95.1
Eccentricity	0.00019	0.004754

The orbital path over the earth's surface for the first few orbits is shown in Fig. 1-13.

1.6 SPACECRAFT DESCRIPTION

The role of the basic spacecraft was to accurately point the pointed instruments at the center of the sun, provide a stable platform for the "wheel experiments", provide inertial aspect and time correlations for the experiments, provide operational control by ground command, and telemeter the experiment data and spacecraft performance (housekeeping) data to earth ground stations. To do this, the spacecraft used ten primary systems:

- (1) Structures and Thermal Control
- (2) Pitch and Roll Control
- (3) Spin Control
- (4) Pointing Control
- (5) Nutation Control
- (6) Launch Sequence Control
- (7) Command
- (8) Telemetry
- (9) Power
- (10) Aspect

In addition to these ten spacecraft systems, there were seven primary scientific experiments; the composite of these systems and experiments (including the basic spacecraft structure) made up the complete observatory.



1.6.1 Spacecraft Structures and Thermal Control

The basic spacecraft consisted of two main structures: the rotating wheel structure, and the solar-oriented sail structure (Fig. 1-14).

Wheel Structure. The wheel consisted of a cylinder divided into nine wedge-shaped compartments arranged around a central hub. Four of these compartments housed the wheel electronics (Fig. 1-15) and the remaining five housed the wheel experiments. Attached to the perimeter of three compartments were three extendible arms that supported the spin-control gas bottles and reaction jets. During the launch phase, these arms were released from the stowed state and moved upward into the plane of the wheel, thus increasing the effective diameter of the wheel. This was done to increase the wheel spin-moment-of-inertia, and thereby increase its gyroscopic rigidity while also providing a longer lever arm for the spin-control jets to act upon. The three arms were latched in the stowed state by squib-actuated latching pins and support brackets; these brackets also served as part of the antenna array. A hydraulic arm damper system was used to prevent damage to the arms when they were released during the launch phase.

The wheel and sail were connected by an azimuth shaft (Fig. 1-16) which extended from the base of the azimuth shaft assembly through the wheel to the base of the azimuth casting which supported the sail. This shaft was held in position by two low-friction azimuth bearings; one at the top and one at the bottom. An azimuth drive motor was located near the uppermost bearing with its stator attached to the azimuth shaft housing and its rotor attached to the azimuth shaft. The azimuth drive motor, in conjunction with the pointing control system, pointed the sail (and, therefore, the pointed experiments) in azimuth during orbit-day by driving the sail at an opposite

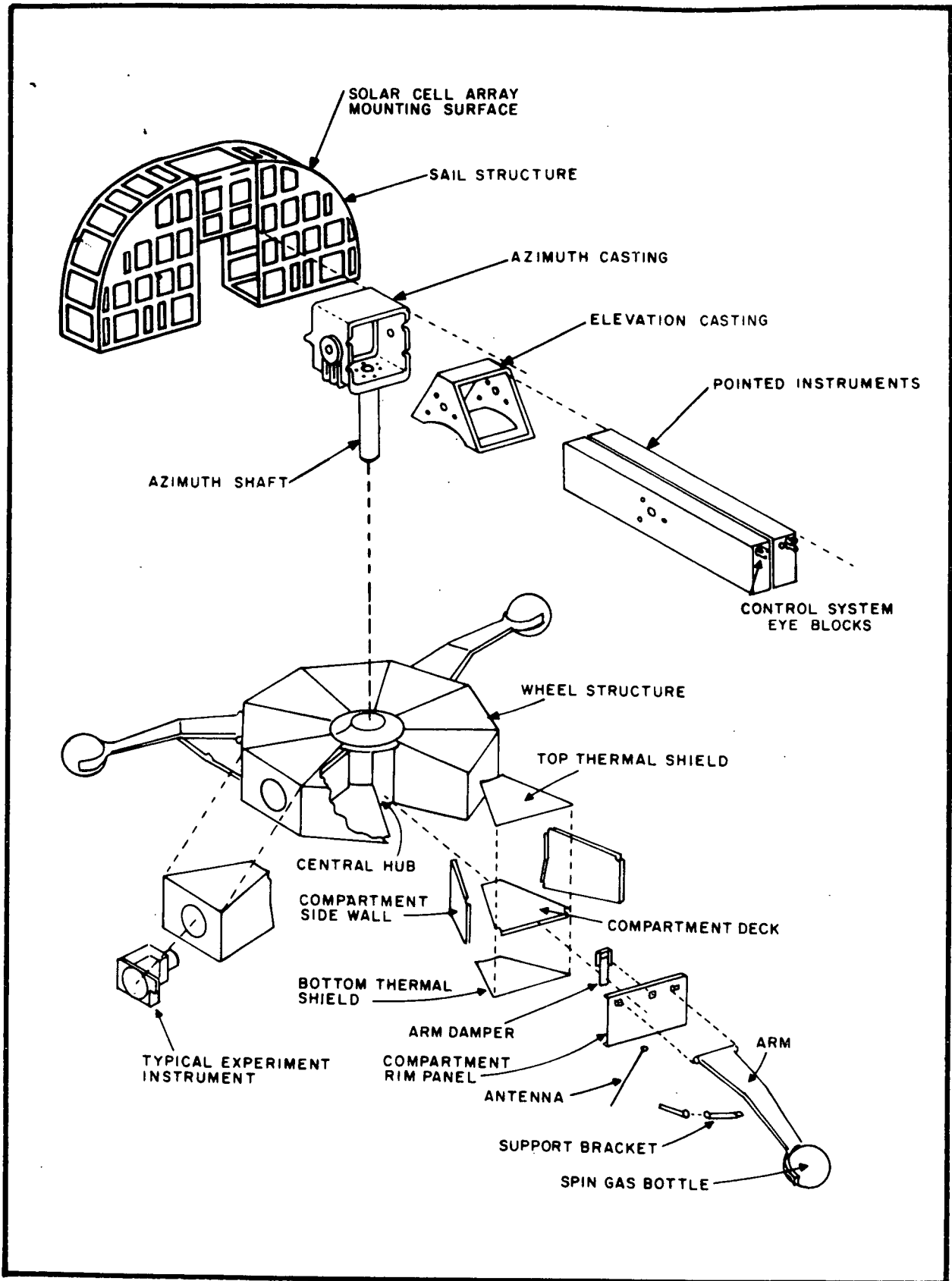


Fig. 1-14 Main Features of OSO Structure

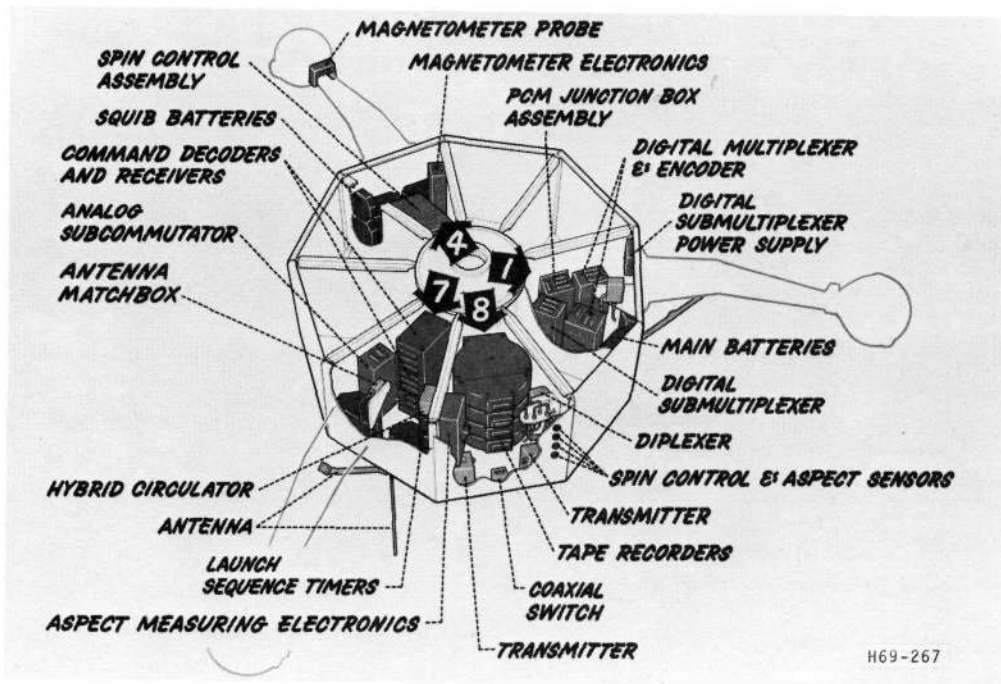


Fig. 1-15 Wheel Electronics Systems

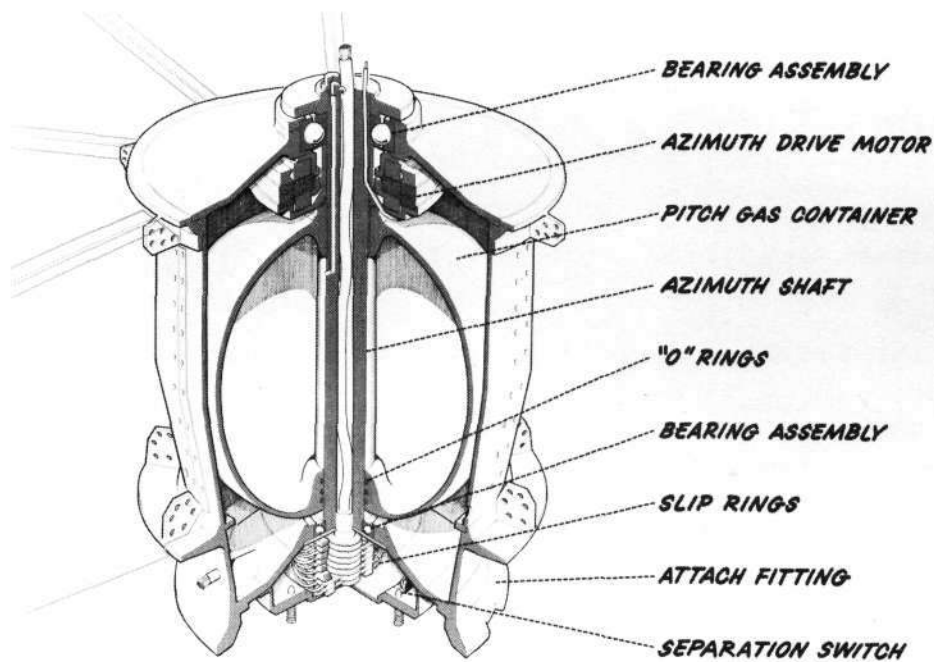


Fig. 1-16 Hub and Azimuth Shaft Assembly



but equal rate with respect to the wheel. Mounted at the base of the azimuth shaft, was a slip ring assembly that transferred power, telemetry signals, and control signals between the sail and the wheel and the separation switches that indicated when separation occurred. Mounted between the two azimuth bearings was a high-pressure nitrogen gas container that stored the gas supply for the pitch control system contained in the sail.

Sail Structure. The sail consisted of a semicircular framework attached atop the azimuth shaft. Solar cells covered the entire sun-facing surface except that part occupied by the pointed experiments. Behind the solar cell array were the electronic, mechanical, and pneumatic components necessary for the operation and orientation of the sail and pointed experiments (Figs. 1-17 and 1-18). The two pointed experiment packages were mounted side-by-side in the elevation casting, which in turn was mounted in the azimuth frame. The elevation casting was supported by two elevation stub shafts and two elevation bearings. An elevation drive motor, connected to one of the stub shafts, provided, in conjunction with the pointing control system, elevation pointing control of the pointed experiments. Both the left-hand and right-hand experiments carried very sensitive solar sensors (fine eyes) that provided "fine" azimuth and elevation pointing error and readout signals for the pointing control system. Also mounted on the sail were other azimuth solar sensors (coarse eyes) that provided "coarse" drive signals for initially despinning the sail each orbit-morning.

Pitch control of the observatory was provided by a nitrogen-gas pneumatic system (Fig. 1-19) contained within the sail and controlled by the pitch control system and a system of magnetic control. The pitch gas was stored in the pitch gas bottle contained in the azimuth shaft assembly and the precession jets were located on either side of the sail.

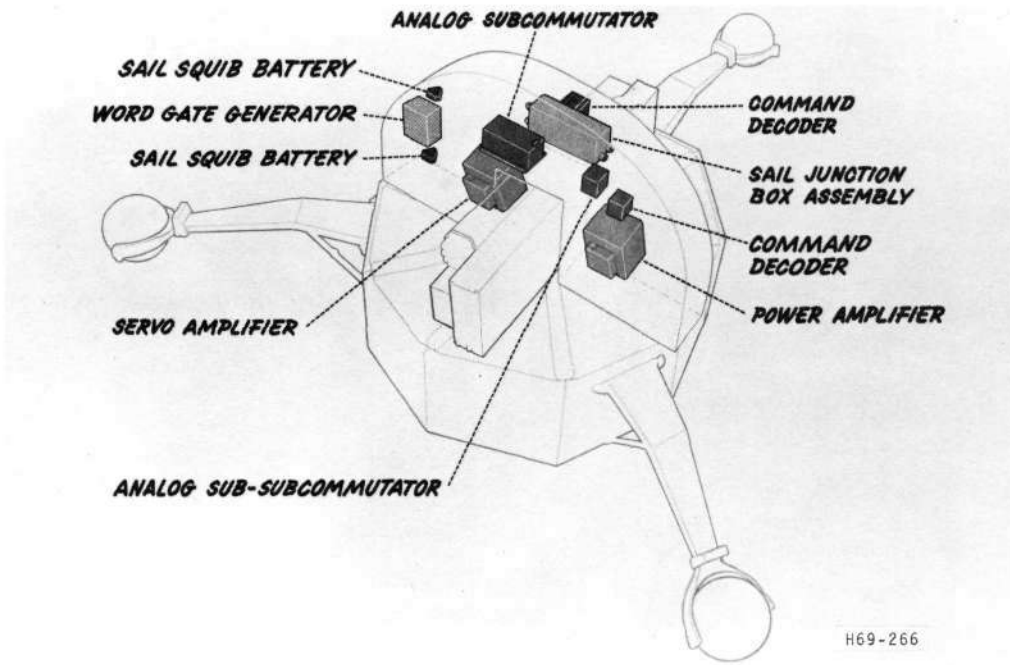


Fig. 1-17 Sail Electronics

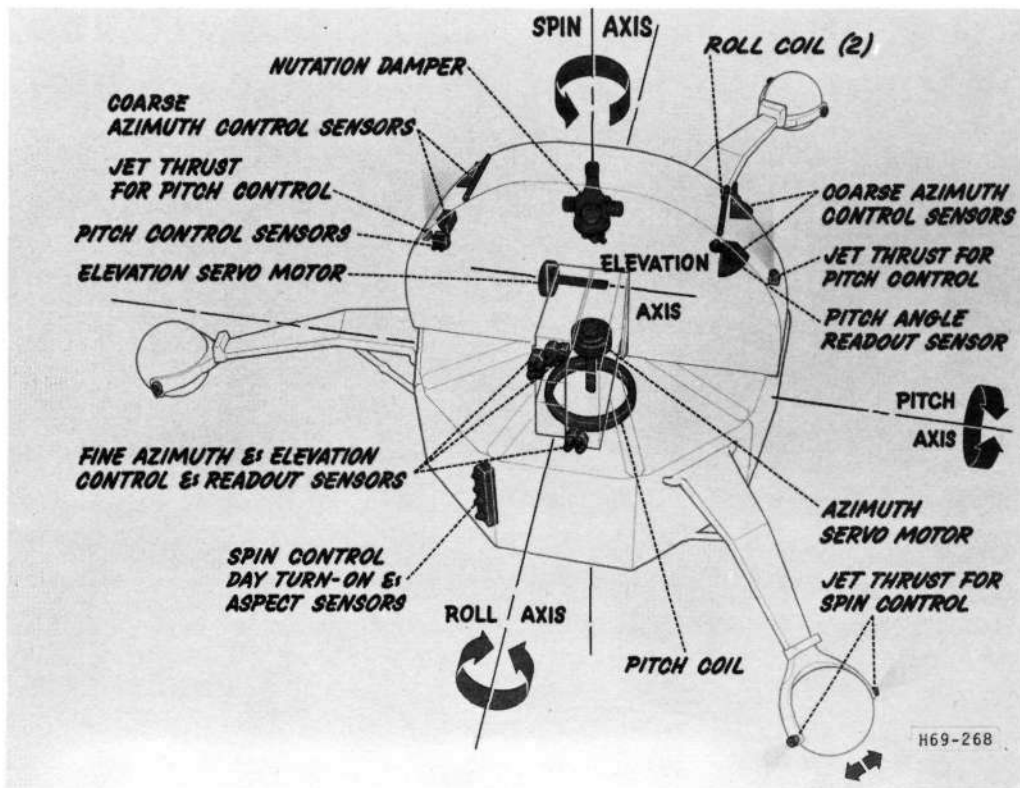


Fig. 1-18 Control Systems

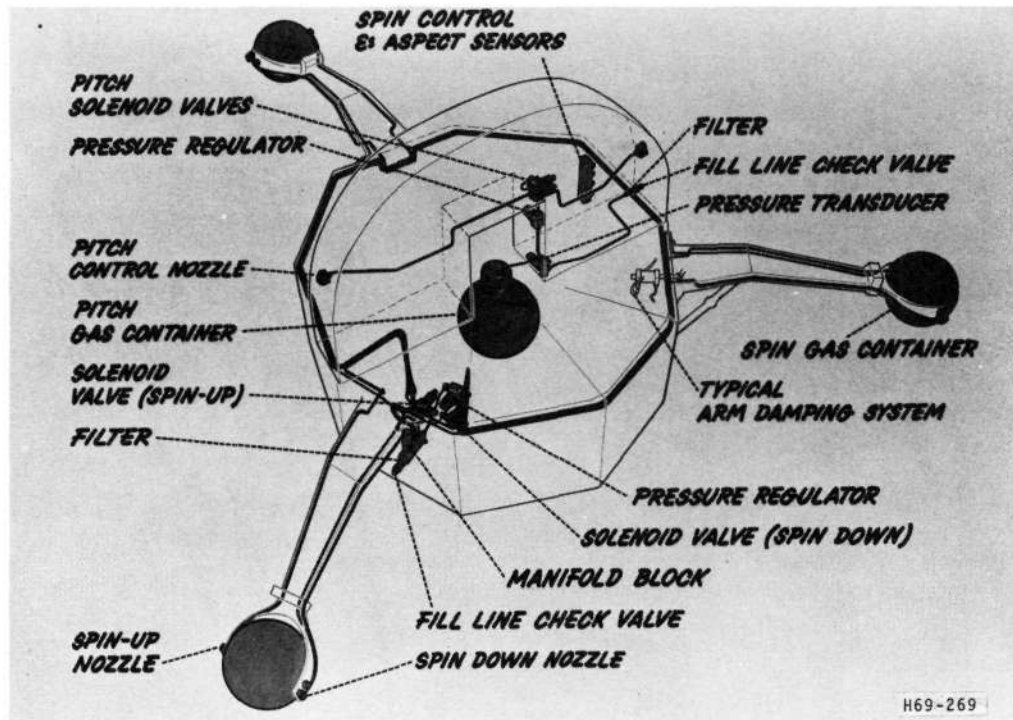


Fig. 1-19 Gas Control Systems

A nutation damper was mounted behind the solar cell array and served to damp any nutational motion the spacecraft may have acquired during its operation.

Spacecraft Dimensions and Mass Properties. The OSO-6 observatory had an overall diameter of about 44 inches and an overall height of about 38 inches including the attach fitting (Fig. 1-20). In

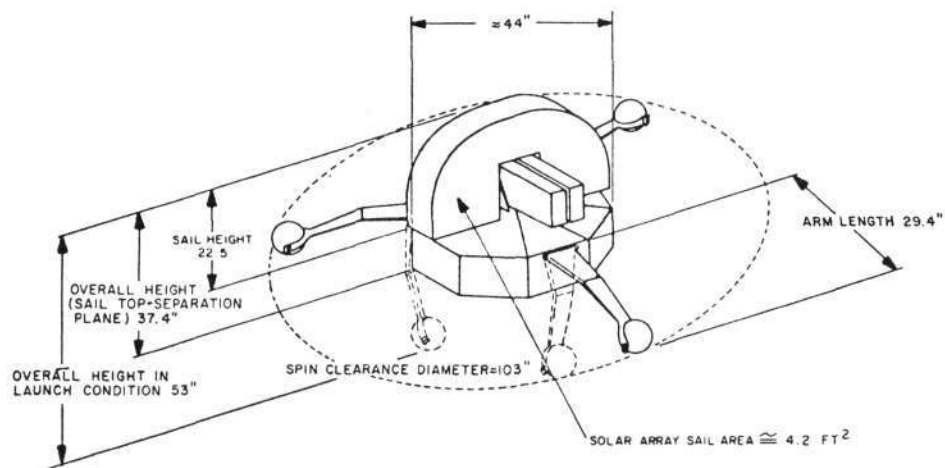


Fig. 1-20 OSO Overall Dimensions



the launch condition, the arms were folded, thereby creating a total payload length of about 54 inches. Table 1-4 lists some of the more important mass properties of OSO-6.

Table 1-4
OSO-6 IMPORTANT MASS PROPERTIES

Property	Value
Total observatory launch weight (Total experiment weight)	639.91 lb. (218.76 lb.) (34.3 percent of total)
Spin MOI (slug-ft ²)	
Wheel only	22.1 (launch); 29.9 (orbit)
Wheel and sail	27.5 (launch); 35.3 (orbit)
Transverse MOI (slug-ft ²)	
X-axis	23.6 (launch); 25.0 (orbit)
Y-axis	24.8 (launch); 23.9 (orbit)
Mean (X & Y)	24.5 (orbit)

Thermal Control. For OSO to accomplish its mission, it is necessary to keep its temperature within specified limits in those sections of the spacecraft that house temperature-sensitive experiment instruments. Therefore, a thermal analysis was performed for the OSO-6 mission with an assumed experiment and spacecraft equipment complement. This analysis considered the thermal characteristics and temperature requirements of each instrument and included such factors as: solar radiation, albedo, earth radiation, electrical heating, radiation to space, conduction and radiation between parts of the spacecraft, and the energy stored by these parts. This analysis also considered typical orbits from the hottest to the coldest during a year, and predicted the temperature changes during each orbit and the orbit mean temperature. From this analysis, we determined the



type of temperature control schemes needed to satisfy the temperature control requirements.

As a result, simple, passive temperature control schemes were used throughout. These schemes consisted of using special paints and surface finishes to control the heat gains and losses and by providing the proper heat conduction paths within the structure.

A more detailed discussion of the structure and thermal control systems is given in Section 11. Summary descriptions of structural components are given in Appendix C.

1.6.2 Pitch and Roll Control

Pitch Control. Because of external torques acting on the spacecraft and the motion of the earth about the sun, the orientation of the spin axis had to be continuously corrected in pitch to maintain the spin axis within ± 3 degrees of normal to the solar vector during the life of the spacecraft. These corrections were made by two independent subsystems: (1) a pneumatic pitch control subsystem, and (2) a magnetic bias coil (pitch-roll coil). The latter was used as the primary control system and the gas system was used only when fast pitch maneuvers were required.

The pneumatic pitch control system consisted, basically, of pitch-angle solar detectors, electronic control circuits, and nitrogen gas thrusters. It has two modes of operation: (1) the automatic pitch mode and (2) the manual pitch mode.

In the automatic pitch mode, this system automatically maintained the pitch attitude by sensing the pitch angle and releasing high pressure N_2 gas through either the pitch-up or pitch-down control nozzles (thrusters) when the ± 3 degree



limits were exceeded. These nozzles were positioned so their impulse caused the observatory to precess in the proper direction (up or down) to correct the pitch error.

In the event of an automatic mode failure, there were circuits that would automatically select the manual pitch mode. The automatic and manual modes could also be selected by ground station command. In the manual control mode, bursts of pitch gas could be released in response to ground commands to change pitch attitude as desired.

The magnetic bias coil consisted simply of a coil of wire placed around the central hub of the spacecraft (Fig. 1-18). When activated by ground commands, this coil would produce a magnetic field that interacted with the earth's magnetic field and caused the spacecraft to slowly pitch in the desired direction. This coil was used to conserve pitch gas and thus greatly increased the operational life of the spacecraft.

The pitch attitude angle was continuously monitored during the day portion of the orbit by a pitch readout solar sensor and telemetered to receiving ground stations.

Roll Control. Roll control was strictly by magnetic means and was provided by the pitch-roll coil (discussed above) and two roll-spin coils mounted in the sail and aligned parallel with the roll axis (Fig. 1-18). These two sets of coils were controlled by ground commands to maneuver the spin axis into the desired roll attitude. The roll attitude was determined by the aspect measuring system.

A more detailed discussion of the pitch and roll control systems is presented in Section 7 of this report. Summary descriptions of this system and its components are given in Appendix C.



1.6.3 Spin Control

It was necessary to keep the wheel spin rate between certain limits for the following reasons: (1) so that the gyroscopic stability of the observatory could be maintained, (2) so that the tuned nutation damper would be most effective (nutation frequency is dependent upon spin rate), and (3) to facilitate the acquisition of wheel experiment data. For these reasons, a pneumatic spin control system was used to automatically keep the wheel spin rate between 0.44 and 0.68 revolutions per second.

The spin control system consisted basically of sun-detecting spin control eyes mounted on the perimeter of the wheel, electronic control circuits contained in the spin control box, and a nitrogen gas pneumatic system. The spin control eyes detected the sun once per wheel revolution, and if the wheel spin rate was outside the range of 0.44 to 0.68 rps, a burst of high pressure N_2 gas would be released from the appropriate spin-up or the spin-down nozzles located at the ends of the three arms.

In the event of a system malfunction in which the spin rate would go too far outside the normal range, the spin control system contained circuits that would automatically switch the system to the manual control mode. In the manual mode, either despin or spin-up bursts could be released by ground command. The selection of either mode of operation could also be accomplished by ground command when desired.

Data from which the spin rate could be computed was continuously telemetered to receiving ground stations. A more detailed description of the spin control system is presented in Section 7. Summary descriptions of this system and its components are given in Appendix C.



1.6.4 Pointing Control

The purpose of the pointing control system was to provide automatic solar acquisition each orbit-morning, and to point the sail and the pointed experiments at desired positions on the sun during the orbit-day.

The pointing control system consisted of three pointing control servo loops: (1) the azimuth-coarse, (2) the azimuth-fine, and (3) the elevation-fine servo loops. These servo loops consisted basically of three separate control sensor assemblies (control eyes), electronic control circuits contained in the servo amplifier and power amplifier, and the azimuth and elevation servo motors (Fig. 1-17 and 1-18).

The OSO-6 pointing control system could be operated in any of four modes: (1) normal center-point mode, (2) large raster mode, (3) offset point mode, and (4) small raster mode (Fig. 1-21).

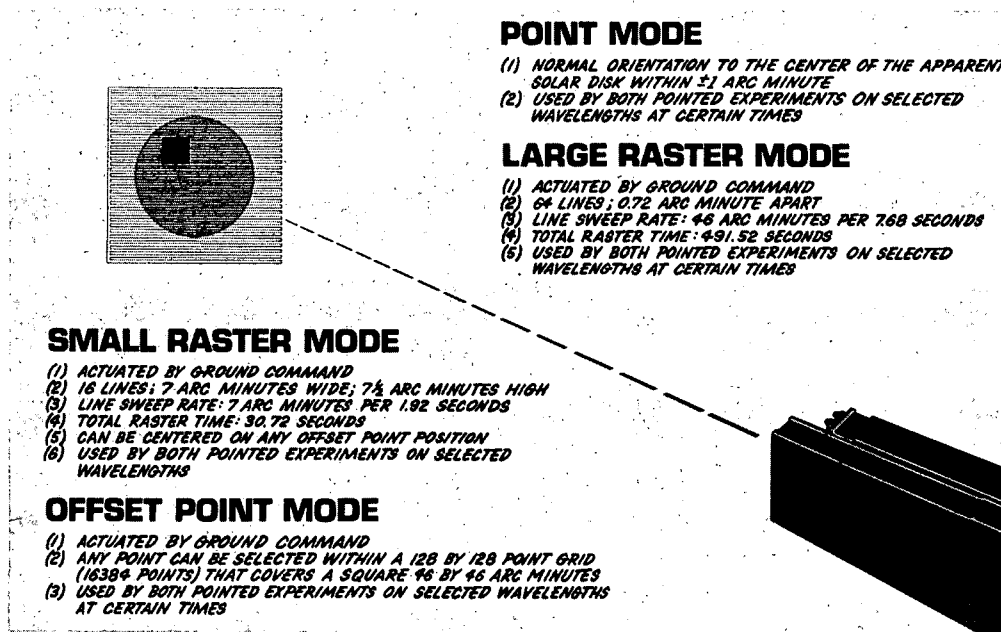


Fig. 1-21 Pointing Modes



In the normal center-point mode, the optical axes of the pointed experiments were pointed at the center of the sun with an accuracy better than ± 1 arc minute. In the large raster mode, the pointed experiments were caused to scan the sun with a 64-line (46 x 46 arc minute) raster pattern centered on the sun. In the offset point mode, the pointed experiments could be pointed at any one of 16,384 points (128 x 128 grid) within the large raster pattern. In the small raster mode, the pointed experiments were caused to raster about any of the offset points with a raster pattern 7 arc minutes in azimuth and 7.5 arc minutes in elevation.

The different modes of operation were selected by command and their use depended on the desires of the experimenters and the GSFC/OSO project personnel. The azimuth and elevation error signals and the point and raster azimuth and elevation readout sensor outputs were telemetered to receiving ground stations.

A more detailed description of the pointing control system is presented in Section 7. Summary descriptions of this system and its components are given in Appendix C.

1.6.5 Nutation Control

Nutation of the observatory from precessional impulses was damped by a "passive" nutation damper located near the top of the sail (Fig. 1-18). This damper consisted of a pendulum bob supported by a wire and emersed in a bath of silicone oil. The bob was tuned to the natural nutation frequency of the observatory when it rotated at 0.5 rps. When the observatory spin axis nutated, the motion of the bob in the oil dissipated the nutation energy in the form of heat.

A more detailed description of this system is presented in Section 7.



1.6.6 Launch Sequence Control

The launch sequence system controlled the unlatching of mechanical assemblies stowed or locked during launch, and supplied activation signals for electrical control functions needed during orbit injection. The system was fully redundant, containing two of each of the following:

- Separation switches
- Electromechanical launch sequence timers
- Squib-firing battery packs in the wheel
- Squib-firing battery packs in the sail
- Squibs in each latch block, and
- Relays and wiring as required.

The timers, which controlled the spacecraft launch sequence events, were started by the separation of the spacecraft from the spin table. The separation signal was provided by the separation switches which were located on the bottom of the OSO attach fitting (Fig. 1-16). The timers provided pulses to control relays which executed the spacecraft functions shown in Fig. 1-22.

This system is described in more detail in Section 7. Summary descriptions of this system and its components are presented in Appendix C.

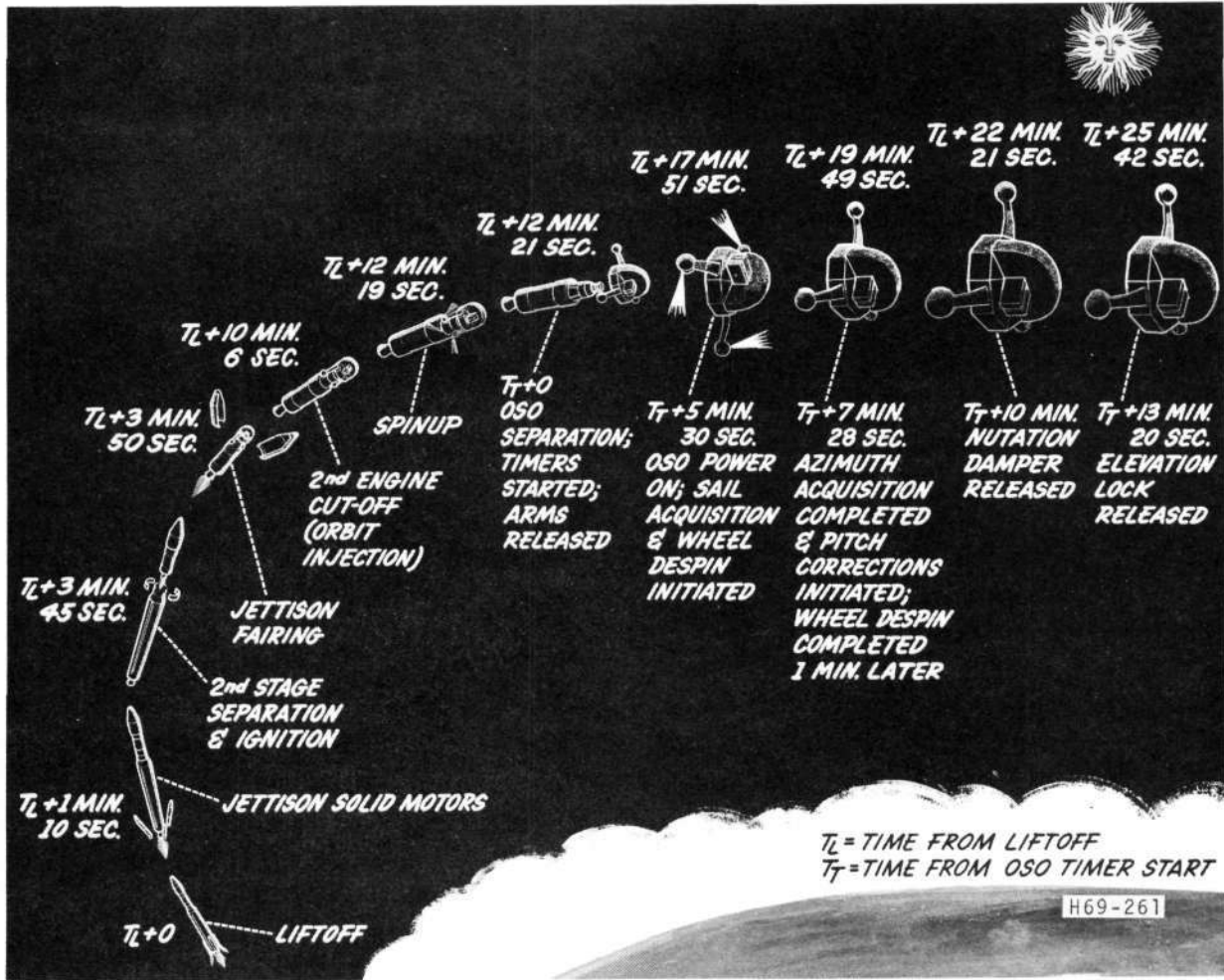


Fig. 1-22 OSO-6 Launch Sequence

1.6.7 Aspect Determination

A knowledge of the orientation ("look" direction) of an experiment when it records a cosmic event assists in the interpretation of the event. This orientation is called "experiment aspect" and was calculated using data from OSO's aspect determination system.

The system consisted of a solar sensor, a fluxgate magnetometer and null detector, the pitch-angle monitor, and associated electronic circuits. The telemetered information after processing yielded:



- (1) The angle between the observatory spin axis and the solar direction
- (2) The roll angle of the observatory spin axis (about the solar direction) relative to ecliptic north
- (3) The angular position of the wheel in its plane of rotation at the time of a detected cosmic event

There were other aspect parameters that were calibrated prior to launch. Examples of these are the tilt of an experiment's look direction relative to the wheel plane, and the angular separation between an experiment's look direction and the azimuth reference axis.

In addition to the spacecraft aspect measuring equipment, some wheel instruments contained their own aspect circuitry. This circuitry usually measured the elapsed time (and hence the amount of wheel rotation) between the passing of an azimuth solar sensor past the sun and the occurrence of a cosmic event. Then, by knowing the roll and pitch angles, the origin of the event could be determined.

The aspect system is described in more detail in Section 5. Summary descriptions of this system and its components are presented in Appendix C.

1.6.8 Command System

The command system provided the means by which the spacecraft and experiments could be remotely controlled by an RF command link between the spacecraft and ground stations. The system



consisted basically of two redundant command receivers, two redundant command decoders in the wheel, two redundant sail decoders, and various control relays and control circuits that provided functional control of the spacecraft and experiments.

The command system used a digital-tone format whereby the address and instruction commands consisted of binary-coded tone bursts. The OSO-6 command system had a complement of 206 commands: 67 for spacecraft functions, 108 for experiment functions, and 31 spares. The command frequency was 149.52 Mhz.

The command receivers detected and amplified the coded RF command signals. Each receiver provided input to an individual wheel decoder, and ground station commands controlled selection of which receiver provided input to each of the two sail decoders. The command decoders accepted the receiver output and, if properly addressed, decoded and executed the instruction commands.

A more detailed description of the command system is presented in Section 10 of this report. Summary descriptions of this system and its components are given in Appendix C.

1.6.9 Telemetry System

The spacecraft and experiment data was sampled, encoded, and telemetered to receiving ground stations by the data handling and RF subsystems. The data consisted of experiment and spacecraft data that originated from spacecraft and experiment transducers, detectors, and monitor circuits. This data was presented to the data handling subsystem in either analog or digital form. Spacecraft and experiment performance data was in analog form; experiment prime data was in digital form. The capacity of the system was 184 8-bit data channels, seven



sync words, and 5 spares. The bit rate was 800 bps and the transmitting frequency was 136.71 Mhz.

The telemetry system processed the spacecraft and experiment data by performing five basic operations. These operations were:

- (1) Commutation (sampling) and analog-to-digital conversion (encoding) of the spacecraft and experiment performance data
- (2) Multiplexing (time sharing) of the digitized performance data, and experiment prime digital data
- (3) Conversion of the multiplexed digital data into biphasic format (Manchester coding)
- (4) Simultaneous data storage and real-time transmitting of data to receiving ground stations
- (5) Transmitting stored data to receiving ground stations in fast playback mode upon command

A more detailed description of the telemetry system is presented in Section 9 of this report. Summary descriptions of this system and its components are given in Appendix C.

1.6.10 Power System

The spacecraft power system converted solar energy into electrical energy, stored this energy in a rechargeable battery, and supplied it to the spacecraft and experiments, upon demand, throughout each orbit. The power system consisted of a solar



cell array, a storage battery assembly, and a power distribution system.

The silicon solar cell array converted the solar energy into electrical energy during orbit-day when the plane of the array was maintained nearly normal to the solar direction. Part of the array output was used to recharge the storage batteries and the balance was consumed by the spacecraft and experiment electrical systems during orbit day. The nickel-cadmium storage battery assembly stored electrical energy for launch and orbit-night consumption, and provided a power reservoir to meet peak power demands. Electrical power was distributed throughout the spacecraft by control relays and associated wiring.

The solar cell array could produce about 40 watts of power during orbit day, which exceeded the power demand by a margin of about ten percent.

A more detailed description of the power system is presented in Section 8 of this report. Summary descriptions of this system and its components are given in Appendix C.

1.6.11 Major Improvements to OSO-6 Systems

The more significant system improvements are briefly described in the following paragraphs:

Pointing Control. Previous OSO's had the capability to point at the center of the sun and to scan the sun with a 40 x 40 arc minute pattern. In addition to the normal sun-centered pointing mode, the OSO-6 was capable of:



- (1) Generating a 46 x 46 arc minute raster centered on and covering the entire sun and some of its atmosphere.
- (2) Providing offset pointing to any position in a 128 x 128 (16,384) point grid pattern centered on the sun. The overall size of this pattern was 46 x 46 arc minutes.
- (3) Generating a small raster of 7 x 7.5 arc minutes that covered about 1/40 of the large raster area. This raster could be centered on any one of the offset points mentioned above.

These improvements meant that the linear region of the control eyes and readout eyes had to be extended and the gain of the pointing control servos had to be changed.

Sail Junction Box. The OSO-6 J-box used plug-in terminal boards and double-density connectors for interfacing with the sail harness and the flex cables. This arrangement made it easy to remove the boards for rework or replacement. In addition, smaller and lighter relays were used on OSO-6.

Flex Cables. The OSO-5 flex cables consisted of printed copper paths thermally bonded between layers of mylar with 37 pin connectors soldered and potted on the ends. The low melting point of mylar caused these cables to be susceptible to heat damage during soldering operations. The flat pointed wire was susceptible to damage by handling during routine spacecraft operations.

The OSO-6 required additional circuits across the elevation axis. In order to reliably provide the additional circuits and maintain flexibility across the elevation axis, OSO-6 flex



cables consisted of shielded and unshielded stranded wires embedded in a flat ribbon of silicone rubber material with 0.070 in. centers and "twist pin" connectors. The resulting cable was more flexible and durable than mylar cables and did not have the melting problem during solder operations.

Roll Control. Because of the requirement of the Rutgers experiment to keep the wheel plane parallel with the ecliptic plane for a minimum of 27 days, a roll coil system was incorporated into OSO-6 to control the roll attitude of the spacecraft.

The system consisted of two electromagnets and associated command and power circuitry. These magnets were located in the sail and aligned parallel to the roll axis. Each magnet was capable of generating a 2500 gauss cm^3 (+10%) magnetic dipole moment in the $+x$ direction with an applied voltage of 19 volts. Therefore, both coils could generate a total magnetic dipole moment of $+5000$ gauss cm^3 . This magnetic moment was capable of rolling the spacecraft by about 1.5 degrees/day.

Transmitter Spectrum. Previous measurements of the PSK 600A transmitter spectrum indicated that the spectrum was not in conformance with NASA Aerospace Data Systems Standards X560-63-2. In order to minimize this nonconformance, the technique of pre-modulation filtering was used. This technique limited the bandwidth of the information signal and consequently the bandwidth of the transmitted signal.

The pre-modulation filter was an active filter with a cut-off frequency of approximately 35 KHz. Functionally, the filter module consisted of a shaping circuit followed by a five pole active filter. The supply voltages for these circuits were derived from zener-diode supplies. An EMI filter was added to minimize the amount of conducted 136 MHz on the spacecraft power lines.



Receiver Sensitivity. In an effort to decrease the sensitivity of the OSO-6 command system to any given RF environment, the sensitivity of the receivers was reduced. The measured command system threshold using these modified receivers was about -103 dbm. This was about a 10 db increase in system threshold when compared to the -110 to -130 dbm measured on previous command systems.

Word Gate Generator. The word gate generator (WGG) was developed and installed in OSO-6 sail in order to minimize the number of slip ring circuits required. The WGG generated selected main frame and digital sub-frame word gates. That is, any 16 of the 32 main frame gates and any 12 of the possible 48 DSM gates could be duplicated in the WGG. The WGG characteristics were essentially identical to those of the wheel gate sources.

HCO/OSO-D Experiment Protection. In order to fly the flight spare HCO/OSO-4 instrument on OSO-6, an adapter was needed to redistribute the HCO interface wiring. This adapter was called the "K-Box". In addition to matching the OSO-4 and OSO-6 interfaces, the K-Box provided filtering originally contained in the HCO Filter Choke Module and contained the relays and wiring required to operate a overload protection circuit.

This circuit monitored the HCO high voltage power supply current. If a high voltage malfunction was indicated by a change in current, the OP circuit automatically actuated the HCO off command to disable the high voltage power supply.



Tape Recorder Operation. On OSO-5 both recorders were turned on by the same command. Separate commands were provided to turn the OSO-5 tape recorders off. On OSO-6, the recorders had all separate on and off commands.

Command Decoders. Previous OSO's used three decoders (two in the wheel and one in the sail). OSO-6 used four decoders (two each in the wheel and sail) to increase the command capability and to increase the reliability by providing redundant commands for critical functions.

Az. and El. PWM-Driver Oscillators. The OSO-6 azimuth and elevation drive oscillators (part of the pointing control servo) were separated in frequency by (nominally) 500 Hz to eliminate low-frequency "beating" and the resulting bus noise.



Section 2 OSO-6 FLIGHT PERFORMANCE

2.1 INTRODUCTION

During the first two years of orbital operation, OSO-6, making over 10,000 orbits around the earth, met every spacecraft mission requirement.

An impressive amount of high-quality data has been gathered from OSO-6's scientific payload. Analysis of this data continues at the facilities of the experimenters. While several of the experiments suffered instrument malfunctions, all experiments fulfilled a major part of their mission objectives.

The performance of the OSO-6 spacecraft is summarized in some detail in this section. Performance of experiments is not covered to any significant extent since analysis of such performance is the prerogative of the experimenter using his proprietary information.

2.2 PERFORMANCE IN THE LAUNCH PHASE

The OSO-6 was placed into a nearly circular orbit. Initial apogee and perigee were about 560 and 495 kilometers, respectively. The inclination of the orbit to the terrestrial equator is about 32.96 degrees. Performance of the launch vehicle was excellent, indicated by the closeness of the predicted and actual orbit parameters. The launch vehicle is described and its performance summarized in Para. 1.5 of this report.

Performance of OSO during the launch and early-orbit phases was likewise excellent in every respect. The launch-sequence timers performed their functions as programmed; solar acquisition, wheel despin, and transition to the orbit configuration occurred without difficulty.



Milestone vehicle and payload events are summarized in Fig. 1-22 and Table 1-3 of this report. Spacecraft spinup and separation were properly sequenced by the launch vehicle control circuits. Spin rate of the OSO just prior to spacecraft separation was about 98 rpm. At separation and spacecraft arm erection, spacecraft spin rate dropped to about 73 rpm due to the change in moment-of-inertia caused by arm deployment. Automatic despin to 0.618 rps took about 63 seconds, exhausting about 300 psi of spin-gas pressure.

The transition from the launch state to the orbit state was properly sequenced by the launch-sequence timers. No pitch correction was required, since the pitch angle at orbit injection was $+2.7^\circ$. Azimuth and elevation solar acquisition occurred normally, and pointing accuracy was within specified tolerance. Battery charging started at solar acquisition. The nutation damper dissipated nutations caused by vehicle separation and initial elevation acquisition.

2.3 POINTING CONTROL SYSTEM IN ORBIT

The observatory pointed instruments were directed to within 0.3 arc minutes of the center of the sun (when in the sun-centered point mode) during the entire life of the observatory.

Figure 2-1 was derived from a computer plot of every readout of sail analog channels 1 and 3 obtained during a typical tape-recorder playback. These channels report elevation and azimuth pointing position. This type of plot is called an orbit profile plot. The computer software for deriving such a plot is discussed in Section 4. As part of the post-launch operational analysis effort, such plots were made and studied periodically. They were generally made within a few days after the pass had occurred, from data supplied by the NASA/GSFC OSO Control Center.

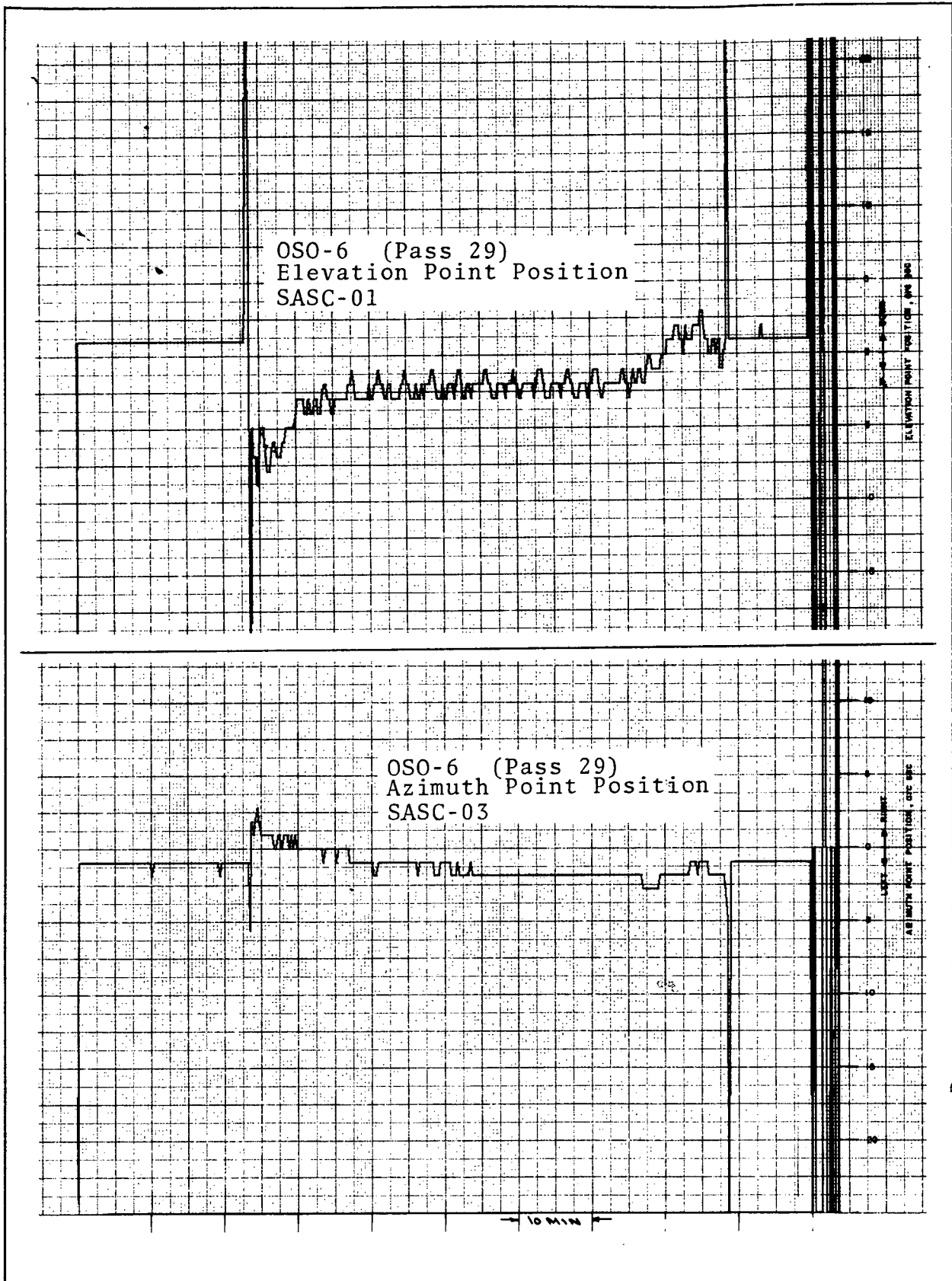


Fig. 2-1 OSO-6 Typical Orbit Profile--Sun-Centered Point



The discrete magnitudes of pointing error shown in the plots are a result of the analog-to-digital conversion resolution of the telemetry equipment. The interval between levels is equal to one telemetry bit. To reduce the effect of invalid samples on the curve, the plot program is designed to average transient samples with previous samples. This smooths the trace somewhat, producing the steps seen in the high-transient areas of the plots.

As can be seen, the "jitter" present in the pointing error was about ± 2 (peak) seconds of arc. The rms value is evidently much smaller, but it cannot be evaluated from the digital data.

Offset Modes. The servo operated well within the design specifications in the offset pointing modes throughout the two-year design life of the observatory. Large raster, small raster, and offset pointing modes were selected by ground command as scheduled by the NASA-GSFC OSO control personnel. Azimuth and elevation position of the pointed instruments in each of the offset modes are shown in Figs. 2-2 through 2-4. These are typical orbit-profile plots, showing the indicated analog channel machine-plotted as a function of time for one full playback of the OSO on-board tape recorders.

Fig. 2-2 shows single-channel plots of elevation and azimuth position in the large raster mode from the playback in Pass 2585. The shift in position which appears from one orbit day to the next is a result of the loss of raster synchronization with the analog subframe through the orbit night. The sampling point in the raster is randomly established at the beginning of each orbit day. The azimuth scan plot, because of synchronization of the raster with the telemetry frame, is a plot of a single point in the scan, and, therefore, appears as a constant position.

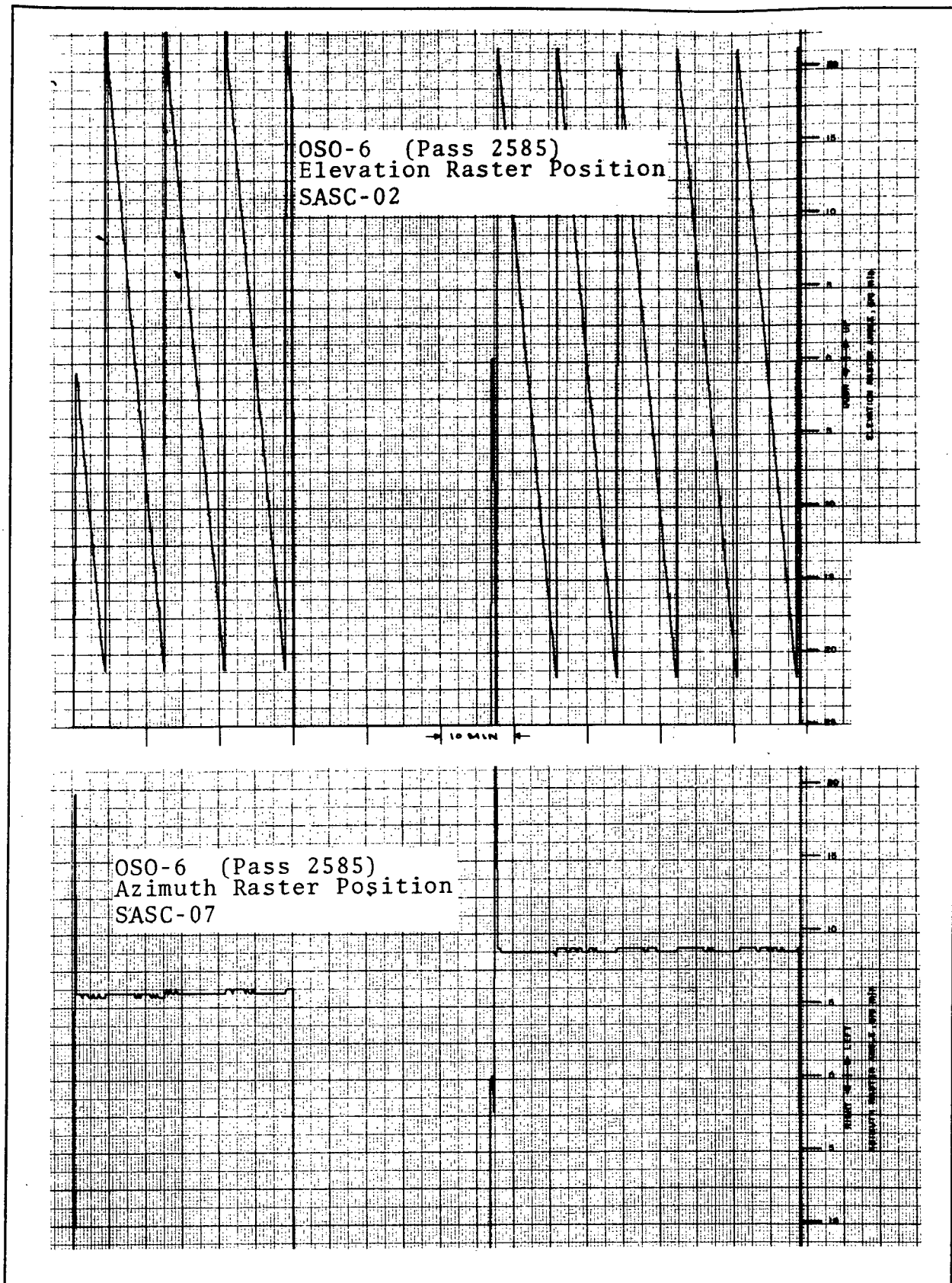


Fig. 2-2 OSO-6 Typical Orbit Profile--Large Raster

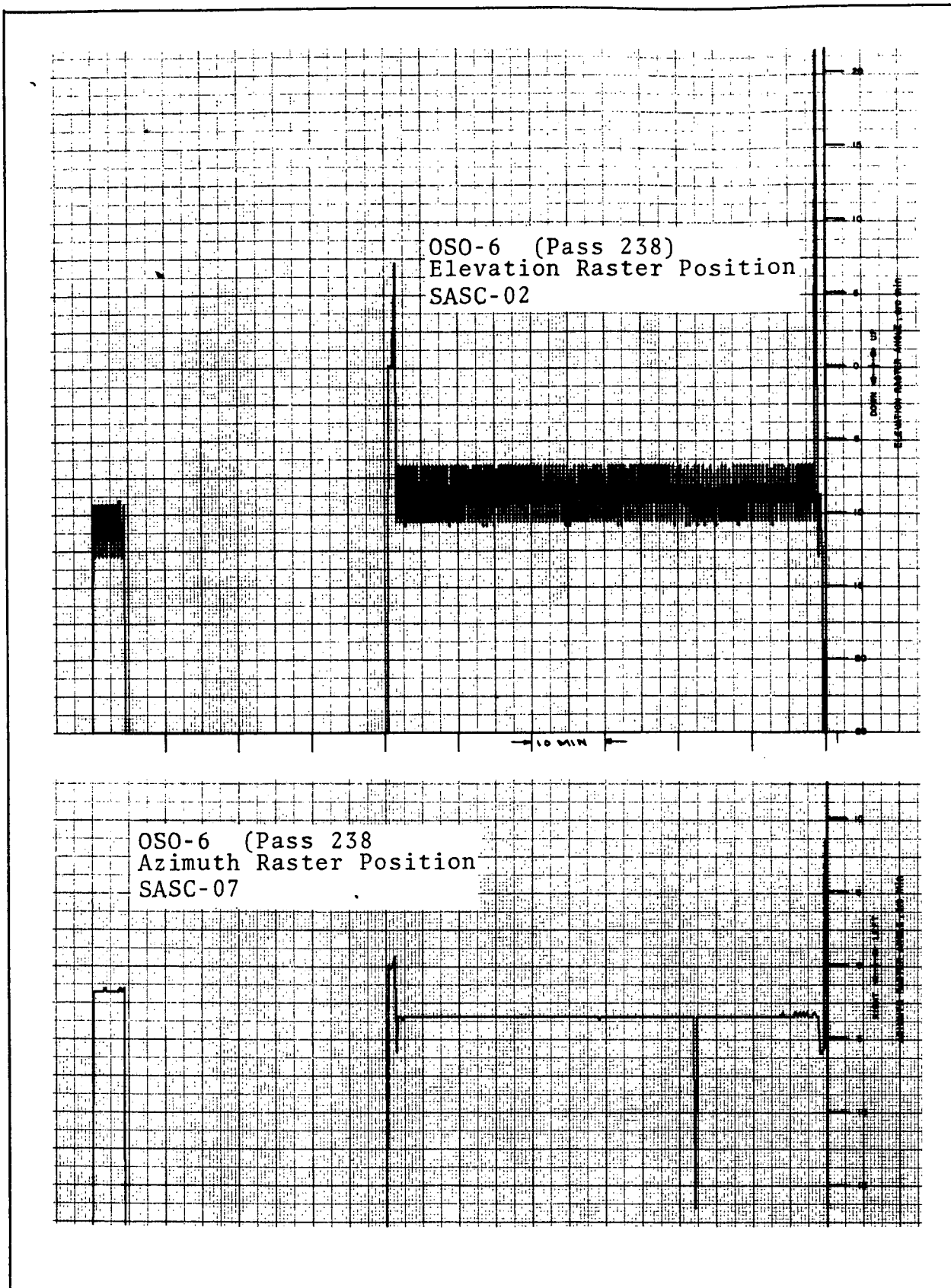


Fig. 2-3 OSO-6 Typical Orbit Profile--Small Raster

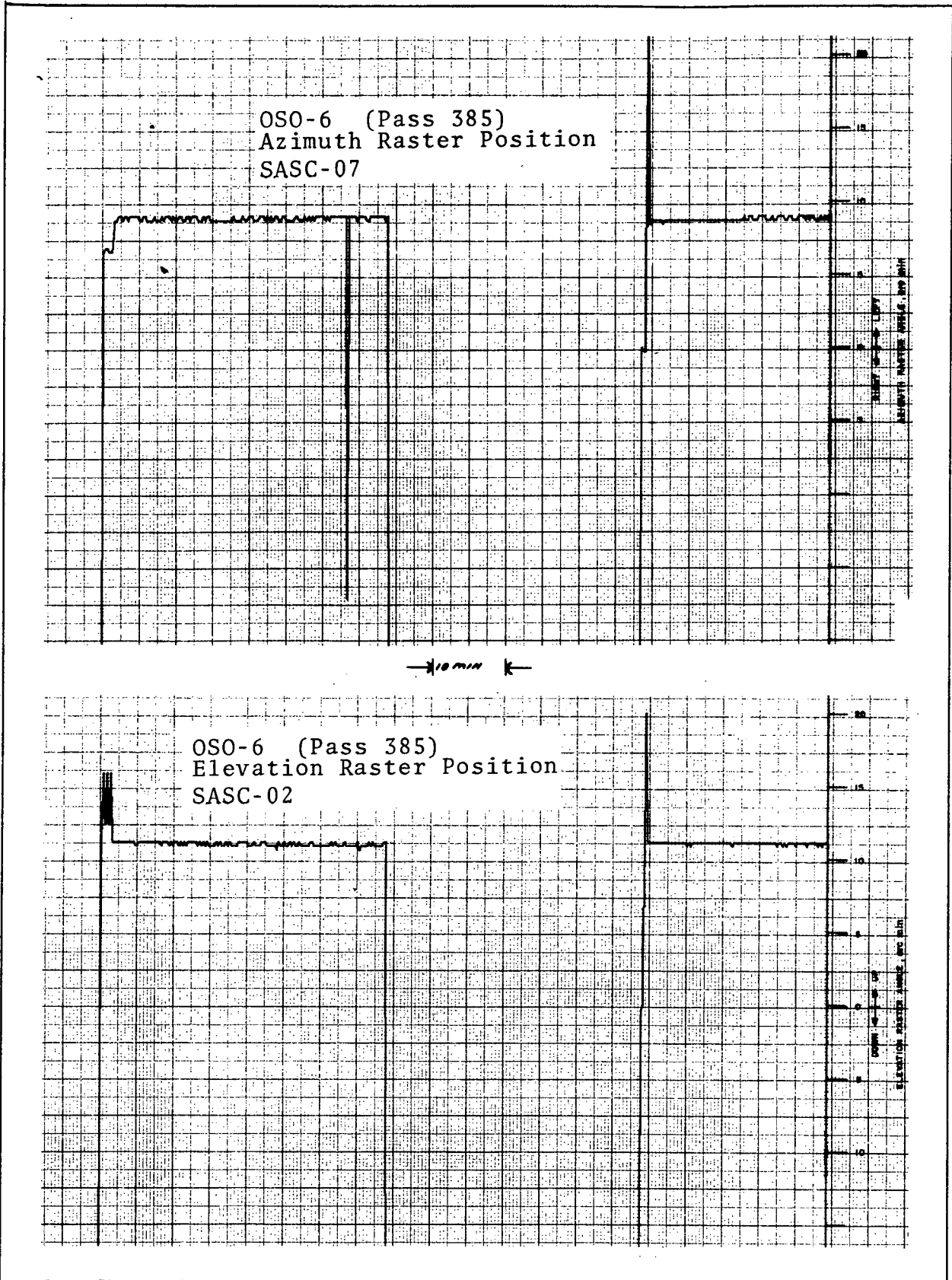


Fig. 2-4 OSO-6 Typical Orbit Profile--Offset Point



Figure 2-3 shows single-channel plots of elevation and azimuth position in the small raster mode from the playback in Pass 238. The shift in position noted through orbit night is the combined effect of telemetry frame resynchronization, and relocation of the small raster in the offset grid in behalf of the Harvard experimenter.

Figure 2-4 shows the elevation and azimuth position in the offset-point mode. The large transients in these plots are due to loss of pointing position at orbit dusk, the transient character of position during solar acquisition at orbit dawn, and telemetry anomalies associated with the splice in the continuous-loop tape of the on-board tape recorders.

Long Term Plots. Performance of the azimuth and elevation servos in the fine point mode is shown in Fig. 2-5. This is a manual plot of the position monitors and motor torque monitors covering one orbit-noon sample per day (when operating in the sun-centered point mode) for the first 100 days. These plots were continued over the two-year period and are summarized as follows:

(1) Elevation Fine Position (SASC-01)

This monitor indicated a gradual downward drift to about -10 arc seconds, with the greatest drift taking place in the first year.

(2) Elevation Raster Position (SASC-02)

This monitor seemed to show a slight upward drift of the instruments over the two-year period, but the drift was too slight to be conclusively identified by the analog monitor.

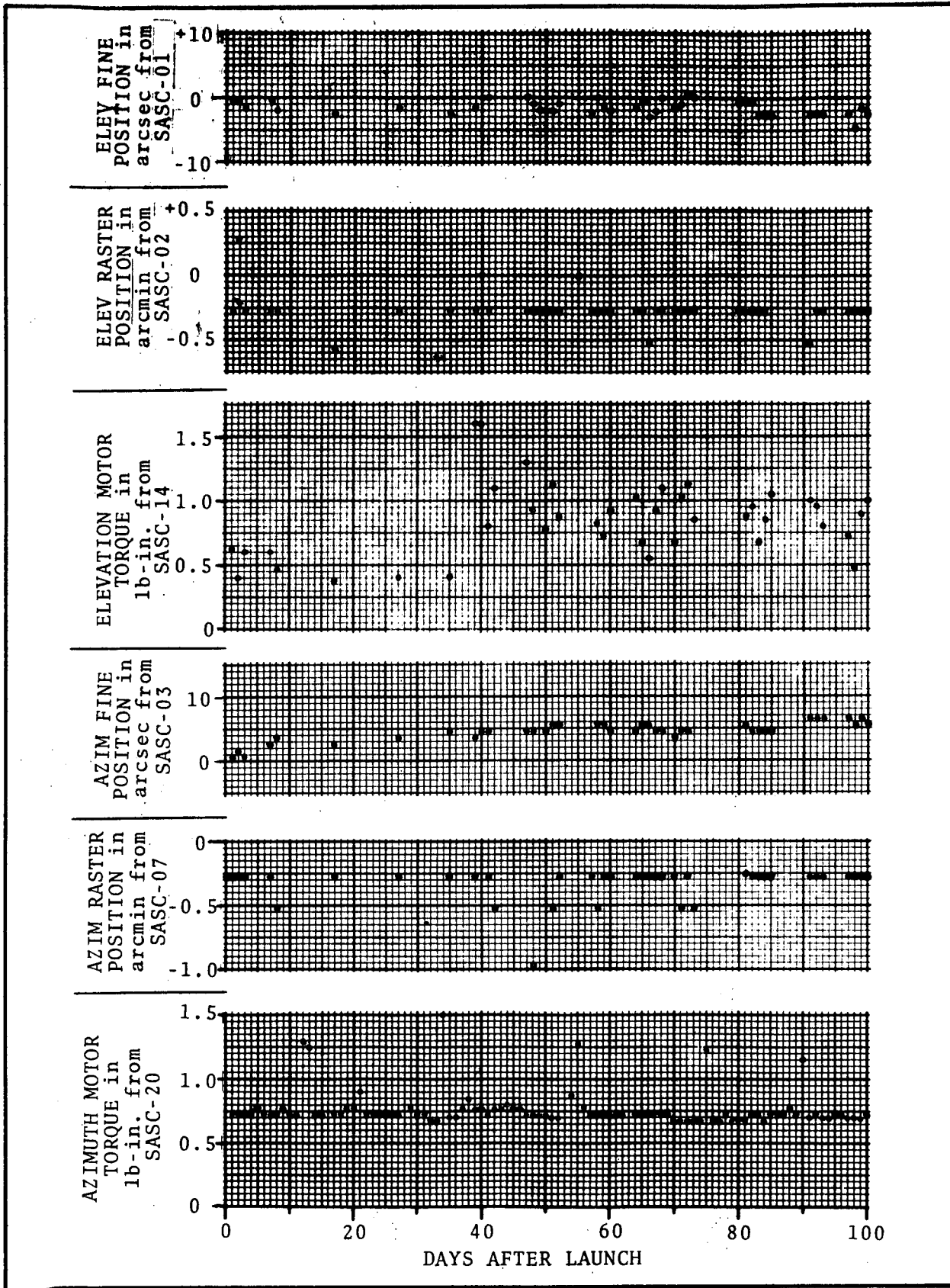


Fig. 2-5 Point Mode Performance -- First 100 Days



(3) Elevation Motor Torque (SASC-14)

No drift trend could be identified from the monitor. Apparently, elevation bearing performance did not degrade during the two-year life of the observatory. Samples of the readout seemed randomly distributed between 0.5 and 1.5 lb.-in., with an average torque about 0.8 lb.-in. Note the jump in torque at about Orbit 38 on Fig. 2-5. Comparison with Fig. 2-6 reveals that this jump is related to OSO pitch angle. Indeed, the torque produced by the flex cables from the sail to the PIA caused elevation motor current to increase with increasing pitch angle. While the increase in motor current has to be considered an undesirable effect, there was another effect which compensated for it to some extent. The torque applied by the flex prints held the PIA against one side of the servo dead zone, thereby decreasing elevation jitter. This is analogous to the azimuth bearing friction's favorable effect on jitter. Prior to these observations, we had considered installing a spring in the elevation gimbal for this purpose. Observing OSO-6 in flight made the desirability of such a spring obvious, and it was therefore incorporated in subsequent OSO designs. Because of this phenomenon, however, the OSO-6 pitch angle had to be controlled within smaller boundaries than planned, to limit the effect of flex-print torque on elevation motor current.

(4) Azimuth Fine Position (SASC-03)

After a leftward drift of about 3 arc seconds early in the flight, position settled at about



7 arc seconds left, and remained fairly constant thereafter.

(5) Azimuth Raster Position (SASC-07)

This monitor seemed to indicate a slight drift to the right over the two-year period. Owing to the limited resolution of the analog-encoded data, and the extremely small drift, the actual drift rate could not be evaluated.

(6) Azimuth Motor Torque (SASC-20)

The motor torque monitor gave no evidence at all of any degradation in performance of the azimuth bearings. The average value over the two-year period stayed at about 0.75 lb.-in.

2.4 ATTITUDE AND SPIN CONTROLS AND MONITORS

The attitude and spin controls and monitors were operated successfully as needed throughout the mission. Fig. 2-6 shows a plot of attitude, spin rate, and roll and pitch coil status during the first 560 days of the flight.

Spin Pneumatic. The pneumatic spin control exhausted about 300 psi of its nitrogen gas supply in the initial despin to 0.618 rps during the launch sequence. In Orbit 10, manual spin bursts were used to lower the spin rate to 0.521 rps. Thereafter, manual spin up or down bursts were used as needed to maintain the desired spin rates, including several changes made in order to observe the effect on the scientific experiment payload.

The use of the pneumatic spin control for spin rate was rarely needed except during times when the roll control coils were



FOLDOUT FRAME

FOLDOUT FRAME

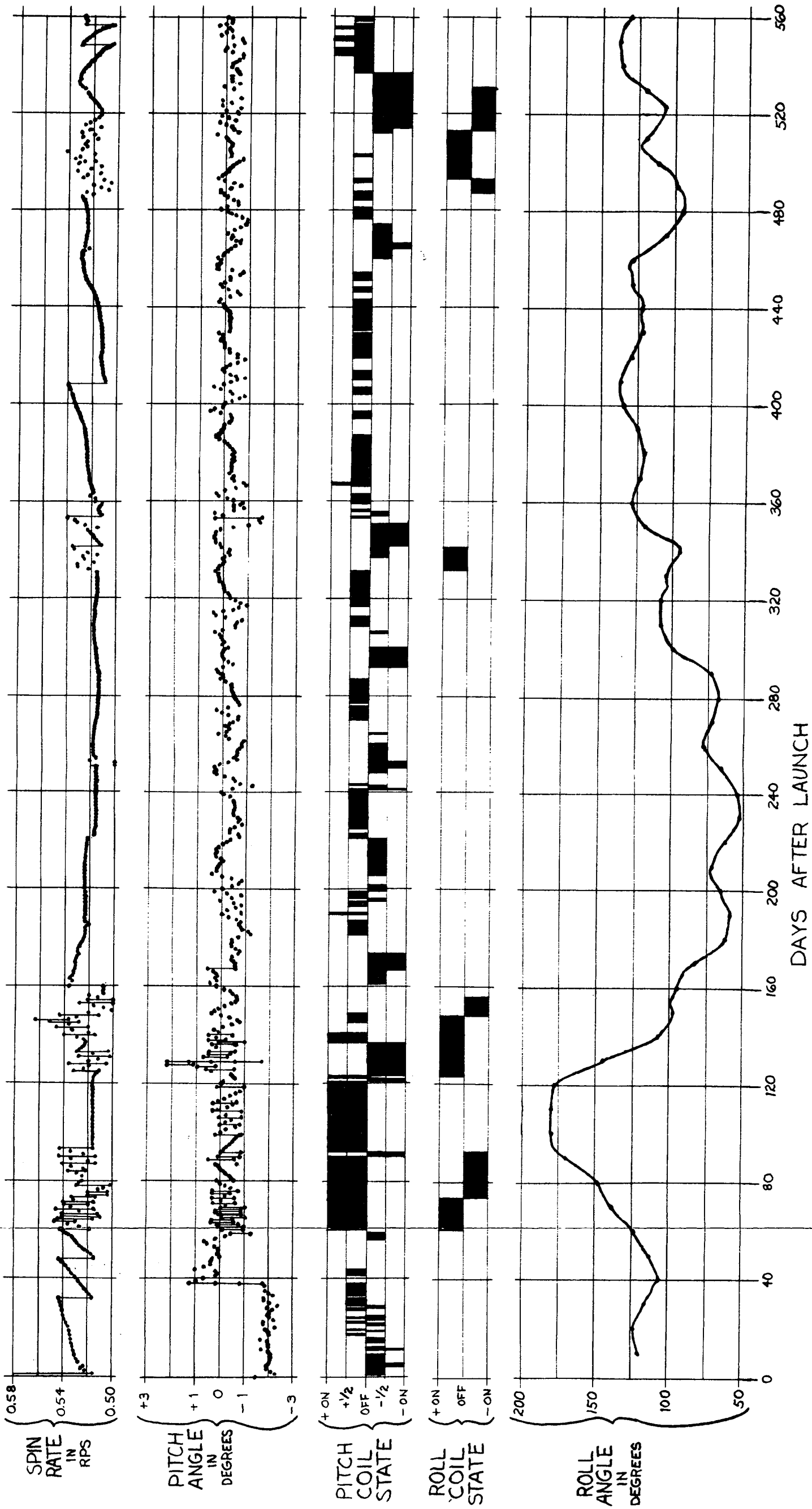


Fig. 2-6 OSO-6 Attitude History

2-12.1



energized. A glance at Fig. 2-6 shows a very strong roll coil/spin rate interaction. At the end of the 560-day period shown in Fig. 2-6, the pneumatic spin control system was still charged to about 1600 psi. Storage pressure at launch was about 2970 psi. During the flight each spin up or down burst exhausted about 20 psi from the system and incremented the spin rate by about 0.025 rps.

Pitch Pneumatic. The pitch attitude of OSO-6 was maintained well within the specified +4-degree limit throughout the life of the observatory. No pitch correction was required in the launch phase since the observatory was placed into orbit with a pitch attitude of +2.7 degrees. It was immediately noticed that the elevation torque motor current was high, however, and after analysis of preflight test data it was concluded that the flex prints were applying a torque to the pointed instruments. Reduction of the pitch angle to -2° during the first two orbits, using the manual pitch pneumatic control, cut torque motor current to its proper level.

Pitch angle history for the first 560 days of the mission is presented in Fig. 2-6. At the end of the 560-day period, pitch gas pressure had diminished from its prelaunch value of about 2950 psi to about 2080 psi. Use of the pitch magnetic bias coil greatly reduced pitch gas consumption.

Magnetic Bias Coils. The magnetic pitch control coil and roll control coils were used successfully throughout the orbit life of OSO-6. Proper switching of the pitch coil power greatly reduced the consumption of the pneumatic system's gas supply, as in earlier OSO flights. Historical data, covering the first 560 days of the flight, are presented in Fig. 2-6.



Use of the roll coils for roll attitude control was complicated somewhat by their effect on the spacecraft spin rate. The roll coils were used early in the flight to establish a 180-degree roll orientation. This orientation was then maintained for about a month, then roll angle was allowed to decrease, giving the rotating instruments an opportunity to scan the celestial sphere.

There were no problems associated with command control of the magnetic attitude control coils except for several instances of coil status being changed by spurious commands. These changes were corrected by subsequent commands, executed in a timely fashion.

Aspect Monitors. As shown by the attitude history in Fig. 2-6, the OSO-6 attitude monitor system operated successfully throughout the mission. Pitch orientation was read out from the pitch-angle sensor through the sail analog subcommutator. The SORE (Spin Orientation and Rate Electronics) system provided data from which spin rate, roll orientation, and instantaneous look direction of the rotating instruments were calculated. Operation of the various attitude controls were based on the information provided by the SORE system.

Wheel spin rate was also successfully calculated from data supplied by the spin rate monitor through the wheel analog subcommutator.

2.5 TELEMETRY SYSTEM IN ORBIT

The OSO-6 telemetry system operated properly throughout the orbit life of the observatory. The OSO-6 government-furnished tape recorders have continued to supply excellent playback data well beyond two years. Real time and playback data were of excellent quality and there was no loss of data caused by malfunction of either the DME or tape recorders.



Receiving ground stations reported no difficulty in receiving or locking-in the OSO-6 transmitted signal.

Proper sampling of all data points, and their timing in the telemetry frame and subframes, were maintained throughout the mission. Data were time-correlated with spacecraft aspect and instrument look direction by using information supplied by the SORE and the telemetry frame counter in the digital subframe. A typical orbit profile of frame count is shown in Fig. 2-7.

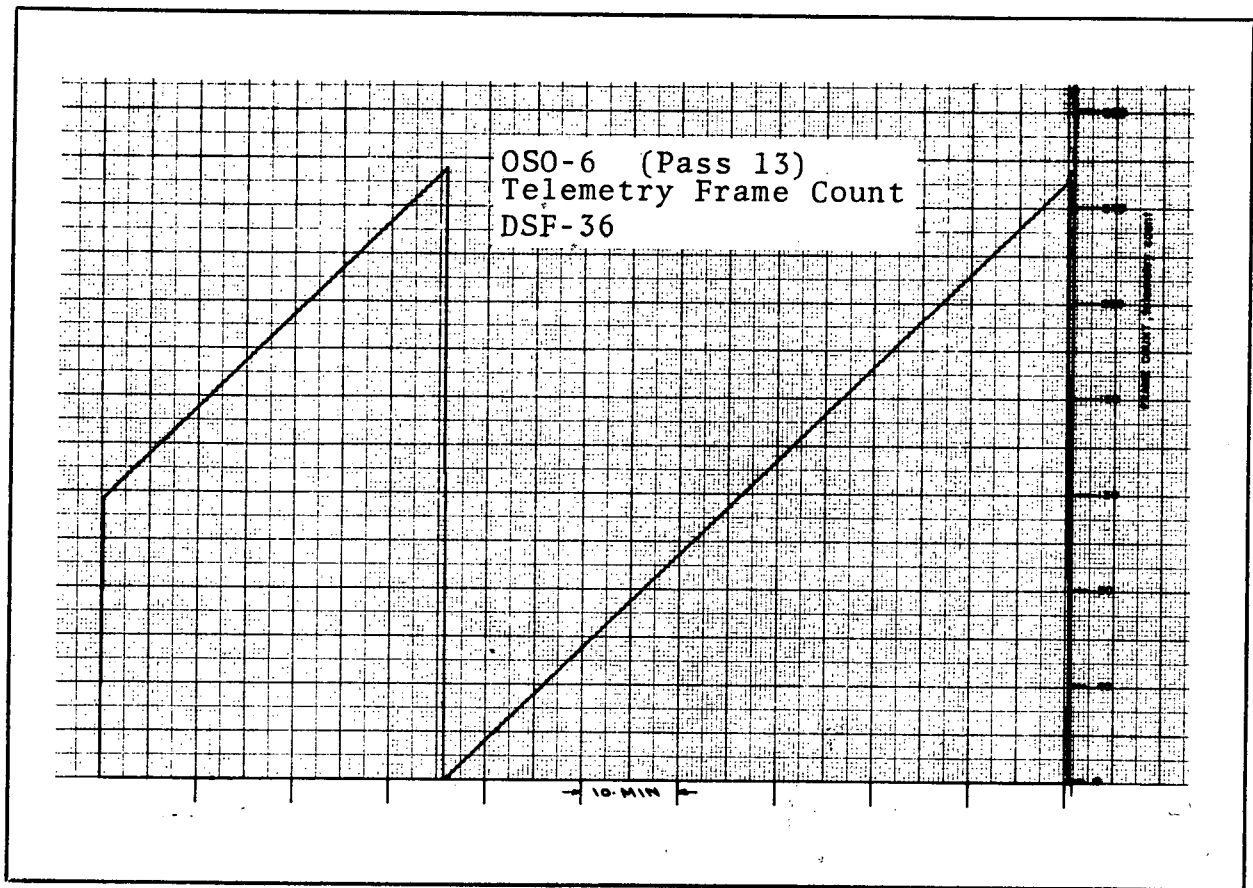


Fig. 2-7 OSO-6 Typical Orbit Profile--Frame Count



2.6 COMMAND SYSTEM IN ORBIT

The OSO-6 command system operated well throughout the first two years in orbit. Transmission of commands to the spacecraft resulted in proper execution of the planned functions.

There were numerous command anomalies reported on OSO-6 during the two year period as follows:

- During the first 6 months, 36 anomalies involving 78 command functions were reported.
- During the second 6 months, 25 anomalies involving 33 command functions were reported.
- During the third 6 months, 16 anomalies involving 20 command functions were reported.
- During the fourth 6 months, 136 anomalies involving 264 command functions were reported

All of the anomalies reported were of the type where a command function was executed which had not been sent by an OSO ground-control facility.

The command functions most often executed in the reported anomalies were:

- 46, Rutgers Manual Sequence (10100011) 69 times;
- 529, NRL Power Off (01101001) 82 times;
- 43, Rutgers Reverse Mode (10011001) 20 times;
- 465, Elevation Vernier Offset Bit (11011000) 20 times; and



- 535, HCO LV On (01111000) 17 times.

There are no apparent similarities in the binary codes for these commands which would indicate a specific design weakness in the decoder matrix.

The command anomaly data available indicate that the reported anomalies occurred during times of high radio frequency interference (RFI). Indeed, testing on OSO-type decoders had shown these decoders to be prone to generate spurious commands under conditions of high RFI. This observation has led to refinements of the command system on OSO's after OSO-6.

The geographical distribution of command anomalies during the two-year reporting period leads to some speculation about the source of the troublesome RFI. Early in the flight the anomalies seemed to occur over the Gulf of Mexico/Caribbean Sea area. Then they seemed most frequent near the eastern coast of China and Southeast Asia. There was then a brief period when many anomalies occurred near New Guinea, after which the China/Southeast Asia area became prominent again.

2.7 POWER SYSTEM IN ORBIT

After two years of in-orbit operation, the OSO-6 power system has shown little, if any, sign of degradation in performance.

Solar array current during the two-year period ranged from about 1.98 amperes to 2.10 amperes, in phase with the solar constant. Long-term trends, if any existed, were not apparent in the orbit-noon data. The temperatures reached by the solar-cell array varied in phase with the length of the orbit-day, as determined by the precession of the orbit.



Solar-cell array degradation generally results from radiation effects, micrometeoritic bombardment, increases in temperature caused by degradation of heat-dumping paths, fractures of solar cells, connecting strips or cover slips, and delamination of cover slips. Apparently no significant loss of output resulted from any of these factors, proving the value of design measures used to minimize array degradation.

The performance of the main storage battery did not change noticeably during OSO-6's first two years of orbit life. The voltage drop at day-to-night transition and during acquisition remained essentially constant, indicating that battery internal resistance did not increase appreciably. The fall in voltage during orbit night likewise remained fairly constant, indicating that no important changes took place in battery capacity.

In the first few days after launch, the main battery showed a tendency to overcharge. The experiment instruments were not energized on a full-time basis at the time. Subsequent application of experiment loads and timely use of the dummy load prevented overcharging throughout the remainder of the two-year period.

2.8 STRUCTURES AND TEMPERATURE IN ORBIT

Throughout the orbit life of OSO-6, the spacecraft structure performed well in meeting the mission requirements. Pointed experiment settling during the launch and subsequent warpage in flight was well within specification. Performance of the azimuth and elevation bearings and the arm-support mechanisms was excellent.

Observatory temperatures were very close to the preflight predictions so no in-depth study was made. Observatory hub temperature varied cyclically between the predicted limits in phase with the length of the orbit day. All temperatures, as indicated by the on-board monitors, varied similarly within acceptable limits.



Both the annual period of the solar constant and the 50-day period of OSO orbit precession were evident in the long-term orbit-noon temperature plots. The solar-cell panel over the pointed instruments showed the greatest temperature excursion, ranging between -24 and +62 degrees centigrade in a single orbit. Orbit noon data showed a variation of about 5 degrees caused by the solar constant, and up to 11 degrees caused by orbit precession. Compensation for these cyclic variations in temperature showed that flight data revealed no significant degradation in OSO-6's passive thermal control.

The spacecraft hub temperature varied between about 8 and 18 degrees centigrade, varying with the above-mentioned cyclic phenomena. Variation of hub temperature in any single orbit was less than about three degrees, well within the five-degree specified limit.

2.9 EXPERIMENT INTERFACES IN ORBIT

Throughout the OSO-6 orbital lifetime there were no verifiable failures in the spacecraft-experiment interfaces. The instruments occasionally received spurious commands, as did the spacecraft. The distribution of spurious commands between the instruments and the spacecraft functions leads to the conclusion that the OSO-6 command decoders, as earlier OSO decoders, were susceptible to RFI, rather than that there were any problems with instrument-spacecraft interfaces.

The OSO-6 instrument initial-turnon history is presented in Table 2-1.



Table 2-1
OSO-6 EXPERIMENT INITIAL TURN-ON HISTORY

<u>Date</u>	<u>Orbit</u>	<u>Time (EDT)</u>	<u>Experiment</u>	<u>Command</u>
9 Aug. 69	001	09:39:00	Rutgers	Squib Arm
"	"	09:39:01	Rutgers	Squib Fire
"	"	10:09:00	UCL	Squib Arm
"	"	10:09:00	UCL	Squib Fire
10 Aug. 69	010	00:17:30	HCO	LV On
"	"	00:18:38	HCO	LV Off
"	014	06:31:00	UCL	LV On
"	"	06:31:15	UCL	LV Off
"	"	06:32:00	Rutgers	LV On
"	"	06:32:05	Rutgers	LV Off
"	015	08:12:35	LASL	LV On
"	"	08:12:43	LASL	LV Off
12 Aug. 69	044	06:01:30	Bologna	LV On
"	"	06:01:35	Bologna	LV Off
"	"	06:01:45	NRL	LV On
"	"	06:03:45	NRL	LV Off
"	054	21:53:30	NRL	PM HV On
"	"	21:53:35	NRL	PM HV Off
"	"	21:53:50	NRL	Prop. Ctr. HV On
"	"	21:54:10	NRL	Bragg HV On
"	"	21:54:15	NRL	Bragg HV Off
"	"	21:54:30	NRL	Burst HV On
"	"	21:54:50	NRL	Rstr. HV On
"	"	21:54:55	NRL	Burst & Rstr HV Off
"	"	21:55:10	NRL	PM HV Off
"	"	21:56:48	HCO	HV On
"	"	21:57:08	HCO	HV Off
13 Aug. 69	056	01:12:45	UCL	HV #1 On
"	"	01:13:16	UCL	Pwr Off



Table 2-1 (continuation)

<u>Date</u>	<u>Orbit</u>	<u>Time (EDT)</u>	<u>Experiment</u>	<u>Command</u>
13 Aug. 69	056	01:13:40	UCL	HV #2 On
"	"	01:14:05	UCL	Pwr Off
"	"	01:14:30	UCL	HV #3 On
"	"	01:14:55	UCL	Pwr Off
"	057	01:55:46	Rutgers	HV On (Cont.)
"	070	23:17:00	UNM	Pwr On (Cont.)
"	"	23:19:30	HCO	HV On (Cont.)
"	"	23:20:30	NRL	All HV On
"	071	23:54:00	NRL	All HV Off
14 Aug. 69	072	02:39:00	UCL	All HV On (Cont.)
"	"	02:40:00	NRL	All HV On (Cont.)
"	073	03:51:34	LASL	LV On
"	"	03:51:39	LASL	HV #1 On
"	"	03:51:44	LASL	HV #1 Off
"	"	03:52:14	LASL	HV #2 On
"	"	03:52:19	LASL	HV #2 Off
"	074	05:30:11	LASL	All HV On (Cont.)
"	"	05:31:21	Bologna	HV On
"	"	05:36:51	Bologna	HV Off
"	075	06:54:20	Bologna	All Pwr On (Cont.)

LEGEND: Cont. = Experiment Turned-On for Continuous Operation
LV = Low Voltage
HV = High Voltage
PM = Photomultiplier
Prop. Ctr. = Proportional Counter
Rstr. = Raster



2.10 IN-ORBIT ONE-YEAR PERFORMANCE SUMMARY

Spacecraft performance during OSO-6's first year in orbit is summarized in Table 2-2, along with specification items which apply to in-orbit performance parameters. As can be seen by the Table, OSO-6 met all of its mission requirements.



Table 2-2
 SUMMARY OF SPACECRAFT SYSTEMS PERFORMANCE
 VS. MODEL SPECIFICATION FOR FIRST YEAR OF OPERATION

Spacecraft System	Model Specification	Actual Performance
<p>In-Orbit Lifetime</p> <p>Pointing Control</p>	<p>6 months minimum in a 300 +50 nmi orbit inclined at 33 +3 deg. to the equator</p> <p>The pointed instruments shall be oriented in the fine control mode within 90 seconds after entering sunlight; while in the sun-centered or offset point modes, the azimuth and elevation pointing error shall be less than +1 min.; jitter shall be <5 sec. in el. and <3 sec. in az.; while in the raster modes the raster size shall be 46 +2 min. for large and 7 x 7.5 +0.5 min. for small.</p>	<p>All systems were operating satisfactorily at the end of one year.</p> <p><u>Azimuth Alignment.</u> The alignment error between the right-hand (reference) instrument and the left-hand instrument increased from 0.03 arc minutes left at launch to about 0.11 arc minutes left by August, 1970.</p> <p><u>Elevation Alignment.</u> The elevation alignment error between the RH and LH instruments increased from about 0.03 arc minutes down at launch to about 18 arc minutes down by June, 1970.</p>
<p>Telemetry</p>	<p>Experiment and spacecraft data shall be continuously time multiplexed at a rate of 100 8-bit words per second; this data shall be continuously transmitted in realtime except during the playback period; during realtime transmission the data shall be continuously stored by tape recorders; the tape recorders shall have a capacity of 98 to 101 minutes; the data format shall remain as assigned; the realtime data rate</p>	<p><u>Raster Size.</u> The large raster size at "mean" sun intensity was 45.2 arc min. in az. and 44.8 arc min. in el.; the small raster varied between 6.9 +0.2 arc min. for el. and 6.8 +0.2 arc min. for az.</p> <p><u>Azimuth Motor Torque.</u> The azimuth motor torque was between 0.60 and 0.80 in.-lb. throughout the first year of orbit life.</p> <p><u>Acquisition Time.</u> Solar acquisition consistently occurred in about 60 seconds after day-power turn-on throughout the first year of orbit life.</p> <p><u>Target Eye Degradation.</u> The target eye readout degraded at 0.12 percent per month rate. At the end of the first year, the target eye had degraded about 1.44 percent.</p> <p><u>Tape Recorders.</u> Both recorders operated properly during first year of orbit life; the pbk. rate was 14.4 k bps +10 bps and the pbk. time was nominal.</p> <p><u>Transmitters.</u> Both transmitters operated successfully throughout the first year of orbit life. The signal strength (with diversity combining) was nominal and varied between -85 and -116 dbm.</p> <p><u>Data Handling Subsystem.</u> Both data handling subsystems operated successfully throughout the first year of orbit life.</p>



Table 2-2 (continuation)

Spacecraft System	Model Specification	Actual Performance
Command	<p>shall be 800 +0.4 bps; the playback rate shall be 14400 +288 bps; the playback period shall be 5.64 +0.083 minutes; the xmtr. carrier frequency shall remain within 5 kHz of assigned; the carrier shall be PSK modulated with a deviation of 57 +5 deg. for both realtime and playback transmission.</p> <p>Any one command sent to the spacecraft results in the execution of a planned function.</p>	<p><u>Receivers.</u> Both of the command receivers operated successfully throughout the first year of orbit life.</p> <p><u>Decoders.</u> All four command decoders operated successfully throughout the first year of orbit life. The only problems noted were a few spurious commands that were accepted. The specific causes were not determined.</p>
Power	<p>19 +3 vdc shall be provided to the spacecraft during both day and night; the output capacity shall be 1.87 amp-hr./orbit minimum; the peak load capacity shall be 8 amps for 5 seconds duration; undervoltage protection shall be provided at 16.2 +0.2 vdc with power being automatically reapplied at 19 +0.2 vdc.</p>	<p><u>Main Battery.</u> The spacecraft main battery operated successfully throughout the first year of orbit life. The battery noontime voltage varied between 18.2 and 20.78 for the "hottest" and "coldest" orbits, respectively. The "dummy load" was used to keep the battery voltage typically between 18 and 20 volts during each orbit.</p> <p><u>Solar Array.</u> The solar array power output remained above the specified value and no degradation was noticed.</p>
Pitch and Roll Control	<p>Automatic pitch control to within +4 deg.; pitch gas pressure of 3000 (+100, -200) psi at launch. No roll requirement.</p>	<p><u>Undervoltage Protection.</u> An undervoltage condition did not occur during the first year of orbit operation and, therefore, this feature was not checked.</p> <p><u>Pneumatic Pitch Control.</u> The pneumatic pitch control system operated successfully throughout the first year of orbit life. A total of 48 manual pneumatic pitch corrections were performed in the first year with an average gas consumption of about 14 psi/degree of pitch motion. The usefulness of the magnetic coils was apparent in that only 600 of the original 2800 psi of pitch gas was consumed in the</p>



Table 2-2 (continuation)

Spacecraft System	Model Specification	Actual Performance
Spin Control	Automatic spin rate control to within 0.44 to 0.68 rps; the spin rate change per correction shall be 0.028 \pm 0.01 rps; switch to manual thresholds shall be 0.39 \pm 0.012 and 0.7 \pm 0.015 rps.	<p>first year. There were no automatic pitch corrections made during the first year and therefore data is not available for this mode of operation.</p> <p>Pitch and Roll Coils. The pitch and roll coils were operated successfully throughout the orbit life and accounted for the greatly reduced consumption rate of pitch gas. Also, the roll coils were used several times to change the roll attitude.</p>
Launch Sequence	The spacecraft shall be placed in the normal orbit mode of operation within 1400 seconds after third-stage spinup.	<p>The pneumatic spin control system operated successfully throughout the first year of orbit life. About 300 of the original 2800 psi of spin gas was used to initially despin the wheel from the third-stage spin rate of 1.63 rps (97.9 rpm) to 0.613 rps. During the first year, six automatic spin-up, one manual spin-up, and 21 manual spin-down maneuvers occurred. The average amount of spin gas used per burst was about 14 psi. The spin gas supply at the end of one year was about 2050 psi.</p>
Aspect Determination	The roll angle shall be determined within \pm 3 deg.	<p>The launch sequence system operated successfully with all launch sequence functions occurring at or near the correct time.</p> <p>The aspect system met the following mission objectives:</p> <ol style="list-style-type: none"> (1) Provided the information necessary for determining the observatory roll attitude to 1 deg. accuracy. (2) Provided information for deriving the wheel spin rate. (3) Provided information for deriving the wheel azimuth position as a function of time. <p>For the first year of in-orbit operation, the OSO-6 spin axis was maintained between 60 and 180 degrees (referenced to ecliptic north).</p>



Table 2-2 (continuation)

Spacecraft System	Model Specification	Actual Performance
Thermal Control	The internal temperature of the wheel compartments shall not deviate more than 5°C per orbit and the mean temperature shall be 15 ±5°C.	The thermal control schemes maintained the wheel in-orbit temperatures very close to those desired.
Mass Balance	As required to meet other design requirements.	About 0.2 degrees of wobble was detected; the cause has not been determined and it did not adversely affect the operation of other spacecraft systems.
Magnetic Balance	As required to meet other design requirements.	The prelaunch magnetic balance adjustments made on OSO-6 produced very nearly the desired effects.



Section 3 OSO-6 DEVELOPMENT AND SUPPORT HISTORY

3.1 INTRODUCTION

The technical effort and program planning behind the OSO-G Orbiting Solar Observatory (OSO-6) are presented in this section. The various aspects of the project are discussed, together with details of their implementation. These include the planning, test programs, development, support activities, and post-launch follow-up efforts.

Fabrication, assembly, integration, and testing of OSO-6 was undertaken by Ball Brothers Research Corporation (BBRC) under Contract NAS5-9300 issued by NASA/GSFC. A prototype/qualification model was not included in the project.

3.2 MANAGEMENT

The OSO-6 project was conducted at the BBRC Boulder facilities using essentially the same organization structure, policies, and procedures as other OSO projects. Technical direction was assigned to the existing OSO project staff. Experienced members of the OSO-5 launch team and key members of other BBRC organizations assisted the Program Manager in completing the OSO-6 project. Work was accomplished in compliance with the applicable portions of NASA Quality Assurance Publication NPC-200-2, and NASA "Reliability" Publication NPC-250-1. The spacecraft's progress was monitored by the project staff with the aid of PERT Status and Cost Control Reports.

Established BBRC policies and procedures regarding work authorization, security of classified data, receiving, shipping, control of nonconforming supplies, project stores control, property control, measurement control, engineering record and release, etc., were used in the OSO-6 program.



3.3 SCHEDULE

Milestone events are listed in Table 1-2 of this report. More detailed breakdown of the OSO-G development and support history is presented in the paragraphs which follow.

3.4 DESIGN REVIEW AND HARDWARE SELECTION

Before hardware fabrication began on the OSO-6 project, a critical review of designs as reflected in documents and drawings from earlier OSO's was conducted. The purpose of this review was to determine the adequacy of this documentation to meet the intent of NASA Document NPC-200-2, Quality Program Provisions for Space System Contractors, and to ensure that the designs were compatible with specific mission requirements.

The major considerations and purposes in the design review before component fabrication and procurement were:

- (1) To develop the basic design definition and documentation for each component, subassembly, and assembly
- (2) To ensure that current design definitions incorporated necessary changes identified in the documentation of previous OSO projects, including failure reports, liaison engineering actions, and engineering orders
- (3) To ensure that all component, subsystem, and system requirements were covered and that the electrical, thermal, and mechanical interfaces were compatible



- (4) To estimate the relative criticality of equipment package input-output circuitry and its vulnerability to failure
- (5) To define possible failure modes and assure that assemblies were interfaced on a noninterference basis
- (6) To provide drawings in a form suitable for OSO-G spacecraft systems analysis work
- (7) To consider weight, balance, materials, thermal, vibration, and stress properties
- (8) To verify that hardware adjustment methods, test methods, installation methods, etc. did not have adverse effects on observatory operational integrity
- (9) To verify that design documentation was of sufficient quality to allow proper fabrication, testing, and quality control of each article, and
- (10) To compile a record of all information developed during the review and the complete revised documentation for design approval and release.

The design review so described was a joint effort of personnel from the Systems Engineering, Quality Assurance and Reliability, Materials, Production, Design, and Integration and Test departments. After the design review of a particular subsystem was completed, it was processed through drawing release so that production work could proceed during review of other subsystems.



Table 3-1 presents a summary identification of the hardware flown on OSO-6 as a result of the design review and subsequent spacecraft development. Items are identified by drawing numbers, serial numbers, specifications, and procedures as appropriate. Functional changes from prior OSO configurations are discussed in later sections covering descriptions of spacecraft systems.

3.5 COMPONENT FABRICATION AND TEST

Component procurement, fabrication, and test was carried out in accordance with a prescribed reliability program (Reliability Program Plan for the OSO Spacecraft). Long-lead-time items were started as early as possible. Procurement of OSO-6 hardware started immediately after design release.

A parts program, providing the best available types and highest quality parts, governed procurement of components. Reliability considerations were based on previous part history, NASA and major space program preferred-parts selection, and audits of currently available types and qualification data. Specifications were tightened to screen out all but the best units that can be made with a given process.

Specification-control drawings (SCD) identified part requirements, source, type and manufacturer, acceptance or rejection criteria, and tied specific parts into assembly drawings and test specifications.

Tests included parameter measurement at room temperature, thermal cycling, power aging and retest, x-ray, high-temperature storage, and other tests as appropriate. Special fixtures constructed for use in earlier OSO programs were used to expedite component qualification and acceptance.



Table 3-1
OSO-6 SPACECRAFT SUBASSEMBLY IDENTIFICATION

Assembly/Subassembly	Serial No.	Drawing No.	Documentation/Notes
<u>Wheel Structure</u>	2	19291-501	MS26493, TS26494
Tube Assy.	2	15481-1	
Arm Installation	45359-1, -4, -7	15495-1	
Rib Assy.	45261	19215-1	
Deck Assy.	37358	19522-1,-501, 503,505	
Purge System	45275	19555-1	
Az Bearing, Lower	122	20324-1	TS18788, TP18789, TN66-82
Az Bearing, Upper	136	20323-1	TS18788, TP18789, TN66-82
Latch Assy, Squib	276, 277, 279	15551-1	(Arm Latches)
<u>Sail Structure</u>	1889A	19302-507	
Latch Assy, Squib	268 (Elev)	15551-1	
Latch Assy, Squib	175 (Nut.)	15559-1	
Elevation Frame	41509	18266-1	
Elevation Bearing	117, 120	20325-1	TS18788, TP18789, TN67-174
Sail Frame Assy.	37329, 37327	19303-1, -502	
Panel Cntr. Front	37324	19307-1	
Panel Cntr. Back	3732	19309-1	
Az Frame Assy.	45016	19534-1	
Nutation Damper	2	19558-501	TS15610, AP15646, QP15614, TN68-130
<u>Pneumatic System</u>	12	19535-501	TS15904, TS19582, TP16704, AP17018, TN68-157
Tubing Assy.		19535-501	TS19582, AP16920, QP15647, TN68-157
Cap Quick Disconn.	28509, 28298	21992-1	TS21999, TP22200, TN67-57
Spin Gas Install.	1920A	19538-501	
Spin Gas Bottle	22,27,29	17518-1	TS15606, TS15904, TN67-171



Table 3-1 (continuation)

Assembly/Subassembly	Serial No.	Drawing No.	Documentation/Notes
Press. Transducer	19339,19340	8380-1	TS15604, TS15904, TP16712, TN67-140, TN68-101
Press. Regulator	108, 109	19549-1	TS15603, TS15904, AP16729, TN67-139, TN68-160
Solenoid Valve	114,115, 116,117	19548-1	TS15602, TS15904, AP16728, TN67-141, TN68-102, TN69-109
Check Valve	105, 106	21884-1	TS15601, QP15642, AP16727, TN67-120, TN68-90
Pitch Gas Install. Pitch Gas Bottle	1959A 13	19539-501 17517-1	TS15605, TS15904, TP20354, TN65-268, TN67-170
<u>Electrical Distr.</u>			
<u>Wheel</u> Temperature Probe	22982, 4507, 105, 22972, 22981, 7661, 22973	21964-1 7737-503	MS18804, TS18805, TP22888, TN69-105
Slip Ring Install	11	15491-1 16093-1	TS16248, TP16249, TN67-144, TN65-250
Terminal Boards	47271, 47272	20835-1	
	1	21993-1	
	1	21965-1	TS21987, TN68-139
	1	21966-1	TS21988, TN68-138
	1	21967-1	TS21989, TN68-137
	1	21968-1	TS21990, TN68-136
	2	21969-1	TS21991, TN68-135
	1	21970-1	
	1	21068-1	
	1	21068-501	
	1	21068-503	
<u>Sail</u> Flex Cable Assy.	12 200	21963-1 30128-1, -501, -503, -505, -507	TS24242 TS24241, TN69-93, TN69-114, TR69-51
Sail Junction Box	3	21790-1	TS24243, TR68-69, TN68-163, TN69-113
Squib Term. Bd. Temperature Probe	2G 22977,4708, 4709,4710, 7670,129	20933-1 7737-503	MS18804, TS18805, TP22888, TN69-105



Table 3-1 (continuation)

Assembly/Subassembly	Serial No.	Drawing No.	Documentation/Notes
RF Choke Module	NRL-2	22684-1	TS24245, TN68-131, TN69-104, TR68-73
Filter Module-HCO	HCO-2	30461-1	TS31225, TN69-69, TR68-68
Overload Protection	2	30750-1	TS31351, TN69-83, TR69-56
<u>Electronic Cont. - Wheel</u>	12	19578-505	
Spin Control Assy.	1	22002-1	MS22194, TS22195, TP22196, TN68-156
Temperature Probe	102,117, 126	7685-503	MS18804, TS18805, TP22888, TN69-106, TN69-105
Spin Sensor Assy.	15	16082-501	MS18818, TS18819, TP18820, TN67-132
Pitch Coil Assy.	41695	15784-1	TS15697, QP15698, AP15699, TN67-62
<u>Electronic Cont. - Sail</u>	6357A	23645-1	
Pitch Control Sensor	15	7865-501	MS18766, TS18821, TP18822, TN68-89
Power Amp Assy.	3	21554-1	MS21556, TS21557, TP21558, TN68-140, TR68-34
15V Regulator		19632-1, -501, -503, 21600-1	MS19469, TS19470, TP19471, TP15476
Temperature Probe	29274, 29277, 8	7685-503, -507	MS18804, TS18805, TP22888, TN69-106
Servo Amp Assy.	3	21581-1	MS21583, TS21584, TP21585, TR68-35, TN68-133
Point Readout Sensor	12	15535-1	MS16689, TS18810, TP18811, TN69-39
Fine Control Sensor	14	15536-503	MS16686, TS18810, TP18811, TN69-41, TN68-155
Coarse Sensor	15	16215-1, -2, -501, -502	MS18815, TS18816, TP18817, TN68-116
Az Torque Motor	64-572-22	19172-1	TS18791, TP18792, TN68-48
E1 Torque Motor	64-573-9	19173-1	TS18791, TP18792, TN68-70
Pitch Readout Sensor	14	8232-501	MS18589, TS18807, TP18808, TN67-138, TN68-93
Scan Readout Sensor	16	19053-505	MS18812, TS18810, TP18811, TN68-150, TN69-38



Table 3-1 (continuation)

Assembly/Subassembly	Serial No.	Drawing No.	Documentation/Notes
Roll Coil Assy.	3A, 2B	30823-1,-2	TS31379, TP31561, TN69-94
<u>Launch Sequence System</u>	1885	19563-503	
Launch Seq. Timer	1190,1191	18851-5	TS16387, TP16388, TN67-152, TN67-153
Press. Cartridge	168, 175 131, 133 164,165, 166,167, 176,178	21974-501 21974-1 21112-1	TS21154, TP22403, TN67-176
Sail Squib Batt.	13, 14	19592-1	DS15864, TS15862, TP15863, TS15860, TP15861, TN69-86
Wheel Squib Batt.	7, 8	19590-501	DS15864, TS15862, TP15863, TS15860, TP15861, TN69-88
Nut. Damper Mon. Sw.	2	28334-1	TS28542, TN69-110
Separation Sw.	2	30884-1	TS30883, TN69-95, TR69-45
<u>Data Handling System</u>	1933A	17416-501	
PCM J-Box	1	22019-1	MS22027, TS22026, TP22028, TN68-147
Frame Counter	1	21942-1	DS17317, TS21956, TP21957, TN68-143
FC Pwr. Supply	601003	16123-3	DS20227, TS20228, TP20290, TN67-130
Tape Recorder	805,808	30418-1	TS30415, TS30416, TP30417, TN68-104
DME-PCM	8; 10	19571-1	DS15342, TS15343, TP17290, TN68-123, TN68-124
ASC-PCM	8, 13	19572-1	DS15342, TS15343, TP17290, TN67-110, TN68-125
ASSC	3	17208-501	DS17191, TS17192, TP21103, TN67-189, TN68-118
Word Gate Gen.	2	28000-501	DS22743, TS22744, TP30776, TN69-76, TR69-22



Table 3-1 (conclusion)

Assembly/Subassembly	Serial No.	Drawing No.	Documentation/Notes
<u>Command System</u>	1932A	17417-501	
Command Receiver	003, 004	20819-1	DS20818, TS20820, TP20821, TN69-78
Command Decoder	G1A, G2A, G3A, G4A	16578-3	DS16846, TS21933, TP22285, TN68-148, TN69-43
<u>RF System</u>	1934A	17415-501	MS21042, TS21043, TP21044, TN69-92
VHF Antenna (Match)	41829, 27286	17350-1	
VHF Transmitter	15, 17	31697-501, 20171-501	DS20329, TS20330, TP20331, TS31698, TP31699, TN68-74, TN68-76
Diplexer Assy.	17	20096-501	MS16116, TS16117, TP16437, TN68-88
Hybrid Circulator	8	17361-1	MS17456, TS17457, TP17458, TN68-87
RF Cable Assy.			MS21042, TS21043, TS21044
Coaxial Relay	2A	21113-1	DS21151, TS21152, TP21153, TN67-194, TR67-83
<u>Aspect Meas. System</u>	12	19568-501	
SORE Package	2	15874-501	MS18784, TS18785, TP16397, TN67-156
Mag. Sensor	1606	16995-1	DS18823, TS18824
Mag. Electronics	1606	19343-1	TP16785, TN68-71
<u>Power System</u>	1900A	19559-503	
Current Monitor Assy.	6, 4F	25106-1	MS27379, TS27380, TP27381, TN67-101, TN68-142
Solar Cell Array	004	17036-1	DS17042, TS20586, TP20587, TN69-107
Power Cell Assy.	14,15,16, 17,18,19	17292-1, 17292-503	TS18872, TP18873, DS17149, TS15856, TP15857, TN69-98



Program personnel visited vendor facilities as necessary to conduct quality surveys and vendor evaluation. These efforts provided criteria for placement of orders and subcontracts. Further visits expedited delivery of items.

Quality assurance test and inspection records, failure reports, and other documentation related to items served to document the history of those items. Records of operating and storage time were kept and used to evaluate items subject to wearout and fatigue.

Major OSO assemblies which were qualified on previous programs and substantially changed for OSO-6 were requalified when necessary. System reliability, failure-mode, and criticality analyses were updated at predetermined milestones during the design, fabrication, and test programs.

BBRC personnel were trained to comply with MSFC-PROC-158B soldering specification. All flight-model printed-circuit boards were epoxy conformal-coated after tests showed that such coating allows two to three times as much power dissipation in certain components. A continuing program of laboratory analyses and tests by the materials and processes section assisted in the resolution of design and production problems.

Acceptance testing of finished subassemblies was accomplished using production-test stations, designed and fabricated for that purpose on this and earlier OSO programs. Use of these stations provided increased efficiency and component safety in testing.



3.6 SPACECRAFT INTEGRATION AND TEST

The spacecraft integration and test phase covered the period from the delivery of the basic sail and wheel structures to the integration and test (I&T) organization to the partial (90 percent) spacecraft buyoff on 29 November 1968. Before such delivery, integration and test personnel reviewed functional drawings and wiring diagrams and prepared and adapted test equipment and procedures for use on OSO-6.

In simplified terms, the activities performed in the spacecraft integration and test phase were:

- (1) Checkout wiring of assemblies before interfacing
- (2) Alignment of sensors and equipment
- (3) Installation of equipment in the sail and wheel structures
- (4) Data collection for dynamic and long-term performance analysis
- (5) Mating of sail, wheel, and azimuth shaft assemblies
- (6) Preparation and installation of dummy pointed instruments to support sail components until installation of flight instruments
- (7) Preparation and execution of tests to cover the applicable spacecraft test specifications
- (8) Identification and resolution of potential and actual trouble areas



- (9) Preparation and maintenance of test equipment supporting the above activities, and
- (10) Spacecraft maintenance.

The OSO-6 spacecraft was tested in accordance with a formal test specification (Dwg. 26494, Test Specification for the OSO-G Spacecraft). All measurable parameters were recorded and analyzed, including the spacecraft functions at the experiment-interface connectors. A summary of spacecraft I&T activity is presented in Figures 3-1 through 3-3.

The spacecraft I&T phase ended with the 90-percent spacecraft acceptance on 29 November 1968. Certain items of spacecraft integration were carried forward for completion during the observatory I&T phase. These were necessitated by late changes to the contract scope-of-work and late delivery of command receivers. The late hardware changes related to offset point mode circuits, word-gate generator development, and adaptation of the launch-sequence system for operation with a two-stage launch vehicle.

3.7 EXPERIMENT ACCOMMODATION

Experiment accommodations personnel worked with spacecraft and experiment designers to accomplish:

- (1) Conciliation of experiment operational requirements and spacecraft dynamic, dimensional, power, command, and telemetry constraints
- (2) Definition of experiment/spacecraft electrical and mechanical interfaces

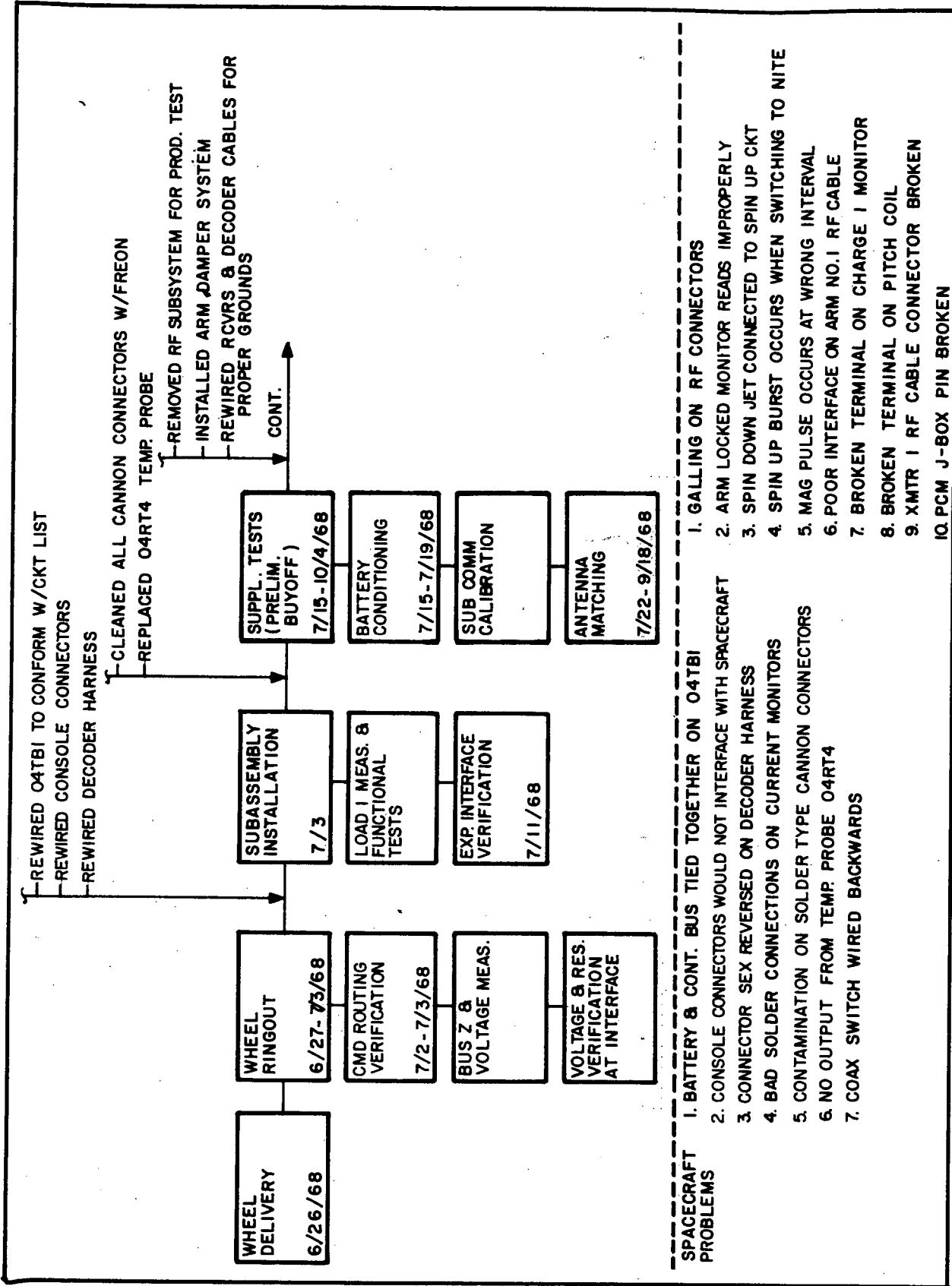


Fig. 3-1 OSO-G Wheel Pre-Mate I and T Activity

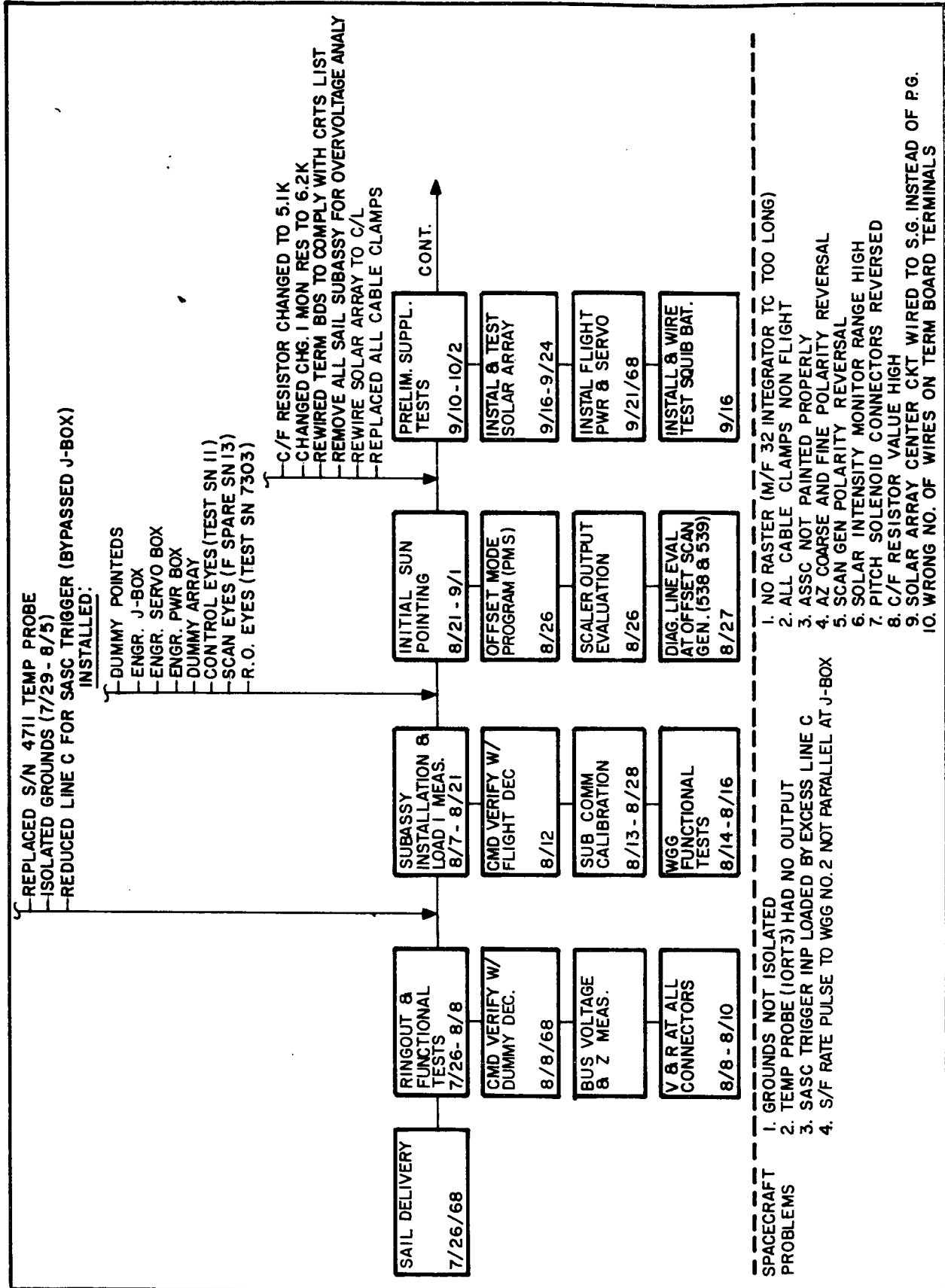


Fig. 3-2 OSO-G Sail Pre-Mate I and T Activity

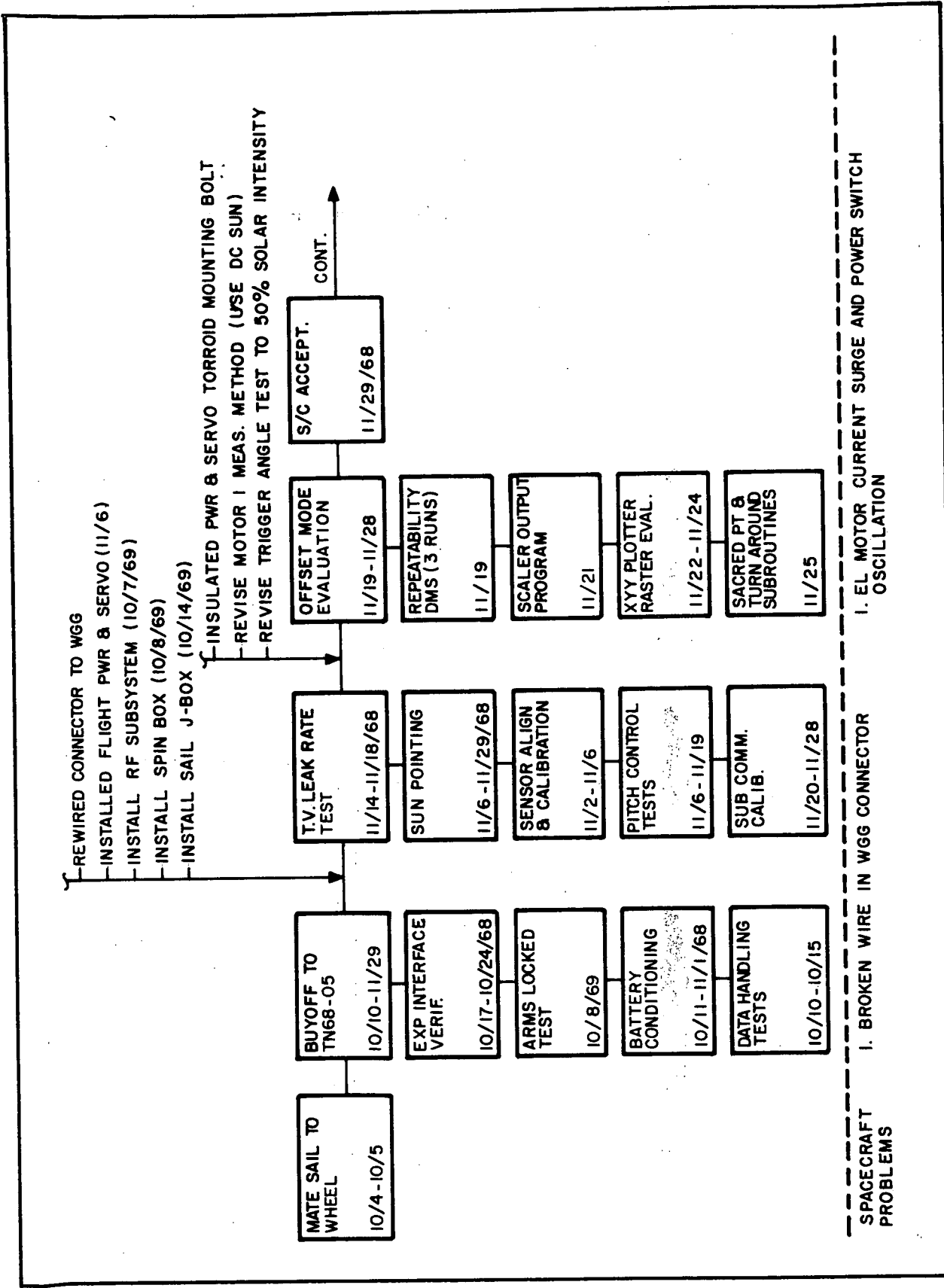


Fig. 3-3 OSO-G Spacecraft Integration and Test



- (3) Preparation and execution of experiment interface compliance test procedures
- (4) Development of policies and procedures for handling experiment hardware (including environmental controls)
- (5) Development of experiment test hardware as needed
- (6) Installation of experiment hardware in the OSO-6 spacecraft (and removal when necessary)
- (7) Preparation of experiment test procedures and their execution as a part of observatory acceptance testing
- (8) Maintenance, repair, and modification of instruments, and
- (9) Development of documentation to support and report experiment activities.

Highlights of the experiment-accommodation effort are presented in this subsection.

3.7.1 Experimenter Coordination

Purpose. The program experiment accommodation personnel maintained constant liaison with the experimenters' organizations throughout the OSO-6 effort. The purpose of this liaison was to ensure continued compatibility of the experiments with the OSO spacecraft and with each other.

Areas of consideration involving the conciliation of experiment operational requirements and spacecraft constraints were:



- (1) Power budgeting, load characteristics, and surges
- (2) Mechanical interfaces, weight, balance, and center-of-gravity locations
- (3) Data word and command allocations
- (4) Electrical interface pin lists
- (5) Non-standard signal allocations
- (6) Radioactive-source requirements
- (7) Specification waivers and changes
- (8) Special-handling and environmental requirements
- (9) Test procedures and equipment
- (10) Spacecraft components mounted to, and signals passing through, the pointed instruments, and
- (11) Magnetic interfaces between spacecraft and experiments.

The initial OSO-6 experimenters meeting was held on 7 October 1965, with GSFC, BBRC, and experimenter representatives attending. Initial allocations and interface definitions were established at this meeting and published in TN65-307, OSO-G Experimenters' Meeting Summary.

Detailed development of the allocations and definitions was thereafter promulgated in TN66-40, the OSO-G Interface Definition Summary (IDS). Evolution of interface specification was coordinated by BBRC with approval by GSFC, and the IDS was updated as necessary.



Handling and test procedures were prepared for each instrument. Table 3-2 shows the evolution of power, command, and telemetry requirements and weight for each instrument. Specific command and telemetry channel assignments are presented in Sections 9 and 10 of this document. To simplify the interpretation of experiment test data, special computerized decommutation and print routines were developed for each experiment (see Section 4).

3.7.2 Experiment Preintegration Testing

During the spacecraft acceptance-test phase, all spacecraft interfaces which would mate with experiment hardware were verified to meet the applicable specifications. Upon receipt of the scientific instruments, each instrument was tested in a spacecraft simulator to verify compatibility with OSO-type electrical signals. Mechanical interface checks were made by trial installation in the spacecraft.

The spacecraft simulator consisted basically of a PCM simulator, power supplies for both the experiments and the simulator, a binary-to-decimal converter, a Franklin printer, and an oscilloscope. Figure 3-4 shows a photograph of the simulator. Details of operation of the simulator are provided in TM70-05, OSO Spacecraft Simulator Model II Operator's Manual.



Table 3-2
OSO-6 EXPERIMENT POWER, COMMAND, TELEMETRY, WEIGHT

	Day Pwr Circuit ma-hrs/orbit	Orbit Pwr Circuit		MF Words	DSM Words	ASC-1 Words	ASC-2 Words	ASSC Words	Sail Cmmd	Wheel Cmmd	Weight Pounds
		ma-hrs/orbit Day	ma-hrs/orbit Night								
HCO (Ptd)	Requested	131.5		4	0	--	6	--	20	--	35
	Orig. Alloc.	131.5	7.9	8	4	--	4	6	28	--	40
	Final Alloc.	131.5	10.5	8	0	--	4	7	41	--	41.6
	Actual Meas.	113.84	7.3	--	--	--	--	--	--	--	36.16
NRL (Ptd)	Requested	191.1	--	14	4	--	2	--	7	--	36
	Orig. Alloc.	191.1	--	6	8	--	10	4	24	--	44
	Final Alloc.	191.1	--	6	8	--	10	0	24	--	44.0
	Actual Meas.	182.1	--	--	--	--	--	--	--	--	49.92
Rutgers (Wheel)	Requested	--	39.5	1	0	2	--	--	--	7	28
	Orig. Alloc.	--	39.5	2	0	2	--	--	--	7	28
	Final Alloc.	34.6	43.1	2	1	2	--	--	--	7	33.0
	Actual Meas.	41.0	58.5	--	--	--	--	--	--	--	33.68
Los Alamos (Wheel)	Requested	52.6	--	1	0	2	--	--	--	4	10
	Orig. Alloc.	52.6	--	1	0	3	--	--	--	6	10
	Final Alloc.	70.3	--	1	0	3	--	--	--	8	19.0
	Actual Meas.	59.4	--	--	--	--	--	--	--	--	20.45
U. of Bologna (Wheel)	Requested	--	43.4	1	0	2	--	--	--	3	10
	Orig. Alloc.	--	43.4	5	2	5	--	--	--	8	25
	Final Alloc.	57.9	43.4	5	2	5	--	--	--	7	25.0
	Actual Meas.	--	31.3	--	--	--	--	--	--	--	23.60
UCL (Wheel)	Requested	31.6	--	1	0	4	--	--	--	3	25
	Orig. Alloc.	31.6	--	1	3(S/B)	3	--	--	--	3	30
	Final Alloc.	31.6	--	1	10	3	--	--	--	7	36.0
	Actual Meas.	19.3	--	--	--	--	--	--	--	--	22.70
U. of N. Mex. (Wheel)	Requested	--	54.7	1	0	4	--	--	--	2	25
	Orig. Alloc.	--	54.7	4	0	6	--	--	--	2	25
	Final Alloc.	--	73.0	4	12	7	--	--	--	2	32.5
	Actual Meas.	--	62.7	--	--	--	--	--	--	--	32.25
Experiment Totals	Requested	406.8	145.5	23	4	14	8	--	27	19	169
	Orig. Alloc.	406.8	145.5	27	17	19	14	10	52	26	202
	Final Alloc.	459.1	149.1	27	33	20	14	7	65	31	231.1
	Actual Meas.	415.64	159.8	--	--	--	--	--	--	--	218.76

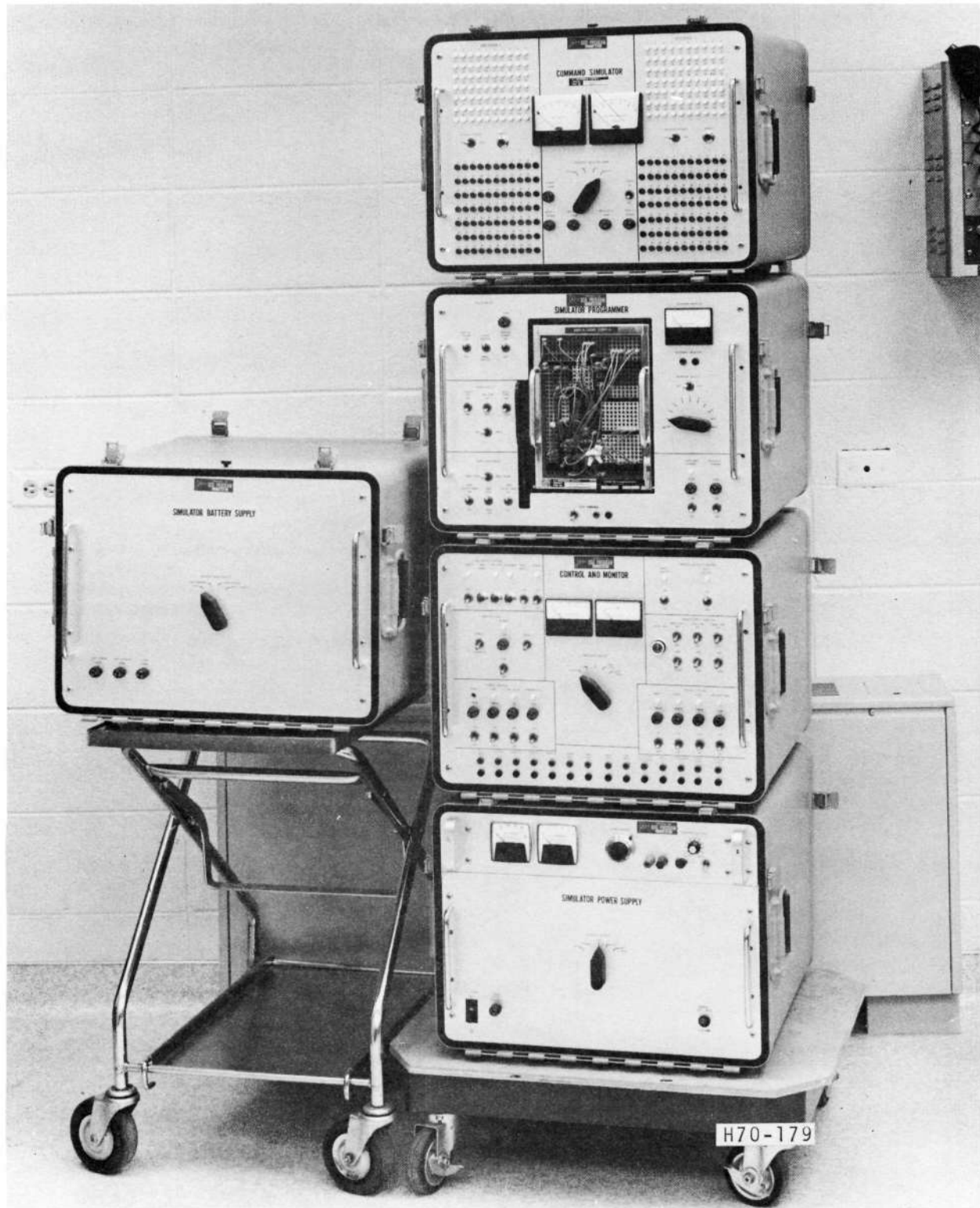


Fig. 3-4 OSO Spacecraft Simulator (Model II)



The purpose of the PCM simulator was to duplicate the OSO telemetry, command, sun pulse, magnetometer pulse, and power distribution signals. The purpose of the binary-to-decimal converter was to convert the experiment serial data into parallel data format which would be compatible with the Franklin printer.

All instrument handling was accomplished in a controlled-access clean room except when otherwise noted in the applicable handling procedure. Each major phase of instrument testing was certified by the cognizant experimenter to have been performed in accordance with the approved procedures.

3.7.3 Experiment Integration and Test

Experiment integration and test activities were conducted in conjunction with the observatory acceptance program. After the interface-compliance tests mentioned in paragraph 3.7.2, experiments were installed in the spacecraft and further tested as a part of the observatory. Normal experiment accommodation activities continued throughout the observatory acceptance and environmental-test program.

Test procedures, handling procedures, telemetry print routines, and special test equipment continued to be refined throughout the observatory test program. Close liaison between GSFC, BBRC, and experimenters, coordinated by the BBRC and GSFC experiment-accommodation organization, expedited the refinement process. Experiment, spacecraft, and test hardware and documentation was updated as necessary.

3.7.4 Experiment Support Documentation

The program experiment-accommodations personnel were responsible for preparing documentation supporting experiment development, integration and acceptance. The documentation was used to



communicate between the experimenters, GSFC, and BBRC, and aided in identification of areas requiring continuing coordination.

The major support documents for OSO-6 experiments are identified in Table 3-3. Additional documentation was provided through daily, weekly, and monthly reports, and observatory logs and records.

All support documentation required experimenter, GSFC, and BBRC approval.

3.8 OBSERVATORY INTEGRATION AND TEST

This phase of the OSO-6 project covered the period between spacecraft buyoff and observatory buyoff. It included the experiment integration and test activities described in the previous paragraphs and spacecraft catch-up items as required. A graphic history of observatory activities during this phase is presented in Fig. 3-5.

The basic purpose of the observatory integration and test phase was to combine the scientific payload with the OSO spacecraft, iron out incompatibilities, and conduct the integrated acceptance-test program. The acceptance tests included testing under the anticipated environmental conditions of launch and in-orbit operation.

Parameters tested under the required conditions were specified in 26494, Test Specification for the OSO-G Spacecraft, and the experiment operation specifications and procedures shown in Table 3-3.

In the paragraphs which follow, major observatory integration and test activities are discussed.

Table 3-3
OSO-6 EXPERIMENT SUPPORT DOCUMENTATION

Mech Interface Control Drawing	Elect. Interface Control Drawing	Experiment Test Procedure	Experiment Test Report		Instrument	Sail		Wheel								
			Flt I	Flt II		HCO	NRL	Rutgers	LAST	Bologna	UCL	UNM				
24782-F 26 May 69	30914-B 11 Aug 69	TN68-08-B 9 Jul 69	---	---	TR68-49 14 Jan 69	TR69-26 7 Jul 69	TR68-50 29 Oct 68	TR68-53 24 Oct 68	TR68-46 16 Aug 68	TR68-44 30 Jul 68	TR68-51 20 Sep 68	TR68-52 30 Aug 68	TR69-28A 25 Aug 69	TR68-13-A 9 Jul 69	21840-D 3 Apr 69	24787-E 26 May 69
24782-F 26 May 69	21842-D 1 Apr 69	TN68-07-B 9 Jul 69	---	---	TR69-27 7 Jul 69	---	---	TR69-29 7 Jul 69	TR68-40 7 Jul 69	TR68-11-A1 9 Jul 69	TR68-09-B 9 Jul 69	TR69-31 7 Jul 69	TR69-41 25 Aug 69	TN68-12-A 9 Jul 69	21834-D 11 Aug 69	24786-D 26 May 69
24782-F 26 May 69	21832-C 2 May 69	TN68-10-A1 9 Jul 69	---	---	TR69-30 7 Jul 69	TR69-32 7 Jul 69	---	TR69-40 7 Jul 69	TR68-44 7 Jul 69	TR68-11-A1 9 Jul 69	TR68-09-B 9 Jul 69	TR69-31 7 Jul 69	TR69-41 25 Aug 69	TN68-12-A 9 Jul 69	21838-D 10 Jan 69	24784-C 4 Feb 69
24782-F 26 May 69	21832-C 2 May 69	TN68-12-A 9 Jul 69	---	---	TR69-32 7 Jul 69	---	---	TR69-32 7 Jul 69	TR68-52 30 Aug 68	TR68-12-A 9 Jul 69	TR68-09-B 9 Jul 69	TR69-31 7 Jul 69	TR69-41 25 Aug 69	TN68-12-A 9 Jul 69	21832-C 2 May 69	24785-F 26 May 69

OTHER DOCUMENTS:

Experimenters' Meeting (TN65-307-A:5 Jan 66)
 Spacecraft Simulator (TM70-05:3 Jun 70)
 Interface Definition Summary (TN66-40-F:5 May 69)
 Experiment Computer Programs (TN68-19:18 Apr 69)
 Test Parameters List (TN65-74-A:23 Apr 68)
 Duty Cycle Plan (TN68-92:16 Aug 68)
 Contamination Tolerance (TN69-07:11 Feb 69)
 Magnetics (TN67-10:15 Mar 67)
 Payload Description (TN69-04:16 Jun 69)
 Interface Specification (29800C:1 Apr 69)

F70-03



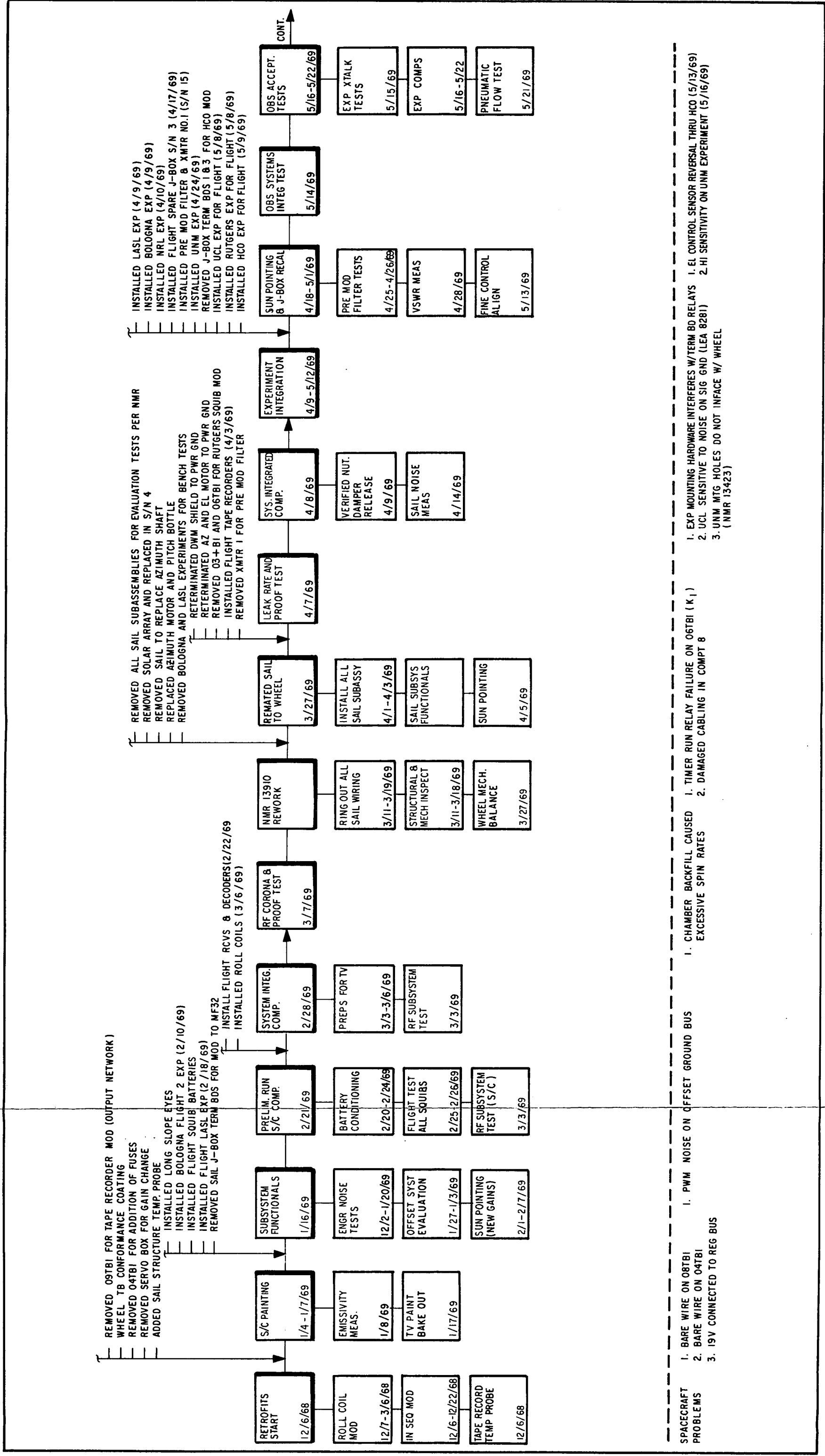
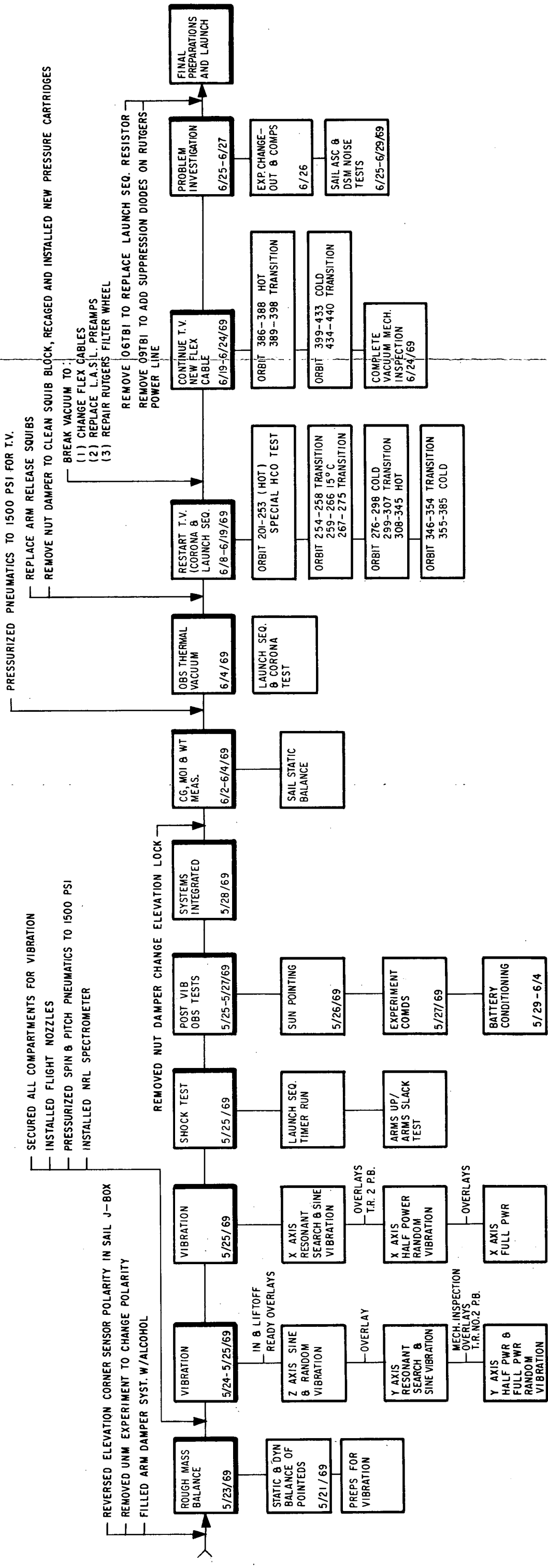


Fig. 3-5 OSO-6 (OSO-G) Integration and Test History (Sheet 1 of 2)



FOLDOUT FRAME



SPACECRAFT PROBLEMS

- 1. LAUNCH SEQUENCE
 - 1. NO OUTPUT ON CHANNELS 4 & 5 OF L.A.S.L. EXP.
 - 2. SUN/ SHADE LOGIC FAILURE (NMR 13918) ON L.A.S.L.
 - 3. FLEX CABLES NON FLIGHT DID NOT FULLY UNCAGE (NMR 15374)
- 2. NUT DAMPER LATCH
 - 1. RUTGERS FILTER WHEEL NO.2 JAMMED
 - 2. SAIL ASC SYNC LOSS W/ SAIL DAY ENABLE CMD.
 - 3. DSM F/C SLIP W/ UNM & RU

- 1. RUTGERS FILTER WHEEL
 - 1. RUTGERS FILTER WHEEL NO. 2 JAMMED
 - 2. BOLOGNA H.V. FAILURE
 - 3. L.A.S.L. CHANNEL 4 FAILURE

- 1. LAUNCH SEQUENCE RESISTOR
 - 1. LAUNCH SEQUENCE RESISTOR MAY NOT BE RELIABLE

3-25

Fig. 3-5 OSO-6 (OSO-G) Integration and Test History (Sheet 2 of 2)



3.8.1 General Procedures

The procedures described in this paragraph are those used repeatedly throughout OSO-6 integration and test activity. They were applied as shown in Fig. 3-5 for acceptance and survival testing, and for maintenance and troubleshooting.

Spacecraft Comprehensive Test (TN68-14). The spacecraft comprehensive test was a combination of test sequences, largely drawn from the supplementary tests, which collected a large amount of test information in a small time. All systems were tested to some extent by the comprehensive. The test was performed in the clean room under controlled atmospheric conditions.

The spacecraft comprehensive test was executed with the help of the CDC-160A computer system, using the special BBRC-developed Observatory Automatic Test System (OATS) program. OATS provided the following advantages in testing:

- (1) More efficient use of test time
- (2) Magnetic tape records of test data were available for subsequent data processing and history
- (3) Reproduction of review and/or data copies of procedures was greatly simplified
- (4) Test accuracy was increased, adding to the safety of the items tested
- (5) Levels of testing which had previously been extremely difficult or impossible were made simple



- (6) An editing routine was used for efficient updating of procedures
- (7) Greater test repeatability was achieved, and
- (8) Records of mistakes and unscheduled operations were automatically inserted with the test data.

Spacecraft Supplementary Tests (TN68-05). The tests in this category were each formed to provide a thorough testing of related spacecraft parameters. In the aggregate, the supplementary tests cover all spacecraft test specifications (except environmental). Some engineering and performance tests not specified were also included.

Supplementary tests were adapted for the OATS technique whenever such adaptation offered a significant net advantage.

A detailed mechanical-inspection procedure was included in the supplementary procedures. It was used to verify mechanical integrity of the observatory after each environmental-test sequence.

A supplementary procedure for conditioning the power and squib batteries was also prepared and used throughout the integration and test phase. The conditioning procedure consisted of fully discharging and recharging the batteries.

Experiment Tests. Experiment tests were published in the operation, specification, and procedures documents shown on Table 3-3. The tests were executed using special computer print routines which arranged and labelled the telemetered experiment data for easy interpretation.



3.8.2 Thermal-Vacuum (T-V) Test (TN68-21)

The purpose of the T-V test was to provide for evaluation of OSO's performance under conditions of temperature and pressure similar to those anticipated for flight. The test was conducted with OSO installed in the large, 10-foot thermal-vacuum chamber shown in Fig. 3-6.

Control of the observatory spin rate during T-V test was exercised through the T-V test console. This console also controlled battery charging, in-chamber stimulus lamps, and observatory switching functions, and provided monitoring of selected status points. Control of the observatory was also maintained through OSO's command system.

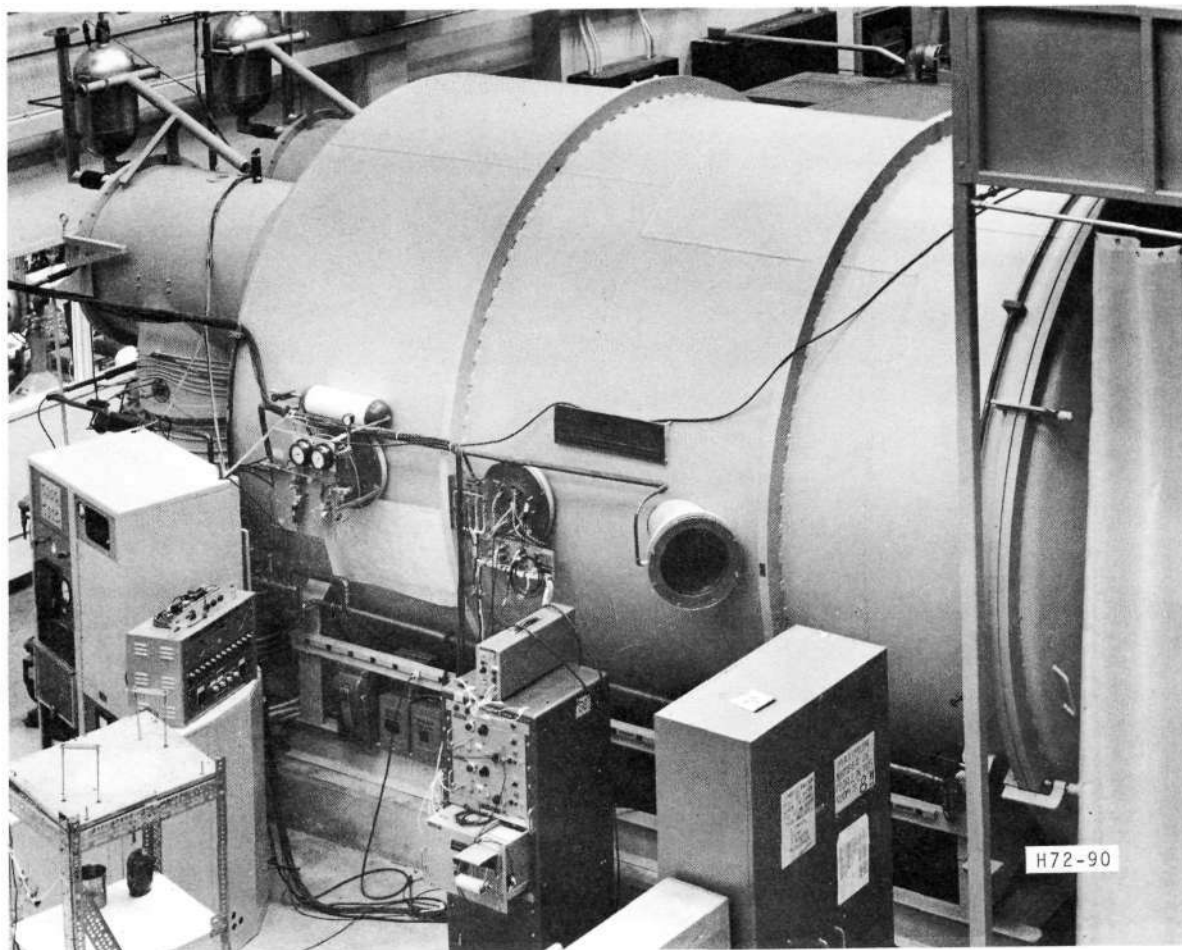


Fig. 3-6 Thermal-Vacuum Chamber



The OSO-6 thermal-vacuum test consisted of 15 days of observatory operation in vacuum ($<10^{-5}$ torr) as follows:

- (1) A full exercise of the launch-sequence control system under simulated flight conditions
- (2) Operation for four days at $+25^{\circ}\text{C}$ (hot exposure, corona, outgas)
- (3) Transition to 0°C and operation at that temperature for one day (cold exposure)
- (4) Transition to $+25^{\circ}\text{C}$ and operation at that temperature for three days (hot soak)
- (5) Transition to 0°C and operation at that temperature for three days (cold soak)
- (6) Transition to $+25^{\circ}\text{C}$ for test-chamber bleedup.

The launch sequence was started by simulating the actuation of the separation switches. This started the launch-sequence timers.

Experiments were not turned on during the first three days of testing, to allow time for them to outgas thoroughly. This provided protection against corona-discharging from their high-voltage circuits.

Spacecraft tests comparable to the comprehensive test (Para. 3.8.1) were conducted periodically throughout the test at selected conditions of temperature and voltage. Experiment tests were conducted as described in the experiment operation, specifications, and procedures manuals (Table 3-3). Tape recorders were played back regularly throughout the test and thoroughly evaluated several times during each test period. A leak check of pneumatic systems



was conducted at the beginning and end of each temperature phase of testing. Voltage-extreme and special tests were included as required by specifications or by the test engineer.

During T-V testing the observatory was operated in a 90-minute day/night duty cycle. This was accomplished by turning spin-eye stimulus lamps on and off by timer control. Telemetry data points were sampled and verified at regular intervals. The flight output of the solar-cell array was simulated by applying battery charge power through a timer and an impedance network.

Spacecraft solar sensors and experiment solar and cosmic ray detectors were stimulated by sources placed in and around the test chamber. The spacecraft communications systems tests and the experiments tests were executed using the 160A computer system.

Contamination Monitoring in T-V. During the observatory thermal-vacuum tests, a series of measurements were made to determine the outgassing and deposition levels of potential contaminants evolving from the observatory.

A mass spectrometer/residual-gas analyzer was used to monitor gases evolved during the tests. Materials that condensed on optical-quality mirrors and refrigerated collectors in the test chamber were analyzed after the test. Analysis of residual gas analyzer data showed that the replacement of outgassing materials discovered in tests of earlier OSO's reduced outgassing to insignificance on OSO-6.

3.8.3 Vibration Test (TN68-20)

The purpose of the vibration test was to verify that the structural members of OSO-6 and its payload were strong enough to survive the



vibration anticipated during launch. Electrical circuits on board OSO-6 were energized in the launch mode to demonstrate that these circuits were not vulnerable to vibration. Comprehensive and supplementary tests (Para. 3.8.1) before and after vibration demonstrated that all electrical circuits and components could survive the launch.

The levels to which OSO-6 was vibrated, predetermined by the characteristic vibration of the launch vehicle, are shown in Table 3-4. The axes of vibration defined for vibration testing are shown in Fig. 3-7. Figures 3-8 through 3-10 show OSO-6 mounted on the driver for each of the three axes of vibration.

Vibration Accelerometers. Before each vibration sequence, accelerometers were mounted to the observatory. The outputs of each of these accelerometers was recorded during the vibration. The accelerometers were classified as control, monitor, crosstalk, or response, commensurate with their use.

The control accelerometers were located immediately below the separation plane on the vibration-fixture adapter. Their sensitive axes were aligned parallel to the axis of vibration. Their outputs were fed to the vibration equipment for amplitude control and to recorders for documentation of control-axis vibration.

The monitor accelerometers (placed adjacent to the control accelerometers) allow real-time visual evaluation of the controlled input. The crosstalk accelerometers were aligned perpendicular to the axis of vibration to record any off-axis motion at the control plane. Response accelerometers were those used as required to study the observatory in vibration.



Table 3-4
OSO-6 VIBRATION ACCEPTANCE TEST LEVELS

Axis	Frequency (Hz)	Acceleration (g, 0 to peak)	Sweep Rate (octaves per min)	
Thrust Z (Sinusoidal)	5-11	0.33 in. D.A.*	4	
	11-17	2.0	4	
	17-23	4.0	3	
	23-200	1.5	4	
Transverse X (Sinusoidal)	5-9.5	0.33 in. D.A.*	4 ↓	
	9.5-11	1.5		
	11-20.5 (1)	0.15		
	20.5-31	1.0		
	31-37	0.37		
Transverse Y (Sinusoidal)	5-9.0	0.33 in. D.A.*	↓	
	9.0-17.5 (2)	0.20		
	17.5-27.0	1.0		
	27.0-32.5 (2)	0.48		
	32.5-200	1.0		
<p>NOTES:</p> <p>(1) Resonance occurs within this range in the X-axis.</p> <p>(2) Resonance occurs within this range in the Y-axis.</p> <p>* Double Amplitude (peak-to-peak)</p>				
Axes	Frequency (Hz)	PSD Level (G ² /Hz)	Acceleration (G-rms)	Duration (min)
Z, X, and Y (Random)	20-300	0.0017 to 0.020 increas- ing 3 db/ octave	6.1 ↓	2 each axis
	300-2000	0.020		

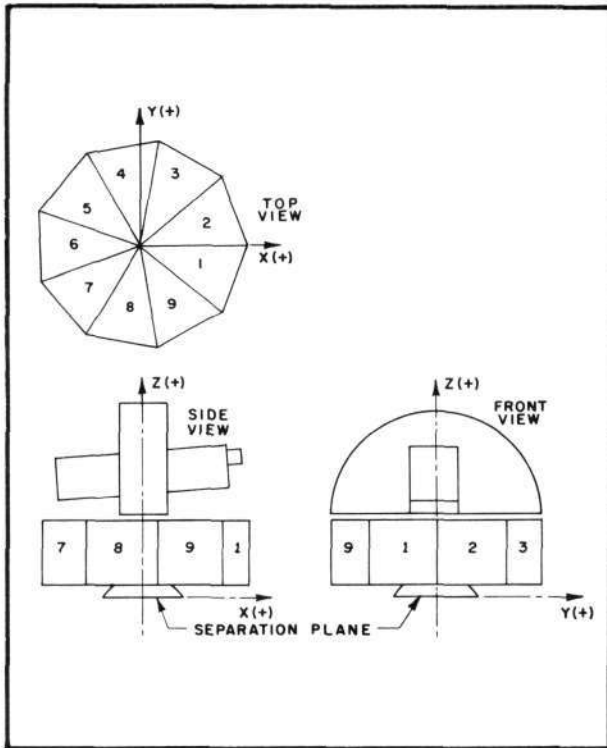


Fig. 3-7 OSO Axes of Vibration

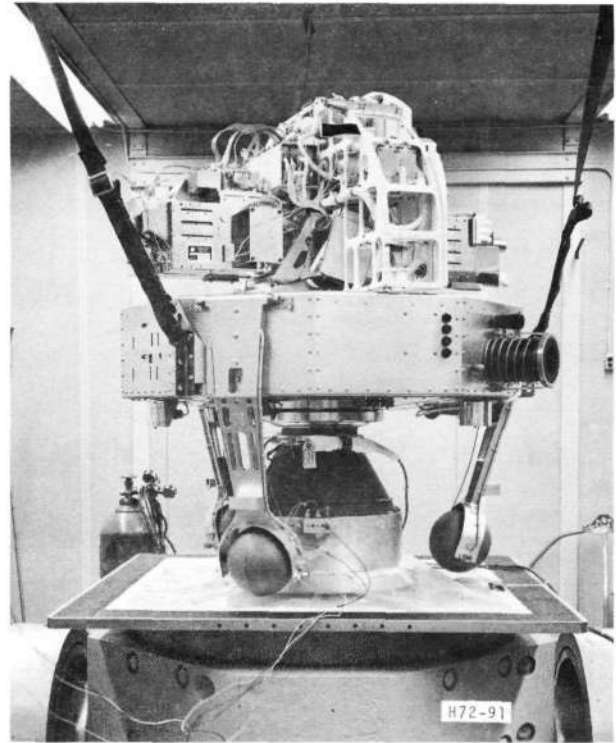


Fig. 3-8 OSO-6 Z-Axis Vibration

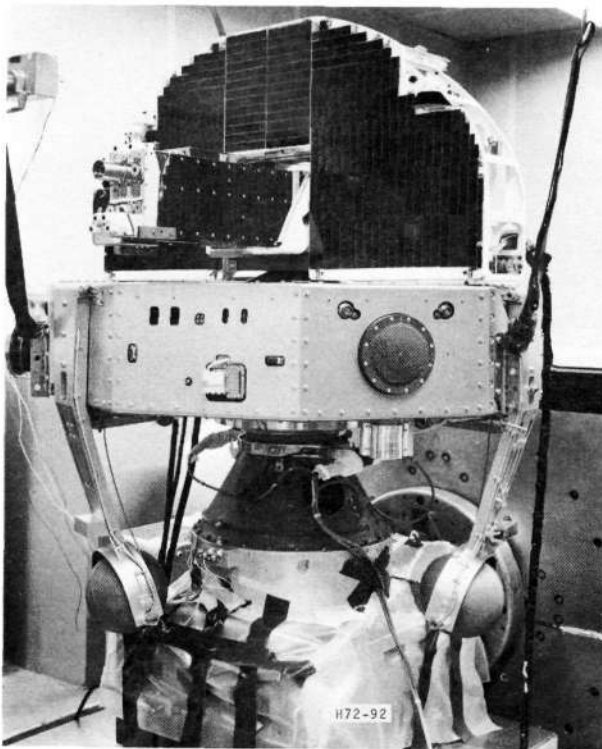


Fig. 3-9 OSO-6 X-Axis Vibration

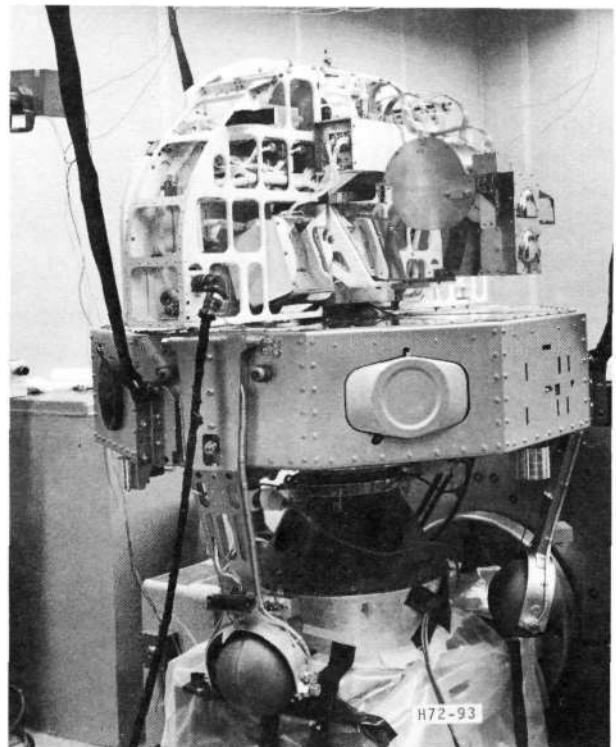


Fig. 3-10 OSO-6 Y-Axis Vibration



Resonance Search. To avoid exceeding the Delta-N vehicle launch loads on the OSO structure, the driver signal was attenuated, or notched, at the frequencies of OSO's mechanical resonances. These frequencies were identified before the transverse-axis vibration runs by conducting resonance searches at about one-half the calculated notch levels.

Monitor during Vibration. During bursts of vibration, the following records were kept:

- (1) Magnetic-tape records of accelerometer outputs (from which both transmissibility plots (db plots) and filtered g-level plots were subsequently made)
- (2) Telemetry-printout of spacecraft housekeeping data, and
- (3) Magnetic-tape record of observatory DME output.

In addition to those records listed above, charts and photographs were prepared to document accelerometer locations.

3.8.4 Dynamic Balance

For proper performance during launch and in orbit, the OSO-6, like other OSO's, had to be balanced statically and dynamically. The launch-condition balance was specified by MDAC to be compatible with the Delta vehicle dynamic characteristics. The in-orbit balance was specified to limit the effects of wobble on spacecraft systems and experiments performance.

Approximate balance is required to prevent excessive wobble during thermal-vacuum and sun-pointing tests. Since removal of equipment from the observatory and its subsequent reinstallation upsets the balance, OSO-6 was balanced several times as indicated in Fig. 3-5.



The balancing machine used on OSO-6 is shown in Fig. 3-11. Each balancing operation required several repetitions of the basic balance procedure, until balance was within the required limits. After the balance machine was erected and aligned, the observatory was mounted to the spin table. The spin axis of the observatory was aligned with the bearing axis of the spin table.

The wheel, with arms extended, was balanced first with the sail tied to the machine frame to prevent rotation. The sail was then tied to the wheel and the balancing process was repeated. The PIA center of gravity was made coincident with the elevation axis by weight additions. The pointed instruments were then allowed to settle at their natural spinning angle during sail balance, and the elevation lock was subsequently adjusted to hold them at that position. The observatory arms were then lowered and the balance was checked in the launch configuration. Balancing was accomplished by adding weights to the spacecraft as needed.

3.8.5 Mass-Properties Measurements

The OSO moment-of-inertia, center-of-gravity, and weight measurements were needed to determine booster performance requirements and the number of spin rockets needed on the second-stage of the launch vehicle. These parameters were also needed for in-orbit performance analysis, the results of which are used to improve future OSO designs.

Moment-of-Inertia (MOI). Two types of MOI measurements were made on OSO-6: spin-axis MOI and transverse-axis MOI.

The spin-axis MOI was measured suspending OSO as shown in Fig. 3-12 and causing it to oscillate as a torsional pendulum. The



oscillation frequency was then measured with the arms both extended and stowed, and with the sail locked and unlocked. MOI for the different configurations was calculated using the formula:

$$I_{\text{spin}} = \frac{Wr^2p^2}{K4\pi^2L} \text{ (slug-feet}^2\text{)}$$

where:

K = 0.995 (amplitude correction factor)

W = weight of OSO (lb)

r = distance from spin axis to cable attach points (ft)

P = period of oscillation (sec)

L = length of cables (ft)

Corrections were made for the lift lug and for the spin gas added for launch.

The transverse-axis MOI was calculated using data obtained with OSO mounted on the transverse MOI fixture (Fig. 3-13). OSO and the pivoted yoke formed a compound pendulum of which the period, mass, and length were measured. The following equation was developed to remove the effects of the pivoted yoke and includes several measured constants necessary to accurately determine OSO transverse MOI:

$$I_{\text{transverse}} = 6.5 \times 10^{-4}T^2 (L + 10) - 6.46 \times 10^{-12}T^2W^2 \\ (L^2 + 11L + 30.5) - 2.22 \times 10^{-2}L^2 - 0.206L \\ - 1.87$$

where:

T = time for 10 oscillations (sec)

L = distance from yoke axis to system CG (in.)

W = weight of OSO (lb)

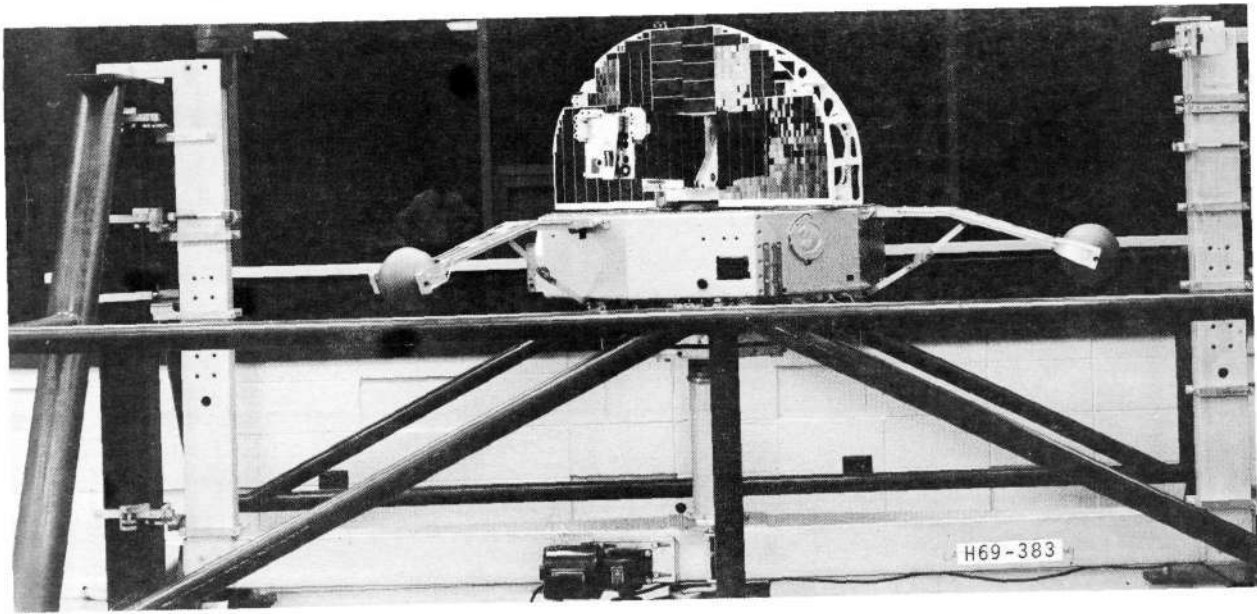


Fig. 3-11 OSO-2 on Balance Machine

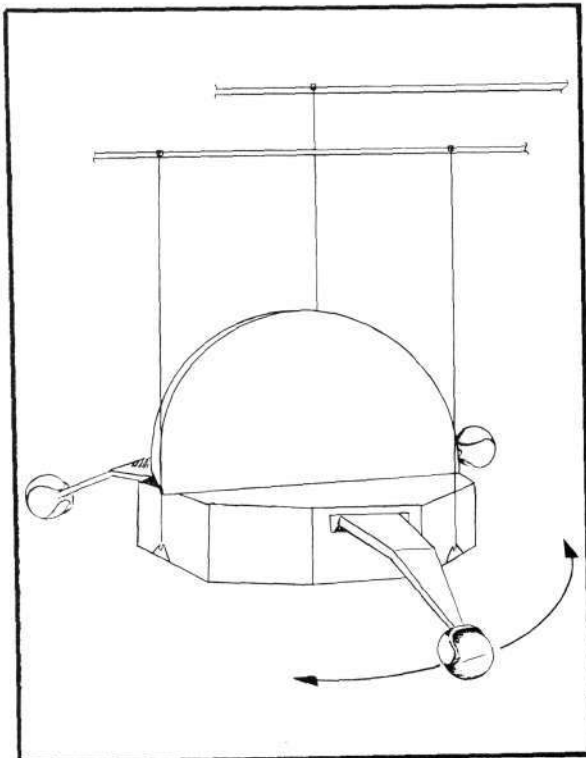


Fig. 3-12 Spin MOI Test Setup

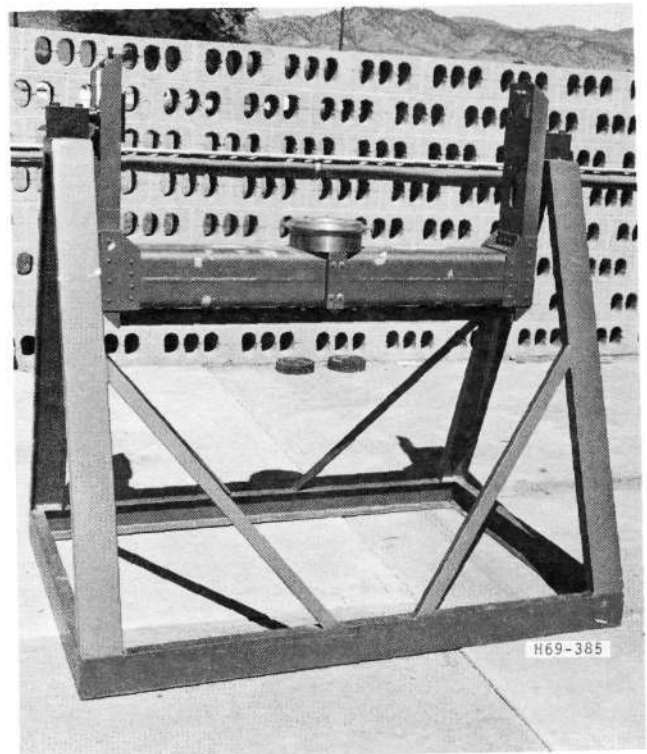


Fig. 3-13 CG/MOI Test Fixture



The maximum transverse MOI about the pitch and roll axes was then calculated using these data, and is shown in Table 3-5. Corrections were made for the addition of spin gas before launch.

Table 3-5
OSO-6 WEIGHT, CG, AND MOI

Item	Measured or Calculated Values
Weight	639.91 lb.
CG (distance from separation plane)	12.42 inches (arms down) 12.97 inches (arms up)
Spin-Axis MOI in Launch Condition	22.1 slug-ft ² (wheel only) 27.5 slug-ft ² (wheel & sail)
Spin-Axis MOI in Orbit Condition	29.9 slug-ft ² (wheel only) 35.3 slug-ft ² (wheel & sail)
Maximum Transverse MOI	24.8 slug-ft ² (Launch condition) 25.0 slug-ft ² (Orbit condition)
Ratio of Spin MOI to Max Transverse MOI in Orbit Condition	1.20 (daytime) 1.41 (nighttime)

Center-of-Gravity (CG). The transverse MOI test fixture (Fig. 3-13) was also used to locate the OSO-6 CG. The yoke was adjusted up and down to the position where OSO would remain at any angular orientation without being reoriented by the pull of gravity. That position defined the CG of the OSO/yoke combination.

This procedure was performed with OSO in both the launch and orbit configurations. The CG location was then calculated for each configuration using the formula:

$$CG = dp + \frac{My}{Ms} (dy + dp)$$



where:

CG = OSO CG location in inches above the separation plane

dp = OSO/yoke CG location in inches above the separation plane

My = mass of yoke = 2.23 slug

Ms = mass of OSO in slugs

dy = yoke CG location in inches below the separation plane = 0.6227 in.

The center-of-gravity locations for OSO-6 are listed in Table 3-5.

Weight Measurement. The OSO weight measurements were made on Hydraset scales (Fig. 3-14). The weight of handling equipment was subtracted from the indicated weight and the weight of nitrogen gas to be added for launch was added to arrive at OSO-6's flight weight. This weight is indicated in Table 3-5.

3.8.6 Magnetic Balance

When OSO is in orbit, its dynamic behavior (including pitch and roll attitude drift) is governed in part by the interaction of observatory magnetic dipoles with the geomagnetic field. Proper adjustment of the OSO-6 magnetic dipoles was used to increase its in-orbit life by reducing attitude gas consumption. From a magnetic control study, it was concluded that the OSO-6 dipole moments should be adjusted as shown in the first column of Table 3-6.

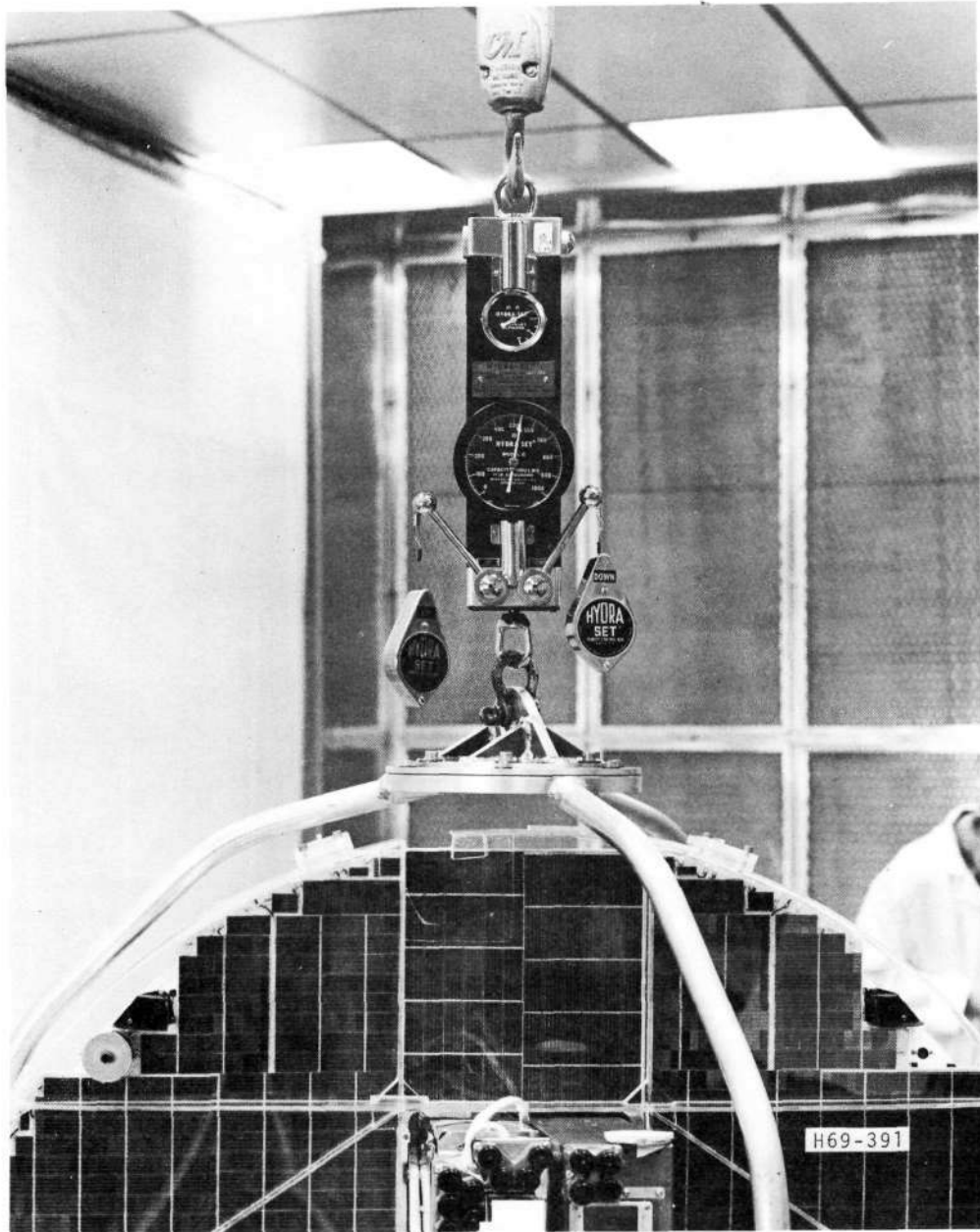


Fig. 3-14 OSO on Weighing Scale

Table 3-6

OSO-6 MAGNETIC DIPOLE MOMENTS *

OSO Axis	Specification	After Demag./ Before Balance	Final Value
X	-200 \pm 200	-84	-84
Y	0 \pm 200	+936	+26
Z	-2200 \pm 200	+792	-2133

* All moments shown are in dyne-cm/gauss



The magnetic balancing operation uses two major pieces of equipment; the observatory demagnetizer and the observatory magnetotropometer. Both these, together with their auxiliary apparatus, are used in the BBRC magnetotropometer building. This building is constructed of extremely-low-magnetic materials in a location far from things which could disturb the local geomagnetic field.

Magnetic balance was performed in four steps:

- (1) OSO was demagnetized to eliminate easily-variable accidental magnets.
- (2) Temporary test magnets were attached, which had dipole moment components that were the negative of the desired values.
- (3) The net magnetic dipole was measured and compensating magnets were permanently installed, making the net moment zero. The dipole moment was then remeasured, to verify that the net moment was near zero.
- (4) The temporary test magnets were removed, thereby bringing the net moment close to the target value.

Condition of OSO for Magnetic Balance. Before magnetic balance was started, OSO was prepared as follows:

- Observatory batteries were fully charged.
- The "launch-turnon plug" was installed so that the pitch coil could be operated by RF commands.



- As much OSO electrical equipment as possible was turned off to reduce the drain on the batteries.
- The pointed instruments were locked with their optical axes perpendicular to the spin axis.
- The OSO arms were in the launch position.
- The sail was wedged to the wheel with the pointed instruments aimed over Compartment 1.
- The solar-array cover was removed.
- All ferromagnetic protective covers were removed.
- Magnetic-equivalent dummy plugs and caps were installed.
- OSO was covered with a polyethylene bag and purged with dry nitrogen.

Demagnetization. Before meaningful dipole moment measurements could be made, the easily-changed parts of the moment had to be removed. This was done using a slowly-decaying alternating field applied by the observatory demagnetizer (Fig. 3-15). The field was not strong enough to affect permanent magnets that were a necessary part of OSO. The field was strong enough, however, to partly demagnetize the accidental magnets so that their value was stabilized.

After the demagnetization was complete, the temporary test magnets were attached, as described above. The test magnets were used so that the final dipole moments measured would be near zero. The magnetotropometer readings are more accurate near to zero than for larger moments.

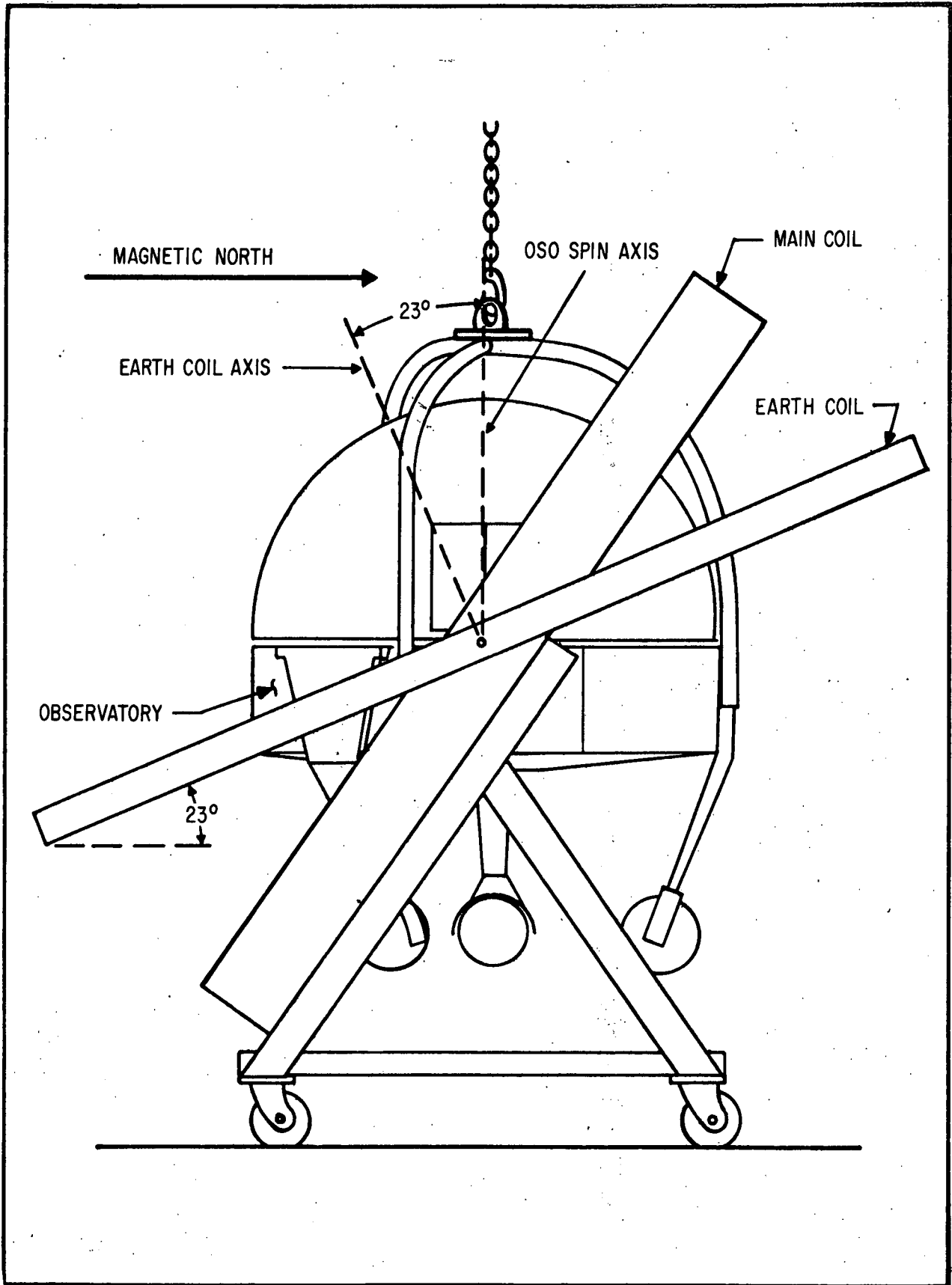


Fig. 3-15 Observatory Demagnetizer



Magnetic Dipole Compensation. The dipole moment was measured by measuring OSO's tendency to act like a compass in the geomagnetic field. The measurement was accomplished on the observatory magnetotropometer (Fig. 3-16).

OSO was suspended, as shown, from a frictionless support, in a region of uniform geomagnetic field. The torque produced by OSO in attempting to align its dipole with the field was then measured. The three components of the dipole were measured by mounting OSO in three mutually-perpendicular orientations on the magnetotropometer.

Permanent compensating magnets were then prepared for each of the three components of the dipole. These were mounted permanently to the sail structure. The observatory dipole moment was then remeasured and verified to be near zero. Removal of the test magnets, then, brought the dipole moment to the desired value, as shown in Table 3-6.

3.9 LAUNCH ACTIVITIES

This phase of the OSO-6 project included shipment to the Eastern Test Range (ETR) at Kennedy Space Center (KSC), Florida, and subsequent activities leading to the launch on 9 August 1969.

3.9.1 Shipment to ETR

OSO-6 was shipped from BBRC, Boulder, to ETR in the OSO shipping container shown in Fig. 3-17 on 17 July 1969. Shipment was via North American Van Lines air-ride truck to Buckley ANG Base, Colorado. Ground-support equipment was packed in 8 by 6 by 6 shipping vaults and transported to Buckley on flat-bed trucks. At Buckley the shipment was loaded into a cargo plane for transfer to ETR.

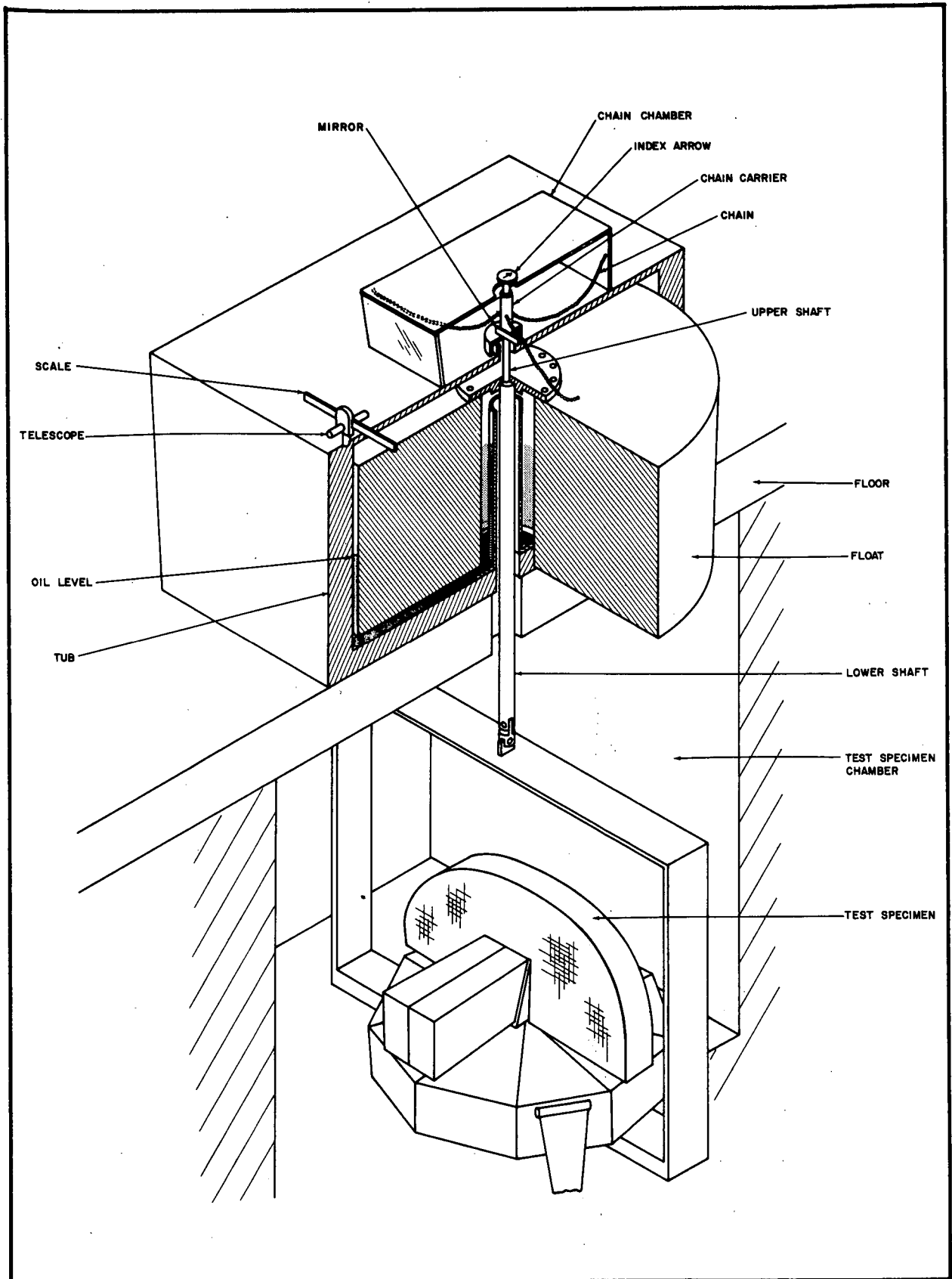


Fig. 3-16 OSO on Magnetotropometer

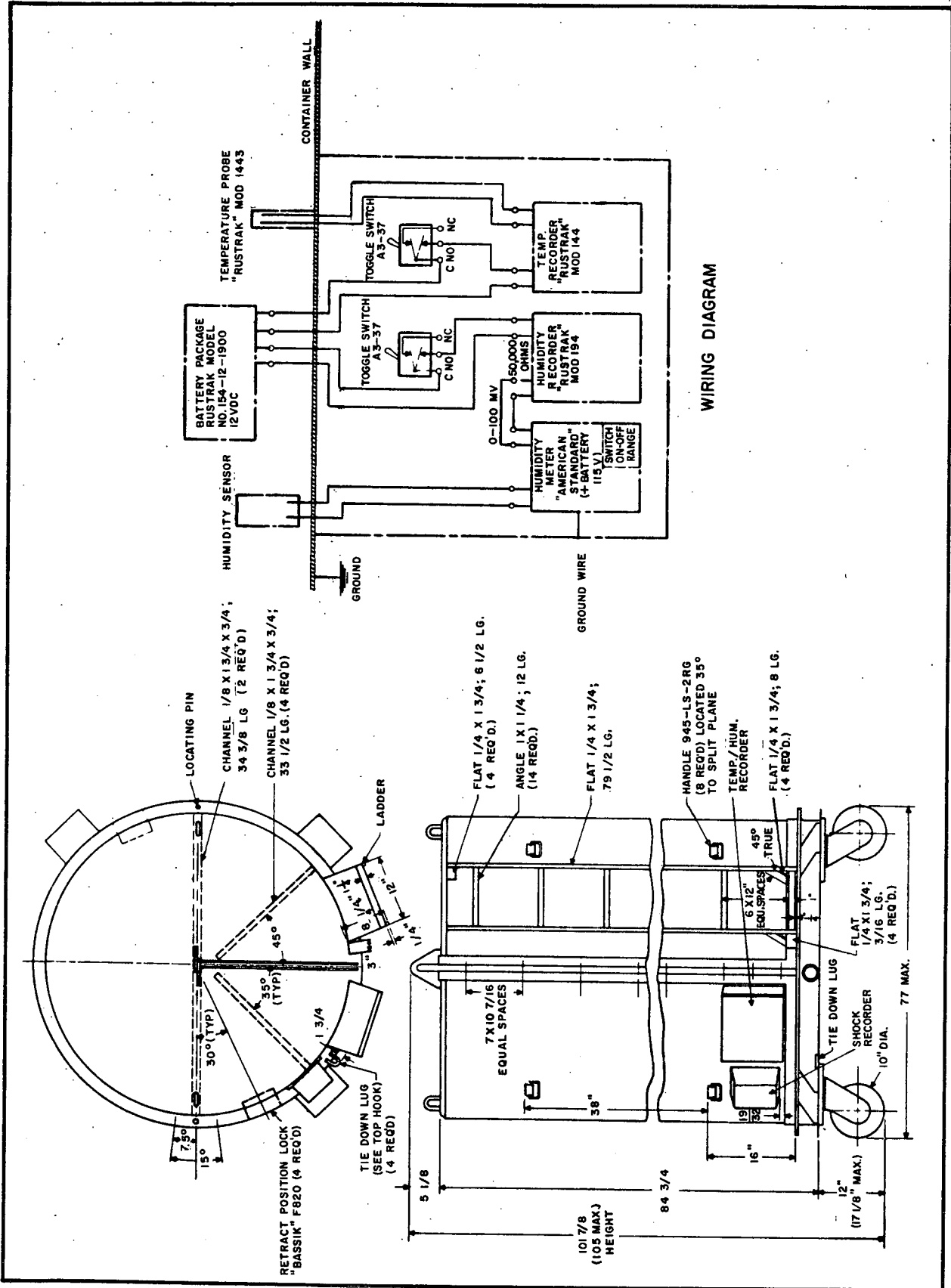


Fig. 3-17 OSO Shipping Container



Before shipment OSO-6 was given a thorough mechanical inspection and appropriate protective covers were installed. The observatory protective capsule, shown in Fig. 3-18, was placed around the observatory before it was installed in the shipping container.

Environmental Controls and Monitors. The OSO shipping container was equipped with eight maximum-reading accelerometers. Four were placed with their sensitive axes vertical, and four horizontal. Each set of four consisted of accelerometers set to trip at 3, 5, 10, and 15g.

The observatory was mounted on three rubber-cushioned shock mounts to isolate it from the canister. A continuously recording accelerometer with a 0-6g range was attached directly to the observatory.

A positive pressure of about 2 psi was maintained inside the canister during shipment. The can was thoroughly purged with dry nitrogen before being sealed and pressurized. A portable nitrogen system was used to maintain the pressure in the can. Seven bags of desiccant (MIL-D03664B) were included as an additional safeguard against moisture.

3.9.2 Prelaunch Activities at ETR

The major items of observatory prelaunch activity at ETR are shown in Table 3-7. Appropriate environmental controls were maintained throughout all these activities. Observatory tests were performed in the assigned hangar clean room whenever possible.

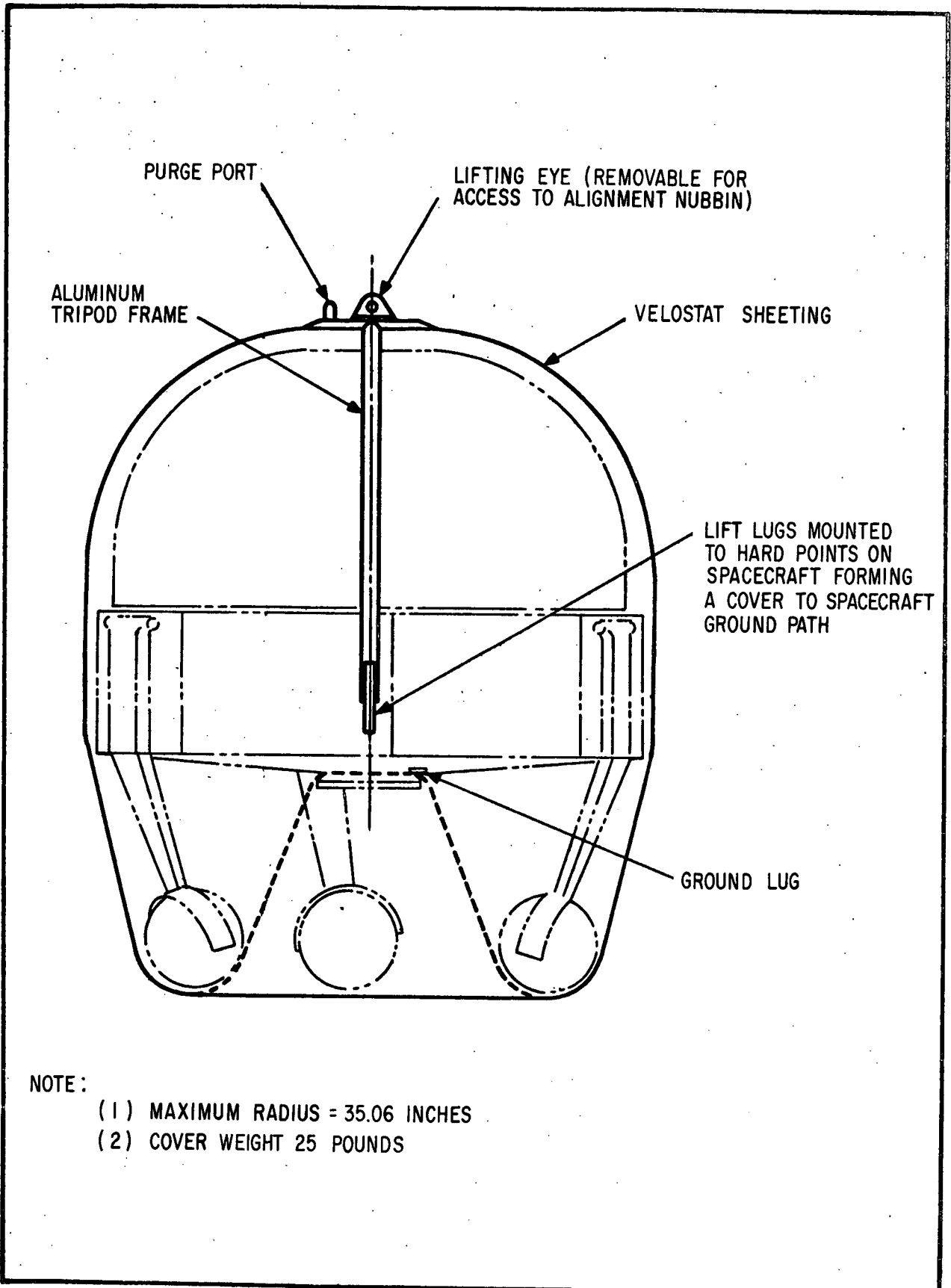


Fig. 3-18 OSO Protective Cover



Table 3-7
OSO-6 ETR PRELAUNCH MILESTONES

Date	Event
7-18-69	Spacecraft and GSE arrived at Cape Kennedy
7-19-69	OSO Ground Station set up and checked out. The spacecraft was removed from the shipping container and placed in the OSO clean room in Hangar AM where a visual inspection was performed.
7-21-69	Spacecraft overlays and experiment comprehensive test were performed.
7-22-69	Spacecraft comprehensive test conducted
7-22 to 7-23-69	Spacecraft supplemental test conducted
7-24-69	Sun pointing, the Rutgers experiment special test, and initial pressurization were performed
7-25-69	F-3 Day procedures were rehearsed
7-26-69	Spacecraft batteries were charged
7-28-69	F-1 Day launch stand rehearsal was conducted
7-29-69	Spacecraft moved to clean room in Building AE
7-29 to 8-1-69	Mechanical balance
8-1-69	Weighed spacecraft
8-5-69	Spacecraft erected on Pad 17A and F-3 Day test successfully conducted

The primary purpose of the OSO tests in the hangar was to verify that the observatory had survived the shipping activities without degradation. The observatory procedures used at Pad 17A are contained in BBRC document TN68-27, OSO-G Launch Tower/Payload



Countdown Procedures. These procedures were executed using the Observatory Automatic Test System computerized technique (Para. 3.8.1) for increased test speed and accuracy.

3.10 POST-LAUNCH ACTIVITIES

Liftoff of the Delta 72 launch vehicle, carrying OSO-6 into orbit about Earth, occurred at 0352 hours (EST) on 9 August 1969. During the following two years, BBRC provided operational surveillance, consulting services, data reduction, and performance analysis as required by the NASA/GSFC OSO Project Office. These post-launch activities are described briefly in this subsection.

Short-Term Activities. During the OSO-6 liftoff and early-orbit phases, selected personnel of the BBRC OSO project team were stationed at Hangars AE and AM at Cape Kennedy, and at GSFC Mission Control Center in Greenbelt, Maryland. Other BBRC personnel were assigned at the BBRC ground station (Fig. 3-19) in Boulder, Colorado. These people were on station during the liftoff, early orbit, and experiment turnon phases to acquire, reduce, and evaluate data from OSO and serve as consultants if needed. No significant problems arose during this part of the mission.

Data acquired during this short-term monitoring activity was used by BBRC in analyzing the initial temperature stabilization and battery charge rates, and in verifying spacecraft injection attitude. Spacecraft-systems performance during flight is presented in Section 2 of this report.

As directed by the GSFC project office, BBRC's post-launch support efforts at Kennedy Space Center concluded after the experiment instruments were energized. All ground-support equipment, including computer facilities and flight spare hardware were shipped back to BBRC, Boulder, Colorado.

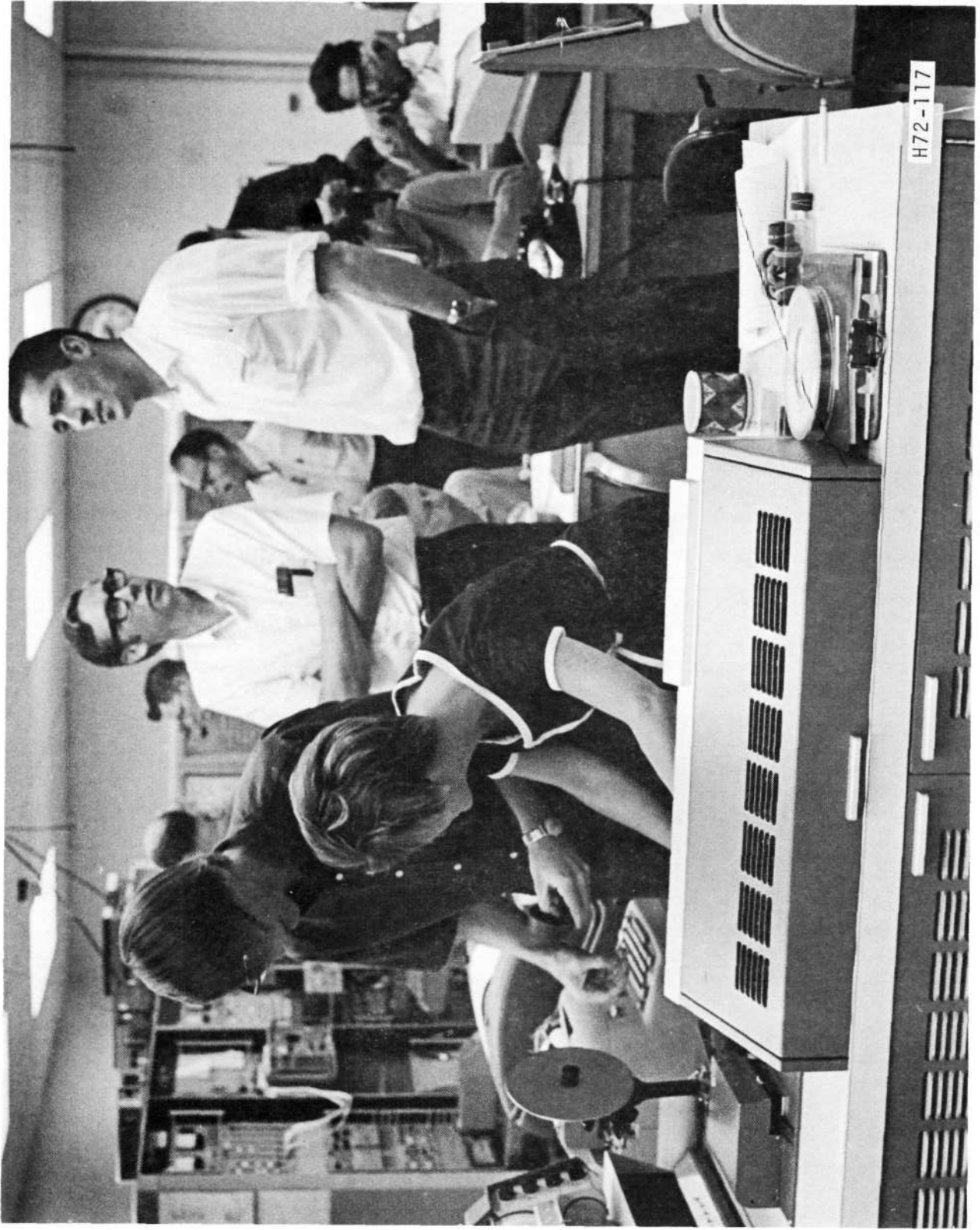


Fig. 3-19 OSO Ground Station During Launch



Long-Term Activities. Post launch support and data reduction continued at the Boulder facility for two years of orbital operation. Daily TWX information, forwarded by GSFC to BBRC, provided readouts of spacecraft performance parameters for timely evaluation by BBRC project engineers. Performance factors were then reported back to the GSFC-OSO project office as part of the monthly progress reports.

Orbit-profile and noontime plots were prepared by the BBRC-OSO data-analysis group as described in Para. 4.3. These plots were used by BBRC engineers to analyze systems performance. BBRC was thus equipped to identify problems as they developed, and to recommend remedial action when necessary.

Ultimately, analysis and interpretation of the reduced and plotted OSO-6 data were used by BBRC engineering personnel to:

- Summarize OSO-6 performance for inclusion in Section 2 of this report
- Predict performance of future observatories, and
- Recommend future spacecraft design improvement.

Subsystem performance analysis was accomplished by the engineering teams responsible for the design of the major subsystems.



Section 4

DATA REDUCTION COMPUTER PROGRAMS

Various computer software systems used to support the OSO-6 program are described in brief in this section.

4.1 EXPERIMENT PRINT ROUTINES

The OSO-G experiment data processing system provided the following basic functions:

- It interfaced with the ground station facility to enable the realtime acquisition of telemetry data and the sending of commands.
- It enabled the operator to establish the operating modes of the system, send commands, or select processing routines to decode and display the data from chosen experiments. (The operation of the system is controlled by operator instructions through the typewriter.)
- It was able to write and process magnetic tape records of the test data.

The OSO-G system employed an integrated array of hardware. The interfacing of the hardware components (observatory systems, ground station facility, and computer facility) is shown in Fig. 4-1.

The observatory data and command systems were an integral part of the system hardware. Measurement and status data from each instrument appeared in the telemetry format as presented in Section 9 (Fig. 9-2) of this report. Commands were allocated to each experiment instrument as shown in Section 10 (Table 10-1).

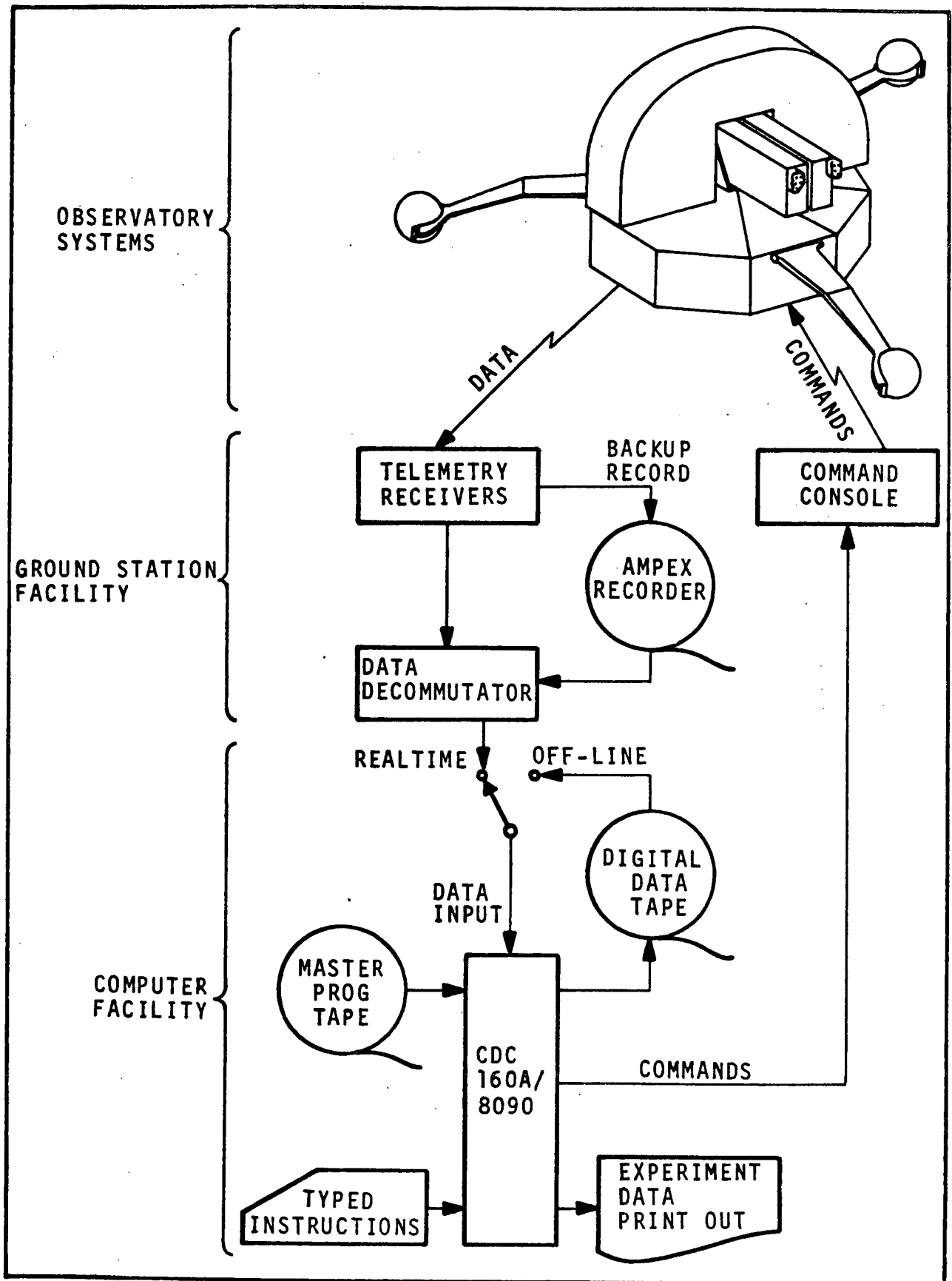


Fig. 4-1 Data Processing System Interfaces



The OSO-6 telemetry data was routed to the computer through the ground station. Radio signals from the OSO's transmitter were sent to the ground station receivers which converted the signals to a bi-phase, 800-cycle, pulse train. This endless data pulse train was grouped into 8-bit words by a telemetry decommutator. The decommutator is able to do this by observing the unique two-word main frame sync pattern. The decommutated data was then sent to the computer.

Commands from the computer were routed to the OSO through the command console which was equipped with a transmitter. This console could be monitored by a command verifier which printed a record of the commands sent.

The computer used for the testing activity was a Control Data Corporation system, consisting of:

- (1) CDC 160-A, main frame core and processing unit (8K)
- (2) CDC 161, input/output on-line typewriter
- (3) CDC 166-2, 300 line/minute printer
- (4) CDC 604, magnetic tape units (2)
- (5) CDC 165-2, plotter
- (6) Paper tape punch and reader
- (7) Friden flexowriter

Items 1, 3, 4, 6, and 7 were used in the preparation and maintenance of the experiment data processing program. Items 1, 2, 3, 4, and 6 were used in the operation of the program during testing.

A second computer system was used to provide faster turn-around times for printing of test data and permitted simultaneous test operations of the spacecraft, and an experiment, or two experiments. This second system was identical to the system specified above except that the central processor was a CDC-8090 unit. There was 100% program compatibility between the two systems.



A large portion of the experiment data processing program remained in core during testing. This portion, called the "Main Program", provided the basic capabilities of the system, including:

- Initialization of the system's operating modes, realtime operator control, and command capability.
- Input and decommutation of realtime telemetry data from the ground station.
- Realtime input/output processing for the control typewriter, printer, and paper tape reader.
- Realtime output of magnetic tape digital history tapes, and the off-line processing of these tapes.

The interpretation and display of experiment telemetry data was performed by special print or evaluation routines. Only one print routine could be selected at a time to print the status and scientific data from a given experiment. One or more special evaluation routines could be selected to run concurrently with a print routine or by themselves. Critical messages from the evaluation routines were sent to the operator via the typewriter.

The interfacing of the computer program routines and experiment print routines is illustrated in Fig. 4-2.

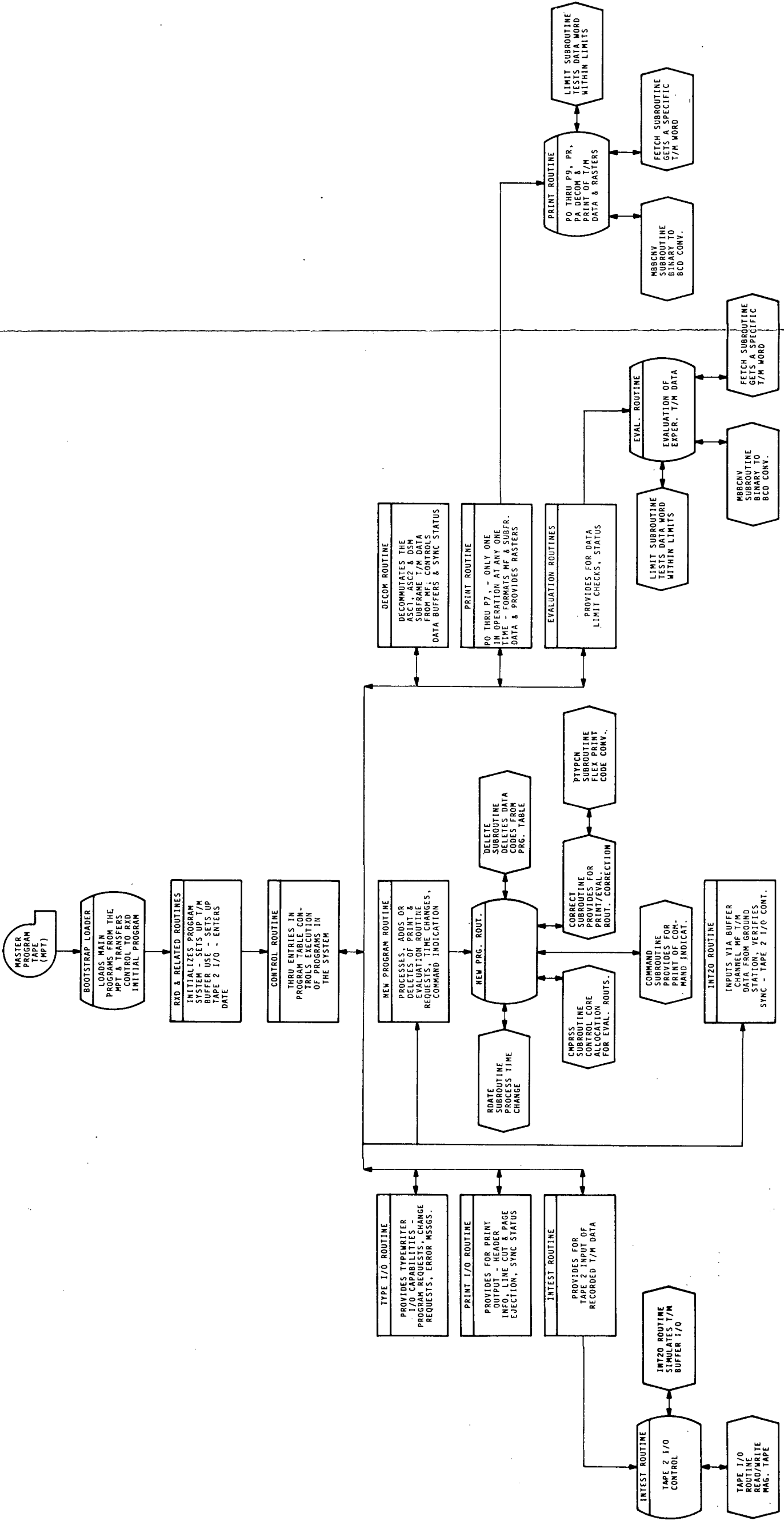


Fig. 4-2 Data Processing System

4-5



The experiment print routines decommutated individual experiment and subframe data and placed this data in the desired format for hard copy output. Each routine indicated the current sync status of the telemetry system on every detail line of print and indicated each OSO command at its occurrence. Only one routine could be in operation at a time. The routines developed were:

- P0 Main Frame Telemetry Data
- P1 Los Alamos Scientific Laboratory (Wheel)
- P2 University of Bologna (Wheel)
- P3 Rutgers State University (Wheel)
- P4 University of New Mexico (Wheel)
- P5 University College, London (Wheel)
- P6 Naval Research Laboratory (Sail)
- P7 Harvard College Observatory (Sail)

The main frame telemetry data routine (P0) extracted the 30 main frame data words from the main-frame buffer area, converted them to BCD, and moved them to a print output area. A sync check was made of the main frame and the three subframes. When any of the frames were out of sync, an asterisk was placed in the first print position; otherwise, an "S" was printed indicating full sync.

Any print routine requested following the operation of P0 required that the complete system be reloaded. This was because the loading of the P0 routine destroyed the sync ID and command indication



heading words in core. See Fig. 4-3 for the main frame print format.

To place the system in operation, a special "bootstrap loader" routine was used to load the main program from the master program tape. The loader then started the program at the initialization routine. After the operator completed his initialization instructions, the control routine started the realtime functions.

Once the system was started, the operator could select print routines, one at a time, which were loaded from the master program tape and executed in realtime. The operator could also select one or more realtime evaluation routines, which were also loaded from the master program tape. Evaluation routines could either run concurrently with a print routine or by themselves. During the realtime test activities, the operator could send commands via the computer to establish observatory or instrument operating modes. In addition, the operator had the option to write digital telemetry data output tapes for historical purposes.

Digital telemetry data tapes which were made during testing could be reprocessed by the system later. All the same data processing options were available for later processing as for realtime processing of data. Commands sent during the acquisition of the data appeared in the printouts of reprocessed data.

A typical experiment print format is shown in Fig. 4-4. The print formats for each experiment included the experiment data and any spacecraft parameters required for proper interpretation of experiment performance. Available information included the following items as appropriate:

- Telemetry sync condition
- Wheel spin rate data
- Telemetry frame count



- Day or Night condition flag
- Cumulative total of commands during print
- Observatory temperatures as required
- Main battery voltage
- Experiment operating mode
- Instrument aspect
- Az and El Raster and Point Position
- Raster signal generator monitor
- Servo coarse/fine (on target) signal
- Offset mode status
- Raster SOL or SOR signals

Use of these experiment print routines contributed greatly to accuracy and efficiency in testing instruments during the I and T phase of OSO-6 development.

4.2 OBSERVATORY AUTOMATIC TESTING SYSTEM (OATS)

The computerized system used to test OSO-6 was called OATS (Observatory Automatic Testing System). It was used with the CDC-160A computer to help execute selected OSO tests, where automation offered significant advantages over manual testing.

The OATS system had two parts - program and procedure. The program prepared the computer to print, read, and interpret steps in the procedure, and to execute automatic-type functions and verifications through ground-station equipment. The procedure was a serial description of the test. It was formatted and coded on magnetic tape for computer interpretation. The format allowed the use of language that is easily read (in printed form), even by a reader not familiar with computer language. Fig. 4-5 presents a sample page of OSO test procedure in OATS format.

The editing system used to prepare or revise OATS procedures was called "Super-Edit". Super-Edit was itself a computerized



7	ACT. BY	DIR. OF	OPERATION	ITEM
2	013 014	160A	READ AND VERIFY DSM CHANNELS SORE SPIN RATE SORE SPIN RATE	D-12(000-255) D-13(000-192) (---)
2			NOTE--THE ABOVE TWO SETS OF DSM-12 AND DSM-13 READINGS MUST BE CONSECUTIVE. USE THE TABLE BELOW ONLY IN THE EVENT OF A BREAK-DOWN IN THE AUTOMATIC-TEST SYSTEM.	
2		160A	COMPUTE SPIN PERIOD	02
2			TABLE 3-2	
	GSE-CT		-- ASPECT SPIN PERIOD CALCULATION IN DAY CONDITION -- OBTAIN TWO CONSECUTIVE SETS OF READINGS OF DSM CHANNELS 12 AND 13 AND CALCULATE SPIN PERIOD IN MSEC. (---)	
2			SET 1	
			DSM-12	--- (---)
			DSM-13	--- (---)
			4(DSM-13)	--- (---)
			TOTAL COUNT = DSM-12 + 4(DSM-13)	--- (S1) (---)
			2.5 MSEC X S	--- (T1) (---)
2			SET 2	
			DSM-12	--- (---)
			DSM-13	--- (---)
			4(DSM-13)	--- (---)
			TOTAL COUNT = DSM-12 + 4(DSM-13)	--- (S2) (---)
			2.5 MSEC X S	--- (T2) (---)
2			DSM FRAME TIME	15360 MSEC
			MINUS T1	- --- MSEC (---)
			DIFFERENCE	--- MSEC (---)
			PLUS T2	--- MSEC (---)
			SUM	--- MSEC (---)
			(SEE NOTE) DIVIDED BY	- (---)
2	011		SPIN PERIOD (1983-2023 MSEC)	---- MSEC (---)
2			NOTE-- IF T2 IS GREATER THAN T1, DIVIDE BY 8, IF T1 IS GREATER THAN T2, DIVIDE BY 7. (THE ANSWER CALLED FOR IN THE ABOVE ITEM IS THE TEST-EQUIPMENT CALIBRATION NUMBER PLUS OR MINUS 20 MSEC OR 1 PERCENT TEST-EQUIPMENT TOLERANCE.)	
2		CT	VERIFY THAT CALCULATED SPIN PERIOD IS WITHIN THE INDICATED LIMITS	(---)
2		OT	VERIFY THAT OSO IS OPERATING ON BATTERY POWER.	(---)
2		OT	CONNECT A VOLTMETER TO THE *MAIN BATT VOLT* TERMINALS AT THE BACK OF THE CONSOLE.	(---)

Fig. 4-5 Sample Page of OATS Procedure



system, consisting of edit instructions and a program which enabled the computer to accept the instructions. The computer accepted existing sources of OATS statements along with the editing instructions to produce or revise an OATS procedure. Using Super-Edit in this way saved a great deal of retyping of procedures.

4.2.1 OATS Background

Early in 1964, Experiment Accommodation personnel started using the 160A to assist in experiment testing. This was required since most OSO experiments provide data so quickly that normal ground-station printing equipment could not keep pace. Special print programs greatly simplified analysis of experiment data.

It became obvious, after a brief experience with computerized testing of experiments, that computerized testing could also be used to advantage in OSO spacecraft-systems tests. OATS proved its value very quickly, and was subsequently adapted for use on all OSO programs.

4.2.2 Description of OATS Functions

In general, there were three types of statements in an OATS procedure:

- (1) Automatic-Type Functions --
These are functions which can be performed by the computer through control of ground-station equipment.
- (2) Manual-Type Functions --
These are functions which must be performed manually by the test operator.



(3) Information Statements. --

These include explanatory notes, cautions, warnings, and information for the test operators. They generally provided all the instructions necessary for manual execution of the test.

The test engineer decided whether to computerize on the basis of his evaluation of the advantages offered in the particular test being considered. This was ordinarily determined by the number of steps in the procedure which could be adapted for automatic execution.

The OATS-system automatic functions were generally limited to ground station activities and to certain calculations. Some of these functions are described as follows:

- (1) The computer could verify main-frame and sub-commutator sync and frame length. It sampled incoming data until the sync appeared, then indicated sync and proceeded to the next step in the procedure.
- (2) The computer could receive telemetry data from any of the spacecraft subcommutators and compare it with predetermined limits. If the reading was out of limit, the computer would print an asterisk (*) next to the reading and cause that group of readings to indicate a "no go" condition. This returned control to the computer operator. If the reading was within limits, the computer advanced to the next step without manual controls.
- (3) The computer could address any OSO command decoder and execute any command. If an attempt was made to send an invalid command or address (one not listed in storage), that command was blocked and control was returned to the operator.



- (4) Several "compute" functions were incorporated into the system. These enabled the computer to perform time-consuming calculations almost instantaneously and with great accuracy.

4.2.3 Improvements in Testing Provided by OATS

When using the automatic-function features of OATS for testing OSO, a great deal of test time was saved. The magnetic-tape records of tests greatly simplified data processing efforts, and reproduction of test records. Test accuracy was improved, providing added safety to the items tested, and variations in testing were substantially reduced.

It should be pointed out that certain types of testing of tape recorders, offset mode, and others, would have been economically impractical without the automatic functions.

During testing, certain types of unscheduled operations were automatically recorded with the test data, providing a more complete record of the test. The editing process used to revise procedures saved an enormous amount of publication effort.

4.3 FLIGHT DATA PLOTTING PROGRAMS

The data-plotting techniques used to support OSO-6 post-launch operational surveillance and performance analysis were essentially the same as those used on earlier OSO's. These techniques were thoroughly tested through use in the observatory integration and test phase.

Computer programs allowed the CDC-160A computer to read OSO data from the BBRC ground station or from the digital history tapes supplied by NASA/GSFC. Special programs were used to process the data and write the processed and edited data on magnetic tape.



Further programs were used to read the processed data tapes and operate the plotter to produce graphs. The programs were designed for maximum modularity. At times when real-time and history-tape data were not available, orbit-noon data for the long-term plots was obtained from available TWX and all-channel-printout communications from GSFC. The manual plots of this data were then available for timely surveillance and analysis.

The three types of plots for which computer programs were written are described below. Samples are included in Section 2 of this report.

Orbit Profile Plots (Type A). These plots each showed the behavior of a particular parameter throughout a period of about 1.2 orbits. The ordinates were in the physical units of the parameter, and the abscissas were graduated in percentage of orbit. These graphs documented performance throughout a full day/night cycle of observatory operation. They were prepared at frequent intervals during the days immediately following launch, and thereafter monthly throughout the first six months of operation.

Long-Term Orbit-Noon Plots (Type B). These were graphs of single-sample orbit-noon values of particular parameters. The ordinates were in physical units and the abscissas were graduated in whole-number orbits. A sample was plotted from each orbit noon. The Type B machine plots gave way to similar manually-prepared plots when difficulty was experienced in obtaining digital history tapes on a timely basis. The manual plots were then used for timely surveillance and analysis of OSO-6 performance.



Refined Orbit-Noon Plots (Type C). These were similar to the Type B plots except for provisions for deleting bad data points and averaging from two to nine samples for each plot entry. Telemetry-system anomalies and transient effects were thus smoothed in the curves, making the Type C plot more useful for identifying long-term trends.



Section 5 ASPECT MEASURING SYSTEM

5.1 GENERAL DESCRIPTION

Generally, data received from an OSO experiment will not be useful unless it can be determined from what direction it came from and at what time. The measuring of these directions and recording the times at which the data was observed is called "aspect determination". An on-board aspect system is used to measure the various aspect parameters. This data is telemetered to the ground where it is processed to determine the desired aspect information such as roll attitude, pitch attitude, wheel spin rate, and the instantaneous azimuth position of any point on the wheel.

The aspect system consists of the Spin Orientation and Rate Electronics (SORE) housed in compartment 8, a flux-gate magnetometer mounted near the end of arm 4, a spin sensor (aspect eye), which is part of the spin sensor assembly mounted on the rim panel of compartment 8, and a pitch readout eye mounted on the front of the sail. This system is identical to that used on OSO-5 and experience has shown that its roll aspect accuracy is about one degree.

The heart of the coarse aspect system is the SORE assembly. Its purpose is to accept inputs from the magnetometer and the aspect eye and measure the time intervals between these signals and DSM word gate 3. The intervals are encoded into eight-bit binary words and telemetered to ground. During the day, the interval between the magnetometer and aspect eye pulses provides a means of measuring the wheel-plane angle between the geomagnetic field vector (known at all points near earth) and the



solar vector. Comparison of this angle with the known angle between the field and solar vector is then used to calculate OSO's *roll angle*. Pitch readout data is used to correct for non-alignment of the wheel plane with the solar vector. This fixes the wheel plane in local coordinates. The roll angle is then fixed in the celestial sphere by simple coordinate-system transformations.

During day, *pitch orientation* is determined from the data telemetered from the pitch readout eye. The accuracy of this sensor is better than 0.2 degree. During night, the pitch angle is extrapolated by using the pitch drift rate measured during the day, and can easily be predicted to within 0.2 degree.

The *wheel spin rate* is found within $\pm 1\%$ by using the period of either of the two once-per-revolution signals. The SORE does this by measuring the intervals between consecutive magnetometer pulses or aspect eye pulses. As a backup, the spin rate can also be calculated using data from channel 12 of the wheel ASC. Of the two methods, the first is the most accurate and can also be used to compute the night spin rate while the latter cannot.

The same data used for spin rate computation is also used to calculate the instantaneous *azimuth position* of a point on the wheel. During orbit-day, the solar vector is used as the reference; during orbit-night, the geomagnetic field vector is used. Time correlation is referenced to DSM word gate 3.



5.2 ASPECT GEOMETRY

5.2.1 Coordinate Reference Systems

The five coordinate systems (experiment, spacecraft, ecliptic, celestial, and topocentric) are shown in Fig. 5-1. It is possible to go from any one system directly to any other; for practical reasons, however, a logical sequence of transformations is performed. For example, instead of direct transformation from the experiment system to the topocentric system, we proceed in four steps: Experiment \rightarrow Spacecraft \rightarrow Ecliptic \rightarrow Celestial \rightarrow Topocentric.

Coordinate system rotations are sufficient to arrive at the final aspect description required of OSO. Translations of systems are not necessary since the center of mass of the observatory can be considered the center of every coordinate system, due to the negligible parallax resulting from the separation of the spacecraft and earth centers.

The experiment coordinate systems and look axes, the magnetometer sensitive axis, and the aspect eye reference all rotate in the spacecraft coordinate system. The relationships between these elements are established by the wheel spin rate and a series of preflight calibration measurements.

Experiment Coordinate Systems. A separate system is defined for each experiment. The X-axis is always defined to be the experiment's line of sight. For convenience, the Y-axis is allowed to lie in the wheel plane so that only two rotations are needed for transformations between experiment and spacecraft systems. The X-axis need not lie in the wheel plane.

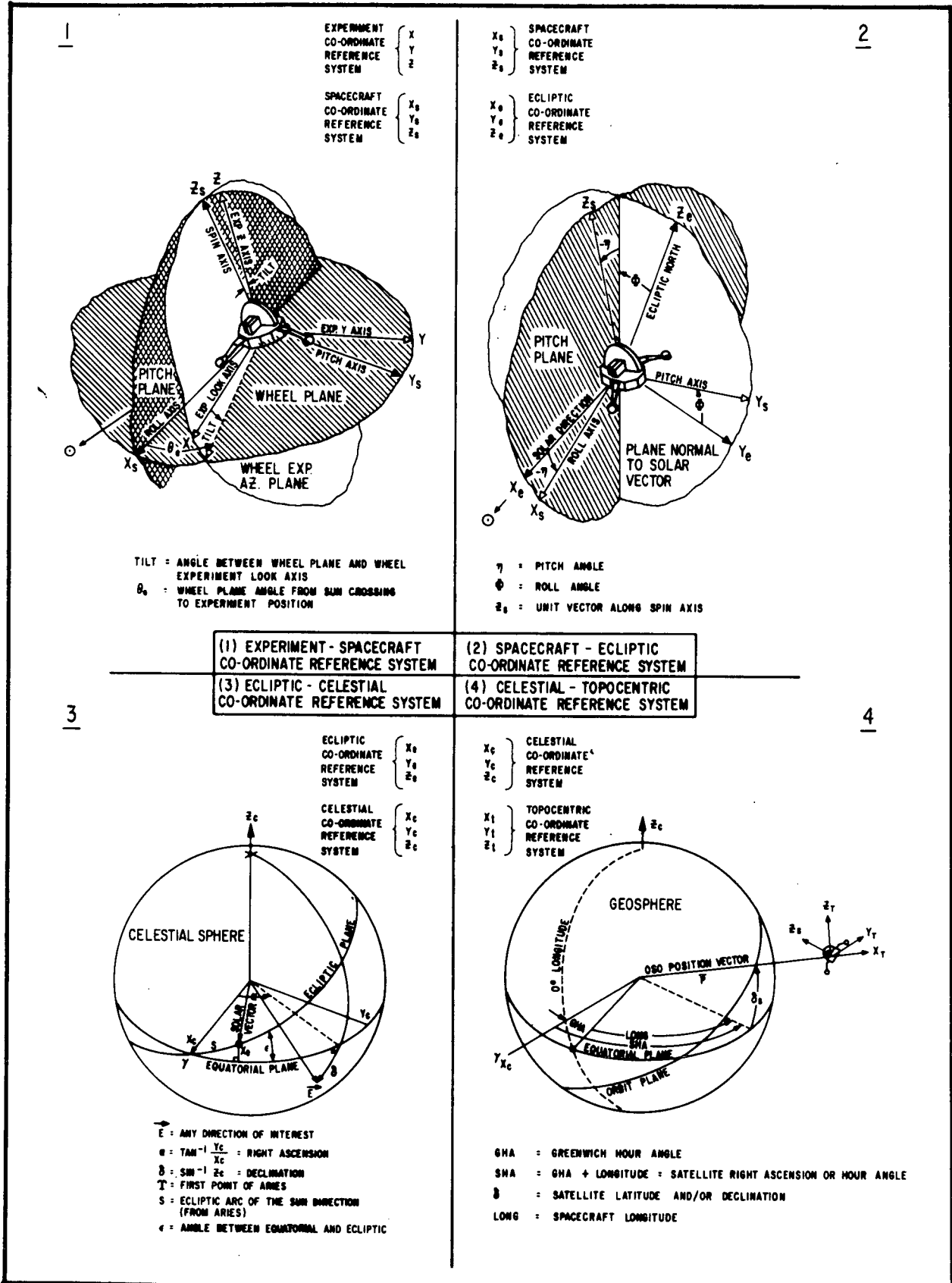


Fig. 5-1 OSO Aspect Coordinate Systems



Spacecraft Coordinate System. As seen in Fig. 5-1 (1), the spacecraft X, Y, and Z-axes are the roll, pitch, and spin axes, respectively. Also, note that the offset between the roll axis and the solar vector is simply the pitch angle (η). The wheel plane includes the roll axis and pitch axis and is perpendicular to the spin axis.

Ecliptic Coordinate System. This system is defined with the X-axis pointing from the center of the spacecraft to the sun's center. The Z-axis lies along the ecliptic pole and the Y-axis forms an orthogonal right-handed system, lying in the ecliptic plane. Note that this ecliptic system differs from the conventional ecliptic system which has the X-axis pointing to the vernal equinox.

Celestial Coordinate System. This is the conventional celestial coordinate system except that the origin may be considered either at the earth's center or at the spacecraft center of mass (interchanged at will without a significant loss of accuracy). Thus, the Z-axis is parallel to the earth's polar axis pointing north, the X-axis points to the vernal equinox and the Y-axis points 90° east of the vernal equinox in the equatorial plane forming an orthogonal system.

Topocentric Coordinate System. The topocentric system is defined with the X-axis directed upward along the local vertical (from spacecraft center of mass out from the earth's center). The Z-axis lies in the local horizontal plane (perpendicular to the X-axis) and points to the north. The Y-axis forms a right-hand orthogonal system pointing east in the horizontal plane.

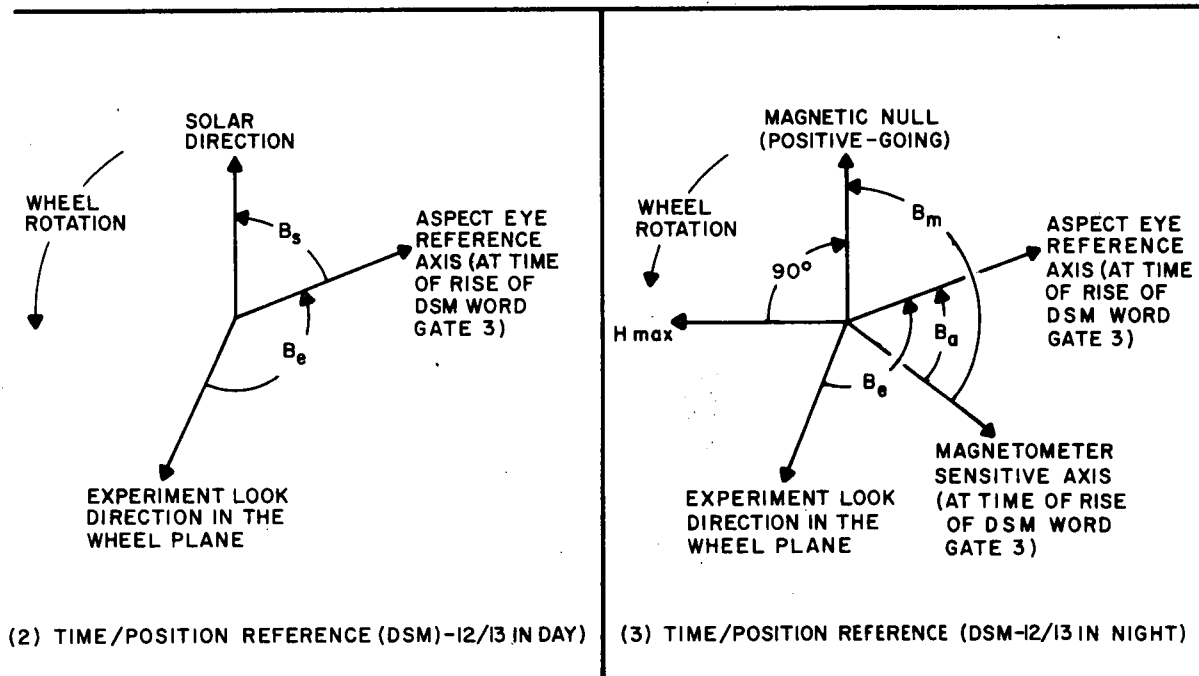
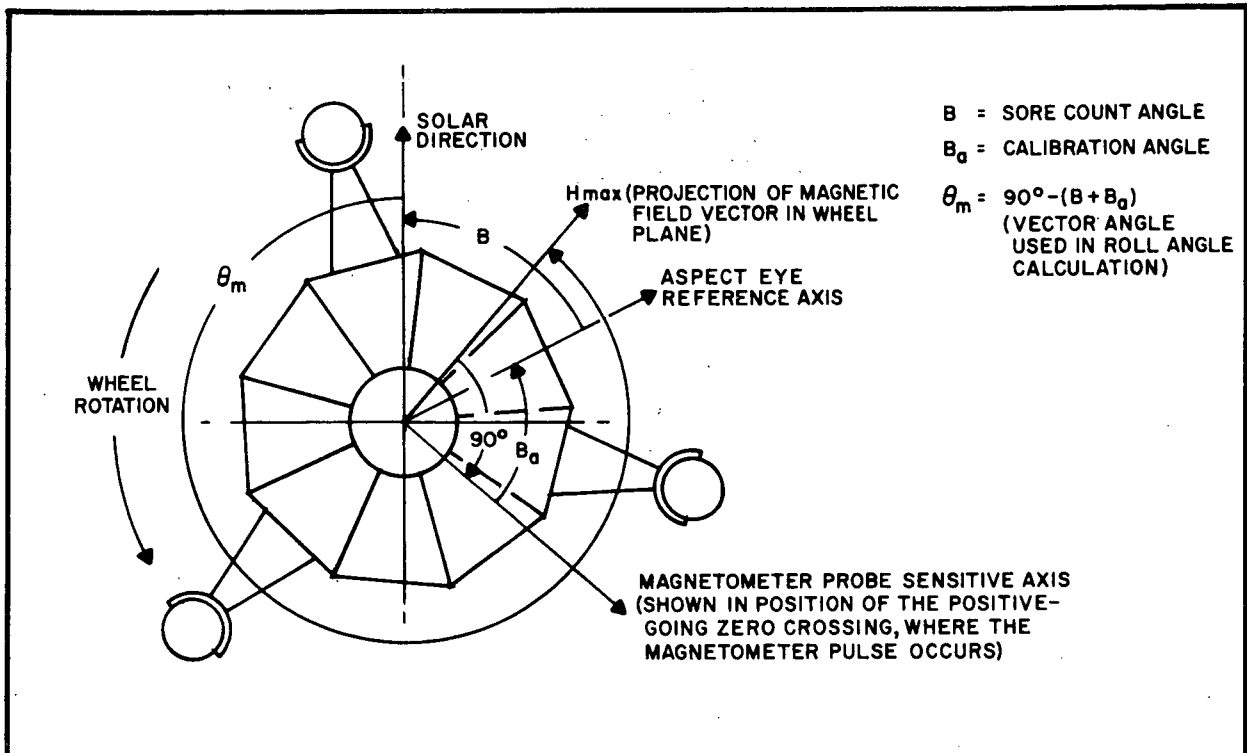


5.2.2 Definitions of Angles Used to Determine Aspect

There are seven angles used in determining the various aspect parameters of OSO and its experiments. These angles are shown in Fig. 5-2 and are described below:

Pitch angle (η)	- The angle between the wheel plane and the solar vector (See Fig. 5-2).
Sun-to-Mag (θ_m)	- The angle (measured in a ccw direction) between the solar vector and the rising zero crossing of the geomagnetic field by the magnetometer.
Mag-to-Sun (β)	- The angle (measured in a ccw direction) between the magnetometer zero crossing and the solar vector.
DSM3-to-Sun (β_s)	- The angle (measured in ccw direction) between the occurrence of word gate DSM-3 and the solar vector.
DSM3-to-Mag (β_m)	- The angle (measured in a ccw direction) between the occurrence of word gate DSM-3 and the magnetometer zero crossing.
Mag-to-Aspect Eye (β_a)	- The acute angle between the magnetometer axis and the aspect eye axis.
Exp-to-Aspect Eye (β_e)	- The angle (measured in a ccw direction) between the look axis of any wheel experiment and the aspect eye axis.

The purpose and the data source for the above angles are listed below. The aspect computations are described in subsection 5.4.



NOTE: ALL ANGLES SHOWN ARE MEASURED IN THE WHEEL PLANE AS SEEN LOOKING FROM THE SAIL DIRECTION. THE ASPECT EYE REFERENCE AXIS, EXPERIMENT LOOK DIRECTION, AND MAGNETOMETER SENSITIVE AXIS, ARE ALL FIXED IN THE WHEEL AND ROTATE WITH IT. THE SOLAR DIRECTION AND H_{max} LINES ARE A FUNCTION OF GEOGRAPHIC LOCATION IN ORBIT.

Fig. 5-2 Geometry of SORE Count Angles



- η - obtained directly from telemetry on sail ASC channel 4 and converted to engineering units by use of OSO-6 Data Conversion Tables (TN68-16); used in the computation of roll attitude.
- θ_m - Computed from relationship of $\theta_m = 90^\circ - (\beta + \beta_a)$; used in the computation of roll attitude and wheel azimuth position at night.
- β - Obtained from SORE telemetry data on DSM channels 32 and 33; converted to an angle by the relationship:

$$\text{Angle(deg)} = \frac{\text{SORE count}}{400 \text{ bps}} \times \text{wheel spin rate (in rps)}.$$
 Used in the computation of θ_m .
- β_s - Obtained (during day only) from SORE telemetry data on DSM channels 12 and 13; converted to angle same as β ; used in the computation of wheel azimuth position during day and during night by a special computation method.
- β_m - Obtained (during night only) from SORE telemetry data on DSM channels 12 and 13; converted to angle same as β ; used in the computation of wheel azimuth position during night.
- β_a - A physical property of OSO and is measured before flight; used in computation of θ_m (day or night) and wheel azimuth position during night only.
- β_e - A physical property of OSO and is measured before flight; used in computation of wheel experiment azimuth position.



5.3 ASPECT SYSTEM ELECTRONICS

5.3.1 Magnetometer

The function of the magnetometer is to indicate reversals of the geomagnetic field by providing a signal when its sensitive axis is perpendicular to the field. OSO-6 used the same type magnetometer used on all earlier OSO's. It is a flux-gate magnetometer built by Schonstedt Instrument Company and produces a dc voltage proportional to the geomagnetic field. A zero-crossing detector in the SORE is used to produce a pulse when reversal of the geomagnetic field is sensed.

The magnetometer consists of an oscillator, sensor, signal amplifier, and demodulator (Fig. 5-3). The oscillator provides an alternating current large enough to cyclically drive the core into magnetic saturation. If there is no external magnetic field acting on the core, the core saturates equally both the positive and negative portions of the cycle. As a result, the flux generated in the core has a symmetrical pattern. If there is a magnetic field acting on the core, the core remains saturated longer on one-half of the cycle than on the other. The flux generated in the core has an asymmetrical waveform containing even order harmonics of the excitation frequency, not present in the symmetrical flux pattern. For weak magnetic fields such as that of the earth, the even harmonics are proportional in magnitude to the intensity of the applied magnetic field.

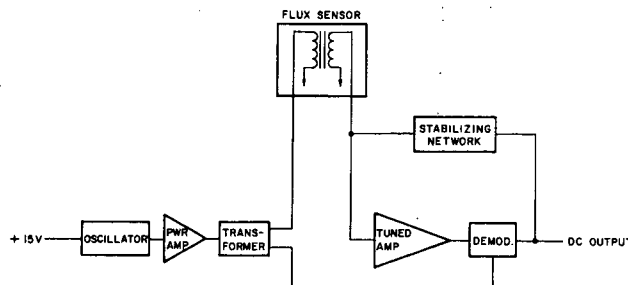


Fig. 5-3 Flux Gate Magnetometer



The amplifier signal from the oscillator excites the primary winding on the sensor. The signal from the sensor secondary passes through an amplifier tuned to the second harmonic of the oscillator frequency. The amplitude of this frequency is proportional to the strength of the magnetic field at the sensor. Using a second harmonic reference voltage (derived from the same transformer that drives the sensor) the signal is demodulated thus producing a dc output voltage proportional to the strength of the earth's magnetic field. A negative feedback network from the output to the sensor secondary is used to temperature-stabilize the circuit and provides automatic gain control.

5.3.2 Pitch Readout Sensor

The pitch readout sensor is identical to the one used on all earlier OSO's. The sensor consists of an analog sun-sensing unit and electronic signal-conditioning circuitry all contained in a common housing. It is mounted on the sail with its optical axis parallel to the spacecraft's X-axis.

The sensing unit consists of a filter/reticle and a pair of silicon photovoltaic cells arranged as shown in Fig. 5-4. The beam of sunlight that goes through the slit in the reticle falls equally on the two cells at null. As the angle between the sun-line and the sensor axis increases, the energy on one cell increases and decreases on the other.

The cells are hooked up in parallel opposition. The resulting output is linear to approximately ± 6.5 degrees (where the light beam no longer falls on one of the cells). Beyond 6.5 degrees, the output continues to increase slightly until the entire beam of light is on one cell. The output then stays constant until the light beam begins to move off the cell. The total field-of-view of the sensor is about ± 25 degrees. The electronics

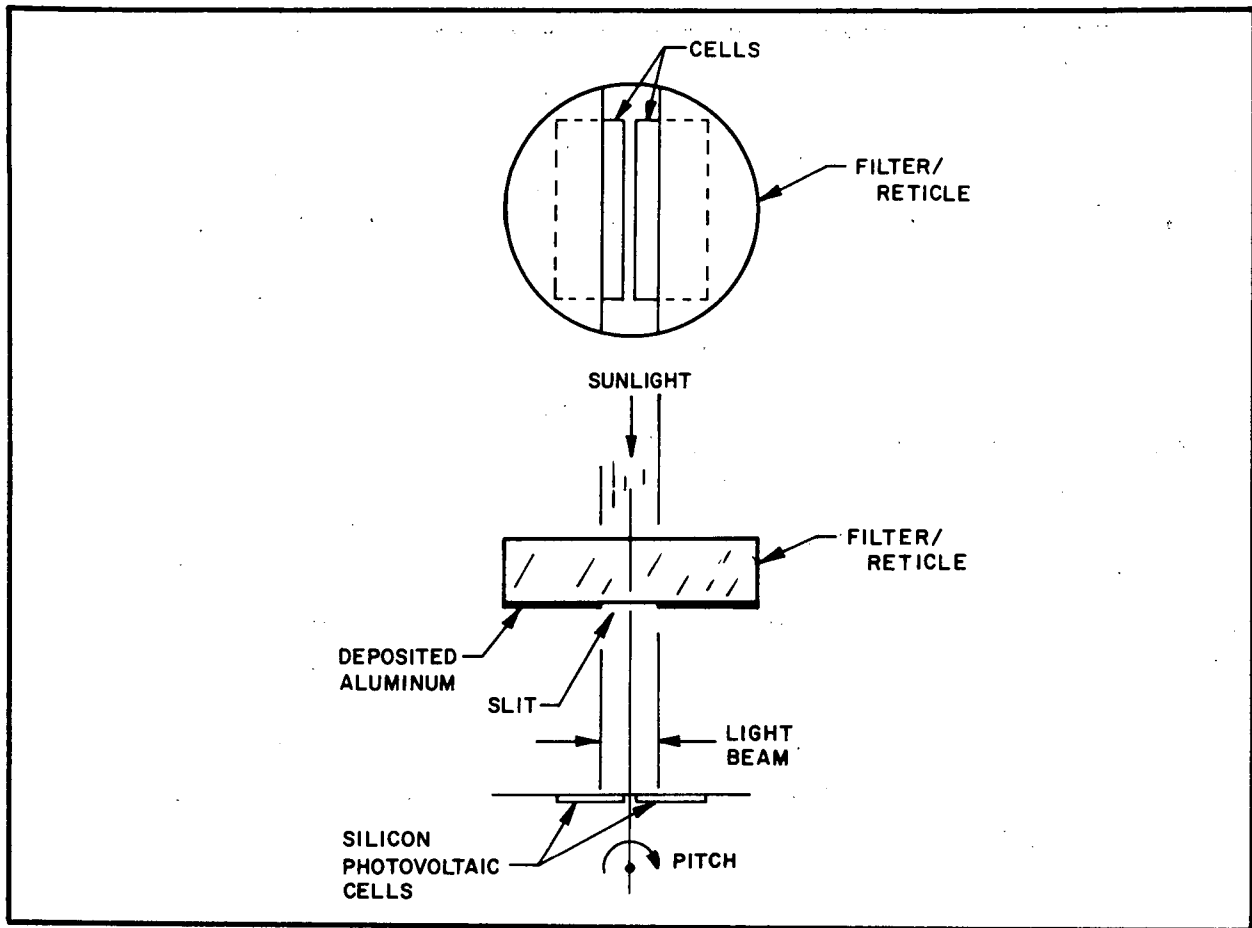


Fig. 5-4 Diagram of Pitch Readout Sensor

serve to limit the output of the sensor at an angle corresponding to about ± 5.5 degrees, resulting in the overall output-versus-angle characteristics shown in Fig. 5-5. This is typical output-versus-angle curve for a unit with a 0 to 5 v output range.

5.3.3 Spin Aspect Sensor

The aspect sensor is part of the spin sensor assembly and is identical to that used on earlier OSO's. The spin sensor assembly is an array of four spin target detectors on an aluminum block, mounted on the rim of the wheel, with its sensing plane parallel to the spin axis. (See Section 7.)

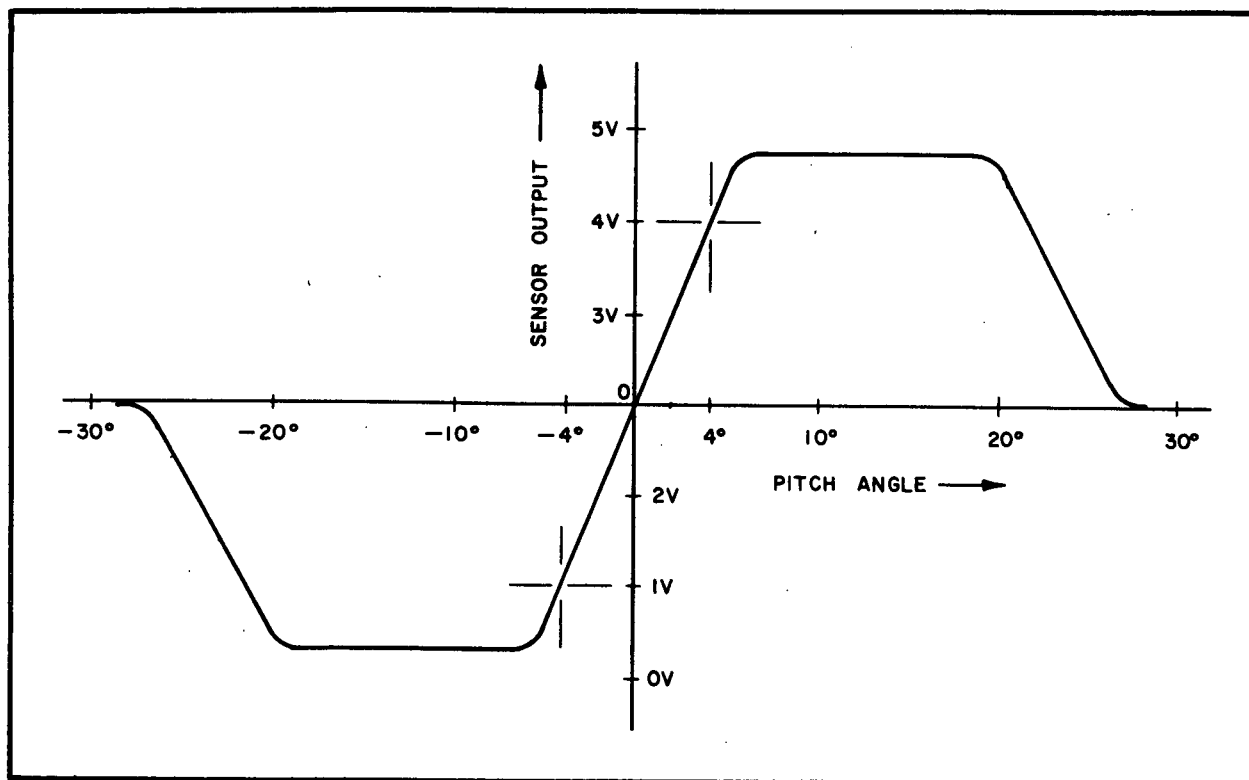


Fig. 5-5 Pitch Readout Sensor Output Curve

Each of the four spin target detectors consists of a housing, lens, aperture plate, filter, and a silicon photovoltaic cell (Fig. 5-6). The copper foil aperture plate is located in the focal plane of the lens and the slit in the aperture plate defines a long, narrow field-of-view, 26 degrees \pm 2 degrees in elevation and 2.5 degrees \pm 0.5 degree in azimuth. The target detectors are mounted so that the field of view of two of them are symmetrical about a line perpendicular to the spin axis while the other two are canted up 3 degrees and down 3 degrees in elevation, respectively. The outputs of the two canted detectors go to the automatic spin control system. The other two detectors provide outputs for the SORE package and the spin rate limit detector in the spin control assembly.

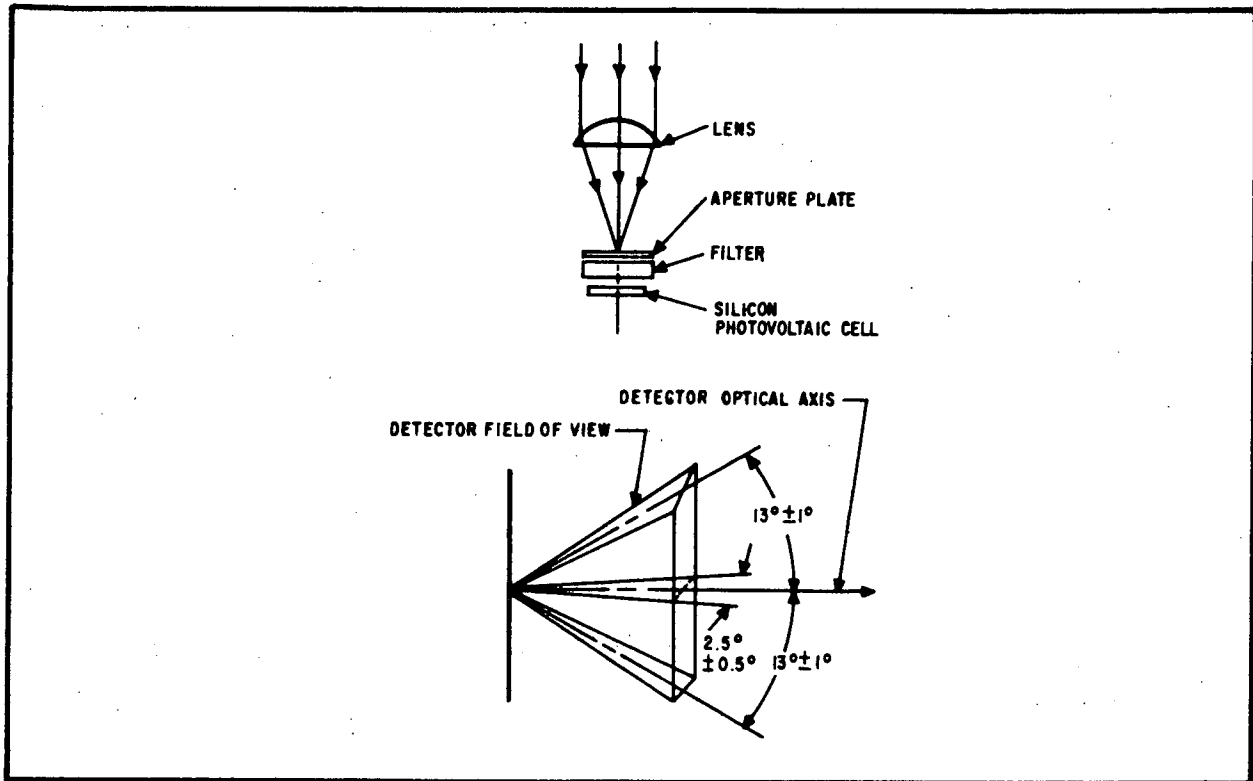


Fig. 5-6 Aspect Detector

5.3.4 Spin Orientation and Rate Electronics (SORE)

The purpose of the SORE is to measure (in telemetry counts) the period between: magnetometer pulse to sun pulse (β), DSM word gate 3 to sun pulse (β_s) and DSM word gate 3 to magnetometer pulse (β_m). These periods are telemetered to the ground where they are converted to angles and used for computing spin rate, roll angle, and wheel azimuth position (see paragraph 5.4). Figure 5-7 is a block diagram of the SORE and Fig. 5-8 is a timing diagram.

- *Measuring DSM-to-sun (β_s) and DSM-to-mag (β_m) Periods*

The sequence starts with the 400 bps clock (the result of dividing the 800 bps clock by 2 in the clock amplifier) being grounded through flipflops (FF) 1, 3, and 4. DSM word gate 3 then occurs and changes the state of FF 1, thus allowing the

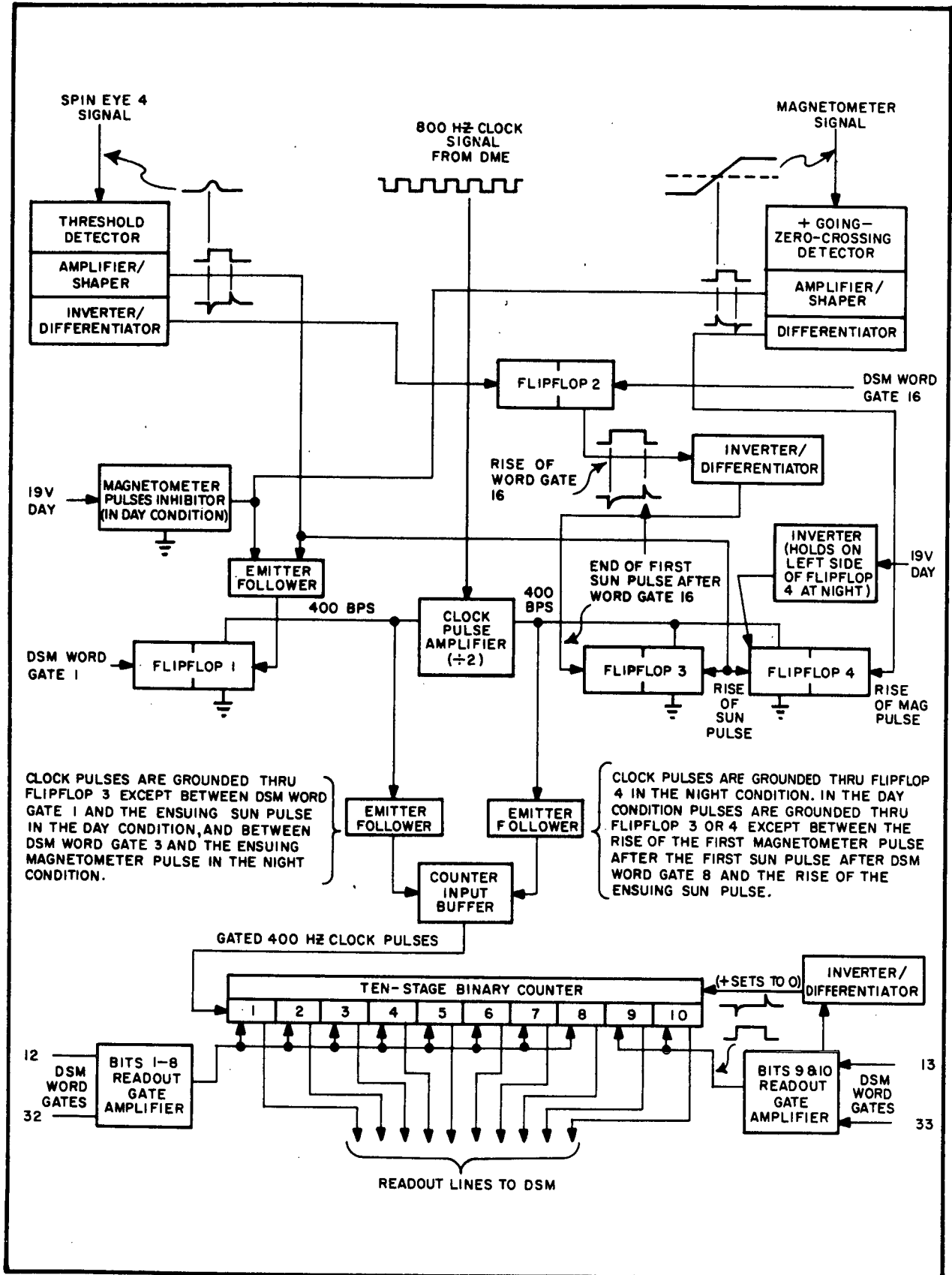
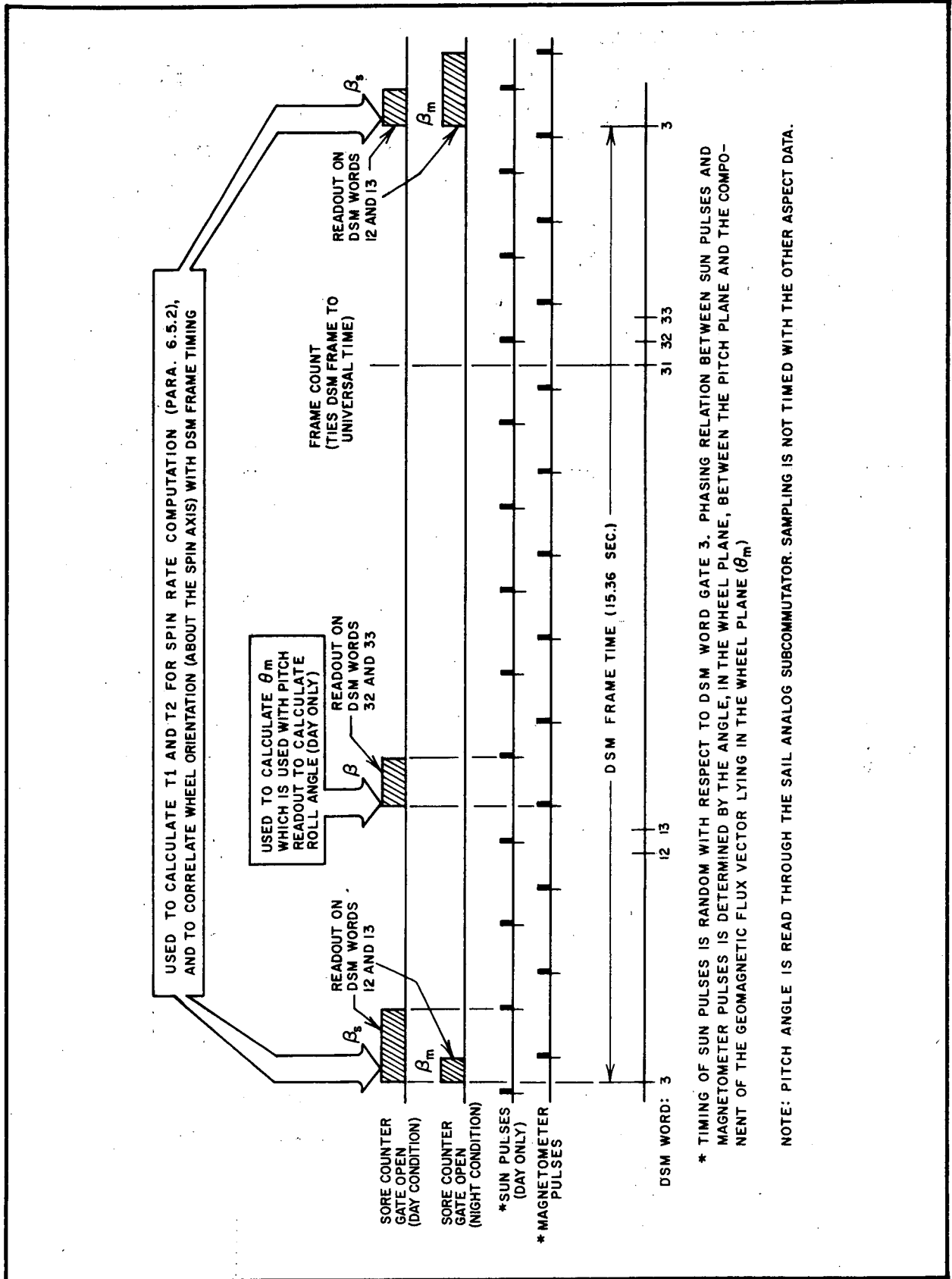


Fig. 5-7 SORE Block Diagram



* TIMING OF SUN PULSES IS RANDOM WITH RESPECT TO DSM WORD GATE 3. PHASING RELATION BETWEEN SUN PULSES AND MAGNETOMETER PULSES IS DETERMINED BY THE ANGLE, IN THE WHEEL PLANE, BETWEEN THE PITCH PLANE AND THE COMPONENT OF THE GEOMAGNETIC FLUX VECTOR LYING IN THE WHEEL PLANE (θ_m)

NOTE: PITCH ANGLE IS READ THROUGH THE SAIL ANALOG SUBCOMMUTATOR. SAMPLING IS NOT TIMED WITH THE OTHER ASPECT DATA.

Fig. 5-8 SORE Timing Diagram



clock pulses to enter the 10-bit counter. The counter registers these clock pulses until the occurrence of either the next sun pulse (when in the day condition) or the next magnetometer pulse (when in the night condition). Either of these two pulses stop the count by setting FF-1 back to the state which grounds the counter input. The magnetometer pulses are kept from reaching FF-1 in the day condition by an inhibitor. The count so loaded into the counter, (which represent β_s in day and β_m at night), remains in the counter until DSM WG-12, at which time the first 8 bits are read out in the DSM subframe. The 2 most significant bits are then read out by DSM WG-13, the trailing edge of which clears the counter.

● *How the Mag-to-Sun (β) Period is Measured*

First, WG-16 sets FF-2 to its positive state. The following sun pulse sets it back to its negative state, and an inverted differentiated pulse sets FF-3 to the state in which it does not ground the clock pulses. The same sun pulse, however, sets FF-4 to the state which does ground the input to the counter. The following magnetometer pulse, then, sets FF-4 to the state which allows the clock pulses to enter the counter. The count registers until the leading edge of the sun pulse, which then grounds the clock pulses through FF-3 and FF-4. The count representing β remains in the register until WG-32. Meanwhile, FF-3 continues to block the input to the counter, while FF-4 cycles on and off with each magnetometer and sun pulse.

The first 8 bits of the count representing β are read out on DSM word 32. The 2 most-significant-bits are then read out on WG-33, the trailing edge of which clears the counter. DSM-3 starts the sequence over again 15.36 seconds later.



During orbit night, the absence of spacecraft day power is used to hold FF-4 in the condition which grounds the DSM 32/33 count, thus inhibiting this count in the night condition.

5.4 ASPECT COMPUTATION

This section describes the methods used in reducing PCM data from which the aspect or orientation of OSO-6 is determined.

Pitch angle reduction, spin rate calculations, frame counter operation, roll angle calculation, and spin axis and wheel azimuth position are covered. Of these, only the pitch angle and frame count are obtained directly from the OSO-G Data Conversion Tables (BBRC Doc TN68-16). The other parameters require calculations. The methods for these calculations follow.

5.4.1 How Wheel Spin Rate Is Calculated

The spin rate of OSO-6 is computed by two independent means. The first uses the data obtained from ASC 1, channel 12; the second uses DSM data. Of the two methods, the latter is the most accurate and can be used to compute the night spin rate while the first cannot.

● *Calculating Spin Rate From ASC Data*

When calculating wheel spin rate using ASC data, the telemetry count received on wheel ASC channel W-12 must be converted to integer steps from the data conversion tables (TN68-16). The 0 - 255 bit count corresponds to steps from 1 to 32. The step count advances one digit each wheel revolution and recycles to 1 after the count reaches 32.



In computing spin rate using this method the following procedure is used:

- (1) Record "n" number of successive data readings from W-12.

NOTE:

The accuracy of spin rate calculation is directly proportional to the value of "n". The actual error term is:

$$\pm \frac{1}{15.36 (n - 1)}$$

- (2) Convert the initial data reading and the final data reading to steps using nomograph W-12 in TN68-16.
- (3) Examine the above data and determine the number of counter resets (a reset is indicated when a data reading is less than the data reading immediately prior to it).
- (4) From the following formula calculate Δ steps (or revolutions):

$$\text{revolutions} = 32 (\text{CR}) + R_f - R_i$$

where

CR = number of counter resets
 R_i = initial reading (step number)
 R_f = final reading (step number)

- (5) Calculate the spin rate (SR) by substituting the values for n and Δ steps into the following formula:

$$\text{SR} = \frac{\text{revolutions}}{15.36 (n - 1)}$$

where

n = number of data readings

C.4



5.4.2 Calculating Spin Rate from SORE Data

The following formula is used when computing the day wheel spin rate, or the approximate night spin rate*, using the data from DSM channels 12 and 13:

$$\text{Spin Rate (rps)} = \frac{N}{15.36 + 0.0025 [(12_2 + 4 \times 13_2) - (12_1 + 4 \times 13_1)]}$$

where

12_1 , 13_1 , and 12_2 , 13_2 are consecutive readings of DSM channels 12 and 13.

N is an integer determined by dividing 15.36 by the approximate period of rotation (normally about 2 seconds). The larger whole integer quotient is used if the quantity $(12_1 + 4 \times 13_1)$ is smaller than $(12_2 + 4 \times 13_2)$. The smaller whole integer quotient is used if $(12_1 + 4 \times 13_1)$ is larger than $(12_2 + 4 \times 13_2)$.

NOTE:

The "15.36" in the equation is the recycle time of the DSM, and is the time between consecutive occurrences of words 12 and 13. The "0.0025" term is the period of the 400 bps clock obtained by dividing the 800 bps clock by 2.

*The computer software systems have provisions for accurately computing night-time spin rate. To do this, the drift in the geomagnetic field between DSM outputs is computed and accounted for in the spin rate computation. Because of the complexity of this operation, the method is not described here.



5.4.3 How Frame Counter is Used to Establish Time Reference

A reference frame count must be established and correlated with the corresponding universal time before roll aspect or wheel night azimuth position can be computed. Also, it must be known approximately when the frame counter will reset, because, with the 800 bits/sec. telemetry system, the frame counter resets twice in each orbit and, therefore, no one frame count number is unique for a particular orbit.

Channel 36 of the DSM contains the DSM frame count and steps once every 15.36 seconds which is the recycle time of the DSM. This channel indicates the frame count from 0 to 255 and resets every 65.536 minutes ($256 \times \frac{15.36}{60} = 65.536$).

The time (T_{θ}) at which the aspect data were taken must be known to determine the observatory's geographic position in the magnetic field. This time is calculated as follows:

$$T_{\theta} = \text{U.T. (ref)} - [\#36 (\text{ref}) - \#36_{\theta_m}] 15.36 \text{ sec.} - 12 \pm 1 \text{ sec.}$$

where

U.T. (ref) is the universal time of frame count reference word #36 (taken near the end of the given orbit by a STADAN station)

$\#36_{\theta_m}$ is the frame count word just preceding DSM words 32 and 33 that were used for the calculation of θ_m .

12 ± 1 sec. is the approximate time interval between the actual measurement of θ_m and the time of frame count word $\#36_{\theta}$.



Section 6 DYNAMICS

6.1 INTRODUCTION

After injection into orbit the OSO spacecraft will try to maintain, because of its gyroscopic properties, a constant orientation with respect to the celestial sphere. The spin rate will remain constant unless the spacecraft is acted upon by external torques. In the absence of external torques, the spacecraft spin axis needs only to be precessed enough to keep it normal to the earth-sun line. If the spin axis is in the ecliptic plane, this requires 360 degrees of correction a year; if the spin axis is normal to the ecliptic plane, no pitch correction is required.

However, both internal and external torques do act on OSO. They cause changes in both the position of the spin axis and in the spin rate of the wheel. Some of these torques also produce nutation which must be damped out. The following is a discussion of the sources of these internal/external torques, their influence on OSO, and how their effects are controlled.

6.2 ROTATIONAL DYNAMICS OF OSO (HOW OSO BEHAVES AS A GYRO)

The OSO behaves much like a simple, single-body gyroscope. Some of the similarities and differences between the OSO and a gyroscope are discussed in the paragraphs that follow.

6.2.1 The Basic Differences Between OSO and the Simple Gyroscope

The simple gyro and OSO are similar in that they both display "gyroscopic rigidity". This characteristic is due to the rotation of a body about an axis (called the spin axis) which



itself may or may not be rotating about some other axis. Because of this single mutual characteristic, the two bodies behave according to basic gyroscopic principles. There are, however, some significant differences that make the motion of OSO much more complicated than the simple gyro. The simplified analysis, then, does not accurately describe this complex motion. Some of the more important differences are:

- (1) The simple gyro is usually considered to be a rigid body (i.e., not consisting of flexible parts); OSO is semi-rigid.
- (2) The spin rate of the simple gyro is normally assumed to be thousands of times greater than any other angular rates (e.g., precession and nutation rates); with OSO these other angular rates are relatively large.
- (3) The simple gyro consists of a single rotating body; OSO consists of two bodies one of which is constantly spinning (the wheel), while the other (the sail) is alternately being spun-up and de-spun as OSO makes transitions from orbit-day to orbit-night and vice versa. Also, the pointed instruments give the MOI of the sail a time-varying character.
- (4) The simple gyro is acted upon only by external torques; OSO is acted upon by both external and internal torques. The internal torques come from the elevation and azimuth servos, the nutation damper, and other non-rigid components.



6.2.2 The Rotational Dynamics of OSO

The following is a discussion of dynamic properties of OSO:

- *Definition of Nutation, Precession and Wobble.*
The OSO is a spin-stabilized satellite with a biaxial pointing control. The satellite "precesses" and "nutates" when external and interbody (internal) torques are applied and "wobbles" when the spinning part is not perfectly balanced. Both nutation and wobble disrupt spin axis inertial stability (with oscillatory periods of a few seconds), and contribute to short-term pointing instability (jitter) of the pointed instruments.

The coning motion of a balanced, symmetrical satellite that is slightly disturbed from a condition of "pure spin" about its symmetry axis is referred to as "nutation". The term "precession" is used to describe the motion of the angular momentum vector during application of external torques. Both precession and nutation occur during application of external torques. Short-term interbody torques are produced only by the azimuth and elevation servos, which also effect the nutational motion of OSO.

The term "wobble" is used to describe the "steady state" motion which results from imperfect balance of the wheel. Wobble and nutation may be present simultaneously.



- *Motion of OSO's Spin Axis During Pitch Precession.*
To adjust OSO pitch attitude, control torques are applied about the X-axis (roll axis) by means of gas jets. These torques cause precessional motion about the Y-axis (pitch axis). The pitch control circuits and gas system, described in detail in Section 7, are designed to keep the spin axis aligned to within 3 degrees of perpendicular to the solar direction. The spacecraft dynamics associated with this system are discussed here. In this analysis of pitch precession we will first present the gyroscopic motion of a rigid, symmetrical OSO being constantly torqued, the motions of the same OSO after the external torquing has been removed, and finally a non-symmetrical OSO being torqued.

Because OSO's spin rate is much slower than that assumed for the simple gyro, the basic equations of motion during precession do not hold true. To be specific, the spin rate of the simple gyro is usually sufficient to essentially eliminate any nutation while the spin axis is being precessed. Thus, the spin vector (\bar{S}) is always coincident with the angular momentum vector (\bar{H}) and, therefore, the precessional motion of the spin axis can be described by simple equations. With OSO, however, the spin rate is low enough (about 0.5 rps) that \bar{S} follows a cycloid path instead of a straight line path as does \bar{H} . This cyclical motion (called nutation) is depicted in Fig. 6-1*.

* The spin axis in Fig. 6-1 is shown laying in the horizontal plane so that an edge view could be obtained of the pitch plane in order to illustrate the motion of \bar{H} and \bar{S} more clearly.

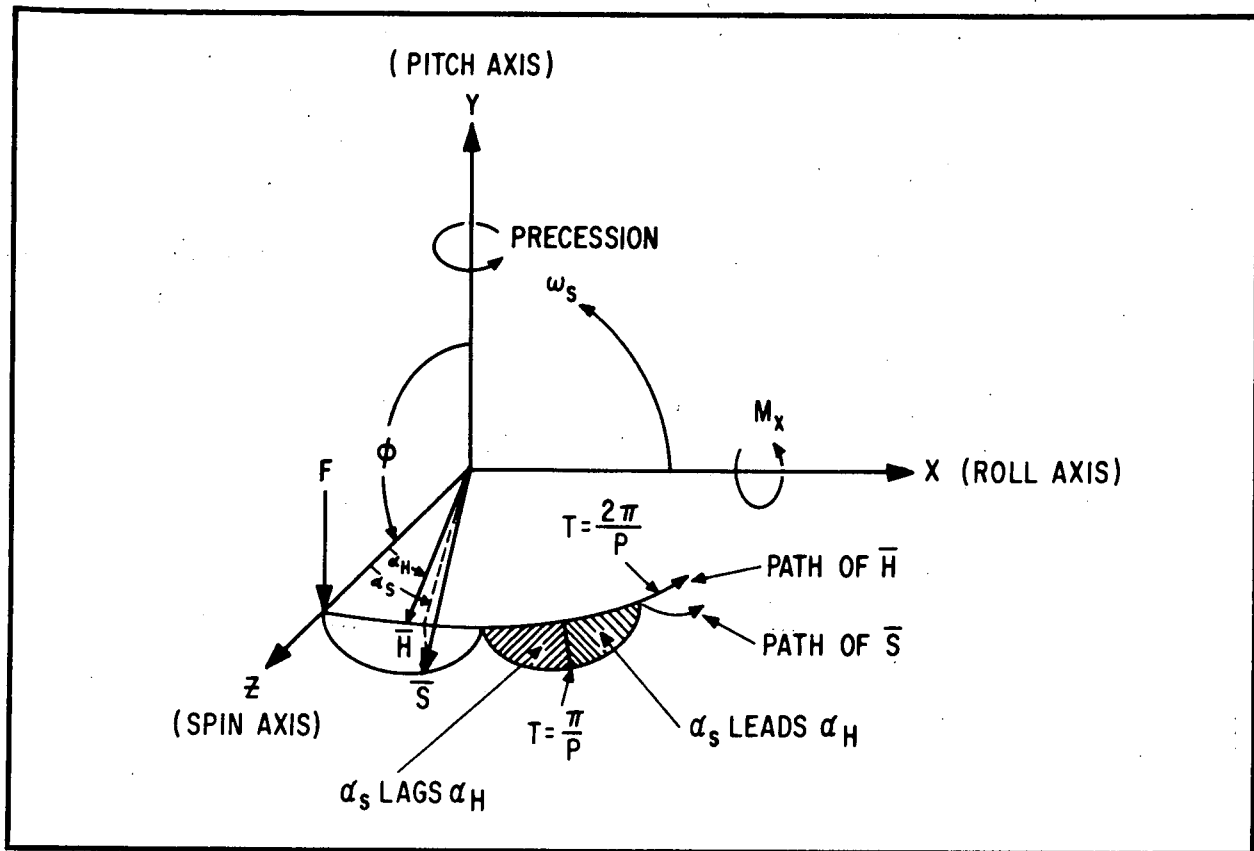


Fig. 6-1 Motion of \bar{H} and \bar{S} During Pitch Precession

In this figure, the x , y and z axes are shown as they would appear before the pitch thrust (F) is applied to the spin axis. After the pitch-down jet is activated, the product of F and its distance from the center of gravity of the spacecraft results in a torque (M_x) about the roll axis. Then by using the RH rule, we find that M_x actually causes the spin axis to rotate (precess) toward the roll axis. The paths of \bar{H} and \bar{S} during precession are shown as vectors with the precession angles in the XZ plane represented by α_H and α_S , respectively. Because the \bar{H} vector moves only in the XZ plane, it always makes an angle of $\theta_H = \frac{\pi}{2}$ radians with the pitch axis. The \bar{S} vector, however, moves



in both the XZ and YZ planes and, therefore, it makes an angle of $\frac{\pi}{2} + \theta_S$ with the pitch axis.

Figure 6-2 is a computer simulation of a 20-second pitch correction showing the nutation produced by such a maneuver. The decaying nature of θ_S is due to the action of the nutation damper.

- *Motion Equations of \bar{H} and \bar{S} During Precession (Symmetrical OSO).* The motion of \bar{H} and \bar{S} during precession can be described by a series of equations that are discussed below.

The position of \bar{H} at any time during the precession is identical to that for the simple gyro, thus:

$$\alpha_H = \frac{M_x t}{I_s \omega_s} \quad (\text{Rad}) \quad (6-1)$$

The rate at which \bar{H} precesses in the XZ plane is:

$$\dot{\alpha}_H = \frac{M_x}{I_s \omega_s} \quad (\text{Rad/sec.}) \quad (6-2)$$

The position of \bar{H} in the YZ plane is always constant; thus θ_H is constant at $\frac{\pi}{2}$ radian = 90°

The position of \bar{S} in the XZ plane at any time during precession is given by:

$$\alpha_S = \frac{M_x t}{I_s \omega_s} - \frac{M_x \sin Pt}{I_s \omega_s P} \quad (\text{Rad}) \quad (6-3)$$

where "P" is the nutation frequency of the OSO and is given by:

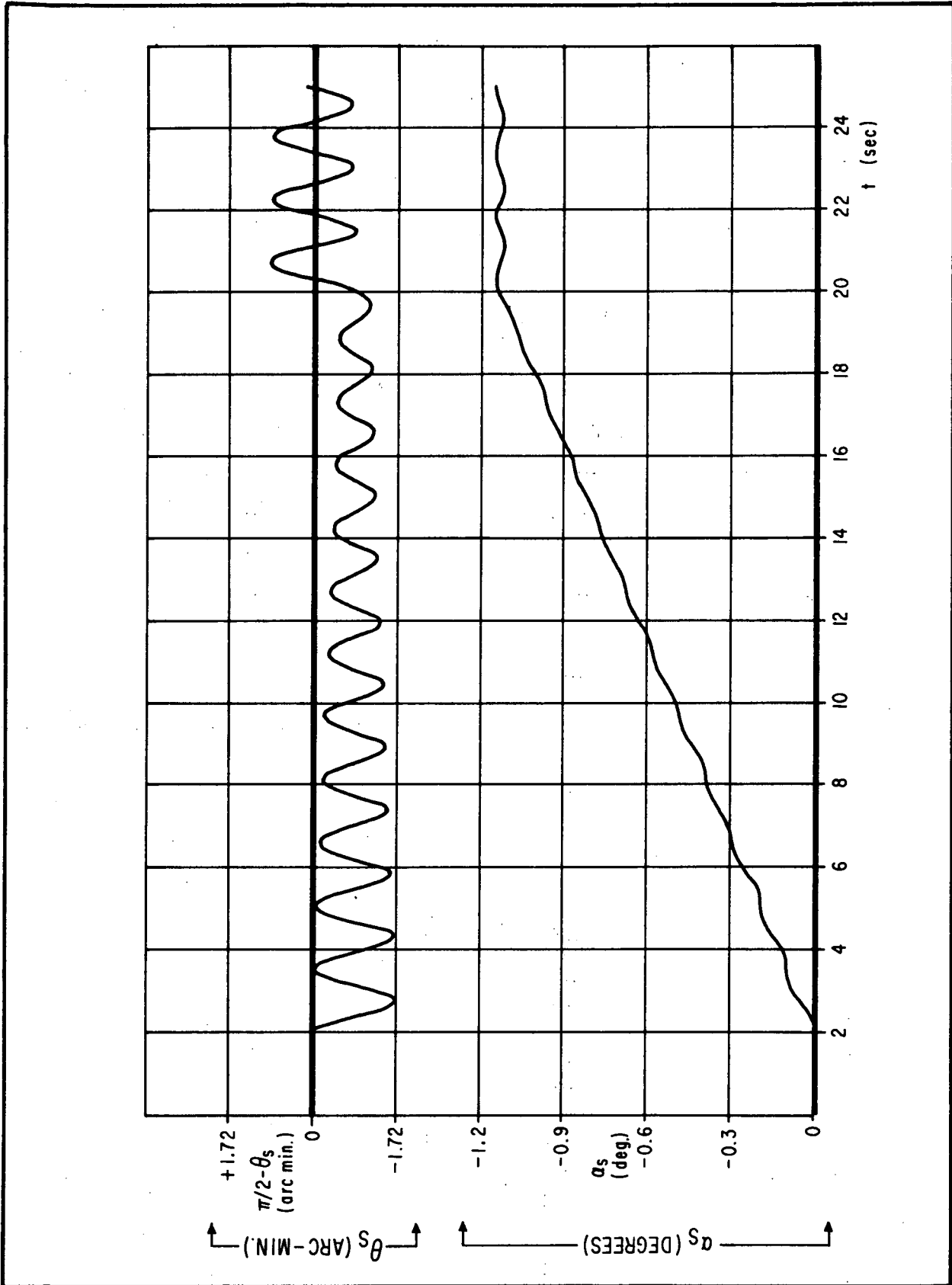


Fig. 6-2 Effect of Pitch Precession Torque (Oriented Sail -- With Nutation Damper)



$$P = \frac{I_S \omega_S}{I_1} \quad (\text{Rad/sec.}) \quad (6-4)$$

where I_S is the spin MOI of the wheel and I_1 is the transverse MOI of the entire spacecraft.

Thus, it can be seen from Eq. 6-3 that \bar{S} leads or

lags \bar{H} by the amount $\left[\frac{M_X \sin Pt}{I_S \omega_S P} \right]$ and in Fig. 6-1 we

have shown that α_S always lags α_H during the first half-cycle of nutation, leads α_H during the last half cycle, and coincides with α_H at the end of each nutation cycle ($t = \frac{2\pi}{P}$).

The rate at which \bar{S} moves in the XZ direction is given by:

$$\dot{\alpha}_S = \frac{M_X}{I_S \omega_S} - \frac{M_X \cos Pt}{I_S \omega_S P} \quad (\text{Rad/sec.}) \quad (6-5)$$

Thus, $\dot{\alpha}_S = 0$ at the end of each nutation cycle ($t = \frac{2\pi}{P}$) and is equal to twice the α_H rate (i.e., $\dot{\alpha}_S = 2\alpha_H$) at the half cycle point ($t = \frac{\pi}{P}$).

The position of \bar{S} in the YZ direction is given by:

$$\theta_S = \frac{\pi}{2} + \frac{M_X (1 - \cos Pt)}{I_S \omega_S P} \quad (\text{Rad}) \quad (6-6)$$

From this it is seen that $\theta_S = \frac{\pi}{2}$ (the same as θ_H) at the end of each nutation period ($t = \frac{2\pi}{P}$) and equals $\frac{\pi}{2} + \frac{2M_X}{I_S \omega_S P}$ at the half cycle point ($t = \frac{\pi}{P}$). The term



$\frac{2M_x}{I_s \omega_s P}$ is, therefore, the maximum nutation amplitude of \bar{S} in the YZ plane and is denoted by:

$$A_n = \frac{2M_x}{I_s \omega_s P} \text{ (Rad)} \quad (6-7)$$

The rate at which \bar{S} moves in the YZ plane is given by:

$$\dot{\theta}_S = \frac{M_x \sin Pt}{I_s \omega_s} \text{ (Rad/sec)} \quad (6-8)$$

Clearly at both $\frac{2\pi}{P}$ and $\frac{\pi}{P}$, $\dot{\theta}_S = 0$.

It can be shown that the amount of residual nutation at any time is given by the following equation:

$$r = \frac{1}{P} \sqrt{\dot{\alpha}_S^2 + \dot{\theta}_S^2} \text{ (Rad)} \quad (6-9)$$

where "r" is the radius of the circular nutational motion (assuming that the transverse MOI's are equal) and $\dot{\alpha}_S$ and $\dot{\theta}_S$ are the velocity components of \bar{S} at the time the torque is removed. Thus, the amount of residual nutation left after a pitch correction is determined by when the pitch torque is removed. This residual nutation is removed (dissipated) by the OSO nutation damper which will be discussed later in this section.

Motion Equations of \bar{S} During Precession (Unsymmetrical Body). The equations of motion given in the previous sections apply to a single-body, symmetrical OSO under constant torque. However, the actual OSO normally consists of both a rotating "wheel" and a stationary "sail" and it is, therefore, necessary to determine



the effects of this stationary sail and the pointed instrument assembly (PIA) on the motion of \bar{S} .

If the total* transverse MOI's of OSO are unequal (i.e., $I_x \neq I_y$) after the effects of the sail and PIA are accounted for, then the OSO is said to be unsymmetrical and both the frequency and amplitude of nutational motion are different than for a symmetrical OSO. For the unsymmetrical case, the nutational frequency equation becomes:

$$P = \frac{I_s \omega_s}{\sqrt{I_x I_y}} \quad (\text{Rad/sec}) \quad (6-10)$$

However, the α_s equation remains the same as in the symmetrical case but the θ_s equation changes to become:

$$\theta_s = \frac{\pi}{2} + \frac{M_x I_y (1 - \cos Pt)}{I_s^2 \omega_s^2} \quad (6-11)$$

Thus, for a composite OSO (wheel + sail + PIA) with unequal total MOI's about the transverse axes, both the frequency and amplitude of nutational motion are different than for a symmetrical OSO.

* The "total" transverse MOI of OSO takes into account, in addition to the transverse MOI of the wheel, the MOI of the sail about the x and y axes and the MOI of the PIA about the x and y axes. Thus, I_x and I_y refer to the total (wheel + sail + PIA) transverse MOI of OSO about the x and y axes.



- *Residual Motion of \bar{S} After Pitch Correction Has Been Completed.* It was shown in the preceding section that the angular momentum vector, \bar{H} , remains in the XZ plane ($\theta_H = \pi/2$) at all times during torquing. When torquing of the gyroscopic body is stopped, the residual motion is a circular motion of the spin vector about the angular momentum vector. From Eq. 6-6 it is seen that the amplitude of this motion is dependent upon the position of \bar{S} on the cycloidal path at the time torquing is stopped. That is, a maximum residual amplitude of $2M_x/I_s \omega_s P$ will remain if $t = n \pi/p$; and no residual motion is present if torquing stops when $t = 2n \pi/p$, or when the spin vector is coincident with the angular momentum vector. This motion is illustrated in Fig. 6-3.

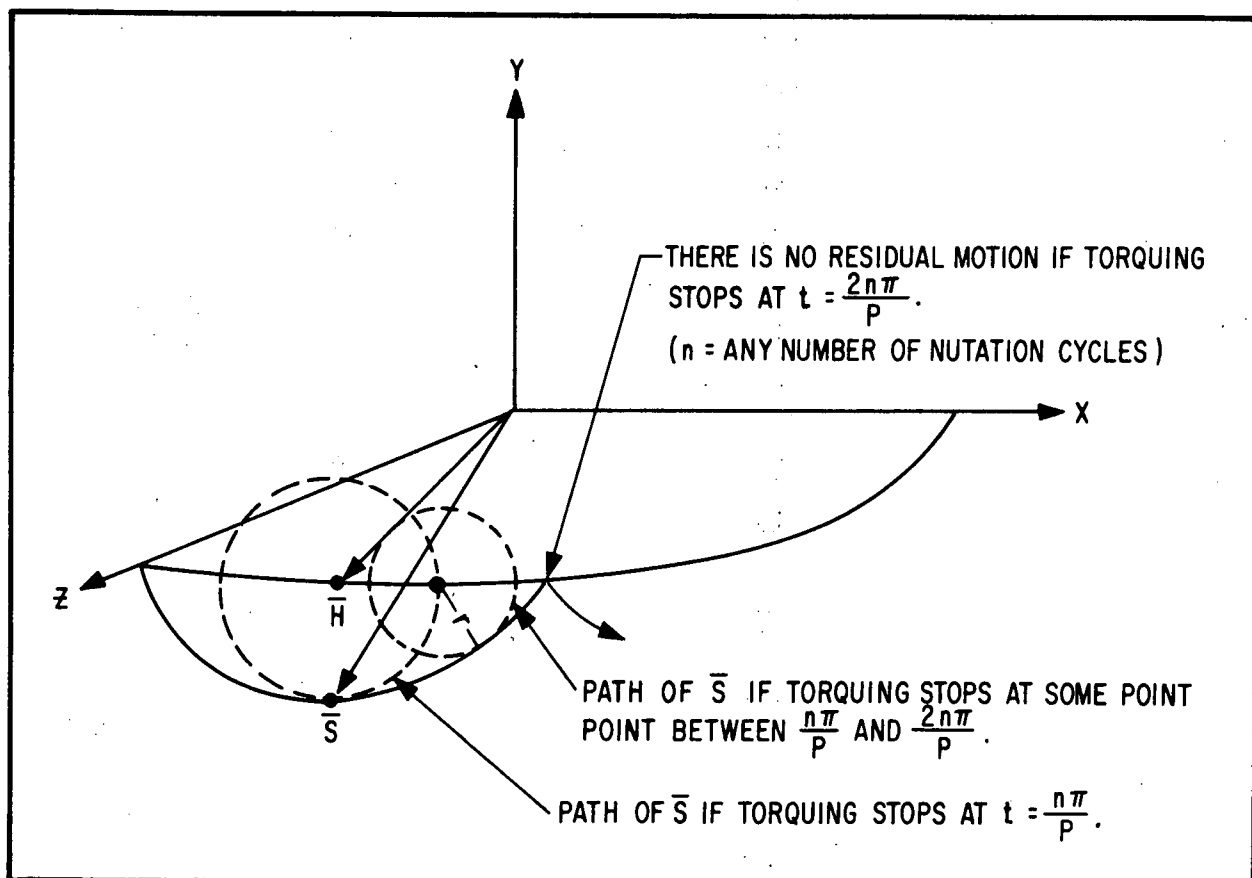


Fig. 6-3 Residual Nutation of \bar{S} After Constant Torquing Stops



- *Values of Some OSO-6 Dynamic Parameters*

Spin MOI of wheel only (orbit condition): I_s
 = 29.9 slug-ft²

Spin MOI of wheel and sail (orbit condition):
 $I_s = 35.3$ slug-ft²

Transverse MOI of wheel and sail (orbit condition):
 $I_1 = 24.5$ slug-ft²

MOI Ratio (orbit day condition): $\frac{I_s}{I_1} = 1.22$

Pitch Torque: $M_x = 0.193$ ft-lb.

Nutation Frequency: $P = \frac{I_s \omega_s}{I_1} = 3.87$ Rad/sec.
 (at $\omega_s = 30$ rpm)

Maximum Nutation Amplitude During Pitch Precession:

$$A_\eta = \frac{2M_x}{I_s \omega_s P} = 1.05 \times 10^{-3} \text{ Rad}$$

Angular Velocity of \bar{H} During Pitch Precession:

$$\dot{\alpha}_H = \frac{M_x}{I_s \omega_s} = 2.04 \times 10^{-3} \text{ Rad/sec.}$$

6.2.3 Interactions Between Pointing Control System and Nutation

The interactions between the OSO azimuth and elevation servos are much more complex, due to the short-duration impulses, than those for steady-state torquing (e.g., torquing by the pitch control system). Thus, the best way to illustrate these complex



interactions is to use the results of a computer analysis that simulated (after some simplification) these interactions. The details of this analysis are reported in Final Report on OSO Dynamic Analysis, (F66-06). In this computer analysis, a set of seven Lagrange equations of motion were used to simulate the effect of nutational motion on the azimuth and elevation servos, the effect of servo operation on nutation, and the effect of the nutation damper on nutation. Some conclusions obtained from this analysis are summarized in the following paragraphs:

- *Effects of the Azimuth and Elevation Servos on Nutation*

The azimuth and elevation control servos form a biaxial pointing control system. When the sail is accelerated in azimuth by the azimuth servo, the reaction torque (acting about the spin axis) causes only a small change in the wheel spin rate (ω). This small change in ω indirectly influences nutation in a small way due to the cross-talk effects on the elevation pointing error when the PIA is moved in azimuth. On the other hand, when the PIA is accelerated in elevation by the elevation servo, the reaction torque is in the "cross-spin" direction (perpendicular to the spin axis) and thus severely affects the nutational motion of the spin axis.

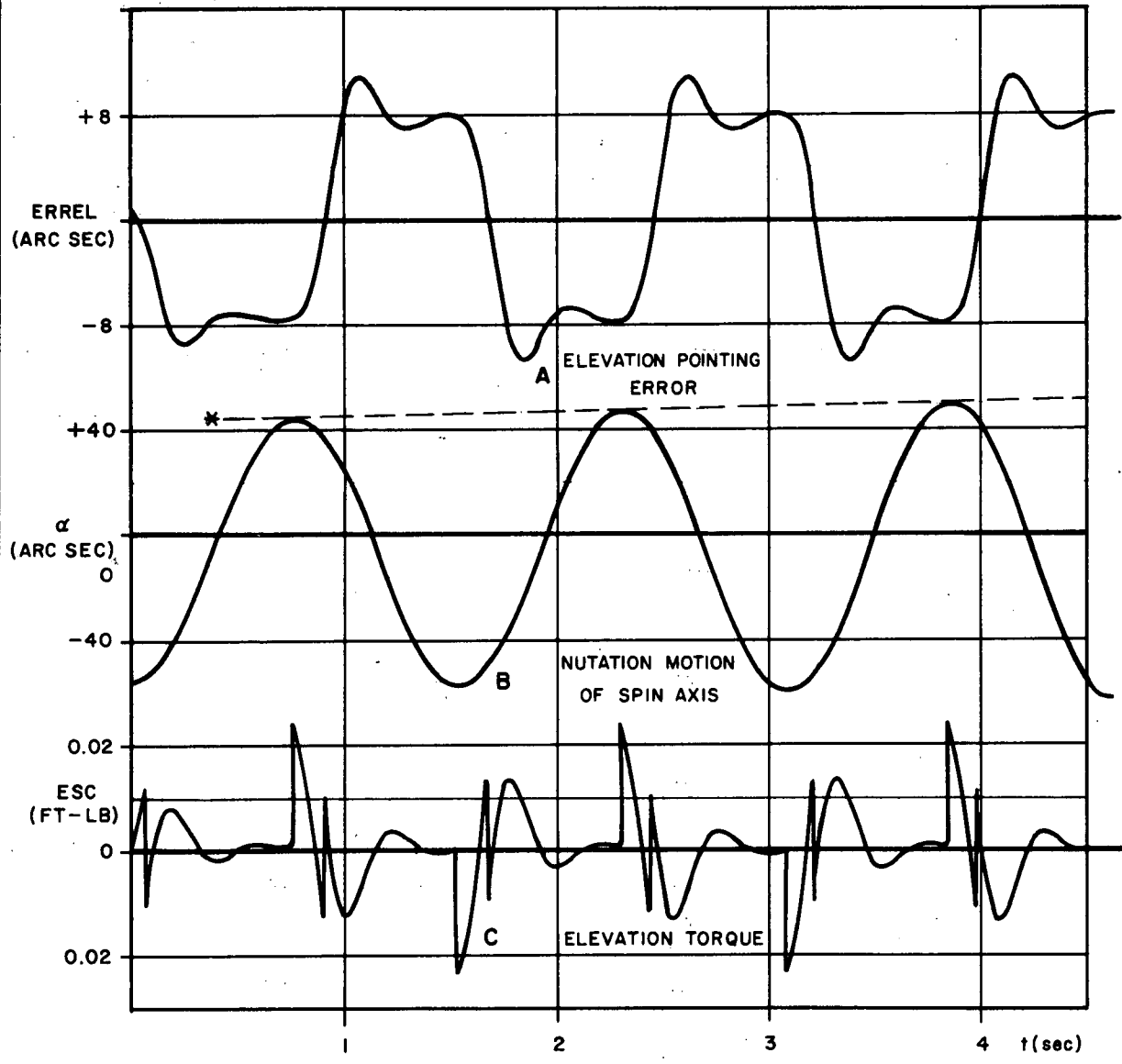
During the normal pointing mode, i.e., after coarse acquisition has occurred, any spin axis nutation causes a periodic disturbing torque to be applied to the PIA about the elevation bearing axis. This disturbance, caused by friction (sometimes called "stiction") in the elevation bearings, causes periodic changes in the elevation pointing error. The elevation servo generates corrective torques proportional to the magnitude and rate of change of the elevation pointing error.



A computer run (see Fig. 6-4) simulating the interactions during the normal pointing mode supports the important conclusion that the elevation servo response tends to increase nutation. In Fig. 6-4, the time histories of elevation pointing error (ERREL), nutation amplitude (α), and elevation torque (ESC) are used to show the interaction between these parameters when an initial nutation amplitude of about 40 arc seconds is assumed. In this run the nutation damper was not simulated because its damping influence would have swamped out the effect of the elevation servo on nutation.

As can be seen in Fig. 6-4a, the elevation pointing error periodically moves between positive and negative values (given by the ratio between the servo gain and friction in the bearings). Also, the nutation amplitude (Fig. 6-4b) is seen to increase by about 2 arc seconds during each nutation cycle. This growth can be accounted for quantitatively by comparing the sense of the net elevation torque (ESC) with α . That is, positive torque causes positive acceleration in α .

- *Interaction Between the Elevation Servo and Nutation During Normal Acquisition.* When the OSO passes into the shadow of the earth, the solar reference is lost and azimuth bearing friction causes the upper structure to spin up until the wheel and upper structure are spinning at the same rate. The sun is reacquired every orbit as both the azimuth and elevation servos develop drive signals in order to point the sail and the PIA in the solar direction. Fig. 6-5 is a computer simulation of a normal acquisition (with the nutation damper effects omitted) in which the PIA is initially displaced about 52 arc minutes from the solar direction. This amount of displacement is normal when it is considered that the



* NOTE INCREASE IN NUTATION AMPLITUDE DUE TO ELEVATION TORQUE.

Fig. 6-4 Interaction of Elevation Servo with Nutation (Normal Pointing Operation; No Nutation Damper)

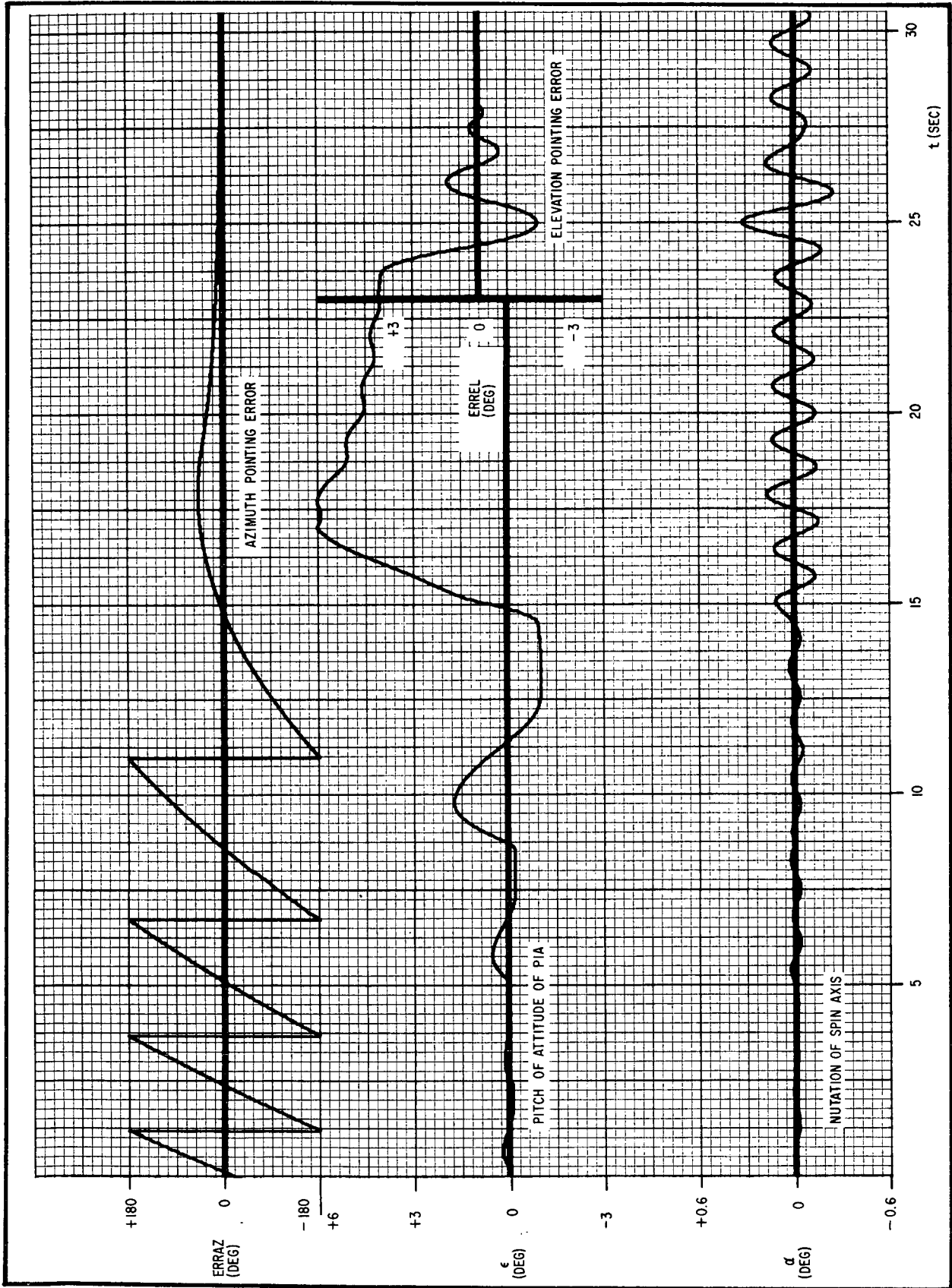


Fig. 6-5 Nutation Generated During Normal Solar Acquisition (no Nutation Damper)



PIA always seeks its dynamic balance position at night. The four parameters plotted in Fig. 6-5 are: azimuth pointing error (ERRAZ); the pitch attitude of the PIA (ϵ) with respect to the wheel plane; elevation pointing error (ERREL) with respect to the sun; and nutation amplitude of the spin axis (α). The azimuth component of pointing error (ERRAZ) is also shown so that the reader can follow the coarse azimuth acquisition and thus know when the sun is in the field of view of the elevation fine control eyes.

During the early phase of solar acquisition, when the sail has a high spin rate, the elevation servo produces torque for brief intervals when the sun is in the field of view of the elevation fine control eyes. At first this torque has little effect on nutation since it lasts only a fraction of a second (note the small perturbations in the α trace during the first 10 to 15 seconds). These short bursts of drive torque do, however, ultimately cause the PIA to begin oscillating about the elevation axis (note the ϵ trace during first 15 seconds) as the bursts get longer.

The centrifugal force due to the sail high spin rate during the early phases at acquisition acts as a spring and thus prevents the PIA from being displaced very much when the elevation torque bursts first occur. As the sail spin rate decreases, the centrifugal force decreases and the amplitude of PIA motion begins to increase (this can be noticed at about $t = 17$ seconds).

As the sail spin rate approaches zero, the elevation servo begins to null the elevation pointing error. The torque produced by the elevation servo during this nulling phase fluctuates at a frequency determined by the response characteristics of the servo. The response characteristics of the servo are a function of:



- (1) The magnitude of the initial error
- (2) The nonlinear response characteristics of the elevation fine eyes
- (3) The torque capability of the elevation torque motor
- (4) The servo lead time constant

The phase relationship between servo torque and spin axis nutation is a major factor in determining the nutation amplitude generated as the error is nulled. That is, large nutation amplitudes are generated when the response frequency of the servo is near the nutation frequency and in phase with it (this can be seen at $t = 25$ seconds in Fig. 6-5).

- *Interaction Between Elevation Servo and Nutation when the PIA Hits the Elevation Stops During Acquisition.*
The PIA can be driven into the elevation stops* if either of two conditions exist during acquisition:

- (1) The initial pitch error is greater than about two degrees and thus one of the stops is closer to the solar direction than the other.
- (2) The PIA is driven hard by a relatively long torque burst as the sail swings past the sun in azimuth, the PIA will coast into one of the elevation stops due to its momentum.

* The elevation stops limit the travel of the PIA to about $\pm 6^\circ$ relative to the solar direction when the pitch error is zero.

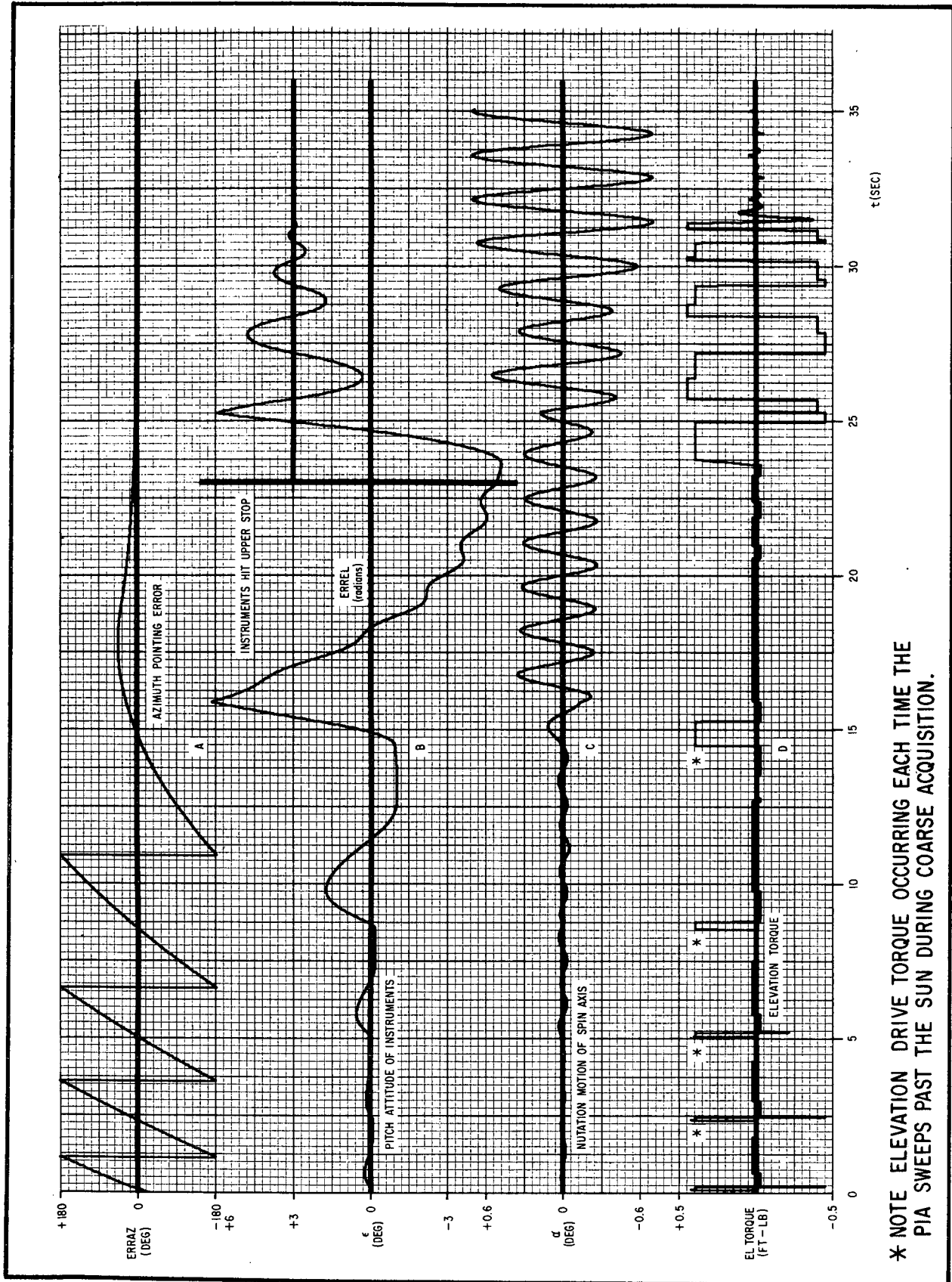


In Fig. 6-6, good examples of both of these situations are shown and we have included the elevation torque in this figure to simplify the interpretation of the interactions. A good example of condition (2) above, is shown at $t = 15$ seconds. Here, the PIA is driven in the positive direction by a relatively long burst of elevation torque. The sail then passes out of view of the elevation control eyes just as the PIA acquires a high angular rate about the elevation axis. At this time the restoring centrifugal force is low due to the sail's low spin rate and the only retarding force is the friction in the elevation bearings. This friction, however, is not enough to prevent the PIA from striking the upper elevation stop (at about $t = 16$ sec.).

An example of condition (1) above, is shown at $t = 25$ seconds. Here, the PIA is driven against the upper stop because this stop is closer to the solar null than the lower stop (i.e., the upper stop is only three degrees from the solar null while the lower stop is about nine degrees from the null).

The violent solar acquisition just described and shown in Fig. 6-6 is a rare occurrence in the actual operation of OSO because the PIA usually stays within two degrees of the solar direction during orbit-night. However, it is possible for this kind of acquisition to occur if the pitch attitude is near one of the $\pm 3^\circ$ pitch limits and if the dynamic balance point of the PIA (at night) is of the opposite sense.

- *How the Nutation Damper Dissipates Nutation.* The damper used on the OSO consists of a bob of dense material attached to the end of a length of piano wire. This bob is immersed in a viscous fluid which applies retarding



* NOTE ELEVATION DRIVE TORQUE OCCURRING EACH TIME THE PIA SWEEPS PAST THE SUN DURING COARSE ACQUISITION.

Fig. 6-6 Nutation Generated During Solar Acquisition when the PIA Strikes the Stops (no Nutation Damper)



forces to the bob. The bob and damping fluid are contained in a compact case which restricts the amplitude of bob motion. In the unrestricted range of bob motion, this damper dissipates the kinetic energy associated with nutation by converting this energy into heat.

The total rotational kinetic energy of a nutating OSO can be expressed as the vector sum of the spin component of kinetic energy ($T_s = 1/2 I_s \omega_s^2$) and the cross-spin kinetic energy ($T_1 = 1/2 I_1 \omega_1^2$). Thus, the total kinetic energy is:

$$T = 1/2 I_s \omega_s^2 + 1/2 I_1 \omega_1^2 \quad (6-12)$$

The cross-spin kinetic energy is associated only with the coning motion (nutation) of the spin axis about the spin angular momentum vector (\bar{H}_s), and must decay to zero if the nutation cone is to collapse onto the angular momentum vector. It can also be said that the total angular momentum (\bar{H}^*) is the sum of its spin and cross-spin components, or

$$\bar{H}^* = \bar{H}_s + \bar{H}_1 \quad (6-13)$$

If it is assumed that the nutation cone collapses strictly as the result of dissipation of energy by the nutation damper, then the total kinetic energy of the spacecraft must change; but its angular momentum, however, remains constant (since no external torque is involved). Because the angular momentum vector is constant, the final spin rate of the wheel (after dissipating the nutation energy) can be calculated as follows:

$$H^{*2} = (I_s \omega_s)^2 + (I_1 \omega_1)^2 \quad (\text{from Pythagoras' theorem for right triangles})$$



The $(I_1\omega)^2$ term in the above equation is reduced to zero as the cross-spin component is dissipated by the nutation damper and thus eventually:

$$H^{*2} = (I_s \omega_s)^2 \quad (6-14)$$

However, since H^* and I_s are both constants, ω_s must increase and the final spin rate (ω_s^*) can be calculated as follows:

$$H^{*2} = (I_s \omega_s^*)^2 = (I_s \omega_s)^2 + (I_1 \omega_1)^2 \quad (6-15)$$

$$\text{or } \omega_s^{*2} = \omega_s^2 + \left(\frac{I_1}{I_s}\right)^2 \omega_1^2$$

The final kinetic energy of OSO after dissipation of the nutation energy is

$$T^* = T_s^* = 1/2 I_s \omega_s^{*2} = 1/2 I_s \omega_s^2 + 1/2 \left(\frac{I_1}{I_s}\right)^2 \omega_1^2 \quad (6-16)$$

The net change in kinetic energy (ΔT) during collapse of the nutation cone is the difference between the kinetic energy expressions in Eqs. 6-12 and 6-16, thus

$$\Delta T = T - T^* = 1/2 I_1 \left(1 - \frac{I_1}{I_s}\right) \omega_1^2 \quad (6-17)$$

$$\text{or } \Delta T = \left(1 - \frac{I_1}{I_s}\right) T_1$$

The conclusions that can be drawn from the above analysis are that:

- H_1 and T_1 have decayed to zero



- T_s has grown to T_s^*
- The total kinetic energy of OSO must decrease if $I_s > I_1$.

The best explanation for why the wheel spin rate increased slightly when the nutational energy is dissipated is by what is called "the modified energy-sink argument". This argument accounts for the increase in spin kinetic energy by assuming that the cross-spin energy is dissipated directly by the nutation damper, and that the azimuth servo adds the increase in the spin kinetic energy (this energy is actually supplied by the solar array).

- *OSO Nutation Damper Performance.* The OSO nutation damper (with a seismic mass of 1/600 of the spacecraft mass) causes a nutation amplitude of less than 1/2 degree of decay to about 1/3 of its initial value in 15 seconds at the nominal spin rate (larger amplitudes force the damper bob against the case). A time interval of 15 seconds corresponds to 10 nutation cycles or about 7 revolutions of the wheel.



Section 7
CONTROL SYSTEMS FUNCTIONAL DESCRIPTION

7.1 INTRODUCTION

This section presents detailed functional descriptions of the five OSO-6 control systems. General descriptions of these systems and their components are presented in Section 1. The five basic control systems are described briefly below:

- (1) Pitch control system - Provides automatic pitch control of the observatory by maintaining the spin axis within 4* degrees of normal to the solar vector; automatically switches to manual control mode in case of malfunction; and provides manual control of pitch attitude by ground station command when necessary. A magnetic bias coil (pitch coil) was used to augment the pneumatic control system. The pitch coil provided a means by which the magnetic dipole moment of the spacecraft could be varied by ground commands.
- (2) Spin control system - Provides automatic spin-rate control of wheel between the nominal limits of 0.45 to 0.66 rps; automatically switches to manual-control mode in case of a malfunction in which the spin rate goes outside the limits of 0.39 to 0.70 rps; and provides manual spin-rate control by ground station command when necessary.

*This is the maximum value allowed by the OSO model specification. The nominal is closer to +3 degrees.



- (3) Pointing control system - Provides automatic solar acquisition of sail each orbit morning and pointing within 1 arc minute of center of sun. Alternate pointing control modes include:
- (a) Large Raster -- a 64-line sun-centered raster covering 46 x 46 arc minutes;
 - (b) Small Raster -- a 16-line raster covering 7.0 arc minutes in azimuth, and 7.5 arc minutes in elevation, centered on any point in the offset grid; and
 - (c) Offset Grid -- an ability to point at or small raster about any point in a 128 point by 128 point grid 46 x 46 arc minutes square.
- (4) Launch sequence control system - Automatically changes observatory from launch to orbit condition by initiating certain control functions at prescribed times; system operation is started by separation of the observatory from the launch vehicle.
- (5) Nutation control system - Damps observatory nutational motion acquired during launch and while in orbit.

7.2 CONTROL SYSTEMS INTERACTION

Basically, the five OSO control systems function independently of each other but there are interactions that should be considered. Some of the more important of these interactions are described below.



7.2.1 Pitch Control System

Operation of this system is affected by the operation of three other systems: First, the pitch control system is not activated until the spin control system has turned day-power on. Also, the spin control system controls wheel spin rate, which in turn governs the angular momentum of the wheel and, therefore, the rate of pitch drift. Although changes in angular momentum will not affect the total amount of pitch gas consumed during the life of the observatory, it will affect the frequency of the pitch corrections. As in several earlier OSO missions, a magnetic bias coil was used to reduce consumption of pitch control gas.

Second, a small amount of nutation is produced each time a pitch correction is made and when the pointed instruments acquire each morning. This motion will modulate the pitch angle unless it is damped by the nutation damping system.

And third, the auto pitch limiter circuits are disabled until coarse-fine switching has occurred. This function is provided by the pointing control system.

7.2.2 Spin Control System

Operation of this system can be affected by the operation of two other systems: the spin pulse amplifiers and the day-power turn-on circuits in the spin control system are first activated when orbit power is turned on by the launch-sequence-control system during the launch phase. These circuits then provide day-power to the auto-spin circuits so that the observatory can be despun from the high spin rate acquired during third stage spinup. Also, the launch sequence system causes the three extendible arms to deploy, thereby decreasing the wheel spin rate from about 120 to 90 rpm while providing a longer lever arm through which the spin jets can act.



Second, the action of the pointing control system during normal orbital operation causes the sail to be despun each morning, and azimuth bearing friction causes the sail to spinup to the wheel spin rate each night. This spinning and despinning of the sail results in a corresponding transfer of sail angular momentum to and from the wheel and, therefore, changes the wheel spin rate. The change in wheel spin rate could cause the spin control system to operate if the spin rate is near the upper or lower limits.

Other factors that define the most desirable spin rate range are as follows:

- (1) The data resolution of certain wheel experiments defines the lower and upper spin rate limits between which data can be most successfully recovered from these experiments. These limits are approximately 0.45 to 0.60 rps.
- (2) The gyroscopic stability of the observatory is proportional to spin rate and thus defines the lowest spin rate at which stability will be acceptable. This limit is approximately 0.05 rps.
- (3) The effective damping range of the tuned nutation damper defines the lower and upper spin rate limits between which the most efficient damping will occur. These limits are approximately 0.44 to 0.57 rps.

7.2.3 The Nutation Control System

Operation of this system can be affected by the operation of the spin control system (because the nutation damper is tuned for a specific spin rate) and by the operation of the launch sequence system. The latter provides the signal that uncages the nutation



damper bob during the launch phase. Also, the pitch and pointing control systems have a significant effect because they generate nutation-producing impulses during their operation.

7.2.4 The Pointing Control System

Operation of this system can be affected by the wheel spin rate and by the pitch attitude of the observatory, i.e., wheel spin rate affects the time required for despinning the sail and also, the pitch plane must be within approximately ± 15 degrees (the vertical view angle of the coarse eyes) of normal to the solar vector before azimuth acquisition can be accomplished.

7.2.5 The Launch Sequence Control System

Operation of this system can be affected only by the separation of the observatory from the launch vehicle.

7.3 CONTROL SYSTEMS OPERATION DURING LAUNCH PHASE

Perhaps the most critical time in the operation of the OSO control systems is the 20-minute period between second-stage spinup and initial solar acquisition shortly after injection into orbit. During this period, the control systems must perform in unison to change the observatory from the launch to the orbit configuration as well as to accomplish initial solar acquisition. The following paragraphs describe some of the launch and early-orbit events.

7.3.1 Launch Requirements

The second-stage spin motors ignite shortly after the second-stage engine provides the final velocity increment to insert the spacecraft into a nearly circular orbit at an altitude of 350 nm. At injection, the spacecraft's spin axis should coincide with the



second-stage velocity vector which in turn should be parallel to the surface of the earth.

The injection point is determined primarily by the launch vehicle capability, the lift-off location, and the orbital parameters desired. Therefore, the injection point is fixed with respect to the earth's surface for the OSO mission.

For successful acquisition of the sun, the spacecraft must be injected into orbit through a time "launch window" determined by the relationship of the fixed injection point and the declination of the sun on the launch day. Proper injection timing is important because the sun must be in the field of view of both the spin eyes and the coarse control eyes mounted on the perimeter of the wheel and on the front and rear of the sail, respectively. The field of view for these sensors is approximately 15 degrees on either side of the wheel plane and 360 degrees in the wheel plane. This +15 degree field of view will allow about a +60 minute "launch window", but for reliability reasons this is reduced to about +20 minutes for OSO. The spacecraft events that occur during the launch and early orbit phases are discussed in the following paragraphs.

7.3.2 Spacecraft Control Systems Operation

At observatory separation, the spacecraft separation switches close, causing the spacecraft arms to deploy and starting the launch sequence timers. Arm deployment causes the spacecraft spin rate to decrease roughly twenty percent from the spin rate achieved during second-stage spinup. This is caused by the increase in wheel moment-of-inertia at arm deployment.

At T + 330 seconds, the spacecraft timers supply a signal that causes "orbit power" to be applied to the spacecraft. The turn-on of orbit power activates the spin eye amplifiers and level detector, and the "day-power" turn-on circuits. The application of



power to these circuits causes "day-power" to be applied to the spin control, pointing control and the pitch control systems.

When day-power is applied to the spin control system, an over-spin condition is immediately sensed. Subsequently, spin gas is released in bursts from the despin nozzles until the spacecraft wheel is despun to a spin rate of about 0.62 rps.

The spin eyes and their associated level-detector circuits have a high turn-on threshold before day-power is turned on and a much lower turn-on threshold after day-power is on. This prevents day-power "chattering" during orbit morning and evening because of varying light conditions.

With day-power turn-on, the pointing control system senses the position of the sun with the azimuth coarse eyes and produces a despin torque that despins the sail. The time required for initial sail despin is approximately 1-1/2 minutes, which is less than the approximately 3-1/2 minutes required by the spin control system to initially despin the wheel to 0.62 rps. Therefore, wheel despin is still progressing after sail despin has ended.

After the sail has been despun and is pointing within ± 3 degrees in azimuth, the target eye (after an eight-second delay) activates the fine pointing circuits, and the sail and pointed instruments are accurately aligned within 1 arc minute (in azimuth only) of the sun's center. Note that at this time, the elevation frame is still locked and, therefore, there can be no elevation pointing. This means that there will be high elevation motor current for approximately seven minutes prior to elevation frame unlatching which occurs at $T + 800$ seconds. Another possibility is that if the pitch angle was greater than the ± 6 degrees vertical view of the target eye, coarse-fine switching could not occur until the pitch control system corrected the pitch to within the range of the target eye.



With the application of day-power, the pitch control system is also activated and, for the first time, the spacecraft's pitch attitude is sensed. If this attitude is outside the range of about ± 3 degrees, this system automatically expels nitrogen gas from the appropriate pitch nozzle to correct the pitch angle to within 1 degree of the solar vector.

At T + 600 seconds, the launch sequence timers produce a signal that releases the nutation damper bob. The nutation damper then absorbs nutation energy originating at separation from the launch vehicle or from the ensuing spacecraft control systems operation; within a few minutes any cross-spin momentum of the spacecraft is reduced to a negligible value.

At T + 800 seconds, the timers produce a signal that unlocks the elevation frame supporting the pointed instruments. The pointed instruments then acquire the sun in elevation by action of the pointing control system. Also, a signal is applied to the auto pitch limiter (APL) and the auto spin limiter (ASL) enabling relays, which enable the auto pitch limiter and auto spin limiter circuits, respectively. At T + 1250 seconds, the timers repeat all of the launch sequence control signals to ensure the occurrence of the launch events.

7.4 CONTROL SYSTEMS IN-ORBIT OPERATION

Control system in-orbit operation is somewhat different from that at launch. As OSO comes into sunlight each orbit morning, the sail and wheel are spinning together because of azimuth bearing friction. Consequently, the spin rate has been reduced to about 87 percent of that for the previous day because of the transfer of a small amount of wheel momentum to the sail. The spin axis attitude at orbit-morning is very nearly the same as it was at the preceding orbit-evening because of the gyroscopic stability of the spacecraft, although it is possible that the very



slow pitch drift during the night might cause a pitch attitude in excess of the ± 3 degrees correcting threshold. At the most, this drift should amount to no more than a few tenths of a degree.

Another spacecraft condition different from launch conditions is that both the nutation damper and the elevation frame are unlocked, the latter assuming a "night" position (because of dynamic unbalance that may exist in the pointed instruments) with the elevation angle being within a few degrees of zero. Also significant is the sun's position at sunrise with respect to OSO. The sun is viewed each orbit-morning as it rises from behind the limb of the earth through the diffused light band (air glow) along the horizon. The presence of this "extra" light, consisting of air glow and albedo, is favorable to battery charging but has little effect on solar acquisition because of the dominating sun intensity.

Control systems operation each orbit-morning will normally occur in the following sequence: The spin eyes sense the sun as it appears above the horizon and "day-power" is subsequently turned on. The low night spin rate is sensed by the spin control system before any appreciable increase in wheel spin rate can occur because of sail despin. Spin-up jets will be activated for a four-second burst if the spin rate is less than the low limit of 0.45 rps. Simultaneously, the coarse control eyes sense the position of the sun, and sail despin is initiated by the pointing control system. The time required for sail despin is approximately 60 seconds (this compares to 90 seconds for initial despin during launch phase caused by the high initial wheel spin rate). The target eye signal causes coarse-fine switching after despin terminates and the pointed instruments are aligned within 1 arc minute of the sun's center. Simultaneous with day-power turn-on, the pitch control system senses the pitch attitude of the spacecraft. If the pitch error exceeds the limits of about ± 3 degrees, the appropriate pitch jets are activated to reduce the error to less than 1 degree. The nutation damper then damps any nutation produced in the above operations.



The above paragraphs have presented a general functional description of each primary control system on OSO during the launch and orbit phases. Each system will now be discussed in detail.

7.5 PITCH CONTROL SYSTEM FUNCTIONAL DESCRIPTION

7.5.1 General Description

The OSO-6 pneumatic pitch control system, like those of earlier OSO's, has two modes of operation: (1) the automatic mode in which the pitch attitude is automatically maintained nearly normal to the solar vector, and (2) the manual mode which is used as a backup in the event of auto-mode failure or when ground station control of the pitch attitude is desired. The auto-mode requires no attention from ground operations other than the routine reduction of the telemetered pitch data to determine the instantaneous pitch attitude and, subsequently, the pitch-drift rate of the spacecraft.

In addition to the pneumatic pitch control system, OSO-6 was equipped with a magnetic bias coil (pitch coil). This pitch coil could be controlled by ground commands to vary the magnetic dipole of the observatory, thereby augmenting the pneumatic system.

7.5.2 Automatic Pitch Control

In the auto-mode, four pitch-angle sensors are used; two for pitch-up control and two for pitch-down control (Figs. 7-1 and 7-2). In Fig. 7-2, these sensors are shown as A-down, B-down and A-up, B-up. The crosshatched areas indicate the turn-on thresholds of the sensors and their amplifiers. Zero pitch error is defined as the condition which exists when the spin axis is normal to the solar direction.

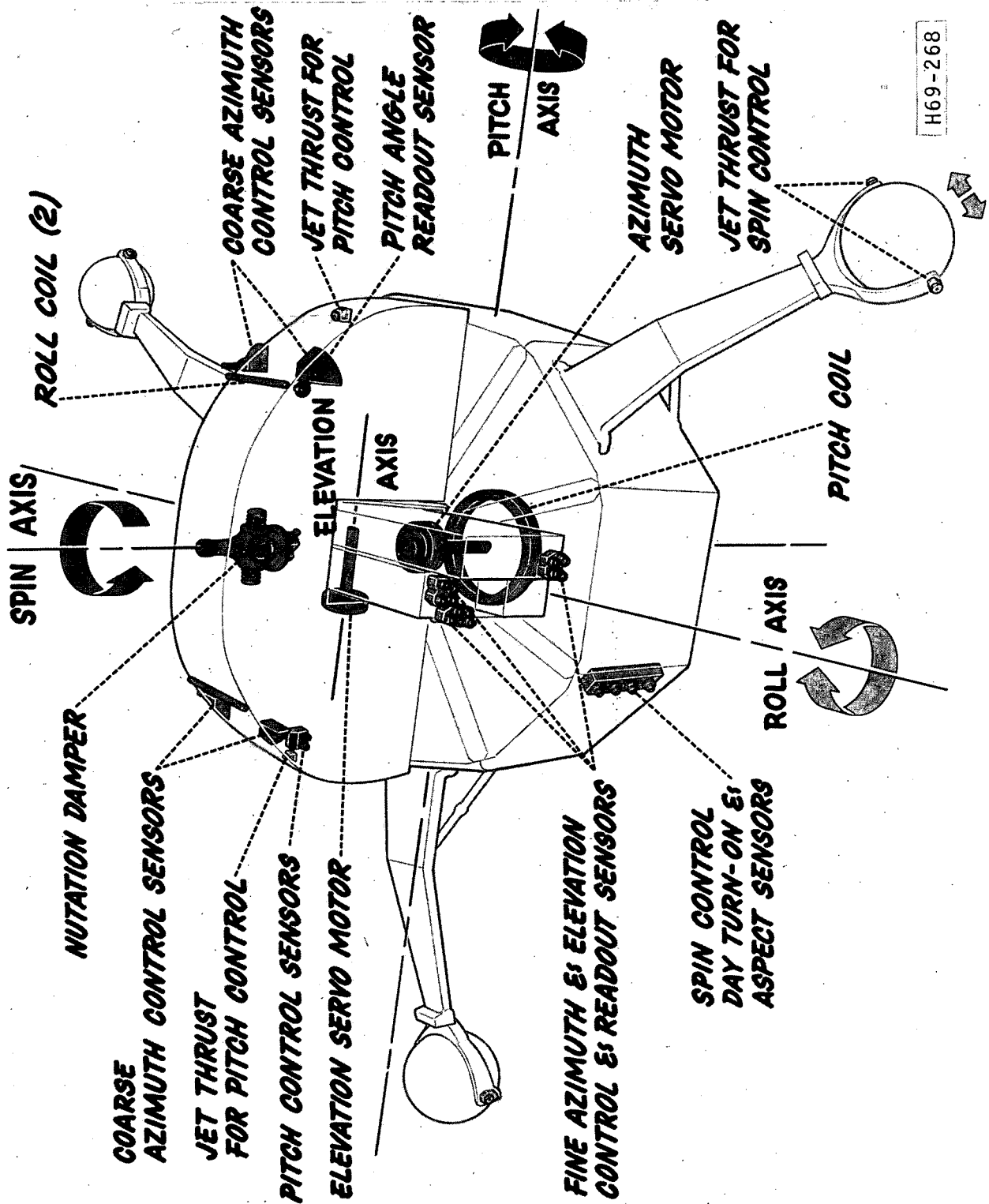


Fig. 7-1 Control Systems Components

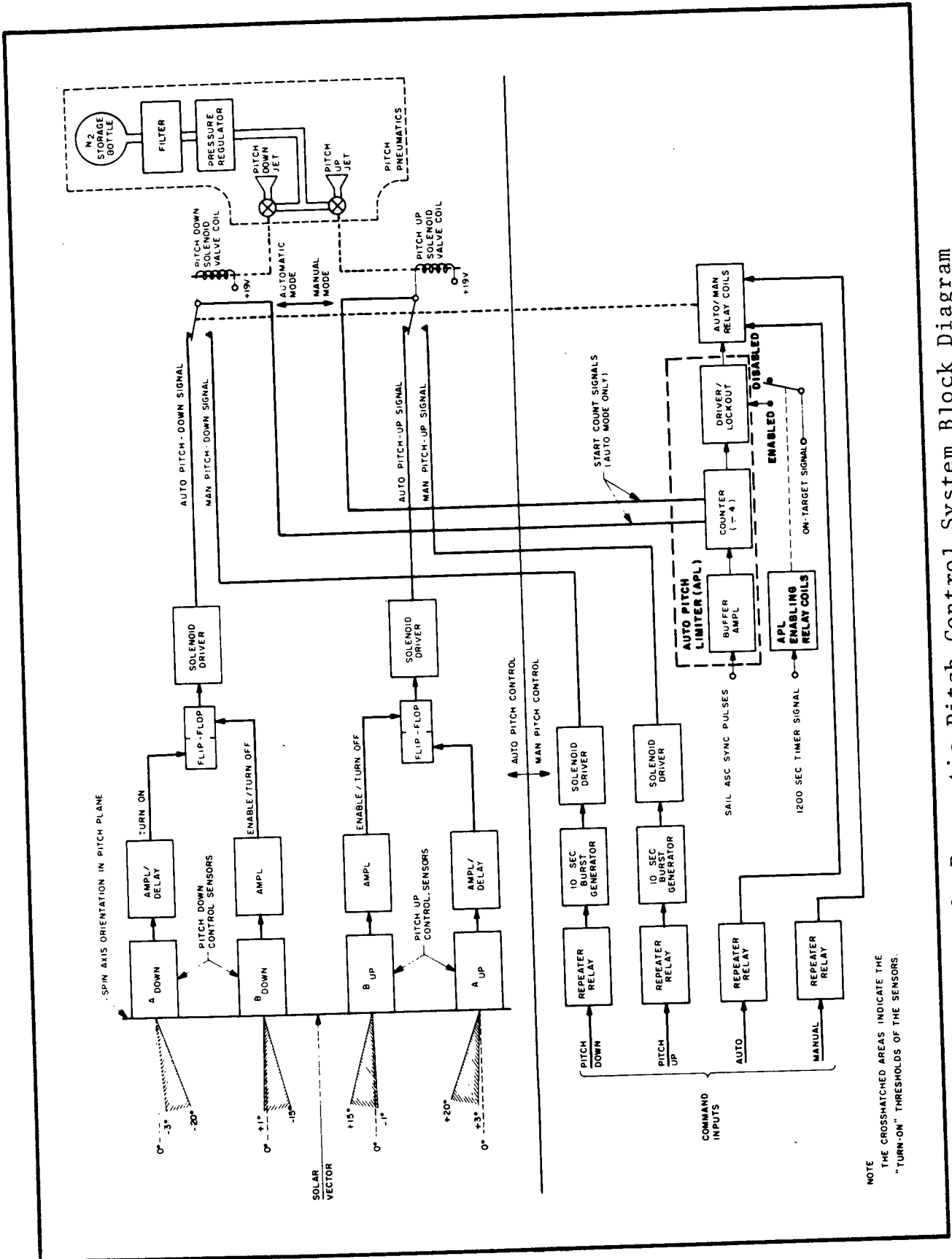


Fig. 7-2 Pneumatic Pitch Control System Block Diagram



First, consider a pitch-up drift of the spacecraft in which the spin axis rotates three degrees clockwise (pitch-up motion) starting from the zero position (Fig. 7-2). The pitch-down flip-flop is initially enabled because the B-down sensor is 1 degree past its turn-on threshold. When the pitch angle has advanced to -3 degrees, the A-down turn-on threshold is reached (assuming that the threshold is adjusted for 3 degrees) and after a delay of approximately 8 seconds, the pitch-down bi-stable flip-flop is set to the "on" state. The output of this flip-flop then drives the solenoid driver, which in turn energizes the pitch-down solenoid valve and pitch gas is exhausted through the pitch-down jet.

As the spacecraft starts to precess counterclockwise (pitch-down motion), the A-down sensor output immediately falls below the turn-on threshold, but the pitch-down flip-flop remains "on" until the B-down sensor output falls below its turn-on threshold. This occurs at +1 degree at which time the flip-flop is reset, and the pitch-down solenoid valve is subsequently de-energized.

The important point to remember in the above discussion is that the purpose of the "B" sensor is to enable and reset the pitch-down, bi-stable flip-flop. That is, when the "B" sensor is "on", the flip-flop is enabled and the "A" sensor can then set it to the "on" state when a pitch error of -3 degrees is sensed. Conversely, when the "B" sensor is "off", the flip-flop is reset; note that this condition normally occurs only at +1 degree because the extreme limit of -15 degrees for this sensor should never be reached.

Automatic correction of a 3 degree pitch-down error occurs in the same manner as does the error correction just presented, except that the pitch-up elements are employed.



The corrective pitch maneuvers just discussed for automatic mode control, as well as those to be considered in pitch manual mode operation below, are actually precessional motions of the entire spacecraft and are governed by gyroscopic principles. A slight amount of spin axis nutation is probable after a pitch correction is made. This motion is damped by the nutation damper, a control system assembly which is discussed later in this section.

7.5.3 Manual Pitch Control

The pitch manual mode of operation is automatically selected by the automatic-pitch limiter (APL) circuits if either solenoid valve is held open under automatic control for a period spanning 108 to 122 seconds. The automatic pitching period, which will cause a switch to manual control, falls at random in the 108 to 122 second range because the switch-over occurs at the moment that eight sail analog subcommutator frame sync pulses have been counted from the time a valve is energized. This starting point may fall anywhere within the subcommutator 15.36-second frame period.

Figure 7-2 also shows the pitch manual control functions. The automatic switch-to-manual functions are shown on the lower right. The sail ASC sync pulses, which occur every 15.36 seconds, are fed to the APL circuits where they are buffered and fed to a divide-by-eight counter. The "start count" signals to this counter are supplied directly from each solenoid valve coil circuit whenever an auto-pitch solenoid driver is turned on. The driver-lockout circuit switches the auto-manual latching relay to the manual position when the counter output provides a four-count switching signal.

During the launch phase, the APL enabling relay supplies no power to the driver-lockout circuit until both the 800 second launch sequence timer signal and the on-target +19 v signal have occurred. This lockout is necessary because orbital injection pitch error can



be as much as ± 5 degrees for normal launch vehicle performance, and the automatic pitching time to correct this error would be a duration that could cause a switch to manual mode and therefore inhibit auto pitch operation. Automatic mode correction of abnormal pitch error at injection can be performed within the pitch control sensor's ± 18 degree viewing angle during the lockout period.

Figure 7-2 also shows the command control functions of manual pitch operation. When manual control is selected, ground stations can command either pitch-down or pitch-up as required. An analog pitch monitor is used to detect the pitch angle and these data are supplied to the telemetry system. For every manual pitch command, the decoder command pulse operates the appropriate repeater relay, which in turn triggers a ten-second monostable multivibrator circuit (called a burst generator). The monostable output signal controls the appropriate pitch valve through a solenoid driver.

The pitch-manual and pitch-auto command inputs are direct switching commands for changing the pitch control mode to either manual or automatic mode. These commands also operate through repeater relays, which in turn directly control the auto-manual latching relay.

7.5.4 Magnetic Pitch, Spin, and Roll Control

Occasionally, the attitude or the spin rate of the observatory must be changed quickly. This takes large torques, so the gas jets must be used. But most of the time, only slow changes are needed; therefore, smaller torques are adequate and they can be produced by magnetic dipoles reacting against the earth's magnetic field. This magnetic torquing conserves gas.



A dipole along the spin axis can produce torque along the roll axis, causing pitch motion (because the observatory acts as a gyroscope) and along the pitch axis, causing roll motion. A dipole along the roll axis can produce torque along the pitch axis, causing roll motion, or along the spin axis, which changes the spin rate. Thus, dipoles along only two axes can produce control torques along all three. And with selective programming, the two dipoles usually can produce the needed torque in the desired direction without producing too much torque in some other direction.

Pitch Coil. The spin-axis dipole is produced by a coil of wire called the "pitch coil". It consists of copper magnet wire wound on an aluminum hoop. Its DC resistance is about 1000 ohms. This coil is mounted in the wheel hub with its axis along the spin axis.

Commands are used to turn the coil on or off, to select full or half power, and select positive or negative polarity. This means that any one of five spin-axis dipole moments can be chosen. The state of the coil is telemetered to the ground.

Roll Coils. The roll-axis dipole is produced by a pair of coils called "roll coils". The coils are mounted on the sail with their axes parallel to the roll axis. They are well separated so they won't interact much. Their mounting location is shown in Fig. 7-1. Different roll-axis dipole moments can be selected by command. The state of each coil is telemetered to the ground.

It would be possible to switch the coils several times each orbit to take advantage of the rapid changes in geomagnetic field direction. That would give strong control and allow fairly fast maneuvers, but it isn't necessary. Working with the orbit-average magnetic fields and switching every few days is good enough. The best coil settings for various times of the mission can be found using a computer program (COIL).



The effects that can be achieved with this system depend strongly on the attitude of the observatory, the position of the ascending node of the orbit, the season of the year, and the maneuver wanted. But they are generally large enough to be useful. This control system can hold the spin rate within its proper limits at all times, and can produce pitch and roll rates roughly on the order of one degree per day most of the time. Careful use of the coils can conserve the gas supply enough to last for several years.

7.6 SPIN CONTROL SYSTEM FUNCTIONAL DESCRIPTION

7.6.1 General

The spin control system, like pitch control, has a primary or automatic control mode of operation as well as a manual or backup control mode. The latter is normally used as a backup in the event of primary control failure, but may be used to manually adjust the spin rate to some specific value between the automatic control limits of 0.45 to 0.66 rps. A block diagram of the spin control system is shown in Fig. 7-3.

The concept of automatic spin control is to electronically measure the time required for each revolution of the wheel. When this time reaches a value of about 2.2 seconds (0.45 rps) as the spin rate drifts downward, a four-second burst of nitrogen gas is expelled from the spin-up nozzles, thus increasing the spin rate an increment of about 0.0245 rps. Similarly, when the time for a revolution reaches a value of about 1.52 seconds (0.66 rps) as the spin rate drifts upward, a four-second burst of gas is expelled from the spin-down nozzles thus decreasing the spin rate an increment of about 0.0245 rps.

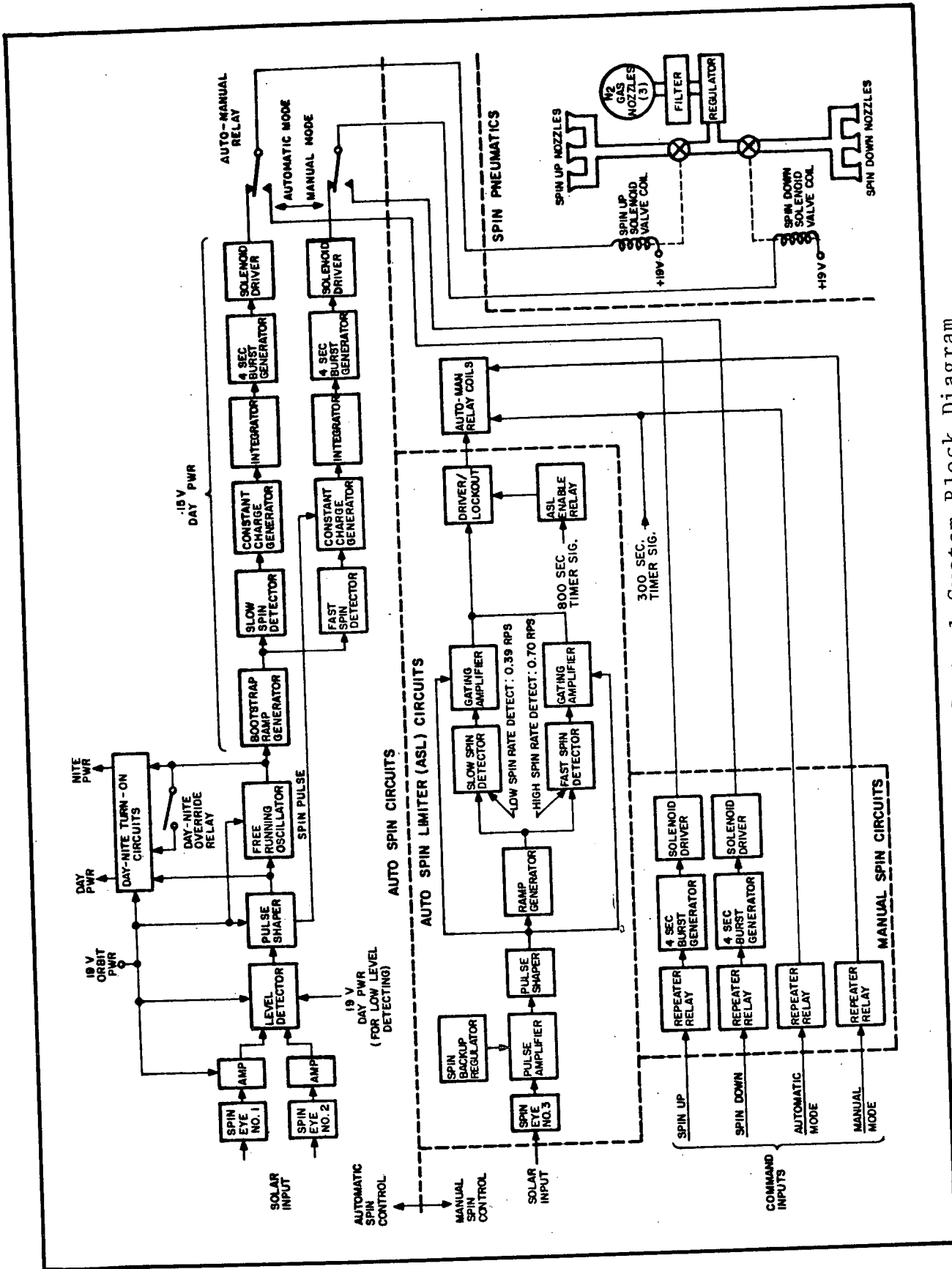


Fig. 7-3 Spin Control System Block Diagram



The manual mode is automatically selected electronically when the time for one revolution falls outside the nominal range of 1.43 seconds (0.70 rps) to 2.56 seconds (0.39 rps). When either of these limits is reached, a failure in the automatic spin control circuits or a stuck solenoid valve is indicated. Manual control can also be selected by ground station command. When the spin rate is corrected manually, a four-second burst of gas is expelled for each spin-up or spin-down command received by the spacecraft.

7.6.2 Automatic Spin Control

Spin Eyes and Amplifiers. The auto-spin control mode uses two identical and redundant solar sensors (spin eyes Nos. 1 and 2), mounted on the perimeter of the spacecraft wheel. As these spin eyes sweep past the sun, they each produce a pseudo-squarewave current pulse (spin pulse) of about 20 milliseconds duration. These two pulses are fed to two current-to-voltage amplifiers where they are amplified and mixed before being fed to a level detector.

Level Detector. The level detector has two modes of operation, i.e., (1) high-level (low-sensitivity) detecting, and (2) low-level (high-sensitivity) detecting. The high-level mode is used during orbit morning when the spin eyes first begin to see the sun. As the sun rises above the limb of the earth, the light intensity varies because of albedo effects. When the instantaneous output level of the spin eyes is sufficient to overcome the high-level detecting threshold of the level detector, a pulse is fed through the pulse shaper circuit and on to the day-night turn-on circuits. These circuits then cause day-power to be applied to the spacecraft during this upward excursion of light intensity. One destination of this day-power is the spin box 15-volt regulator. The output of this regulator is then fed back to the level detector bias circuit and causes the



detector to operate in the low-level detecting mode. This action effectively "latches" the level detector on, once its high-detecting threshold has been overcome and any varying light levels are thereby prevented from causing intermittent application (chattering) of day-power.

Pulse Shaper. As previously mentioned, the output of the level detector is fed to a pulse shaper circuit. Here the spin pulses, which are roughly rectangular, are inverted twice and, in the process, become more square. After the first inversion, the positive-going trailing edge (originally a negative-going trailing edge) is used to turn day power on (this will be discussed in a later paragraph) and also to synchronize a free-running oscillator. After the second inversion, the positive-going leading edge is used as gating pulses in the constant charge generator in the overspin loop. The importance of this double inverting is that the free running oscillator is synchronized by the trailing edge of the spin pulses and the inhibitor constant charge generator circuit is gated by the leading edge.

Free-running Oscillator. The free-running oscillator has a free period of about 2.9 seconds which corresponds to 0.345 rps. This rate is much slower than the normal wheel spin rate expected (0.45 to 0.66 rps) and, therefore, the spin pulses will synchronize and simultaneously increase the oscillator's free-running frequency to match the spin rate. The oscillator output is fed to the day turn-on circuits and to a bootstrap ramp generator.

Bootstrap Ramp Generator. The bootstrap ramp generator develops a sawtooth voltage waveform that increases linearly with time. The period of this sawtooth (or ramp) is identical to that of the spinning wheel since the ramp generator is controlled by the oscillator, which in turn is synchronized by the trailing edge of the spin pulses. The peak voltage reached by the ramp



is then directly proportional to the wheel period. That is, the higher the value of this peak voltage, the slower the spin rate.

This ramp voltage is fed to two detector circuits - an overspin detector and an underspin detector.

Overspin Detector. The overspin detector functions as an under-voltage detector. As the ramp (Fig. 7-4a) increases from zero volts up to the level at which it is reset by the trailing edge of the spin pulse (Fig. 7-4b), the overspin detector produces a positive output pulse (Fig. 7-4c) that starts at a preset point on the ramp (called the overspin threshold) and ends when the ramp is reset. The overspin threshold is preset for a nominal wheel spin period of 1.52 seconds (0.66 rps). This means that for spin rates above 0.66 rps (Fig. 7-4e), the output from the overspin detector is at ground level (Fig. 7-4g).

When the detector output is positive, a storage capacitor is charged and then slowly discharged. This produces the decay function shown in the detector output (Fig. 7-4c). When the output from the detector is zero, the charge on the storage capacitor drops to zero as shown in Fig. 7-4g. This output from the overspin detector is used as an input to the constant charge generator.

Overspin Constant Charge Generator. The purpose of the constant charge generator is to generate a fixed amount of electrical charge (coulombs) each time an overspin condition is sensed by the overspin detector.

When the overspin detector output is positive (corresponding to a normal spin rate condition, Fig. 7-4c), there is no output from the constant charge generator (Fig. 7-4d). However, when the detector output is zero (indicating an overspin condition, Fig. 7-4g), the constant charge generator generates a pulse of current

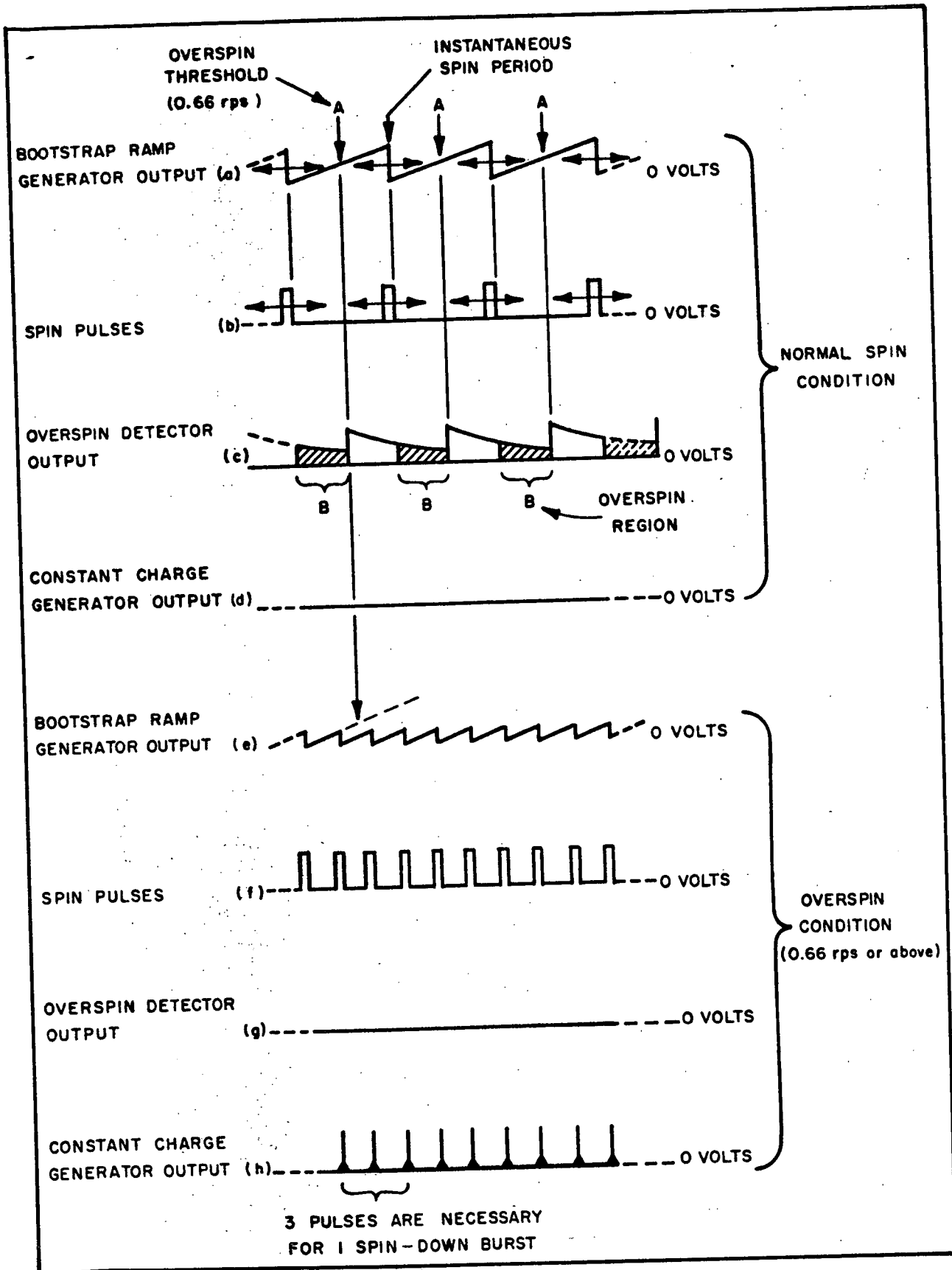


Fig. 7-4 Spin-Down Loop Timing Diagram



for a fixed period of time (Fig. 7-4h). The length of this pulse is governed by the differentiated leading edge of the spin pulse (Fig. 7-4f) which is used as a gating pulse.

The timing relationships of the ramp, spin pulses, overspin thresholds, and constant charge generator outputs are shown in Fig. 7-4.

Integrator, Spin-Down Burst Generator, and Solenoid Driver. The output pulses from the constant charge generator are fed to an integrator circuit where they are stored on a capacitor. This summing action continues for three consecutive pulses at which time the charge is sufficient to forward bias a uni-junction switch. The output pulse from the uni-junction circuit is then fed to the spin-down burst generator.

The spin-down burst generator is a mono-stable multivibrator with a four-second time constant. For each integrator pulse, this circuit generates a four-second rectangular wave output. This output is fed to a solenoid driver circuit which provides a ground path for the spin-down solenoid. A four-second burst of gas is then released from the spin-down nozzles.

Underspin Detector, Constant Charge Generator, Integrator, Spinup Burst Generator, and Solenoid Driver. The other destination of the ramp discussed in the Bootstrap Ramp Generator subsection, is the underspin detector in the underspin loop. This detector functions as an overvoltage detector.

As the ramp voltage increases (signifying a decreasing spin rate), the turn-on threshold of the underspin detector is ultimately reached. This turn-on threshold corresponds to a spin rate of about 0.45 rps.



The output of the underspin detector is used to trigger another constant charge generator. This generator differs from the overspin constant charge generator in that the latter was gated by the spin pulses and this one consists of a mono-stable multi-vibrator and, therefore, provides its own timing. The purpose, however, is the same in both cases.

As in the overspin loop, the output of the constant charge generator is stored by a capacitor in the integrator circuit. After three pulses are received, the integrator triggers the spinup burst generator and a four-second pulse is fed to the spinup solenoid driver. A ground path is then provided for the spinup solenoid and a four-second burst of gas is released from the spinup nozzles.

The timing relationships of the ramp, underspin detector, and the constant charge generator are shown in Fig. 7-5.

Initial Despin. The automatic spin control circuits also provide the initial despinning of the wheel from about 99 rpm (1.67 rps) to 0.62 rps during the launch phase.

7.6.3 Manual Spin Control

Manual spin control can have two separate functional operations: (1) if a spin rate outside the limit of 0.39 to 0.70 rps is detected, the auto spin limiter (ASL) circuits automatically disable the automatic spin circuits to prevent spin rate run-away, and (2) a ground command control capability permits spin rate correction when the manual mode is selected.

Detection of the ASL overspin and underspin rates is similar to spin rate sensing in automatic control operation. Spin detector No. 3 (Fig. 7-3) provides a spin pulse to the pulse amplifier

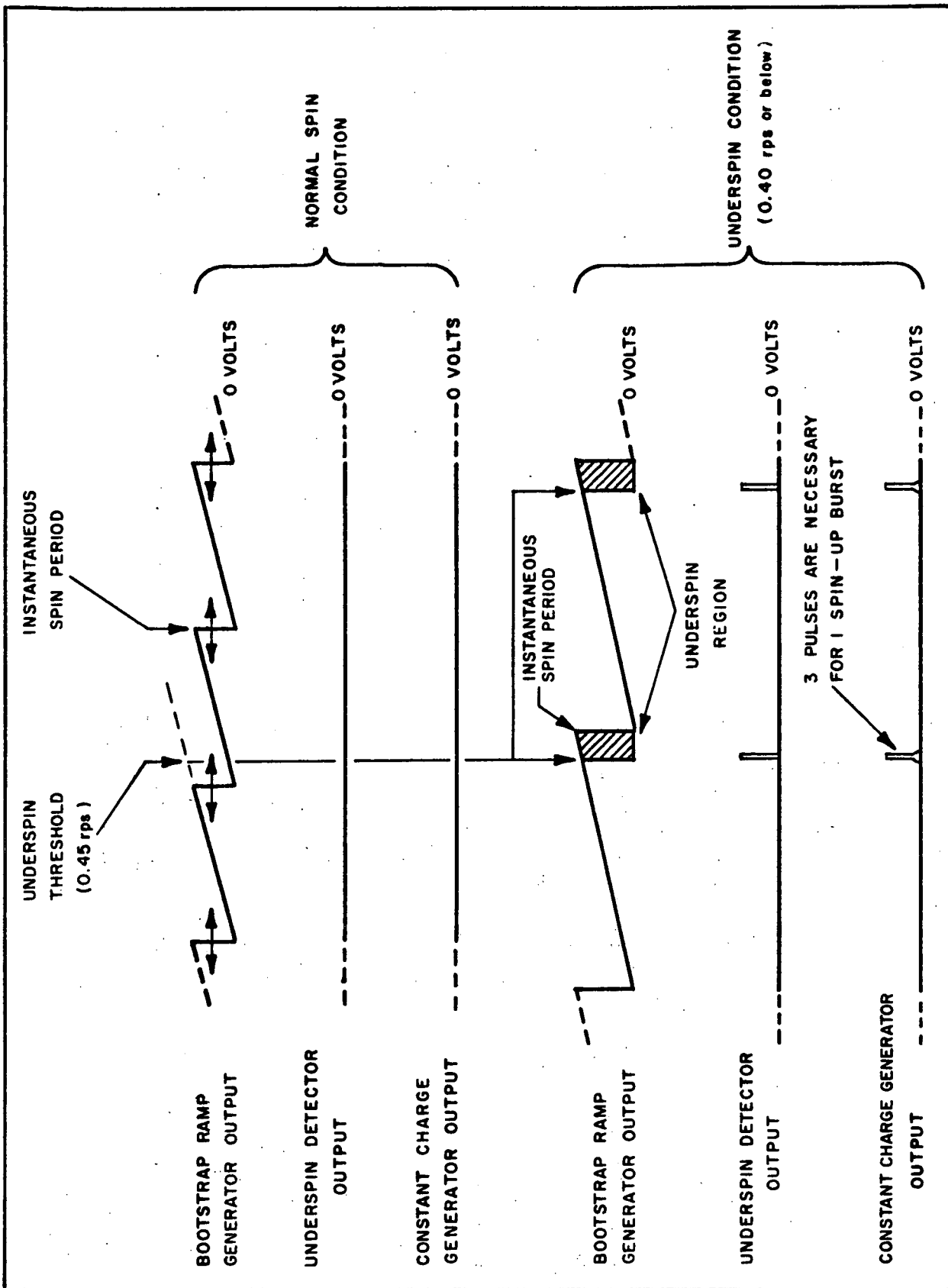


Fig. 7-5 Spin-Up Loop Timing Diagram



once every wheel revolution. The amplifier output is fed through a pulse shaper and then to a ramp generator whose output voltage rises linearly with time. The ramp generator output reaches a peak level which is a measure of the wheel revolution period. Both overvoltage and undervoltage detectors are then used to sense the low and high triggering rates of 0.39 and 0.70 rps, respectively.

The undervoltage (overspin) detector is very similar to that used in the auto spin-down circuits. When the spin rate goes above 0.70 rps, the output from the overspin detectors drops to zero. When this happens, the first unsuppressed spin pulse energizes the gate amplifier, which in turn energizes the driver-lockout circuit and latches the auto-manual relay to the manual position. The underspin detector responds to the high ramp voltage peaks occurring with wheel spin rates of 0.39 rps or less, and also causes the auto-manual relay to switch to the manual position.

The ASL circuits are disabled during the launch sequence phase so that the auto spin control circuits can perform the initial despin. Disabling of the ASL circuits is accomplished by latching the ASL enabling relay in its disabled position during launch. This prevents power from being applied to the driver-lockout circuit. At the 800 second timer signal, the ASL enabling relay is latched in the enabled position, thereby enabling the ASL circuits. The despin operation will have normally been completed before the 800 seconds timer signal occurs.

When the manual control mode is in effect, ground commands must be sent to initiate four-second spin-up or spin-down bursts. Repeater relays drive their respective burst generators and solenoid drivers when commanded. The required command functions



for switching to either manual or automatic operation are also shown in Fig. 7-3.

7.6.4 Day Power Turn-On

As mentioned, the spin pulses are also used to turn day-power on and off at sunrise and sunset, respectively. A block diagram of the day-night circuits is shown in Fig. 7-6.

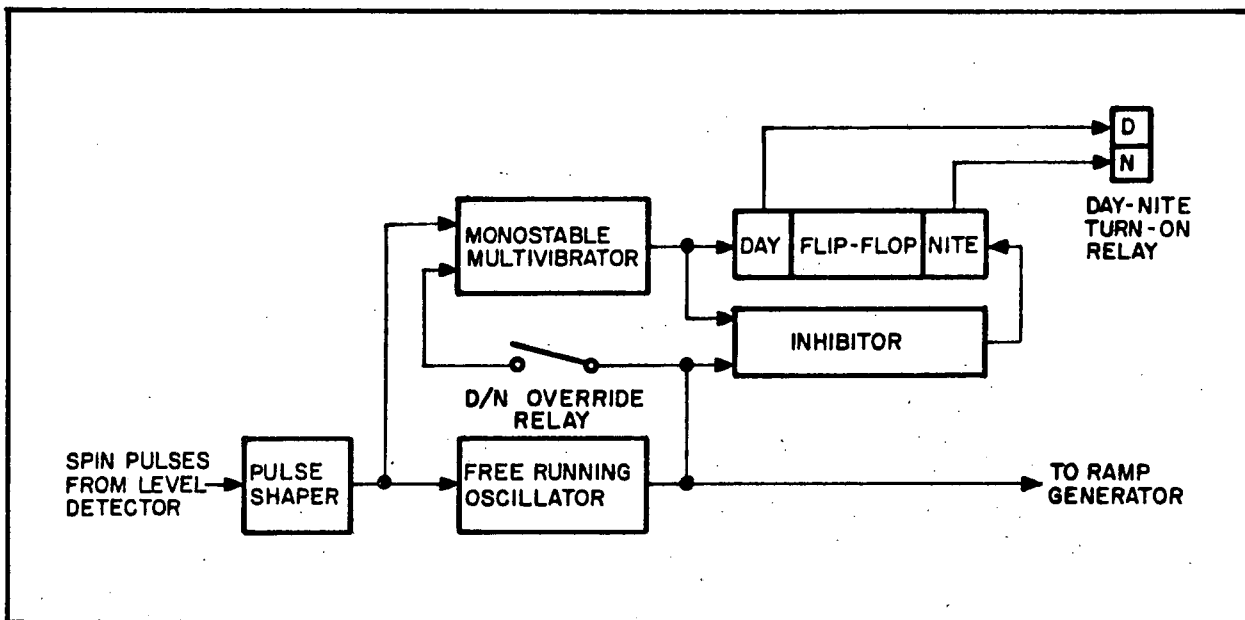


Fig. 7-6 Day Power Turn-On Circuits



First, consider the night condition, where there are no spin pulses, and, thus, the free-running oscillator is operating at its low rate. Also, the mono-stable multivibrator is not producing an inhibiting signal to the inhibitor because there are no spin pulses. Therefore, the output of the oscillator is not inhibited and it keeps the day-night flip-flop set to the night state.

When the spin pulses are present (during day only), the free-running oscillator is synchronized with the wheel spin rate. Also, the mono-stable multivibrator is triggered by the spin pulses and it outputs a pulse about 0.2 seconds long. This pulse is used to set the day-night flip-flop in the day state and also to inhibit the oscillator output from resetting the flip-flop. This action continues until the spin pulses are no longer present, which signifies night, and the flip-flop is again set to the night state by the oscillator pulses.

A means has also been provided by which day-power, during test operations, can be turned on when there are no spin pulses. This is done by feeding the oscillator output through the day-night eye override relay (which can be commanded from the test console only), and using this signal as an input to the mono-stable multivibrator. In this case, the output of the multivibrator is used to set the day-night flip-flop to the day state and also to inhibit itself from resetting the flip-flop.

It is important to note that this function can be used only during ground testing because the D/N eye override relay cannot be operated through the spacecraft command system. However, another relay is provided (the day-night bypass relay), which can be used to bypass the auto day-night turn-on circuits. This relay is commandable through the spacecraft command system.



7.7 OFFSET POINTING CONTROL FUNCTIONAL DESCRIPTION

The OSO-6 pointing control system can be operated in any of four modes:

- (1) normal center-point mode
- (2) large raster mode
- (3) offset point mode
- (4) small raster mode

In the normal center-point mode, the optical axes of the pointed experiments are pointed at the center of the sun with an accuracy better than ± 1 arc minute. In the large raster mode, the pointed experiments are caused to scan the sun with a 64-line (46 by 46 arc minute) raster pattern centered about the sun. In the offset point mode, the pointed experiments can be pointed at any one of 16,384 points (128 by 128 grid) within the large raster pattern. In the small raster mode, the pointed experiments can be directed to raster about any of the offset points with a raster pattern 7 arc minutes in azimuth and 7.5 arc minutes in elevation.

7.7.1 Large Raster Mode

In the large raster mode, the pointed experiments scan at the rate of one line every 24 main frames, or $0.32 \text{ sec/MF} \times 24 \text{ MF} = 7.68$ seconds per line. The period for a complete large raster pattern is then $7.68 \text{ sec/line} \times 64 \text{ lines} = 491.52$ seconds or 8.2 minutes. The nominal size of the large raster pattern is 46 by 46 arc minutes which means that each line is separated by $46 \div 63 \text{ spaces} = 0.73$ arc minutes. The size of the large raster is affected by changes in solar intensity due to the elliptic orbit of the earth. This effect is approximately six percent over a period of one year.



Figure 7-7 illustrates the OSO-6 raster pattern together with the offset point grid coordinates. Point A represents the on-point position (center of the solar disc). The large raster pattern centers about this point.

When the large raster mode is selected, a start-of-raster (SOR) pulse is generated by the raster synchronizing generator which causes the raster generator to begin the large raster at the center of raster line 1. Thereafter, a SOR pulse is generated each time a new raster pattern is begun (each 8.2 min). Also, a start-of-line (SOL) pulse is generated each time a new line is begun (every 7.68 sec).

7.7.2 Small Raster Mode

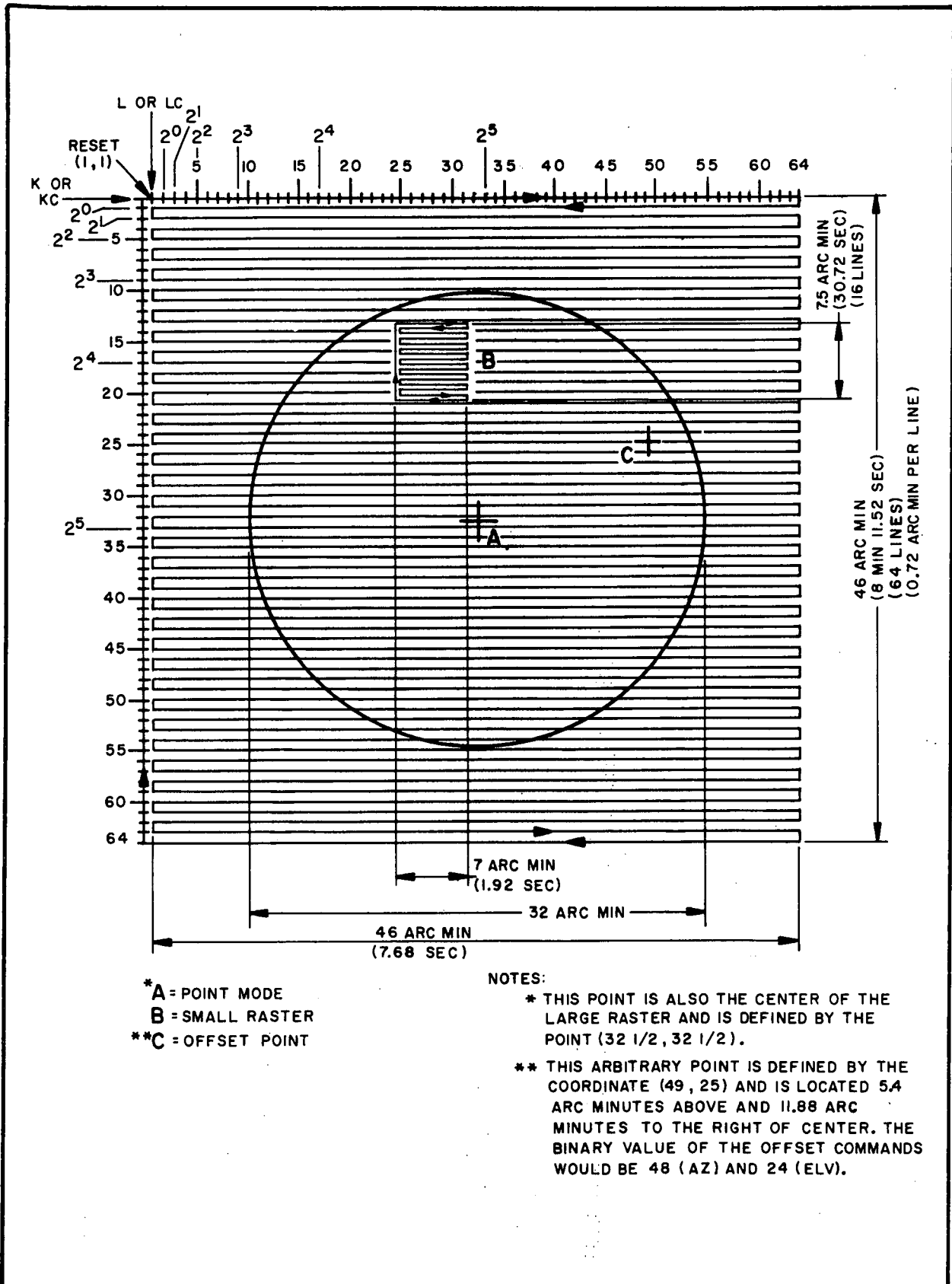
Point B (Fig. 7-7) illustrates the small raster mode. The size of this raster is 7.5 arc minutes in elevation and 7 arc minutes in azimuth and consists of 16 equally spaced lines. This means that each line is separated by $7.5 \div 15$ spaces = 0.5 arc minutes. The total time for each raster is one main frame or 30.72 seconds. The sweep time for each line is then $30.72 \div 16 = 1.92$ seconds.

The small raster is always centered around whatever offset point coordinate is programmed into the offset point generator.

7.7.3 Offset Point Mode

By means of the offset point mode, the pointed instruments can be pointed at any one of 16,384 points within a square pattern about the size of the large raster pattern.

In Fig. 7-7, the numbers 1 through 64 (in both azimuth and elevation) define the offset pointing grid (excluding the vernier offset). Any coordinate point on this grid can be selected by sending the proper combination of offset commands.



- *A = POINT MODE
- B = SMALL RASTER
- **C = OFFSET POINT

NOTES:

- * THIS POINT IS ALSO THE CENTER OF THE LARGE RASTER AND IS DEFINED BY THE POINT (32 1/2, 32 1/2).
- ** THIS ARBITRARY POINT IS DEFINED BY THE COORDINATE (49, 25) AND IS LOCATED 5.4 ARC MINUTES ABOVE AND 11.88 ARC MINUTES TO THE RIGHT OF CENTER. THE BINARY VALUE OF THE OFFSET COMMANDS WOULD BE 48 (AZ) AND 24 (ELV).

Fig. 7-7 OSO-6 Raster Patterns



In addition, the 64 by 64 offset point grid can be expanded to 128 by 128 by using the azimuth and elevation vernier offset commands. The azimuth vernier command will move the pointed experiments one-half step (or 1/2 bit) to the right of whatever point the experiments were previously pointing at. The elevation vernier command will move the experiments 1/2 bit up.

Note: When the vernier offset commands are used, the actual size of the offset grid has been enlarged by 1/2 bit up and 1/2 bit to the right. This means that the center of this new grid is 1/4 bit up and 1/4 bit to the right of the center of the large raster.

7.7.4 OSO-6 Offset Circuit

Incorporation of the offset point and small raster into the OSO-6 scan system required the following:

- (1) Addition of a new PC board, containing the circuitry for the selection of offset points.
- (2) Modification of the existing large raster circuitry to incorporate the small raster electronics and also to update the design.
- (3) Modification of timing circuits to incorporate small raster and also to enable the offset system to be versatile.
- (4) Addition of monitors to allow verification of offset mode and offset point selected.

The above changes were incorporated into the existing power amplifier and servo amplifier assemblies.



Figures 7-8 and 7-9 are functional block diagrams of the offset point/offset scan system.

Voltage levels, corresponding to the offset points on the offset grid pattern, are generated by changing the gain of an operational amplifier in discrete steps. The op-amp gain is changed on ground command by setting a flip-flop which turns on a field effect transistor (FET), connecting a selected resistor to the summing junction, thus changing the input impedance of the op-amp. All the offset point flip-flops are reset by one ground command. Although this adds slight complexity to ground operation, it decreases the number of commands required, thereby increasing system reliability. The offset point generators (azimuth and elevation) are identical and are summed at the input to the azimuth and elevation output operational amplifier by ground command.

Generation of a raster pattern requires a highly-linear triangular voltage waveform (azimuth) and a staircase function of uniform steps (elevation). The triangular wave form is produced by the azimuth integrator, with the peak-to-peak voltage and period dependent upon the pattern selected (large or small). The staircase waveform is produced by summing currents which result from six binary-weighted positioning currents that are controlled by their respective counter stages. The period of the clock input to the counter is dependent upon whether large or small raster is selected.

Azimuth and elevation signal generator outputs are summed at the input to their respective scale amplifier along with the offset point generator output. In addition to providing a summing point for the offset point and scanning signals, the scalar amplifiers permit fine adjustment of the amplitudes to obtain precise pattern sizes. The outputs of the scalar amplifiers are connected to their respective current generators where the scalar output

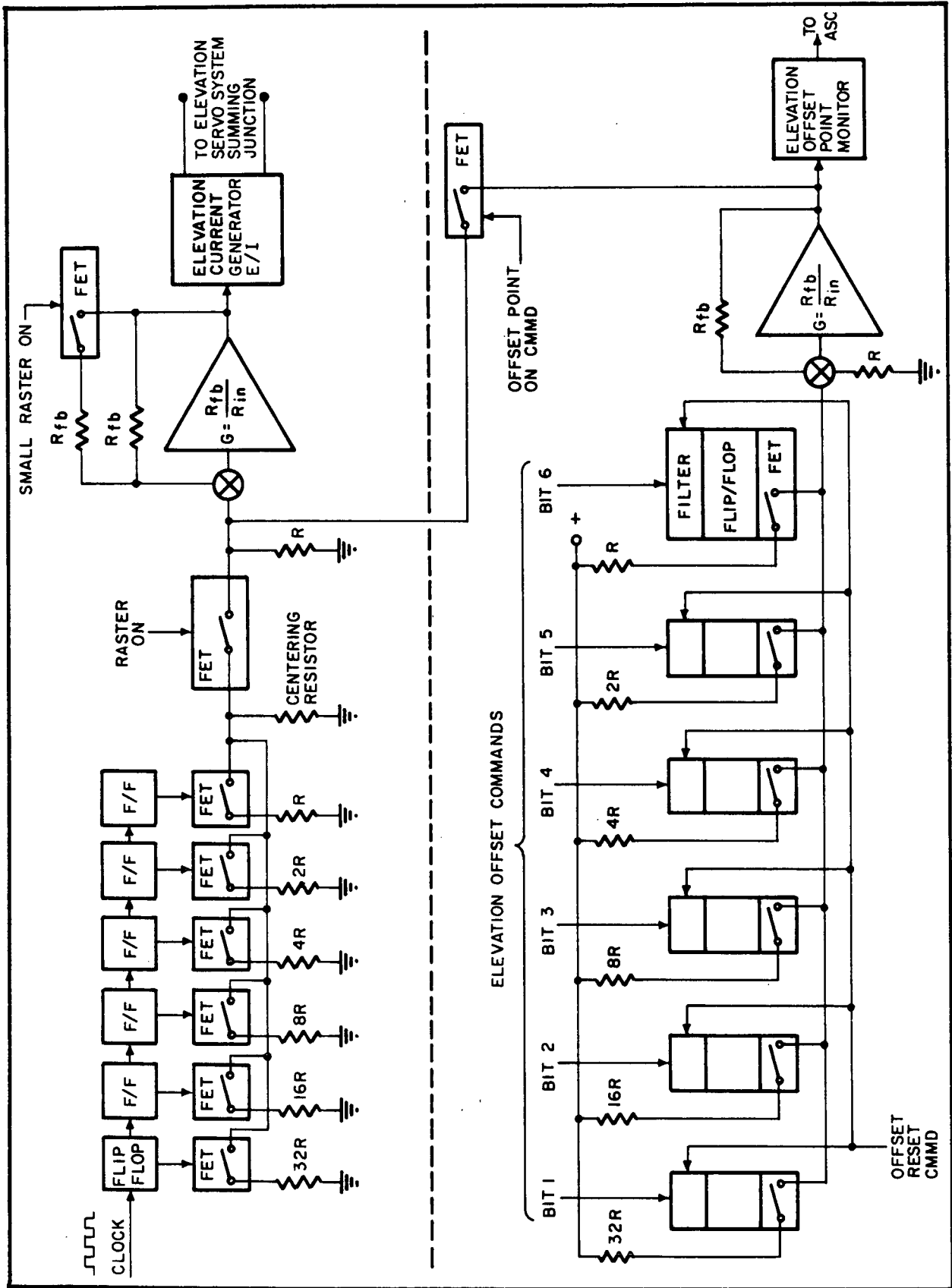


Fig. 7-8 Elevation Offset Channel

C.5



voltages are transformed into proportional current signals. The current signals are then summed with the servo control sun sensor signals for offset mode operation.

7.8 COARSE SERVO FUNCTIONAL DESCRIPTION

The pointing control system provides automatic solar acquisition and pointing of the sail and pointed experiments beginning each orbit morning. The system also provides offset-mode operation as described in Paragraph 7.7. The pointing servo consists of three servo loops; namely, the coarse azimuth, fine azimuth, and fine elevation. These servo loops consist of three separate control sensor assemblies (control eyes), electronic control circuits contained in the servo amplifier and power amplifier assemblies, and the azimuth and elevation torque motors.

The azimuth and elevation servo loops differ in operational concepts in only a few respects. The most important difference is that the azimuth control requires two solar sensing functions (one for coarse sensing and one for fine sensing) while the elevation control requires only fine solar sensing because the pitch control system performs the coarse elevation pointing function. The dual azimuth sensing design requires an additional preamplifier and compensation network as well as an on-target relay that switches azimuth servo control from coarse to fine sensing circuitry when on-target pointing is achieved.

Each orbit morning, day power is applied to the pointing control circuits by the day-night sensing circuits in the power distribution system. The coarse azimuth servo loop then despins the sail from the wheel spin rate to within 3 degrees of stationary azimuth pointing. Control is then transferred to the azimuth fine loop by the coarse/fine control (on target) relay. The azimuth fine and elevation fine loops then complete the acquisition, aligning the pointed instruments to within one arc minute of the center of the sun.



In steady-state pointing, the azimuth servo drives against the unidirectional friction drag of the azimuth bearings contained in the wheel hub. Thus, the azimuth servo must develop a drive torque to counteract this ever-present, and nearly-constant, drag. The elevation servo, on the other hand, must overcome the elevation bearing friction only when a correction in elevation is required. Because of the extremely slow drift rate of the observatory in pitch, no elevation drive is necessary unless there is spin axis nutation or wobble present or if the pointed instruments are dynamically unbalanced so that they assume a different position at night, which would then require elevation drive in the morning to bring them back to the on-point position. Also, a small amount of elevation drive may result from unsymmetrical loading by the flex-cables that provide electrical connection between the pointed instruments and the sail electronics.

Because the functional differences between the azimuth and elevation servos are minor, a detailed functional description of the azimuth servo loop is first presented, followed by a brief discussion of the elevation servo. A block diagram of the OSO-6 pointing control system is shown in Fig. 7-10.

The main difference between the OSO-5 and OSO-6 pointing control systems consists of the offset mode capability described in Paragraph 7.7.

7.8.1 Coarse Azimuth Servo Sensors

The coarse azimuth servo despins the observatory upper structure from the night spin rate each orbit dawn. It aligns the pointed instruments with the sun to within three degrees in azimuth. The on-target sensor then enables the fine azimuth servo. This discussion of the coarse azimuth servo will cover the operating characteristics of the coarse sensors, circuits unique to the

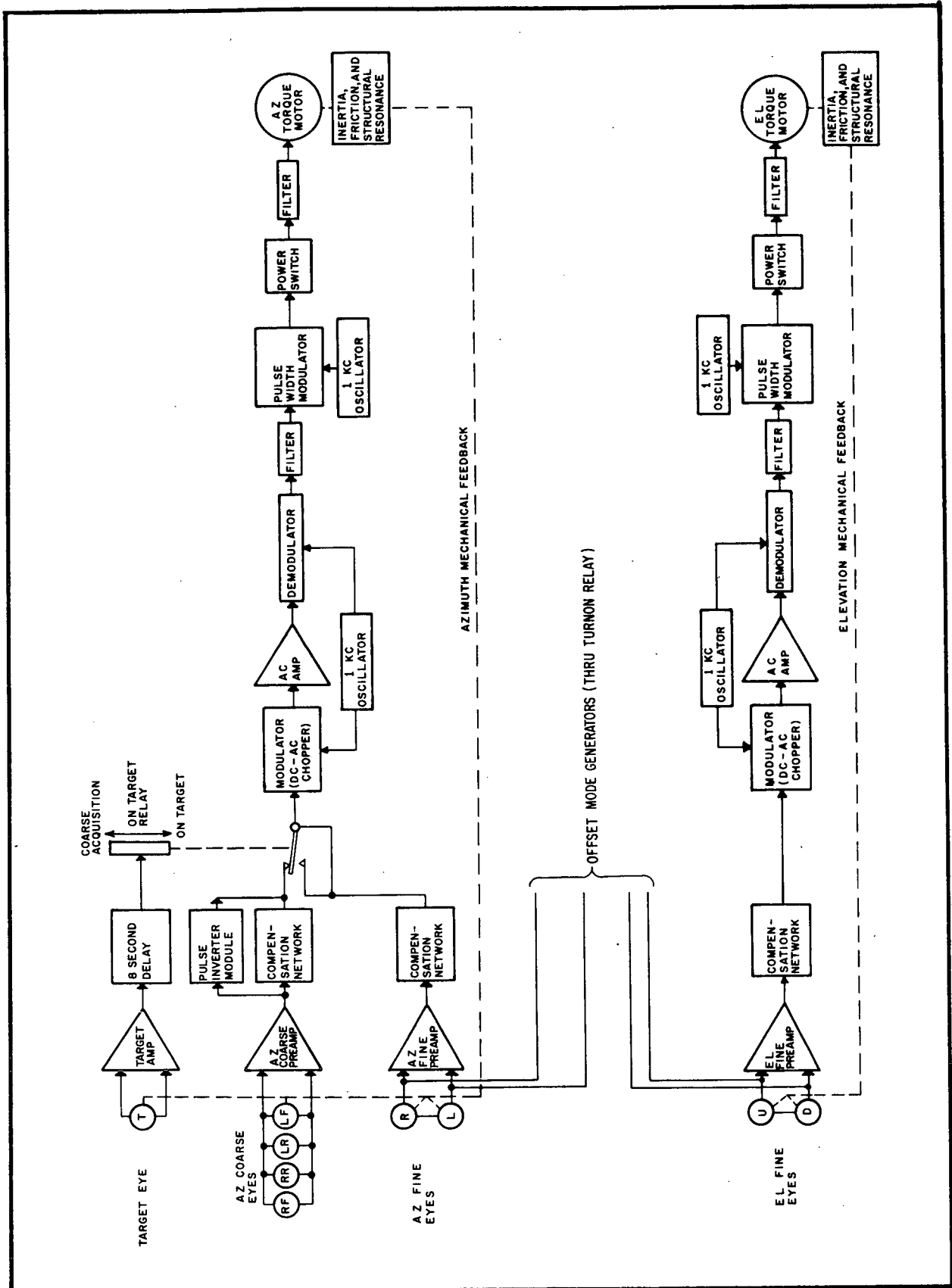


Fig. 7-10 OSO-6 Pointing Control Block Diagram



coarse-acquisition mode, circuits common to the coarse and fine modes, and the functions of the target eye and its circuits.

Each of the four azimuth-coarse eyes consists of a silicon photoelectric sensor mounted to an aluminum block and covered by a Corning No. 2600 red glass filter. Each eye assembly is protected from radiation damage by a 0.1-inch quartz cover slip installed over the filter. The eyes are mounted in holders which establish the desired view angles. The completed eye assemblies are shown in Fig. 7-11.

The vertical field-of-view of the eyes is from 15 degrees above to 15 degrees below the wheel plane. This restricted field-of-view prevents the eyes being affected by light reflected from the top of the wheel or from earth albedo. It also prevents solar sensing and servo drive when the spin axis is not perpendicular to the solar vector within 15 degrees. The composite field of the eyes in azimuth is 360 degrees. The static view angle, however, is about 110 degrees for each front eye, and 95 degrees for each rear eye (see Fig. 7-12).

As the sail rotates, the coarse eyes produce a current waveform (error signal) shown in Fig. 7-12. The figure shows the location of each eye and the output waveform of each as the sail rotates. The four individual outputs are summed as shown on their way to the azimuth coarse preamplifier.

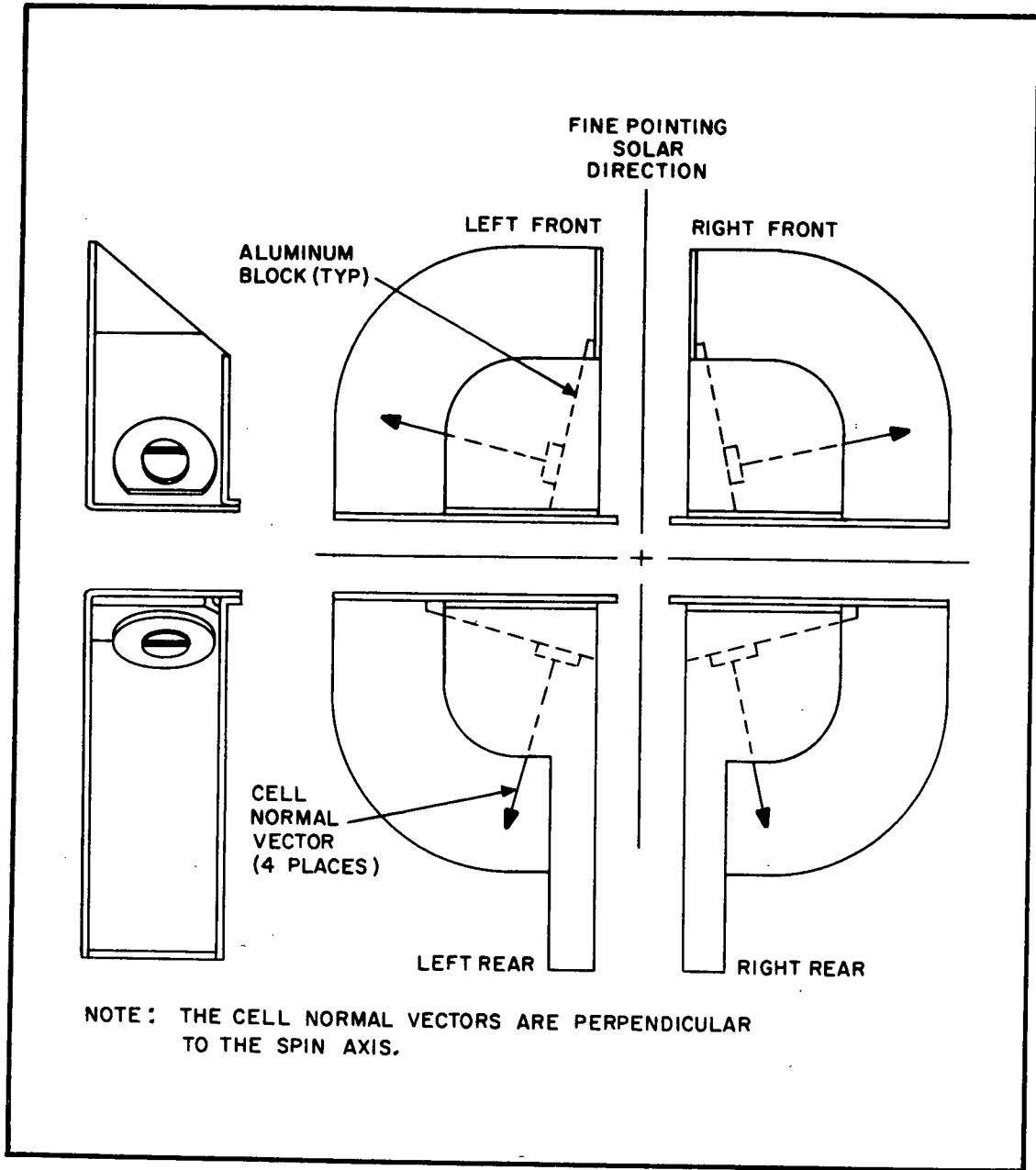


Fig. 7-11 Coarse Sensor Assemblies

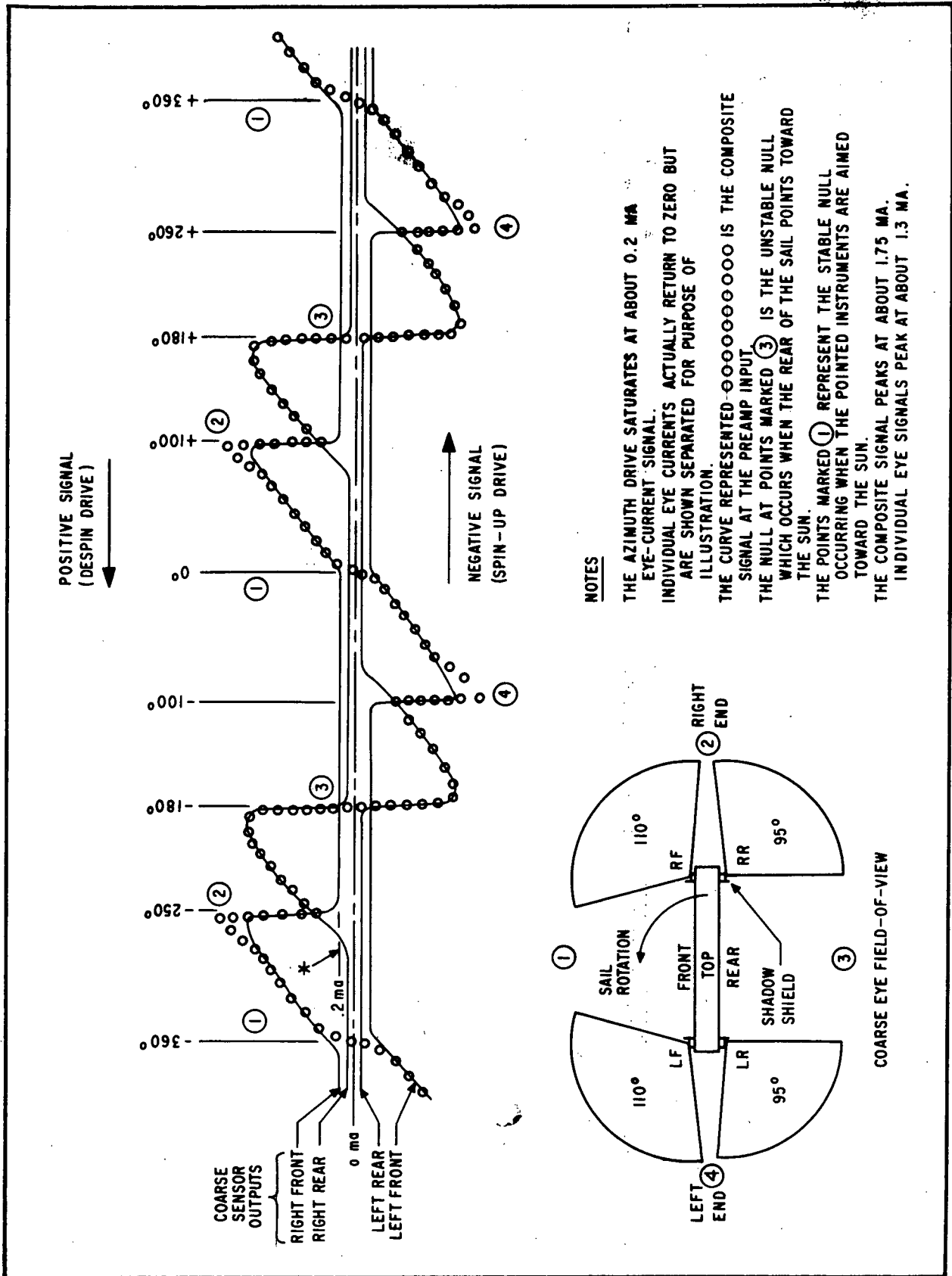


Fig. 7-12 Coarse Sensor Signal



The composite signal from the coarse eyes has two important terms: a position term and a time-rate-of-change term. The position term is the instantaneous amplitude of the signal. The rate term reflects the rate at which the position term changes. Each of these terms plays an important role in the coarse-acquisition function.

The polarity of the position term is such that the positive area of the signal (shown on Fig. 7-12) causes the sail to be driven in the despin direction. This portion of the signal is produced by the right-front (RF) and right-rear (RR) eyes. The negative area of the signal causes the sail to be driven in the spinup direction. This portion of the signal is produced by the left-rear (LR) and left-front (LF) eyes.

Note that the drive produced by signals in the region of the unstable null (③ on the curve) are away from the null, while those near the stable null (① on the curve) are toward the null. This assures that the sail will only stop at the stable null, which is the desired position.

The rate term dominates while the sail rotates quickly. A rate network and pulse-inverter circuit (which will be discussed later) convert most of the negative (spinup) signal into a positive signal. This action continues until the spin rate is reduced to about 0.07 rps. The position term then becomes dominant and remains so throughout the rest of the acquisition. Thus, the rate term is dominant at high spin rates and the position term at slow spin rates.



7.8.2 Coarse-Servo Circuits

The circuits described in this paragraph are those peculiar to the coarse-mode operation of the azimuth pointing control.

The coarse preamplifier converts the coarse-eye output (Fig. 7-12) from a current waveform to a voltage waveform. The preamp is a differential, low drift amplifier and incorporates automatic compensation circuits for changes in its own gain. It provides a low-impedance load for the eyes and a high-impedance output to the rate network. The preamp is designed for unsaturated operation between +1.5 ma of input eye current.

The output of the azimuth coarse preamp is fed into a compensating network and a pulse-inverter module (PIM) as shown in Fig. 7-10. Rate sensing and the conversion of spinup signals are accomplished in these circuits.

The compensating network consists of a resistor-capacitor coupling arrangement which provides dc coupling for low-spin-rate eye signals and predominantly-despin signals for higher spin rates. This network provides for a positive (despin) drive signal when the eye signal is positive-going and spin rate is greater than about 0.07 rps. Figure 7-13(a) and (b) show the relationship between the eye signal and the ideal output of the compensating network. Notice how this compensation turns the symmetrical waveform into a predominantly positive signal.

Part of the despin signal is lost, however, due to differentiation of the ideal output. The resultant waveform is shown in Fig. 7-13(c). The negative portion of this waveform represents spinup drive and therefore decreases net despin efficiency. The effect of the negative signal is substantially reduced by the addition of the PIM circuit.

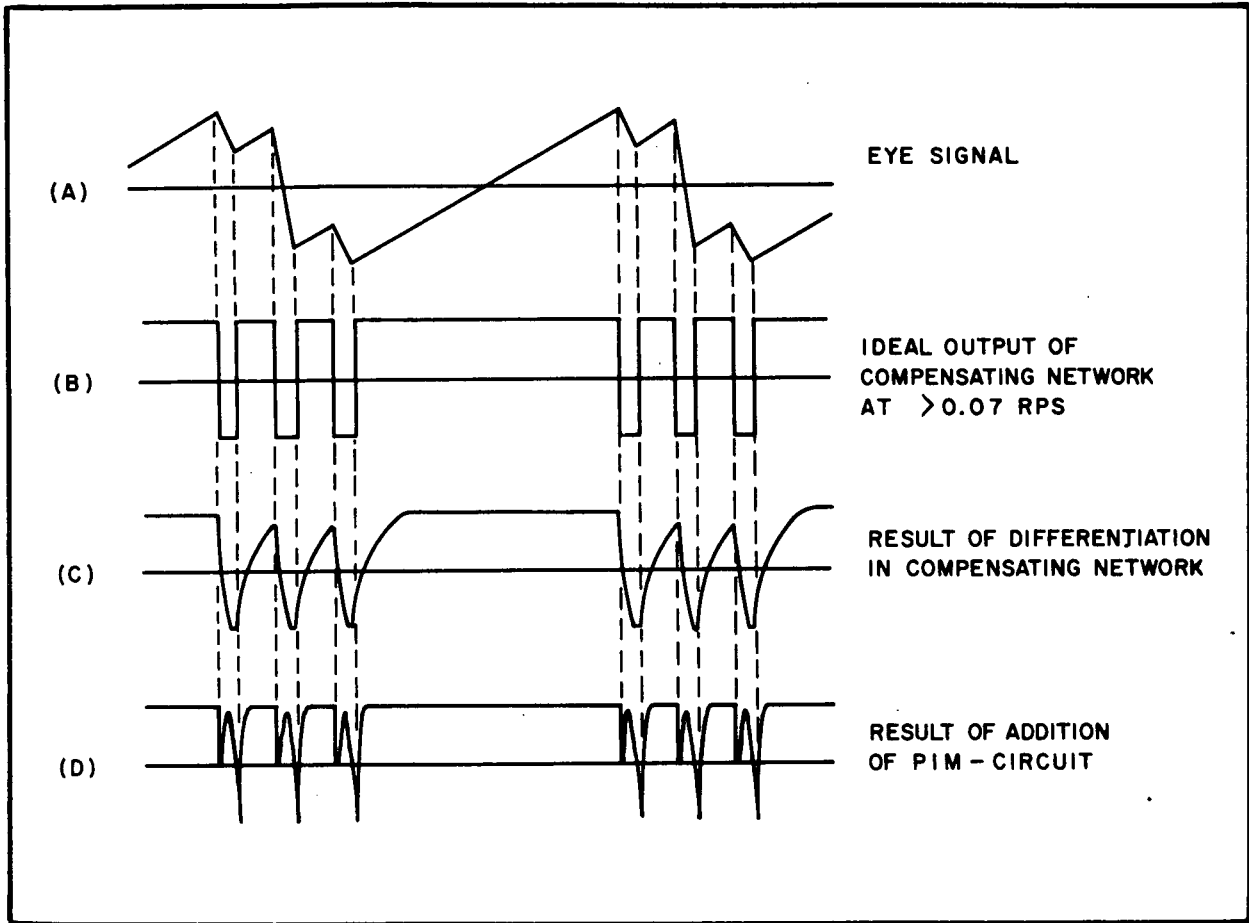


Fig. 7-13 Rate Signal Compensation

The pulse-inverter module (PIM) tends to superimpose a positive signal on the negative output of the compensating network. It does this through a time constant which prevents it from interfering with spinup drive in the final phase of solar acquisition. The PIM also peaks up the leading edge of the positive output of the compensating network. Both of these actions of the PIM increase net despin drive efficiency as shown in Fig. 7-13(d).

When the sail rotation is reduced to about 0.07 rps, the compensating network and PIM give way to direct dc coupling of the eye signal to the modulator (Fig. 7-10). The position term of the



error signal then becomes dominant and controls the final stages of coarse azimuth acquisition.

The net efficiency of the azimuth coarse servo is expressed in a term known as net despin drive. It is found by subtracting the percent of time the drive is negative (spinup) from the percent of time drive is positive (despin) during a revolution of the sail. Net despin drive is expressed as a percent and plotted as a function of sail spin rate.

The output of the coarse-servo circuits is fed to the circuits which are common to the azimuth servo in both the coarse-acquisition and fine-pointing modes (Para. 7.8.3).

7.8.3 Common Azimuth Circuits

The characteristics of the azimuth modulator, ac amplifier, demodulator, pulse-width modulator, power switch, and torque motor are described in this paragraph. These are circuits which are common to the azimuth fine and coarse servo loops.

The output of the rate network is fed through the on-target relay to the modulator.

The modulator is a dc-to-ac chopper, which samples the differential output of the coarse preamplifier and rate network at a 1,000 Hz rate. The output of the modulator is a square wave with a peak-to-peak amplitude equal to the differential input signal. This output is fed to the azimuth ac amplifier.

The ac amplifier saturates with an input corresponding to coarse-eye currents of about ± 0.2 ma. Thus, during acquisition, this amplifier is saturated most of the time, providing a clipped output. This output goes to the demodulator for reconditioning.



The demodulator is driven by the same oscillator that drives the modulator. It reconditions the output of the ac amplifier as a dc signal. The output of the demodulator is an amplified and clipped reconstruction of the error signal, except that it is referenced to a 7.5 v bias level, and has 1,000 Hz transients in it. The response curve for the coarse-preamp/ac-amplifier combination is shown in Fig. 7-14.

The output of the demodulator is fed through a filter which removes the 1,000 Hz transients and any other system noise down to about 50 Hz. This filtered signal then goes to the PWM circuit.

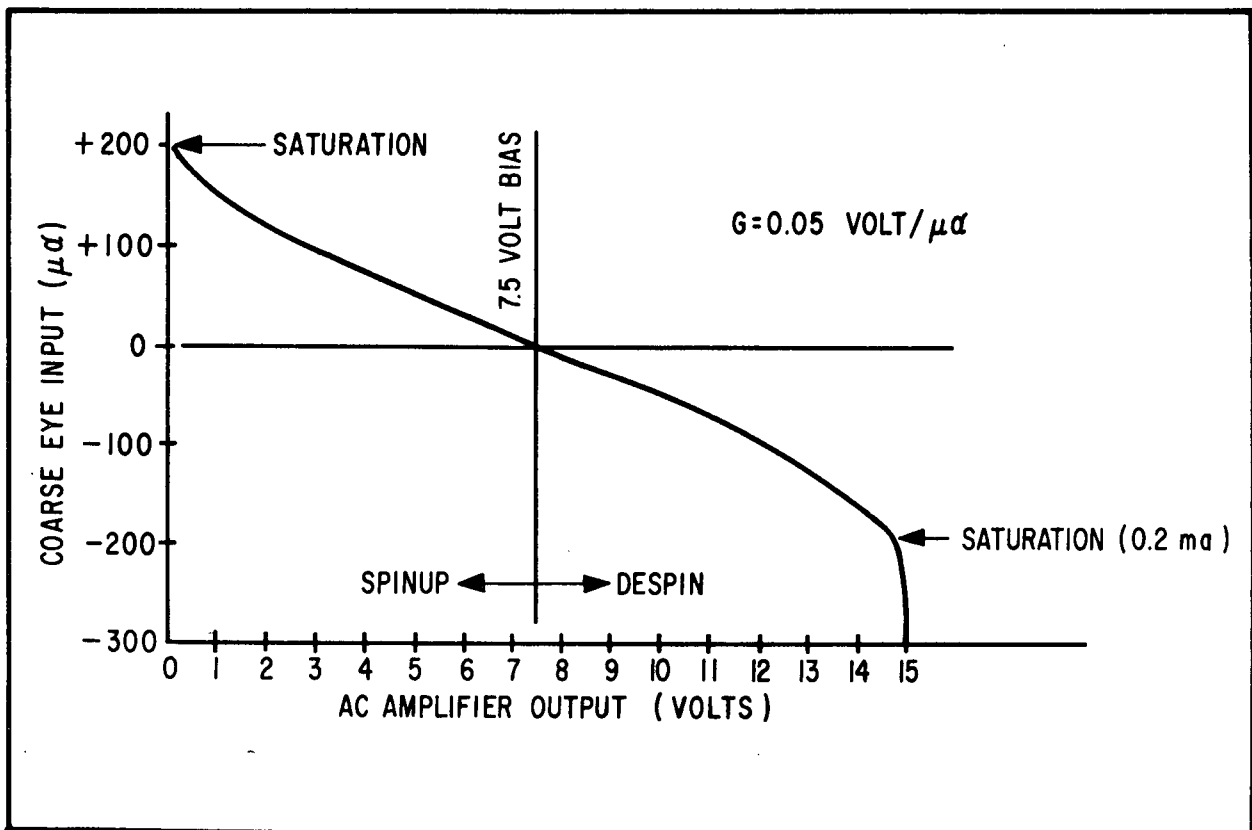


Fig. 7-14 Typical Coarse Azimuth Preamp/AC Amp Response



The pulse-width modulator (PWM) converts the amplitude modulated error signal into a constant-amplitude 1,000 Hz waveform in which pulse width (or duration) is proportional to the amplitude of the dc error signal. The principle reason for using a PWM design is to reduce power dissipation in the power switch. This eliminates a potential component-reliability problem in these circuits.

The PWM is designed to produce an output only when the input varies above or below the 7.5 v bias level. This variation is typically between about +2 and +13 v as the sail rotates. The PWM has a dead zone (no output) at about 7.5 ± 0.25 v. The dead zone has no effect on the operation of the azimuth loop since the wheel always spins in the same direction, holding azimuth-loop operation on one side of the dead zone (except during acquisition). The PWM dead zone is shown in Fig. 7-15.

The PWM actually consists of two separate PWMs that work together. One converts despin signal (>7.5 v) into pulse-width waveform and the other converts spinup signal (<7.5 v). Outputs of both PWM circuits are positive. Each output is fed to one side of the power switch for power amplification. Obviously, outputs from both PWM circuits cannot occur simultaneously since the inputs are separated at 7.5 v.

The power switch consists of two pairs of saturable transistor switches. One pair of transistors is controlled by the despin PWM and drives the azimuth torque motor in the despin direction. The other pair is controlled by the spinup PWM and drives the motor in the spinup direction. The outputs from the power switch are filtered before being applied to the torque motor to reduce power losses in the motor windings. The drive current is averaged by the filter.

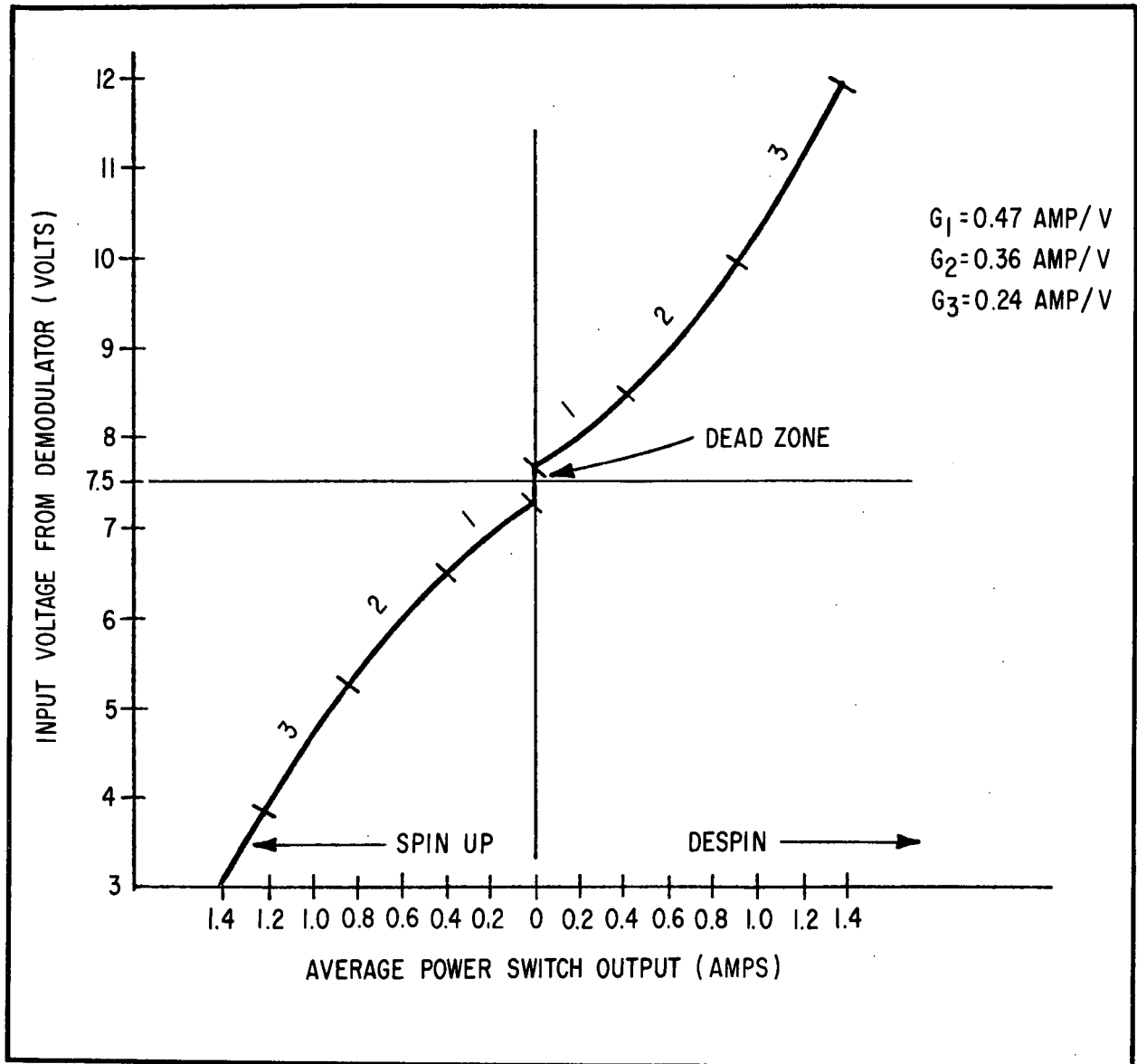


Fig. 7-15 Typical PWM/Power-Switch Response

Operation of the power switches in the region of saturation and cut-off avoids the heat dissipation and power waste inherent in other areas of the transistor load line.

Figure 7-15 shows a typical overall response of the PWM and power-switch circuits to inputs from the demodulator.



The azimuth torque motor consists of a permanent-magnet stator attached to the azimuth shaft (fixed to the sail), and a rotor attached inside the wheel hub. The drive power from the power switch (located in the power box in the sail) is fed through a brush assembly to the commutator of the rotor.

7.8.4 Target Eye and Coarse/Fine Switch

The target eye and coarse/fine switch are the link between the azimuth coarse and fine servo loops. When the coarse loop has brought the pointed instruments within 3 degrees of the solar direction, the target-eye senses the sun. After about an eight-second delay, coarse/fine switching occurs. The input to the azimuth ac amplifier is then developed in the fine-mode sensors and circuits.

The target eye is mounted in the fine-control-eye block, presented in subsection 7.9. The eye produces about a 2 ma current when the pointed instruments are aimed within the capability of the coarse pointing control. The elevation field-of-view of the target eye is about +6 degrees. Operation of the elevation servo is, therefore, not required for coarse/fine switching. The field-of-view of the azimuth fine-control eyes is greater than +8 degrees, providing the necessary overlap for smooth coarse/fine transition. The output of the target eye is fed through the target-eye amplifier to the coarse/fine relay driver and the telemetered target-intensity monitor.

The azimuth coarse/fine switch is often called the "on-target relay" for brevity. After the target-eye has been illuminated for the 8-second delay period, the on-target switch is released to the "fine" position. The switch is a momentary-operation relay and is energized in the coarse mode. This conserves power, since the servo operates in the fine mode for more than 98 percent of the time powered.



The on-target relay switches out the signal from the azimuth coarse eyes and completes the azimuth fine-control servo loop. This function is illustrated in Fig. 7-10. In addition, the relay generates an "on-target" signal which is monitored by telemetry, and enables the auto-pitch limiter (APL) circuits as described earlier in this section.

The target-intensity monitor is a telemetry sampling of the output of the target-eye amplifier. The linear characteristic of this amplifier provides for in-flight evaluation of target intensity and sensor degradation.

7.9 FINE AZIMUTH AND ELEVATION SERVO LOOPS

Fine azimuth and elevation servo control begins at the completion of coarse acquisition (coarse-fine switching). These servo loops function very much like the coarse azimuth servo loop, with the following exceptions:

- (1) The error signals are produced by the azimuth and elevation fine eyes.
- (2) A different azimuth preamplifier is used.
- (3) The rate-sensing and PIM circuits are replaced by compensation networks designed to adjust servo stability and response characteristics to other servo parameters such as static gain and structural resonances.
- (4) The elevation torque motor produces about one-half the torque that the azimuth motor produces.



The fine-control eyes for the azimuth and elevation servos each consist of a pair of BBRC FE-5 fine sensors. Each FE-5 sensor has a focusing lens, a red-glass filter, and a silicon solar cell. One half of each red filter disc is masked by a thin aluminum film. The output of each cell is a function of the direction it is pointing, as shown in Fig. 7-16.

The electrical leads from each sensor are connected in opposing polarity to the other half of the sensor pair. The sensors of each pair point slightly away from each other so that, on point, each sensor produces about ten percent of its maximum output. The two opposing currents produce a stable null in the on-point direction.

An azimuth or elevation error signal results when the sensor assembly is rotated from the on-point position. Figure 7-16 shows the output curve for a typical fine-eye pair. The figure also shows the front view of the eyeblock (including the Target eye), the aluminum shield orientation, and the behavior of individual eye outputs near the null region.

The fine-servo circuits are similar, in many ways, to those of the coarse azimuth loop already discussed. The areas presented here are those which are peculiar to the fine-control mode. The fine azimuth and elevation servo loops seek a precise null position, and maintain pointing accuracy within +1 arc minute.

As can be seen in Fig. 7-10, the fine-servo loops differ from the azimuth coarse loop primarily in the development of the sensor signals. The fine azimuth and elevation preamplifiers convert the current signal from the eyes to a voltage signal for the ac amplifiers.

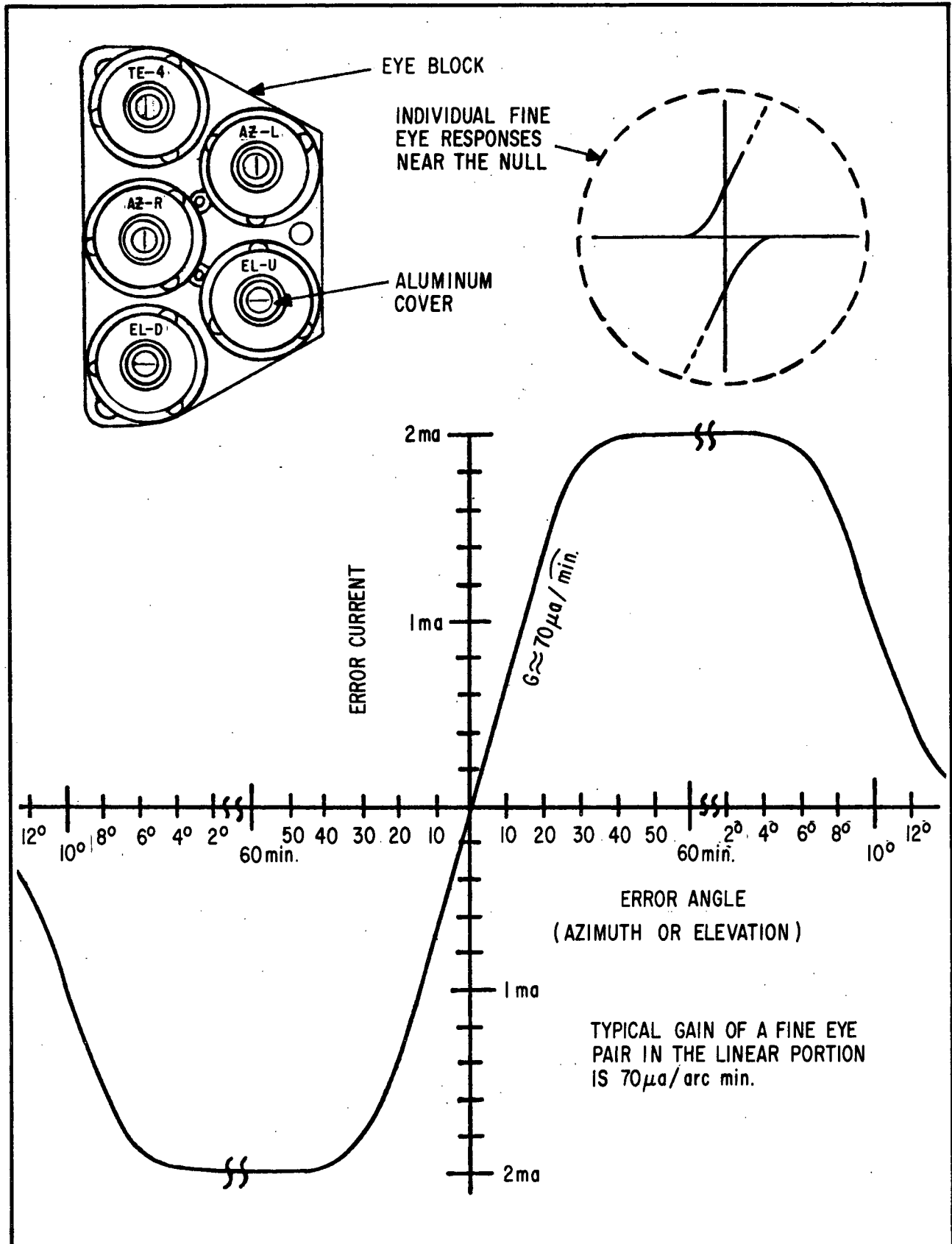


Fig. 7-16 Typical Fine-Eye Response



The circuits of the azimuth fine control loop are common to the coarse loop beyond the preamp stage. The elevation loop has its own modulator, ac amplifier, demodulator, PWM, power switch, and torque motor, similar to azimuth.

The fine servo performance characteristics are effected by such factors as friction, motor back-emf in azimuth, and flex-cable loading in elevation.

The azimuth fine eyes are aligned to produce zero pointing error when driving against the normal friction of the azimuth bearings. A 0.5 in-lb increase in shaft friction will cause a pointing change in the direction of spin of about 2 arc seconds. Similarly, a 0.2 rps increase in spin rate would cause a shift in the direction of spin of about 2.7 arc seconds. These examples show that the azimuth servo can tolerate reasonable friction and rate changes. Normal friction of the azimuth bearings is about 1.1 inch-pounds.

The PWM dead zone is reflected in the fine-servo gain curve shown in Fig. 7-17. This dead zone has no effect on azimuth operation since wheel spin always holds the sail to the side of the zone in the direction of spin.

Appreciable pointing errors in the fine elevation servo loop can be caused by elevation motor shaft friction, flex cable loading, and electronic and mechanical alignment drift. The friction errors would be the result of wobble or nutation of the spin axis. These motions tend to displace the elevation gimbal above and below its average pointing position and the pointing error would appear as an approximate squarewave. If wobble were causing the motion, the frequency would be identical with the wheel spin rate. If nutation were causing the motion, the frequency would be a function of wheel spin rate. Note that the spin rate/back-emf changes that can cause pointing errors in azimuth do not apply to the elevation servo.

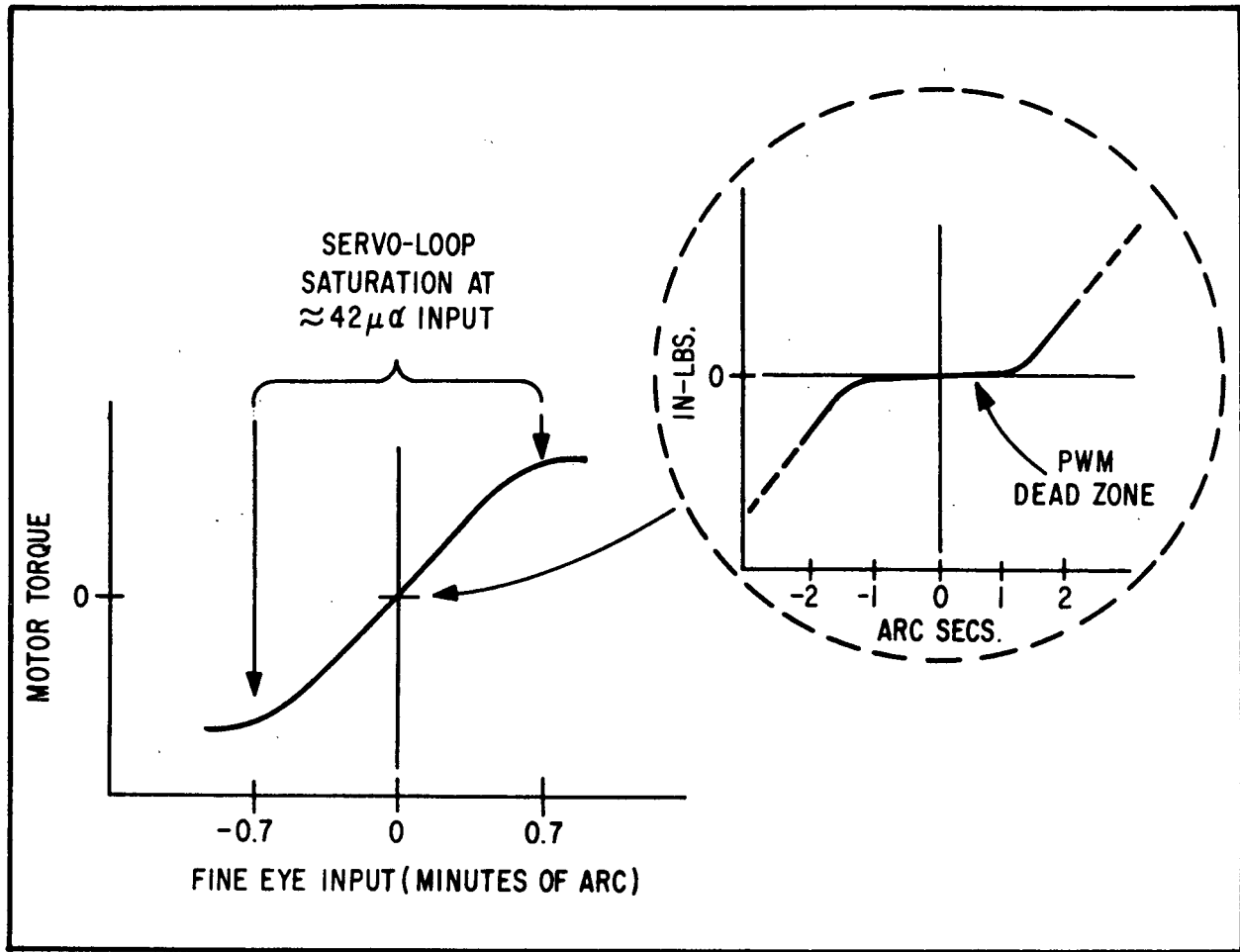


Fig. 7-17 Overall Fine Servo Gain Showing Dead Zone

The PWM dead zone can cause a 2.5 arc second instability in elevation pointing. This instability is small compared to the desired 1 arc minute pointing accuracy. Rather than raising the gain of the loop and risking oscillation, the dead-zone is tolerated as it is.

The combined friction and flex-cable-loading torques were determined to introduce negligible error contribution.

During booster operation at launch, a relative alignment change between the right and left pointed instruments could occur. Such a change would cause a pointing error in the left instrument. The error would show in the telemetered pointing data since the fine



control and pointing readout eye blocks are mounted on the right instrument and the raster readout block is on the left instrument.

After considering all the disturbing drifts, the steady-state azimuth pointing accuracy is well within the +1 arc minute requirement.

7.10 POINTING CONTROL INTERACTION WITH OTHER SYSTEMS

The pointing control system influences the operation of other control systems. Other systems, likewise, produce an effect on the operation of the pointing control. These interactions of the pointing control are herein presented briefly.

The spin-control system normally makes spinup corrections at orbit dawn because the night spin rate is slower than the day rate. Spin-control circuits are not powered in the night condition. During orbit night, azimuth-bearing friction brings the sail up to the wheel spin rate. Due to the conservation of angular momentum, the larger spinning moment of inertia at night results in a decreased wheel spin rate. When day power is first applied, before the angular momentum of the sail is imparted to the wheel through the azimuth servo, the spin control system senses its lowest spin rate. If a spinup correction is needed, it will occur at this time.

Spin rate has an effect on coarse-acquisition time since it takes the servo longer to slow down the sail from higher spin rates. The motor back-emf is an increasing function of spin rate, causing a shift in azimuth in the spin direction for higher spin rates. This can result in pointing error and increased azimuth-drive power consumption.

Pitch corrections by the pneumatic pitch control can only be triggered when steady-state pointing is achieved. The pitch-eye block is directional and must be aimed by the pointing control for



at least eight seconds before an excessive pitch error can be detected. The pneumatic jets must likewise be held at a fixed angular orientation to produce a pitch correction.

Pitch error must be less than 15 degrees for azimuth acquisition, limited by the field-of-view of the coarse eyes. Error must be less than 5 degrees for elevation pointing, limited by the freedom of traverse of the elevation gimbal. Pitch attitude within the 5-degree limit will influence the effect of flex-cable rigidity on pointing accuracy in elevation and the resultant drive power consumed.

The action of the Auto-Pitch Limiter circuit is disabled in the azimuth-servo coarse mode.

Nutation is caused by elevation acquisition at orbit dawn, by the torques produced in the elevation motor in the scan mode, and by pneumatic pitch corrections. Such nutations have a minimal effect on the pointing control, since servo gain is high enough to overcome them. Nutation energy is quickly absorbed by the nutation damper.

7.11 POINTING PARAMETERS AND MONITORS

The servo parameters and performance monitors used to evaluate the pointing control both before and during flight are described in this subsection. Other monitors in the pointing-control system are the "target intensity" and "on-target" monitors presented in earlier paragraphs. The conversion tables for translating telemetered binary-coded data into engineering units are contained in BBRC document TN68-16.



7.11.1 Position Readout

There is a set of position-readout eyes mounted to the front of each pointed instrument. These eyes are the same type fine-eye pairs used for fine-pointing control. Their response is about the same as that shown in Fig. 7-16. In addition to their use in analyzing servo performance, the two sets of eyes provide for evaluation of relative displacement of the pointed instruments. Such displacements may occur due to vibration during the launch sequence, or thermal warpage in orbit.

The "point" position readout eyes are mounted on one pointed instrument and the "raster" readout eyes on the other. The difference between the eyeblocks, other than their location, is their gain.

The pointing readout eye amplifiers' gains are set for about ± 2 arc minutes full-scale telemetry readout. These provide for a high-resolution of pointing accuracy readout. The raster eye amplifiers, however, are adjusted for a gain to provide accurate position data in the range of the servo raster-mode operation. All eye amplifiers are of an extremely stable type.

The azimuth and elevation position data are read out, each assigned a single channel, through the sail analog subcommutator.

7.11.2 Error-Signal Monitors

The dc-voltage levels of the inputs to the azimuth and elevation PWMs are each read out through a channel of the sail subcommutator. The conversion tables (TN68-16) translate the binary data into error-voltage readout. In the event of excessive in-flight pointing errors, analysis of error-signal voltage data would aid in determining the causes of the problem.



7.11.3 Motor-Current Monitors

The average currents supplied to the azimuth and elevation torque motors are each read out through a channel of the sail subcommutator. The data from these monitors are used to study the long-term in-flight performance of the azimuth and elevation bearings, and miscellaneous torques operating against the servo system. These may be friction, balance, flex-cable, or oscillatory anomalies.

7.12 LAUNCH SEQUENCE SYSTEM FUNCTIONAL DESCRIPTION

The OSO launch sequence system performs the following:

- (1) Sequences the unlatching of mechanical assemblies, which are stowed or locked during launch
- (2) Supplies control signals which activate electrical and control functions required during observatory orbital injection

Figure 7-18 is a block diagram of the launch sequence system. With zero-time starting at observatory separation from the launch vehicle, the spacecraft controlled launch sequence functions occur in the order indicated on the figure. These launch sequence functions were discussed in subsection 7.3.

Several requirements are placed on the Delta launch vehicle before the OSO launch sequence events can occur. First, the final spin rate achieved by the second-stage/payload combination before separation must be greater than 80 rpm. Second, the launch vehicle must sequence its separation from OSO after spinup. Finally, the OSO spin axis must lie within five degrees of normal to the solar direction at separation and the OSO center of gravity should be translating in a circular orbit of about 556 km (300 nm) altitude and a 33-degree inclination to the equator.

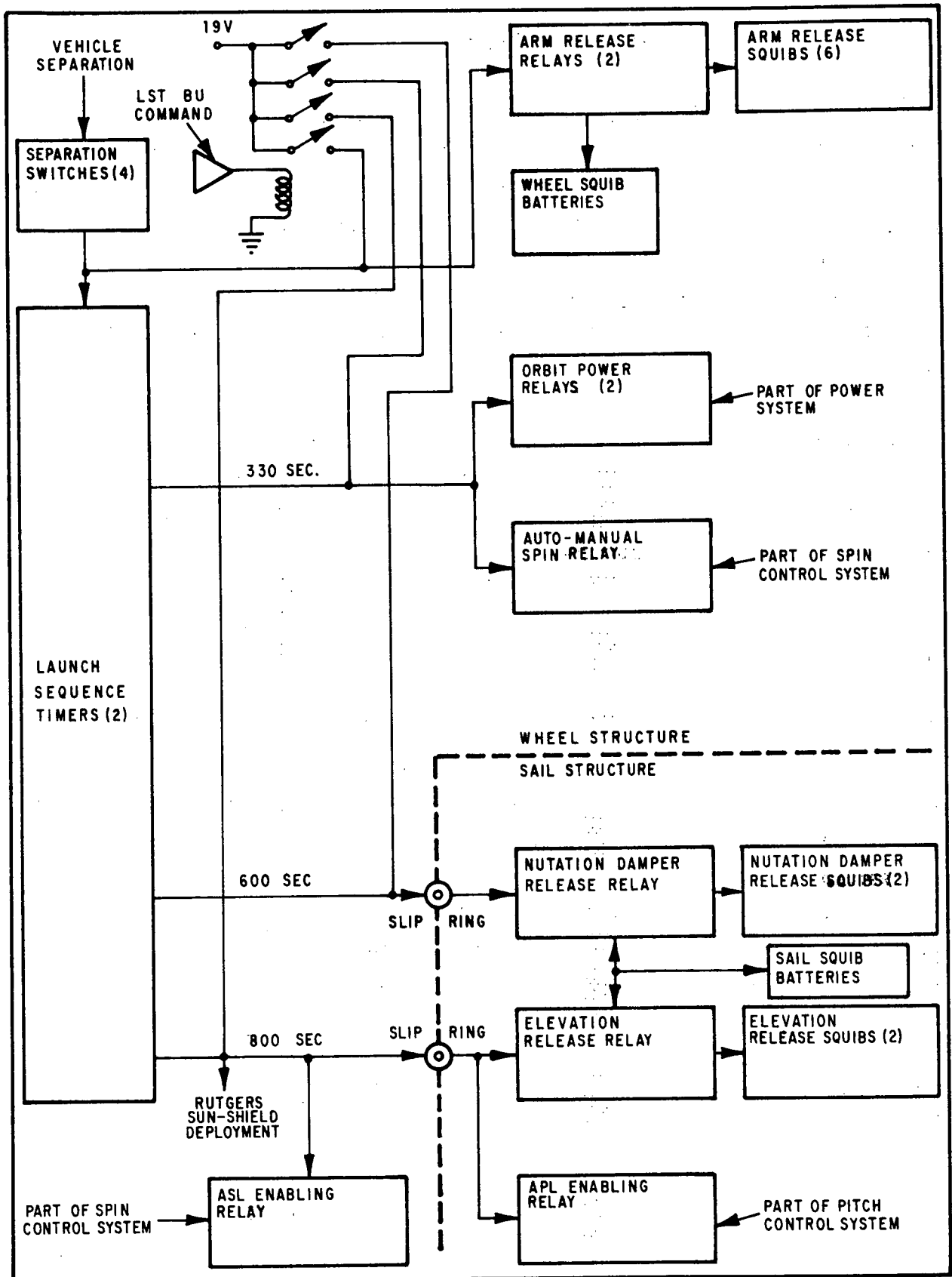


Fig. 7-18 Launch Sequence System Block Diagram



7.12.1 Launch Sequence Timers

Each of the two launch sequence timers consists of a constant speed drive motor which drives a cam-laden mandrel (Fig. 7-19). The cams on the mandrel make momentary contact with wire brushes, thereby providing 15-second closure signals for sequencing events. A dc voltage regulator contained within the timer drives the dc motor at a speed of approximately 4,800 rpm. By means of gear reduction, the motor drives the mandrel through one rotation in about 1,600 seconds.

Once a separation switch actuates, the timer motors are supplied power through the timer-run relay (latching type) and the timer-run contacts internal to the timers. The timer motors then run until the timer-run contacts open at a nominal 1,450 seconds. The fastest-running timer then shuts off the power to both timers. To reset the timer to zero time during ground tests, a timer-reset contact is provided which supplies power from the test console to the timers until zero-time is reached.

Each timer motor consumes about 40 ma of current. The tolerance of the timing sequences is ± 5 percent. Due to the large variance in friction with temperature, it is extremely difficult to maintain timer accuracy over a wide temperature range. To partially compensate for speed change due to temperature, the voltage regulator is designed to provide a higher voltage to the motor at low temperatures.

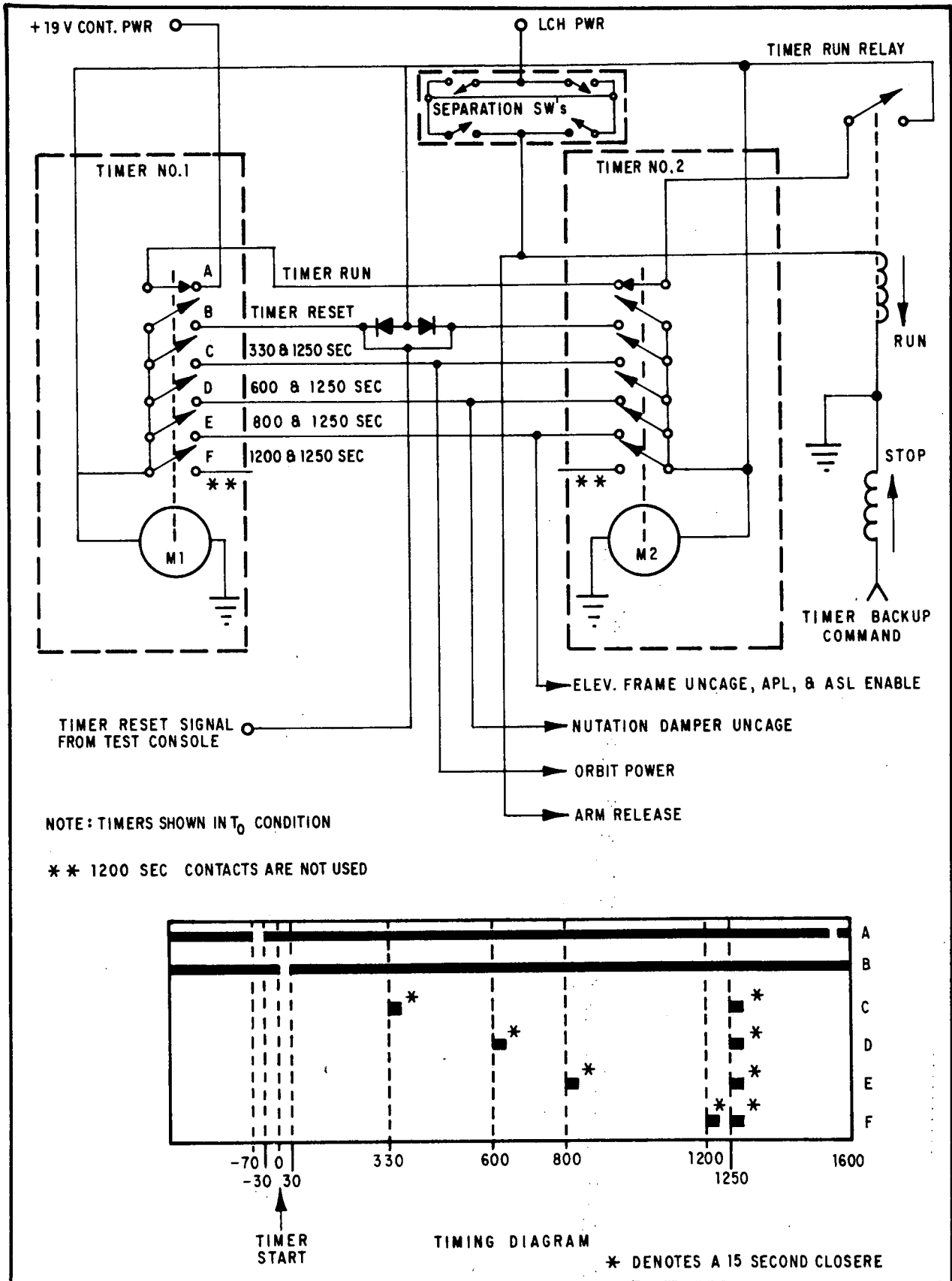


Fig. 7-19 Launch Sequence Timer Schematic Diagram



7.12.2 Pyrotechnic Pin-Pullers

The five pyrotechnic pin-pullers used on the OSO-6 spacecraft are as follows:

- (1) 1 through 3 - Arm release (1 on each arm)
- (2) 4 - Nutation damper bob release
- (3) 5 - Elevation frame release

Each pin-puller consists of a latching block, two pressure cartridges (squibs), and a latching pin. The purpose of the pin-pullers is to release the various mechanical components stowed or constrained by latching pins during the launch phase. The detonation signals originate from the separation switches and the launch sequence timers.

Arm Release Pin-pullers. When in the launch state, the spacecraft arms are folded down alongside the wheel and a folding linkage extends under the spacecraft. A latching block is used on each arm to pin the linkages to the wheel. The latching pins are pulled simultaneously at observatory separation from the launch vehicle, and the arms are then deployed to their extended or orbit condition by the centrifugal force exerted by the spinning wheel.

Power for the arm release pin-pullers is supplied through two parallel relays with contacts rated at 10 amps. These relays switch power from the two wheel squib batteries to fire the six (two on each arm) arm release squibs. Each squib has two filaments that are fused separately so that short circuits to ground, as a result of firing, do not drop the voltage available to fire the other circuits. Also, the circuit design is such



that normal functioning of either relay, either battery, or either squib on each arm will cause the three arms to deploy. A typical squib firing circuit is shown in Fig. 7-20.

Nutation Damper Bob Pin-Pullers. The nutation damper bob is secured during the launch phase by two spring loaded cones pinned by a latching block. The latching pin is pulled at $T + 600$ seconds, and the bob is then allowed to move freely.

The $T + 600$ seconds timer signal (15 seconds duration) is fed to the nutation damper release relay through a slip ring. This relay also has contacts rated at 10 amps and is used to fire two squibs in the nutation damper latch block. In this case, the power is provided by the two sail squib batteries. Again, each of the four filaments (two per squib) are individually fused.

Elevation Frame Release Pin-Puller. The elevation frame is latched to the azimuth frame during the launch phase by the elevation latching block. A $T + 800$ seconds, the latching pin is pulled, and the pointed instruments are allowed to move in elevation.

The $T + 800$ second timer signal (15 seconds duration) is also supplied to the sail through a slip ring. In the sail, this signal actuates a relay, which in turn fires the elevation release squibs. The elevation release design is similar to that of the nutation damper described above.

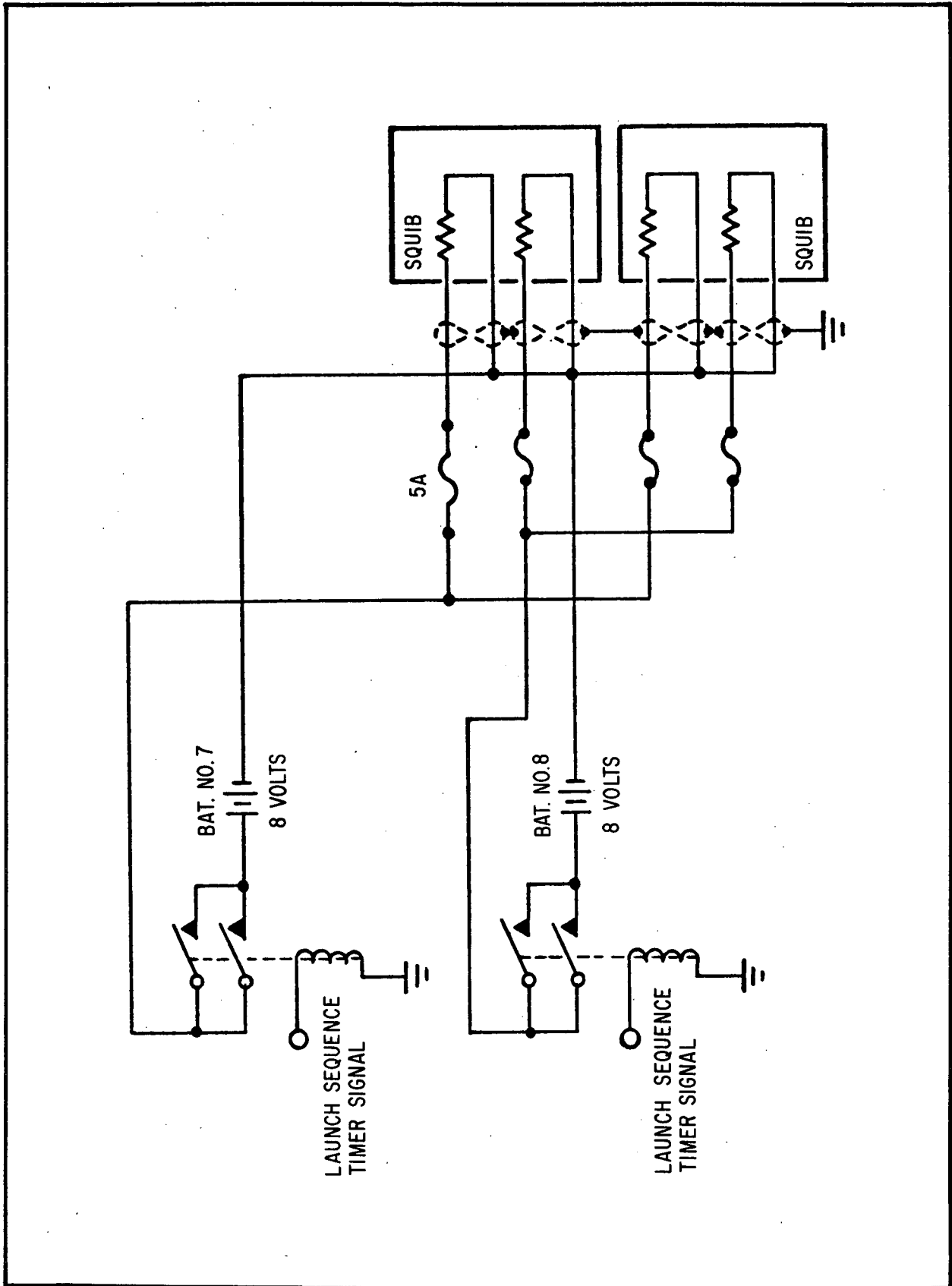


Fig. 7-20 Typical Squib Firing Circuit



7.12.3 Squib Batteries

There are two redundant wheel squib batteries whose only function is to fire the arm release squibs. When connected to the bridge wires of the squibs, each battery is loaded with a 1/4-ohm load.

Each wheel squib battery consists of two parallel strings of 1/2 C-size nickel-cadmium cells with seven cells in series in each string. The battery is capable of supplying 20 amp into a 1/4-ohm load for two seconds.

There are two sail squib batteries; their function is to fire the squibs that uncage the nutation damper and the elevation lock. Each sail squib battery consists of two parallel strings of three 1/2 C-size nickel-cadmium cells connected in each string. At 600 seconds and again at 800 seconds, each sail squib battery is loaded with 1/2-ohm. Each battery is capable of providing 6 amp into a 1/2-ohm load for 2 seconds.

7.13 NUTATION CONTROL SYSTEM FUNCTIONAL DESCRIPTION

During the orbit life of the OSO spacecraft, many external torques act on the spacecraft structure. These torques are caused by the earth's unsymmetrical gravity field, interaction with earth's magnetic field, solar radiation pressure, aerodynamic drag, elevation drive torques, and pitch corrections by the pitch pneumatic system. All these torques can cause the spacecraft spin axis to precess in pitch and produce nutation of the spin axis. However, only the reaction of the pitch jets and the elevation drive torques have any significant effect because of the high impulses they produce.

Another important nutation source is the initial nutation imparted to the spacecraft when the second-stage motor is separated after



orbit injection. This nutation is attributed to unsymmetrical thrust of the separation spring and to unsymmetrical motion of the arms as they are deployed into position.

Because the primary mission of the spacecraft is to provide a stable platform from which the pointed experiments can operate and also to allow the wheel experiments to uniformly sweep the celestial sphere, a passive nutation control system is used to damp any nutation that the spacecraft may acquire. To summarize, the spacecraft is "put to sleep" after the following events have occurred:

- (1) Orbit injection (to dissipate any nutation produced by separation, arm deployment, initial solar acquisition of the pointed experiments and initial pitch corrections)
- (2) Orbit morning (to dissipate the nutation produced by elevation motor torque)
- (3) Pitch correction (to dissipate the nutation produced by pitch jet activation)

The nutation control system consists of a tuned nutation damper (Fig. 7-21) mounted in the sail. The damper consists of a pendulum bob supported by a wire and immersed in a bath of silicone oil. This type of damper is termed a passive device because it is driven by the nutational motion which it eventually damps out. This means that it has good reliability, simplicity of operation, and requires no external power source.

The nutation damper pendulum consists of a 0.8 pound spherical bob suspended by a steel wire with a length of about 2.9 inches and a diameter of 0.020 inches. The exact length of the pendulum wire is adjusted to suit the mass properties of the spacecraft.

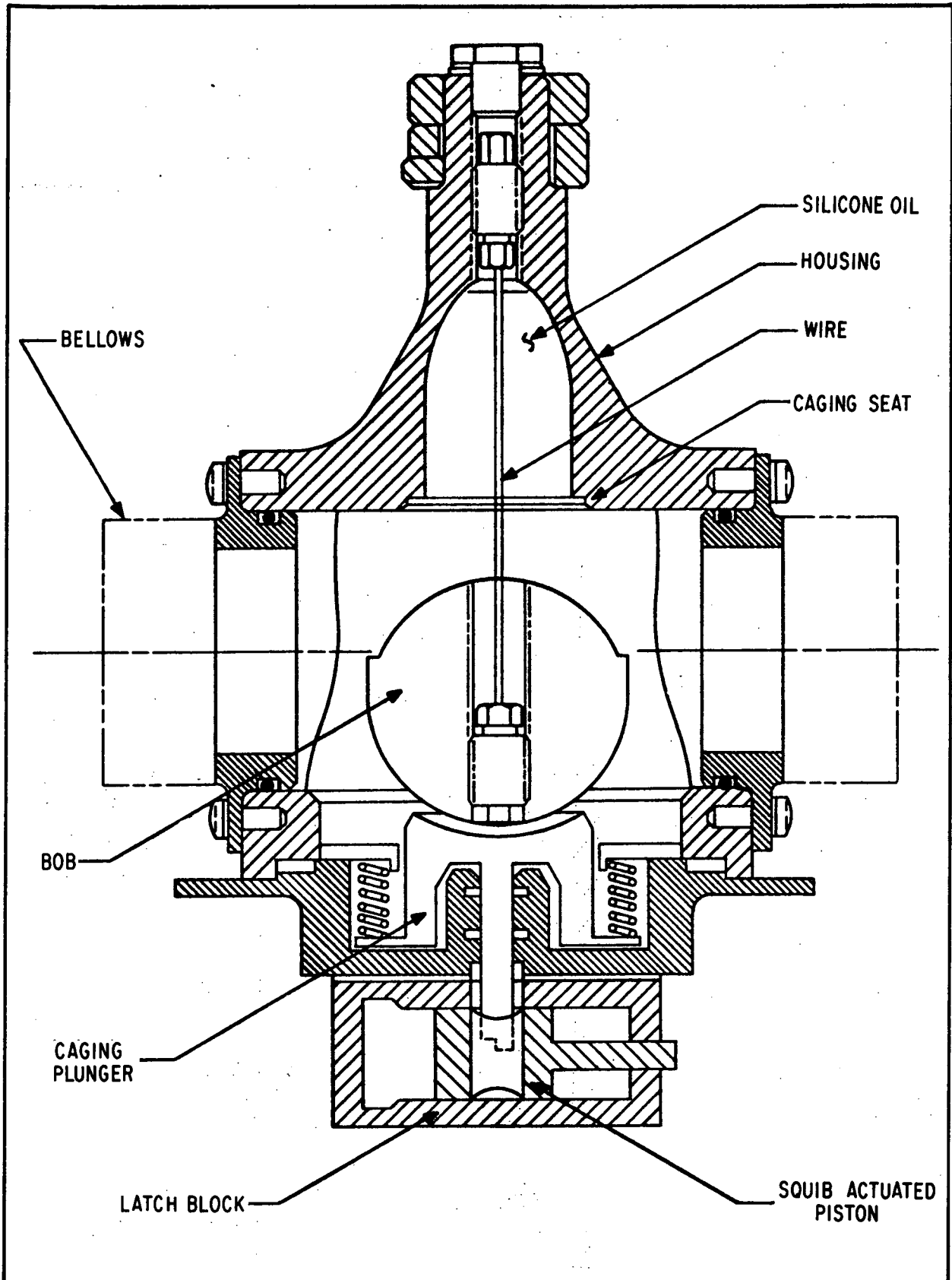


Fig. 7-21 Nutation Damper



The main body of the nutation damper and the bellows contains silicone oil. The bellows accommodate any volume change in the oil due to temperature changes, and thereby maintain a positive pressure upon the oil.

The bob is caged with the squib-actuated caging plunger in the up position during the test, transportation, and launch phases. The bob is uncaged at $T + 600$ seconds (spacecraft time) by the firing of the squibs in the latch assembly. The spring forces the caging plunger to the down position and frees the bob. The bob is then able to oscillate in the oil bath with a 2-degree freedom of movement.

The nutation damper absorbs nutational energy by converting the kinetic energy of the pendulum bob into heat energy as the bob moves in the oil bath. The heat energy is a result of fluid friction and is dissipated by the nutation damper casting. Monitoring of nutation damper performance is accomplished by analyzing pitch readout data.

The design damping range of the nutation damper is approximately 0.45 to 0.55 rps although the damper is effective over a much wider range than this.



Section 8 POWER AND DISTRIBUTION DESCRIPTION

8.1 INTRODUCTION

The OSO power system consists of the power supply, power control, and distribution circuits. The power supply consists of a solar-cell array assembly and a battery assembly. The power control is provided basically by an undervoltage switch and the day-night turn-on circuits. The power distribution consists of the wiring and relays that connect the electronic equipment to the various power buses.

A simplified functional diagram of the power system is shown in Fig. 8-1. This diagram shows which "black boxes" are powered from the various power bases and also shows the commands that operate the power control relays and the location of the protective fuses.

8.2 POWER SUPPLY

Electrical power for the spacecraft is derived from sunlight by a solar-oriented array of silicon solar cells (Fig. 8-2). Part of this power is used to operate the spacecraft and experiment electrical components during the day part of the orbit. The balance of the solar array power is used to charge a storage battery which stabilizes the voltage, supplies peak demands, and provides power during the dark part of the orbit. The solar array produces about 40 watts which allows a comfortable power margin to meet the observatory load requirements.

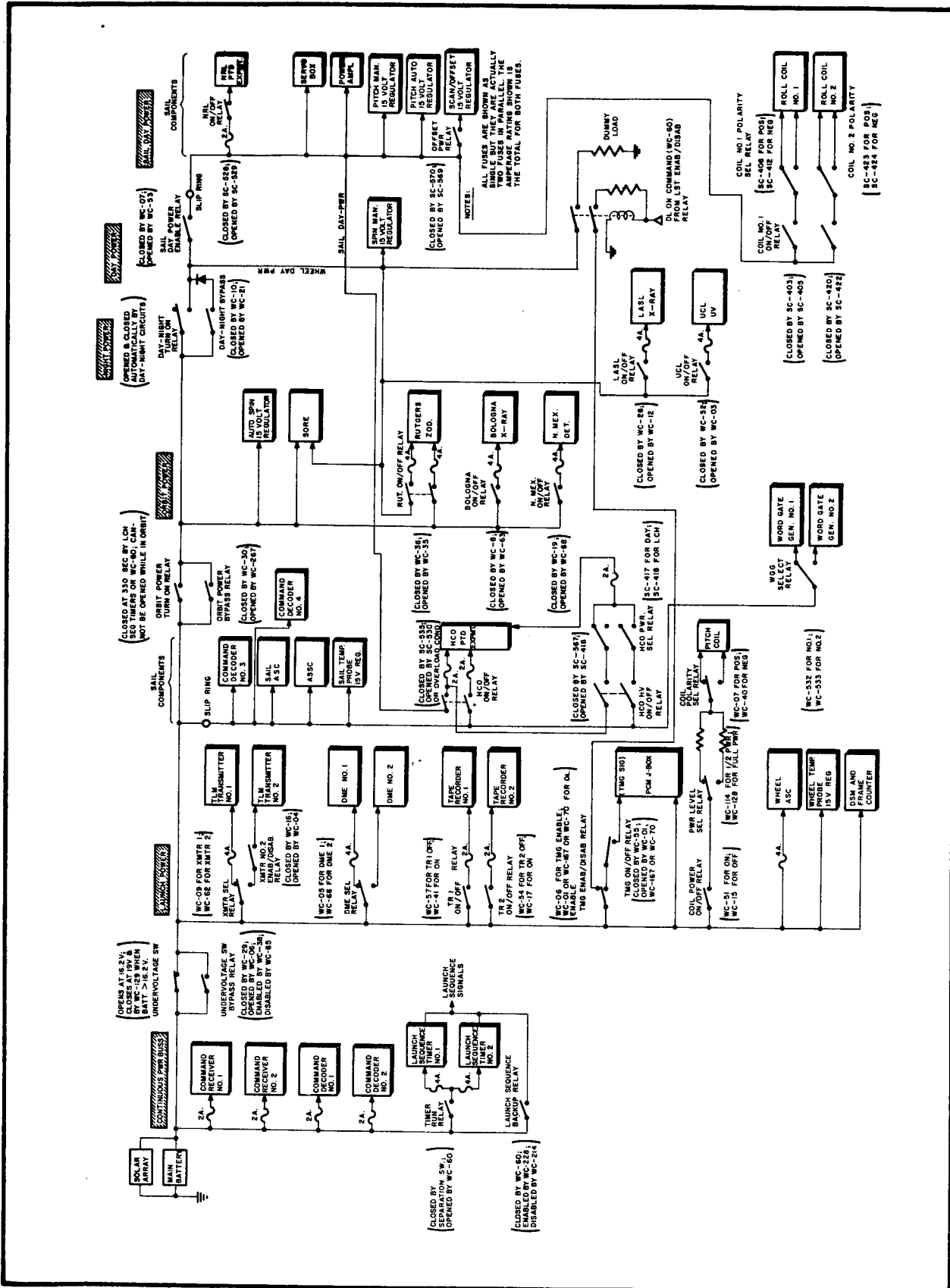


Fig. 8-1 OSO-6 Power Distribution Diagram

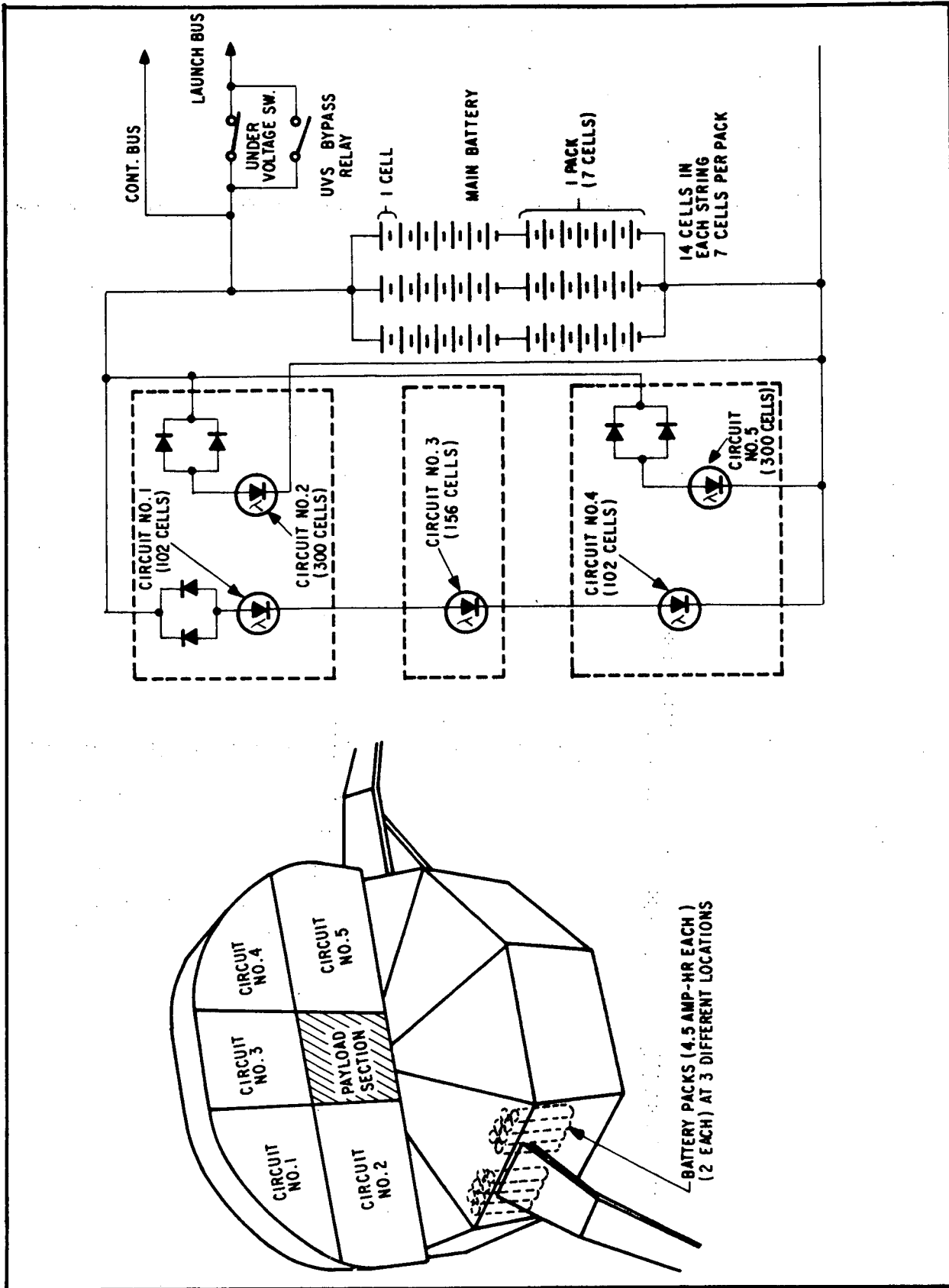


Fig. 8-2 Main Battery and Solar-Cell Array



The greatest demand on the power supply occurs at each satellite dawn. During the 40 to 60-second acquisition period there is nearly a three-ampere load on the power supply.

During the day, the main battery is charged at a rate of about 0.8 amperes. The charge rate is highest immediately after acquisition (about one amp) due to low battery voltage and low temperature of the solar array. During satellite night, the main battery is discharged at a rate of about 0.5 amperes for a maximum of 35 minutes.

8.2.1 Solar-Cell Array

The solar array consists of flat mounted N-P type silicon solar cells mounted on three panels (see Fig. 8-2). Flat mounting of solar cells requires less cells, fewer interconnections, and lower cost. The array output response was designed with margin for errors in temperature predictions. This placed the maximum power point near the higher end of the anticipated range of OSO operating voltages. Thus, a shift in the response curve caused by higher-than-predicted temperatures will not cause output current to fall sharply.

Solar Cells. The Spectrolab N-P type cells (Fig. 8-3) have five tapered solder grids on the sunlight side to collect current with a minimum amount of power loss from resistance. The back side of the cell is prepared to take solder by means of an electrolysis plating method. The response characteristics of the solar cells are shown in Fig. 8-4.

Solar Array Wiring. The 960 cells, most of which measure 2 by 2 centimeters, are arranged in five circuits (see Fig. 8-2). The center panel supports one circuit matrix (circuit No. 3) of six cells in parallel by 26 cells in series. This is connected in series with circuits No.'s 1 and 4 each of which have six cells

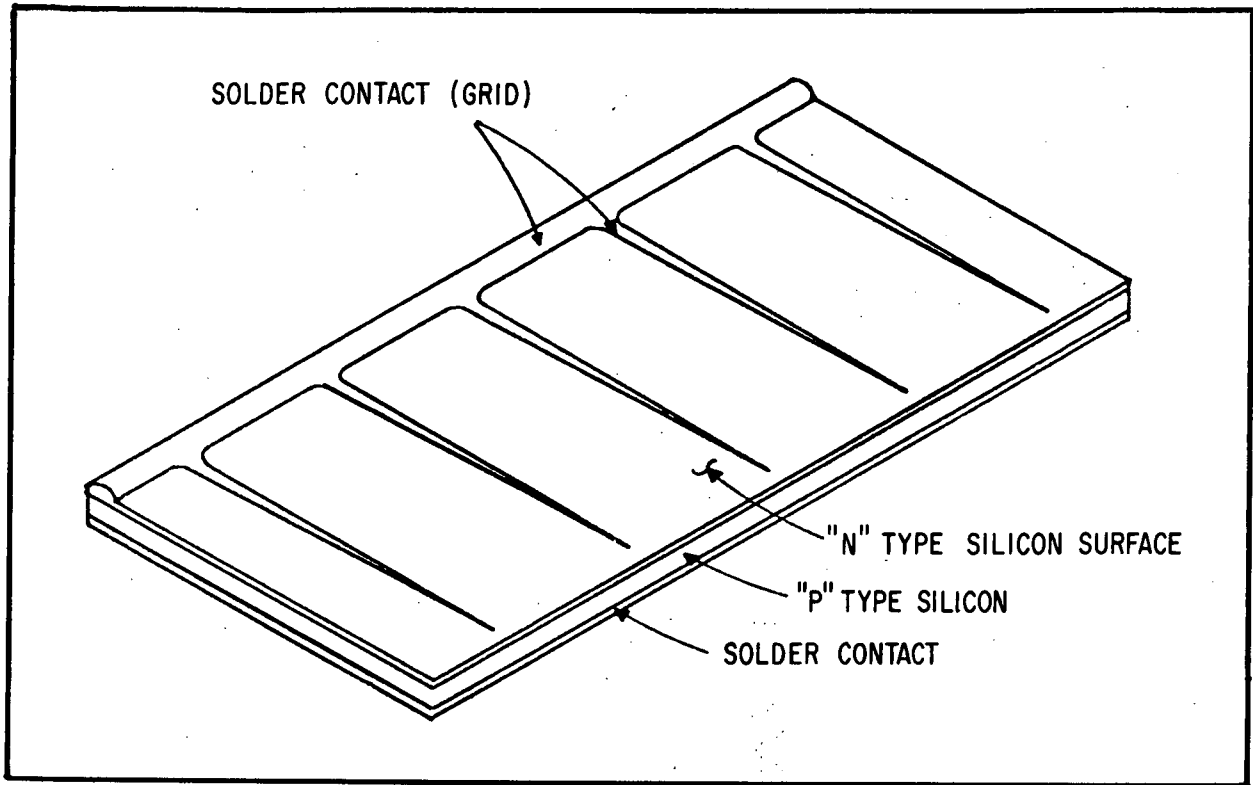


Fig. 8-3 N-P Silicon Solar Cell

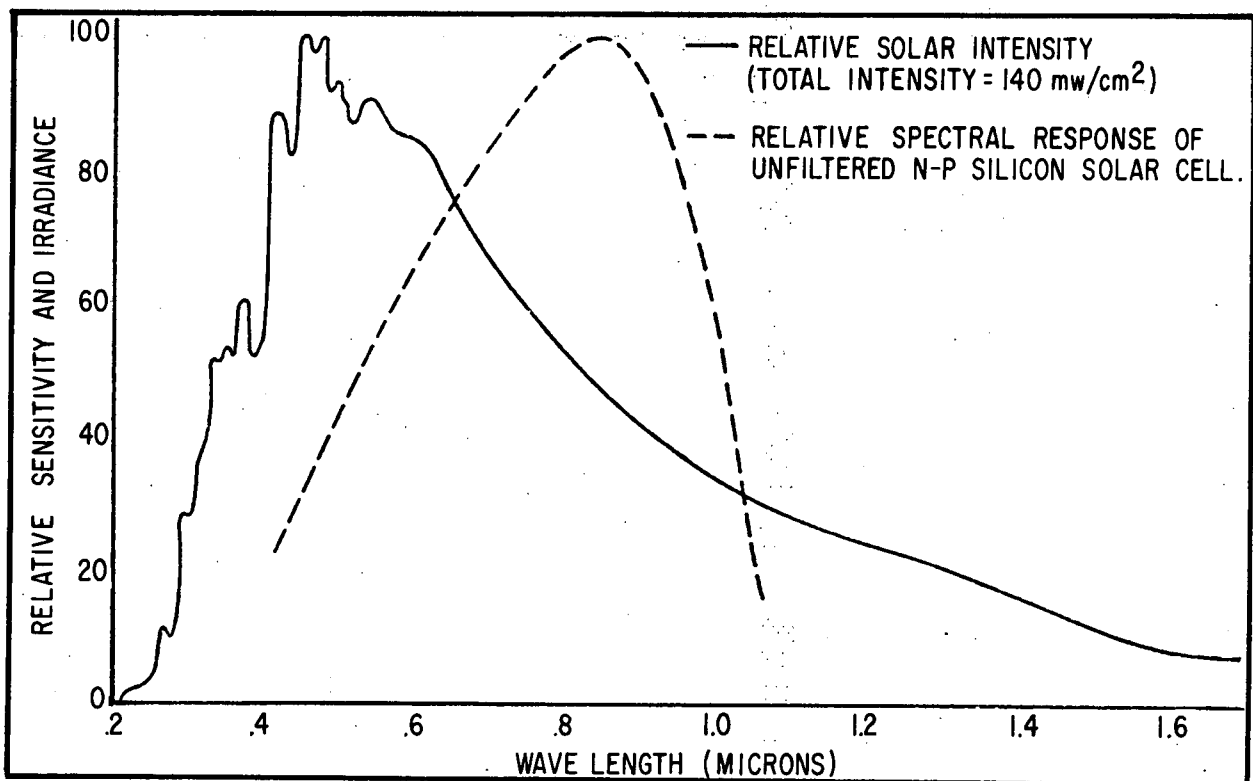


Fig. 8-4 Solar-Cell Response



in parallel and 17 in series. On the bottom of the side panels there is a circuit matrix of five cells in parallel by 60 cells in series. Mechanically, the solar cells are flat mounted modules of five or six cells per module (except along the rounded edges of the solar array substrate when some of the modules are broken into smaller blocks.) The modules include the necessary interconnecting contact strips between cells on the module. Each series circuit is isolated by means of two blocking diodes connected in parallel.

Cover Glass. Each cell has a 30-mil thick fused silica cover glass which is cemented to the cell with a silicone-based adhesive. On the face of the cover glass is an anti-reflective coating and on the side nearest the cell is an ultraviolet reflective coating. The ultraviolet reflective coating has a cutoff point at about 4 microns. This is slightly higher than the shortest wavelength to which a cell will respond. The anti-reflective coating has a cutoff point of 0.625 microns. By means of these coatings and the use of proper thermal coating on the back side of the panels, the orbital temperature of the array is kept below 70°C.

Solar Array Tests. The most severe environmental test for the solar array is a thermal shock test. The greatest stresses occur during this test between the intercell connections due to the difference in thermal expansion between the cells and the panels on which they are mounted. The solar array is, therefore, subjected to 20 thermal shock cycles. Each cycle consists of about nine minutes in a cold chamber at 45°C and about nine minutes in an oven at 80°C. This test is performed before power-output measurements are made.



Power-output measurements are made on each circuit of the solar array with the panels operating at orbital temperature in order to minimize errors that might occur from extrapolating from a lower temperature.

With a panel oriented so that it is perpendicular to the sun, I-V curves of each of the circuits on that panel are made together with measurements of the solar intensity by means of a standard cell under collimated and uncollimated conditions.

Other tests are also conducted as part of the OSO acceptance test program. One of these tests consists of measuring the current output of the array at different voltages and temperatures, and the results are adjusted for nominal space conditions. The I-V power curve for a typical solar array is shown in Fig. 8-5.

The maximum-power point for the solar array is about 1.95 amp at 20 v. A voltage drop across the solar-array blocking diodes is between 0.7 and 0.8 v and the drop across the charge-current monitor can be as high as 0.3 v. The voltage at the battery terminals, then, is about 19 v. It is this voltage (19 v) which is used in all calculations, and which is plotted in Fig. 8-5.

8.2.2 Main Storage Battery

The main battery is charged by the solar array and effectively limits the maximum supply voltage to 21 v. It also provides power during launch, during night, and for surges during the day.

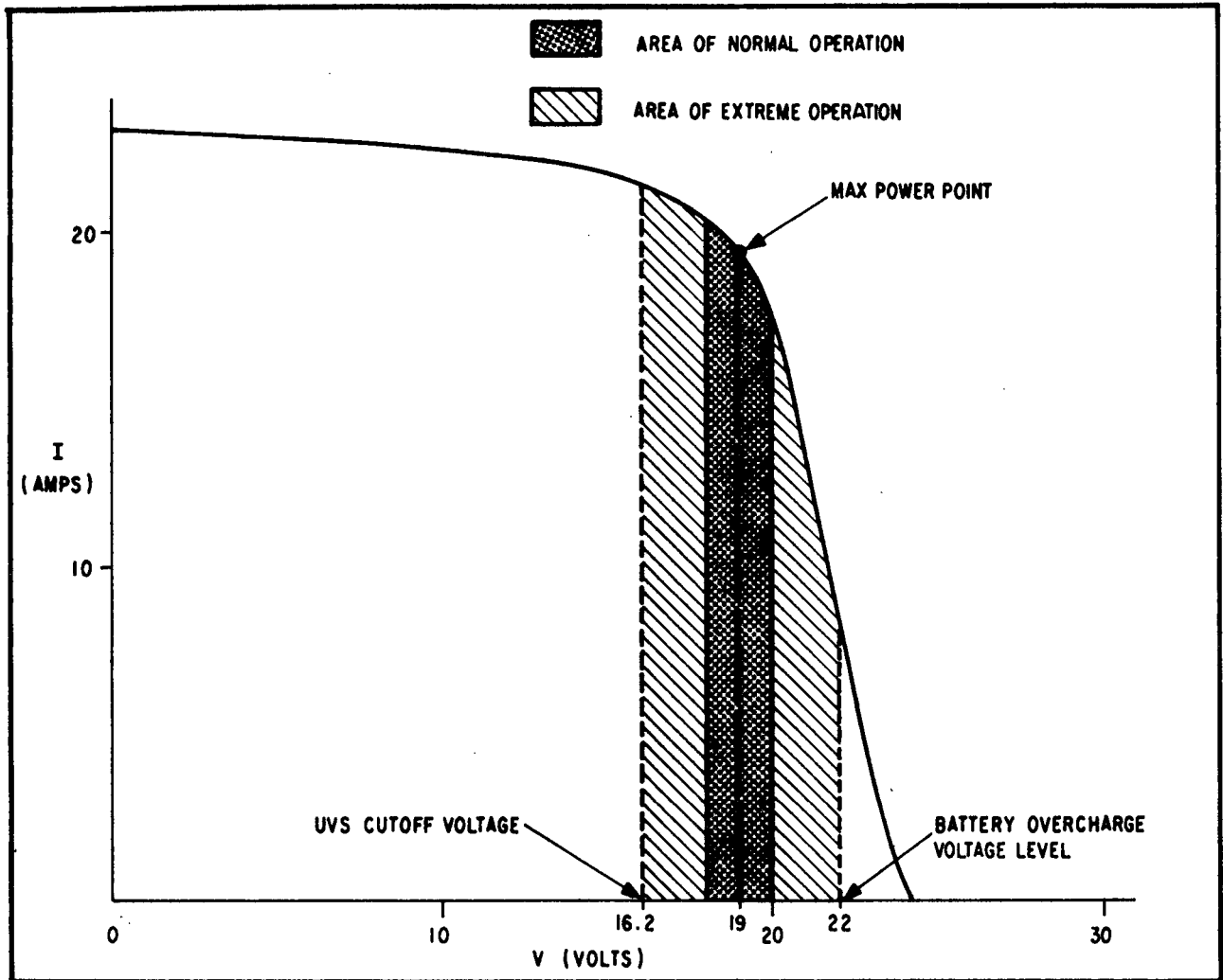


Fig. 8-5 Solar Array Power

The cell selected for use in the main battery is a Sonotone Type F hermetically sealed nickel-cadmium (Nicad) cell, with two plates 32-mils thick and a poly-propylene separator. This cell has a measured capacity of at least 4.2 amp hr above 1.2 v at room temperature. It can stand continuous overcharge of 0.45 amp with a maximum voltage of 1.48 v.

The battery consists of 42 cells arranged in three parallel strings of 14 cells each. Each string consists of two packs of seven cells each. At time of launch, the battery capacity is about 13 amp hr above 16.8 v. It can stand a continuous



overcharge of at least 1.35 amp. for additional safety margin, however, 0.6 amp was used as a maximum overcharge rate for system-design calculations.

In normal operation, the battery is cycled to a discharge depth of about 3-1/2 percent. If the solar-cell array should fail, the battery alone could power the basic spacecraft for about eight orbits at the time of launch.

8.3 POWER CONTROL AND DISTRIBUTION

The power control and distribution circuits provide for operation of the spacecraft in variously-powered modes, such as the day, night, and undervoltage modes.

As shown in Fig. 8-1, all power control is exercised by ground command, with the exception of the undervoltage switch, the orbit power relay, and day-night switching. Orbit power turnon is normally controlled by the launch-sequence timer (Section 7) and is irreversible in flight. Day-night power switching is incorporated into the spin-control system and is also discussed in Section 7.

OSO has a command-controlled dummy load, which can be used to prevent excessive battery overcharging. This component is described below.

8.3.1 Undervoltage Switch Operation

An undervoltage switch (UVS) is used on OSO to prevent an excessive power consumption problem from depleting the batteries



to the point of no return. This point would be that at which it would be impossible to execute corrective commands. (The voltage threshold of the command decoders has been shown, in engineering tests, to be below 15 volts.)

When the spacecraft is in the undervoltage state, the sail can no longer be solar oriented, and the solar array therefore charges the batteries in a pulsating dc fashion (at about a 25 percent rate) until the voltage rises to about 19.1 v. At this time, power is reapplied to the observatory, and normal functions can be resumed. Such an undervoltage condition could be caused by battery failure--but it is more likely to be caused by some excessive current demand due to an electronic circuit failure.

The undervoltage switch consists of a voltage sensing circuit that automatically opens the UVS relay (Fig. 8-1) when the battery voltage drops to 16.2 v and that closes the relay when the voltage rises to 19 v.

A bypass relay can be commanded to bypass the UVS circuits. Because of the inherent danger of using this bypass capability, it is used only when the automatic undervoltage circuit has failed in an open condition. The danger in closing the UVS bypass when it is not needed is that the protection offered by the UVS is no longer effective. If battery voltage drops below the command-system operation level, there is no way to remove the excessive load from the power supply. The battery, therefore, cannot be recharged to its operating level.

The UVS bypass command closes the undervoltage switch. It may therefore be followed immediately by the "not bypassed" command and if battery voltage stays above 16.2 v, the under-voltage switch will remain closed. In this way, power may be reapplied to QSO safely before the battery is fully recharged.



8.3.2 Dummy Load

The dummy load feature on OSO-6 consists of a 90-ohm load resistor and a parallel circuit consisting of a control relay and a feedback resistor. The total resistance is about 75 ohms and this load is applied or removed by ground commands. The resistor forms a holding loop on the dummy load on/off relay. The dummy load is connected to the day power bus and, therefore, only diverts charge current from the solar array and thus prevents battery overcharging.

Battery overcharging, while not desirable, can be tolerated up to a limit of approximately 600 milliamperes continuously. Therefore, excessive overcharging poses no serious problem unless some of the experiments are turned off. In this event, the batteries may be subjected to overcharging in excess of 600 milliamperes. Charging above this level has the adverse effect of decreasing battery life.

Therefore, the dummy load is normally used early in the flight since the solar-cell array output is high during this time because none of the anticipated degradation factors have yet come into effect. Also, later in the mission it is possible that some of the scientific payload will have been turned off, and the dummy load is then used to bleed off the resultant surplus power.

BATTERY VOLTAGE VERSUS DUMMY LOAD CURRENT AND POWER

Battery Voltage (v)	Load Current (ma)	Power (w)
22	292	6.4
21	278	5.8
20	265	5.3
19	250	4.7
18	238	4.3
17	225	3.8



8.4 SOLAR ARRAY OUTPUT AND OBSERVATORY POWER BUDGET

Table 8-1 shows the predicted solar array output in ma-hr per orbit at 19 volts for 6 month increments of orbit life. The output at launch was calculated to be about 1980 $\frac{\text{ma-hr}}{\text{orbit}}$ and degradation was predicted to be a maximum of two percent during the first 6 months and a maximum of two percent per year thereafter (the actual in-orbit performance is described in Section 2).

The solar-array output prediction is influenced by many factors, including:

- Preflight measurements have an uncertainty due to varying atmospheric attenuation
- Degradation of the array in flight due to solar-radiation damage
- Solar flux varies from the mean by ± 3.4 percent in the course of a year
- The daylight portion of the orbit was predicted to be between 60.1 and 70.9 minutes. The lower limit was used for power budgeting and thus represents a worst-case situation.
- The earth's albedo increases the array output every orbit morning and evening. The amount of the increase depends, to a degree, on spacecraft aspect
- Output from the solar array varies sharply with array temperature and load voltage



Actual power availability is also influenced by variations in battery-charging efficiency, which can be expected to degrade with age.

Table 8-1
OSO-6 PREDICTED SOLAR ARRAY OUTPUT

Orbit Period	Radiation Degradation (%)	Output Energy ($\frac{\text{ma-hr}}{\text{orbit}}$)
Launch	0.0	1980.0
6 months	2.0	1940.4
12 months	3.0	1921.0
18 months	4.0	1901.8
24 months	5.0	1882.8

The observatory power budgets for spacecraft systems and the experiments are shown in Tables 8-2 and 8-3, respectively. By using the worst case prediction of $1980 \frac{\text{ma-hr}}{\text{orbit}}$ for solar array output at launch, it can be seen from Tables 8-2 and 8-3 that the predicted power pad at launch was about $1980 - (1162 + 792) = 26 \frac{\text{ma-hr}}{\text{orbit}}$. However, if a sunlight period of 70.9 minutes is used the power pad would be about $358 \frac{\text{ma-hr}}{\text{orbit}}$.

The values in Tables 8-2 and 8-3 were computed before launch using the following assumptions and factors:

- (1) A 96-minute orbit period (1.6 hour per orbit) was used and divided as follows:

$$96 \text{ min. orbit} \left\{ \begin{array}{l} 60 \text{ min. day} = 62.5\% \\ 36 \text{ min. night} = 37.5\% \end{array} \right.$$



- (2) The orbit day only energy (E_d) was computed as follows:

$$E_d = (0.625) \left(1.6 \frac{\text{hr}}{\text{orbit}} \right) I_d = I_d \frac{\text{ma-hr}}{\text{orbit}}$$

- (3) The orbit night only energy (E_n) was computed as follows:

$$\begin{aligned} E_n &= (0.375)(1.25) \left(1.6 \frac{\text{hr}}{\text{orbit}} \right) I_n \\ &= 0.75 I_n \frac{\text{ma-hr}}{\text{orbit}} \end{aligned}$$

where the 1.25 term represents the battery loss factor.



Table 8-2
OSO-6 SPACECRAFT POWER SUMMARY

Subsystem	Assemblies	Day Power		Night Power	
		milliwatts	ma-hr per orbit	milliwatts	ma-hr per orbit
Pointing Controls	Servo Amplifier	1,710.0	90.0	190.0	7.5
	Power Amplifier	3,420.0	180.0	-----	---
	Pitch Readout	57.0	3.0	-----	---
	Raster	1,026.0	54.0	380.0	15.0
Spin Control	Spin Box	1,330.0	70.0	855.0	34.0
Attitude	SORE	266.0	14.0	152.0	6.0
Monitor	Magnetometer	209.0	11.0	209.0	8.3
Telemetry	PCM (DME & 2 ASC)	1,235.0	65.0	1,235.0	49.0
	DSM	551.0	29.0	551.0	21.7
	PCM Junction Box	361.0	19.0	361.0	14.8
	Tape Recorder (1)	1,837.0	96.6	1,837.0	72.5
	Transmitter (1)	2,242.0	118.0	2,242.0	88.5
	Terminal Boards	95.0	5.0	95.0	3.8
	ASSC	76.0	4.0	76.0	3.0
Command	Word Gate Generator	975.0	25.0	975.0	18.8
	2 receivers/4 decoders	304.0	16.0	304.0	12.0
Power	Charge monitor current	142.5	7.5	-----	----
	TOTAL	15,836.5	807.1	9,462.0	354.9

Summary
 Night current: 354.9 ma-hr per orbit
 Day Current: 807.1 ma-hr per orbit
 Total Spacecraft Current: 1162.0 ma-hr per orbit



Table 8-3
OSO-6 FLIGHT INSTRUMENTS ACTUAL POWER BUDGET

Experiment	Day Bus		Night Bus		Orbit Bus			Exmt. Current Subtotals ma-hr orbit
	pwr (mw)	ma-hr orbit	power (mw)	ma-hr orbit	power (mw)	ma-hr orbit		
						Day	Night	
<u>Pointed</u>						Day	Night	
HCO	2163	113.8	-0-	-0-	182.0	9.6	7.3	130.7
NRL	3460	182.1	-0-	-0-	-0-	-0-	-0-	182.1
<u>Wheel</u>								
Rutgers	779	41.0	-0-	-0-	1482.0	78.0	58.5	177.5
LASL	1129	59.4	-0-	-0-	-0-	-0-	-0-	59.4
Bologna	-0-	-0-	-0-	-0-	832.2	43.8	32.8	76.6
UCL	367	19.3	-0-	-0-	-0-	-0-	-0-	19.3
UNM	-0-	-0-	-0-	-0-	1558.0	83.6	62.7	146.3
Totals	7898	415.6	-0-	-0-	4054.2	215.0	161.3	791.9



8.5 POWER SYSTEM DIFFERENCES

8.5.1 OSO-4/HCO Instrument Conversion

In order to fly the HCO/OSO-4 flight spare instrument on OSO-6, an adapter was installed on the HCO instrument to redistribute the interface wiring. This adapter is called the "K-Box". In addition to matching the OSO-4 and 6 interfaces, the K-Box provides the filtering originally contained in the HCO filter choke module and contains the relay and wiring required to operate the overload protection (OP) circuit which connects at the rear of the K-Box.

The OP circuit monitors the HCO high voltage power supply current. If a high voltage malfunction is indicated by a change in current, the OP circuit automatically actuates the "HCO off" command to disable the high voltage power supply.

8.5.2 Flex Cable Modifications

The OSO-5 flex cables consisted of printed copper paths thermally bonded between layers of mylar with 37 pin connectors soldered and potted on the ends. The low melting point of mylar caused these cables to be susceptible to heat damage during soldering operations. Furthermore, the flat printed wire was susceptible to damage by handling during routine spacecraft operations.

The OSO-6 required additional circuits across the elevation axis. In order to reliably provide the additional circuits and maintain flexibility across the elevation axis, a different type of cable was selected.



The OSO-6 flex cables consist of shielded and unshielded stranded wires embedded in a flat ribbon of silicon rubber material with 0.070 in. centers and "twist-pin" connectors. The resulting cable is more flexible and durable than mylar cables and does not have the melting problem during solder operations. Refer to Para. 2.3 of this report for a discussion of the in-orbit performance of these redesigned flex cables.



Section 9
TELEMETRY SYSTEM DESCRIPTION

9.1 INTRODUCTION

The spacecraft and experiment data is sampled, encoded, and telemetered to the GSFC Satellite Tracking and Data Acquisition Network (STADAN) system by means of an on-board pulse code modulation/phase modulation (PCM/PM) telemetry system. This system consists basically of a data handling subsystem and a RF subsystem (Fig. 9-1). The data handling subsystem provides communication (sampling), multiplexing (time sharing), encoding, and on-board storage of the observatory data. The RF subsystem provides RF transmission of both real-time and stored data to the STADAN stations.

The OSO-6 telemetry system is very similar to OSO-5's. The main differences consist of: the addition of the word gate generator, changes in the sail J-box, decreasing the bandwidth of the transmitter spectrum, and changing the transmitter frequency to 136.71 MHz.

9.2 DATA HANDLING SUBSYSTEM

9.2.1 General

The data handling subsystem provides the interface between all observatory data sources and the RF subsystem. Its primary function is to assemble the observatory data into a form suitable for transmission and to store these data for playback when the observatory is over a selected STADAN station.

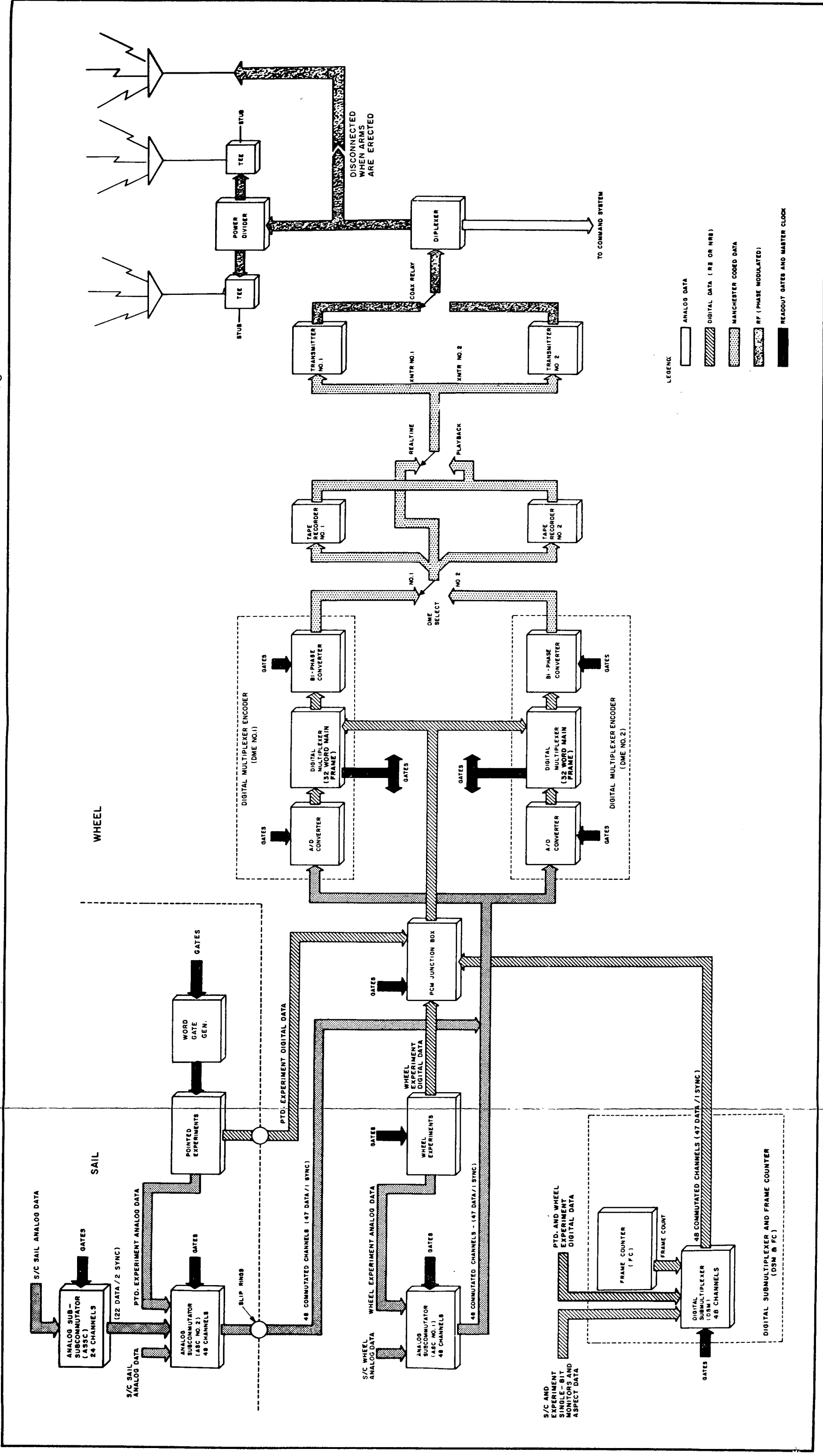


Fig. 9-1 OSO-6 Telemetry System Block Diagram



The data-handling subsystem uses time multiplexing techniques wherein each data source is assigned a time interval (channel) for transmission of the parameter being measured. This source data can be in either digital or analog form.

The OSO-6 telemetry system provides 26 channels of a 32-channel main-frame format for experiment prime (digital) data. Most of the spacecraft status and performance data are in analog form, and the system provides 47 data channels in each of the two 48-channel analog subcommutators (ASC's) and 22 data channels in the 24-channel analog sub-subcommutator (ASSC) for this type of data. Some of the analog channels are used for experiment performance data. A 48-channel digital submultiplexer (DSM) provides additional digital channels for aspect, spacecraft housekeeping, and experiment data. There is a total of 196 telemetry channels (184 data, 7 sync, and 5 spares) available on OSO-6. Additional submultiplexing is done internally in some of the experimenter's instruments.

The multiplexed PCM signal has a bit rate of 800 bps. Each of the 32 main-frame channels (or words) contains eight bits. Two words (16 bits) are used for a main frame synchronization code, one word is assigned to each of the two analog subcommutators (ASC), one word is assigned to the digital submultiplexer (DSM), and the remaining 27 words are assigned to the experiment instruments. The two ASC's, the ASSC, and the DSM subframes contain their own synchronization codes.

All signals into the two redundant digital multiplexer encoders (DME) are connected in parallel, and the internal circuit design is such that failure in one will not affect the other. The redundant DME output is selected by the same ground station commands that control DME power switching.



The experiments have self-contained storage shift registers for their digital data. The spacecraft data handling subsystem provides gate pulses to shift the stored data into the telemeter at the assigned time interval. The assignment of words on OSO-6 for both digital and analog channels is shown in Fig. 9-2.

Data are stored by redundant, continuous-loop, magnetic tape recorders which have the capacity to record data for 100 ± 2 minutes. Either of the two recorders is selectively powered in response to ground station command and, upon receiving a "playback command", the selected recorder reproduces the recorded data at 18 times the realtime rate (14,400 bps). The recorder automatically reverts to the record mode at the end of the playback.

9.2.2 Digital Multiplexer and Encoder

The digital multiplexer and encoder (DME) assembly provides the following five basic functions:

- (1) Generates telemetry master clock (800 Hz)
- (2) Generates gate pulse signals for multiplexing digital and analog signals
- (3) Generates sync codes for main frame and ASC subframes
- (4) Encodes the analog data into eight-bit digital words, and
- (5) Provides signal conditioning to convert the multiplexed digital data into a biphase (Manchester) code.



TELEMETRY FORMAT

MAIN FRAME	
1	NRL SAIL
2	NRL SAIL
3	HCO SAIL
4	HCO SAIL
5	RUTGERS WHEEL
6	BOLOGNA WHEEL
7	RUTGERS WHEEL
8	NRL SAIL
9	NRL SAIL
10	BOLOGNA WHEEL
11	HCO SAIL
12	HCO SAIL
13	NRL SAIL
14	UNM WHEEL
15	UNM WHEEL
16	UNM WHEEL
17	UNM WHEEL
18	BOLOGNA WHEEL
19	HCO SAIL
20	HCO SAIL
21	LASL WHEEL
22	BOLOGNA WHEEL
23	UCL WHEEL
24	NRL SAIL
25	SAIL ANALOG SUBCOMMUTATOR
26	WHEEL ANALOG SUBCOMMUTATOR
27	HCO SAIL
28	HCO SAIL
29	DIGITAL SUBMULTIPLEXER
30	BOLOGNA WHEEL
31	SYNC
32	SYNC

WHEEL ANALOG SUBCOMMUTATOR (WASC)	
WORD	MONITOR
1	UNM COUNT RATE DATA 1
2	UNM COUNT RATE DATA 2
3	UNM COUNT RATE DATA 3
4	UNM VOLTAGE MONITOR
5	UNM VOLTAGE / TEMP MONITOR
6	UNM ASSC ID
7	BOLOGNA HV MONITOR
8	BOLOGNA SPARE
9	BOLOGNA SPARE
10	BOLOGNA LV MONITOR
11	RCVR 1 AGC
12	SPIN RATE
13	BOLOGNA TEMP
14	BOTTOM SKIN TEMP
15	TEMP PROBE 15 V REGULATOR
16	MAIN BATT PACK 3 TEMP
17	MAIN BATT PACK 4 TEMP
18	SPIN GAS BOTTLE TEMP
19	TOP SKIN TEMP
20	UCL LA MONITOR 1
21	RIM SKIN TEMP
22	TR 2 TEMP
23	HUB TEMP
24	SORE 5V REGULATOR
25	SORE 15 V REGULATOR
26	LASL HV1 MONITOR
27	LASL HV2 MONITOR
28	LASL TEMP
29	SPACECRAFT LOAD CURRENT
30	LCH BUS VOLTAGE
31	UCL SQ DISARM MONITOR
32	UCL LA MONITOR 2-CALIB OFF
33	SPIN AUTO 15 V REGULATOR
34	SPIN MANUAL 15 V REGULATOR
35	RUTGERS VOLTAGE MONITOR
36	RUTGERS DATA SAMPLE
37	SPIN GAS PRESSURE
38	SPIN BOX TEMP
39	RIB TEMP
40	DECK TEMP
41	SOLAR ARRAY CURRENT
42	UCL TEMP MONITOR-CALIB ON
43	UCL HV 3 MONITOR
44	UCL HV 2 MONITOR
45	RCVR 2 AGC
46	UCL HV1 MONITOR
47	PITCH COIL STATUS
48	SYNC

OSM	
WORD	MONITOR
1	UCL MODE AND HV STATUS
2	UNM BIT ERROR CODE
3	SINGLE BIT
4	RUTGERS CMMD-OPTICS STATUS
5	UCL MODE AND HV MONITOR
6	UNM BIT ERROR CODE
7	BOLOGNA TOTAL COUNT
8	BOLOGNA CMMD STATUS
9	SINGLE BIT
10	UNM BIT ERROR CODE
11	UCL MODE AND HV STATUS
12	SORE SPIN RATE
13	SORE SPIN RATE
14	UNM BIT ERROR CODE
15	UCL MODE AND HV STATUS
16	SPACECRAFT SPARE
17	NRL BURST-BACKGROUND
18	UNM BIT ERROR CODE
19	HCO SPARE
20	UCL MODE AND HV STATUS
21	NRL CMMD STATUS
22	UNM BIT ERROR CODE
23	NRL BRAGG POSITION
24	NRL BRAGG POSITION
25	UCL MODE AND HV STATUS
26	UNM BIT ERROR CODE
27	NRL CMMD STATUS
28	NRL BURST-BACKGROUND
29	HCO SPARE
30	UNM BIT ERROR CODE
31	UCL MODE AND HV STATUS
32	SORE COUNT ANGLE
33	SORE COUNT ANGLE
34	UNM BIT ERROR CODE
35	UCL MODE AND HV STATUS
36	FRAME COUNT
37	SINGLE BIT
38	UNM BIT ERROR CODE
39	NRL BURST-BACKGROUND
40	UCL MODE AND HV STATUS
41	SINGLE BIT
42	UNM BIT ERROR CODE
43	HCO SPARE
44	NRL BURST-BACKGROUND
45	UCL MODE AND HV STATUS
46	UNM BIT ERROR CODE
47	SPACECRAFT SPARE
48	SYNC

WORD 3 - SINGLE BIT ALLOCATION	
BIT NO.	MONITOR
1	DME 1 ON (MSB)
2	DME 2 ON
3	XMTR 1 ON
4	XMTR 2 ON
5	XMTR 2 DISAB
6	TR 1 ON
7	TR 2 ON
8	SEPARATION SWITCH ENAB

WORD 9 - SINGLE BIT ALLOCATION	
BIT NO.	MONITOR
1	UVS BYP CMMD DISAB (MSB)
2	UVS NOT BYP
3	ORBIT RELAY NOT BYP
4	D-N RELAY NOT BYP
5	SPIN AUTO
6	ASL DISAB
7	TMG DISAB
8	DL ON

WORD 37 - SINGLE BIT ALLOCATION	
BIT NO.	MONITOR
1	ORBIT PWR ON (MSB)
2	WHEEL DAY PWR ON
3	SAIL DAY PWR ON
4	UNM ORBIT PWR ON
5	BOLOGNA ORBIT PWR ON
6	UCL DAY PWR ON
7	LASL DAY PWR ON
8	RUTGERS DAY PWR ON

WORD 41 - SINGLE BIT ALLOCATION	
BIT NO.	MONITOR
1	LSBU DISABLE
2	LST RUNNING
3	ARM 1 ERECT
4	ARM 4 ERECT
5	ARM 7 ERECT
6	ARM 1 STOWED
7	ARM 4 STOWED
8	ARM 7 STOWED

SAIL ANALOG SUBCOMMUTATOR (SASC)	
WORD	MONITOR
1	EL ANGLE POINT MODE
2	EL ANGLE 1, RSTR-OFST MODE
3	AZ ANGLE POINT MODE
4	PITCH ANGLE
5	HCO HV MONITOR
6	HCO GRATING POSITION MONITOR
7	AZ ANGLE 1, RSTR-OFST MODE
8	HCO +4.3 V MONITOR / PULSE AMP OUT
9	HCO +4.3 V MONITOR / PULSE AMP OUT
10	RSTR-OFST MODE POSITION EYE TEMP
11	EL SERVO ERROR
12	EL ANGLE 2, RSTR-OFST MODE
13	AZ ANGLE 2, RSTR-OFST MODE
14	EL MTR CURRENT
15	OFST MODE STATUS
16	NRL PM HV MONITOR
17	AZ ANGLE 3, RSTR-OFST MODE
18	NRL PROP HV MONITOR
19	NRL BRAGG HV MONITOR
20	AZ MTR CURRENT
21	NRL BURST HV MONITOR
22	EL ANGLE 3, RSTR-OFST MODE
23	AZ ANGLE 4, RSTR-OFST MODE
24	SOLAR INTENSITY
25	AZ SERVO ERROR
26	NRL RSTR HV MONITOR
27	NRL +9 V MONITOR
28	NRL +12 V MONITOR
29	NRL CRYSTAL TEMP
30	NRL FRONT TEMP
31	NRL +4 V MONITOR
32	WG GEN TEMP
33	SOLAR ARRAY (CENTER) TEMP
34	SOLAR ARRAY (LWR RT) TEMP
35	AZ ANGLE 5, RSTR-OFST MODE
36	EL ANGLE 4, RSTR-OFST MODE
37	AZ ANGLE 6, RSTR-OFST MODE
38	EL OFST GEN STATE
39	AZ OFST GEN STATE
40	SAIL ANALOG SUB-SUBCOM (ASSC)
41	SASC TEMP
42	AZ ANGLE 7, RSTR-OFST MODE
43	DAY PWR / HCO HV LCH AND DAY
44	NRL DAY / HCO LV LCH AND DAY
45	PITCH MODE / APL STATUS
46	AZ ANGLE 8, RSTR-OFST MODE
47	PITCH GAS PRESSURE
48	SYNC

ANALOG SUB-SUBCOMMUTATOR	
WORD	MONITOR
1	PWM 15 V REGULATOR
2	SERVO 15 V REGULATOR
3	TEMP PROBE 15 V / VERNIER OFST BITS
4	ON TARGET/FINE POINT MODE
5	PITCH MANUAL 15 V REGULATOR
6	HCO ELECTRONICS TEMP
7	HCO DELTA TEMP
8	PITCH AUTO 15 V REGULATOR
9	SERVO AMPLIFIER TEMP
10	AZ CASTING TEMP
11	PWR SWITCH TEMP
12	OFST DAY 15 V REGULATOR
13	WG GEN STATUS
14	RT STRUCTURE TEMP/NUT DAMPER REL
15	OFST LCH 15 V REGULATOR
16	ROLL COIL 1 STATUS
17	HCO -5.2 V / READ-IN GATE
18	HCO ELECTRONICS TEMP
19	HCO DELTA TEMP
20	HCO OP CKT RST/EXCT MONITOR
21	HCO OP CKT ENAB/DISAB MONITOR
22	ROLL COIL 2 STATUS
23	SYNC
24	SYNC

NOTE:
See Table 10-1
for abbreviations.

16 JULY 1969

Fig. 9-2 OSO-6 Telemetry Format



Figure 9-3 is a functional block diagram of the data-handling subsystem, and 9-4 is a logic diagram of the DME.

The basic timing-signal generator is a crystal-controlled oscillator operating at 102.4 kHz. This basic frequency is divided down through a binary divider consisting of five flip-flops. The output of the 6.4 kHz flip-flop is fed to another binary counter in the bi-phase modulator. The 800 Hz (master clock) output of this divider is used to provide all of the necessary timing signals in the system. The master clock is also brought out to be used as shift pulses in the experiment and spacecraft shift registers.

The main-frame word-gate signals are generated by the word-gate generator consisting of a matrix of AND gates. This circuit is essentially a sequential pulse generator that produces 32 sequential pulses. The timing is such that each pulse is one word-length in duration (10 msec). These 32 pulses are referred to as "word gates". Word gates 31 and 32 are connected internally to the main frame sync-code-generation circuits. During the time of word 31 and 32, a pseudo-random code, "00011110/10110010" (which corresponds to a count of 30 and 178 respectively), is multiplexed into the output for main-frame identification and ground equipment synchronization.

Twenty-eight of the remaining word gates are routed outside the DME to the PCM junction box (J-Box) patch panel where they are interconnected to make up the desired multiplex format for the wheel and pointed experiments and the DSM. Two of the word gates are connected back into the DME at the inputs designated "word A" and "word B" for generation of the analog subcommutator timing signals. These two inputs activate trigger generation circuitry that develops two gates, 156 μ sec wide. These gates are routed outside the DME as ASC-1 trigger and ASC-2 trigger.

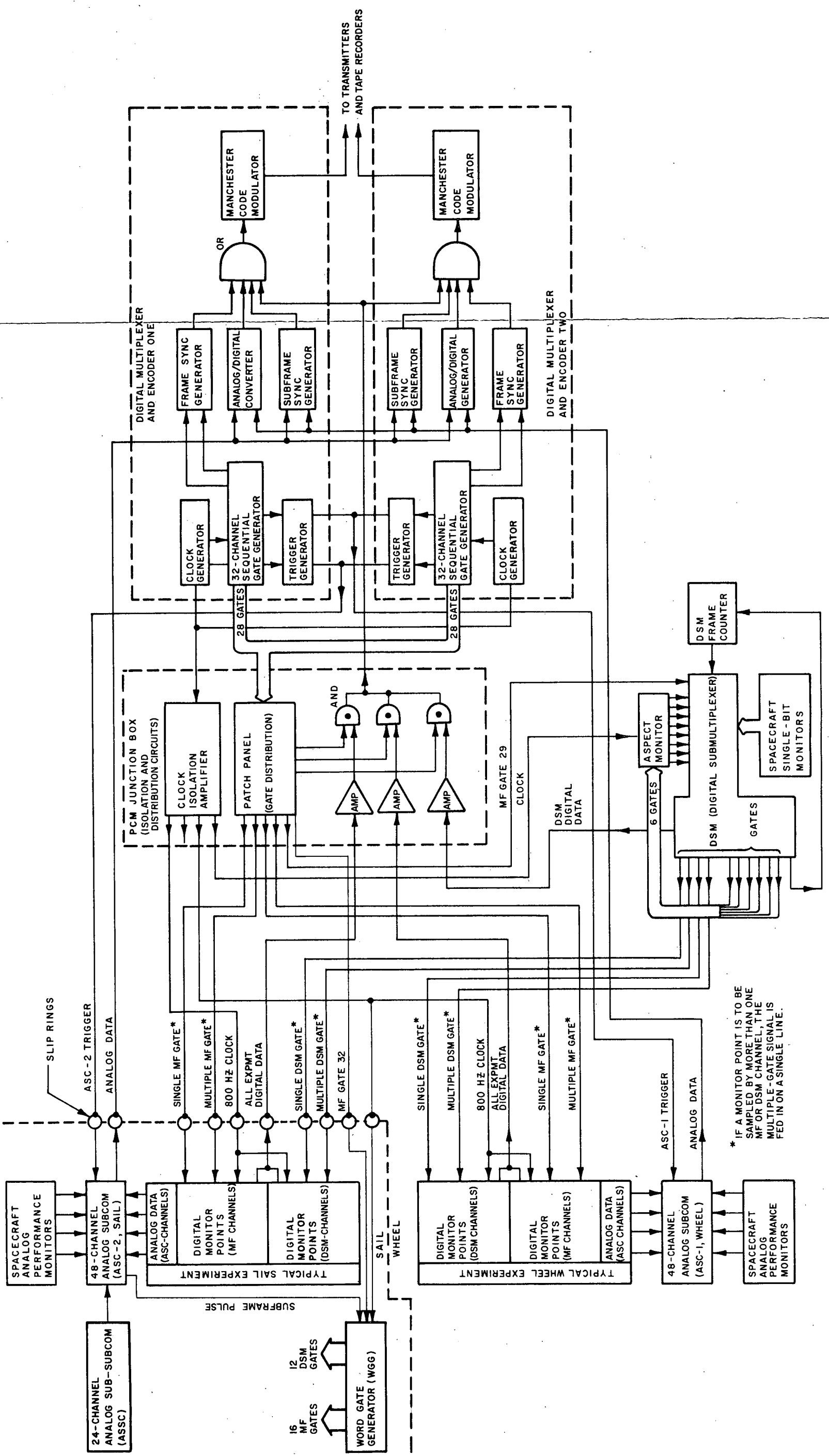


Fig. 9-3 Data-Handling System Functional Diagram

9-7.1

9-7



FOLDOUT FRAME

FOLDOUT FRAME

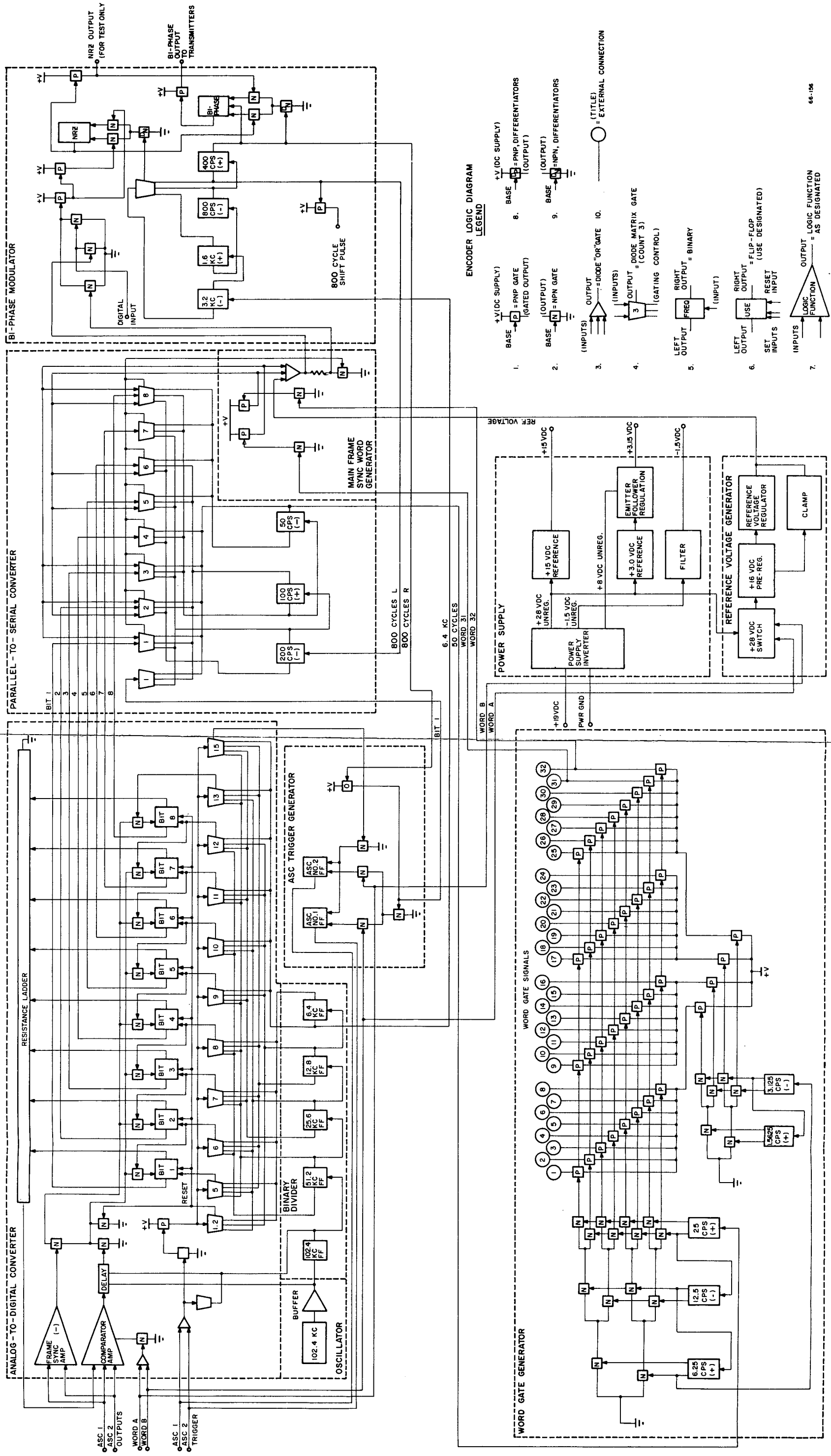


Fig. 9-4 Digital Multiplexer and Encoder Logic Diagram

9-8.1



The "word A" and "word B" inputs also operate a power switch that applies power to the analog-to-digital converter (ADC) portion of the DME. Although the circuitry required to do the analog-to-digital conversion takes appreciable power, a significant power savings is accomplished by switching the ADC on only when it is required to operate. (See Fig. 9-5 for the DME timing diagram.)

The PCM J-Box also provides gate pulses to the DSM to generate the 48 DSM words, to the individual experiment instruments to shift out their data at the proper time, and to the word gate generator (a new feature on OSO-6) which in turn provides gates to the HCO pointed experiment.

Analog-to-Digital Encoding. The analog-to-digital encoding is accomplished by a successive-approximation method. The analog input from the ASC's is fed to a comparator in the DME's where it is compared against a series of reference voltages and the result of each comparison is stored in a flip-flop. For example, during the first comparison interval, a voltage is applied to the resistance ladder network to develop a one-half-scale voltage reference at the comparator. When the input voltage is more than half scale, a "one" will be set into the first flip-flop and if it is less than half scale, a "zero" is set into the first flip-flop. During the second comparison interval a voltage is applied to the resistance ladder network to develop a one-quarter-scale reference voltage. If a "one" is set into the first storage flip-flop during the first interval, the half-scale reference will remain and is added to the one-quarter-scale reference. If a "zero" is set, then only the one-quarter-scale reference will be retained.

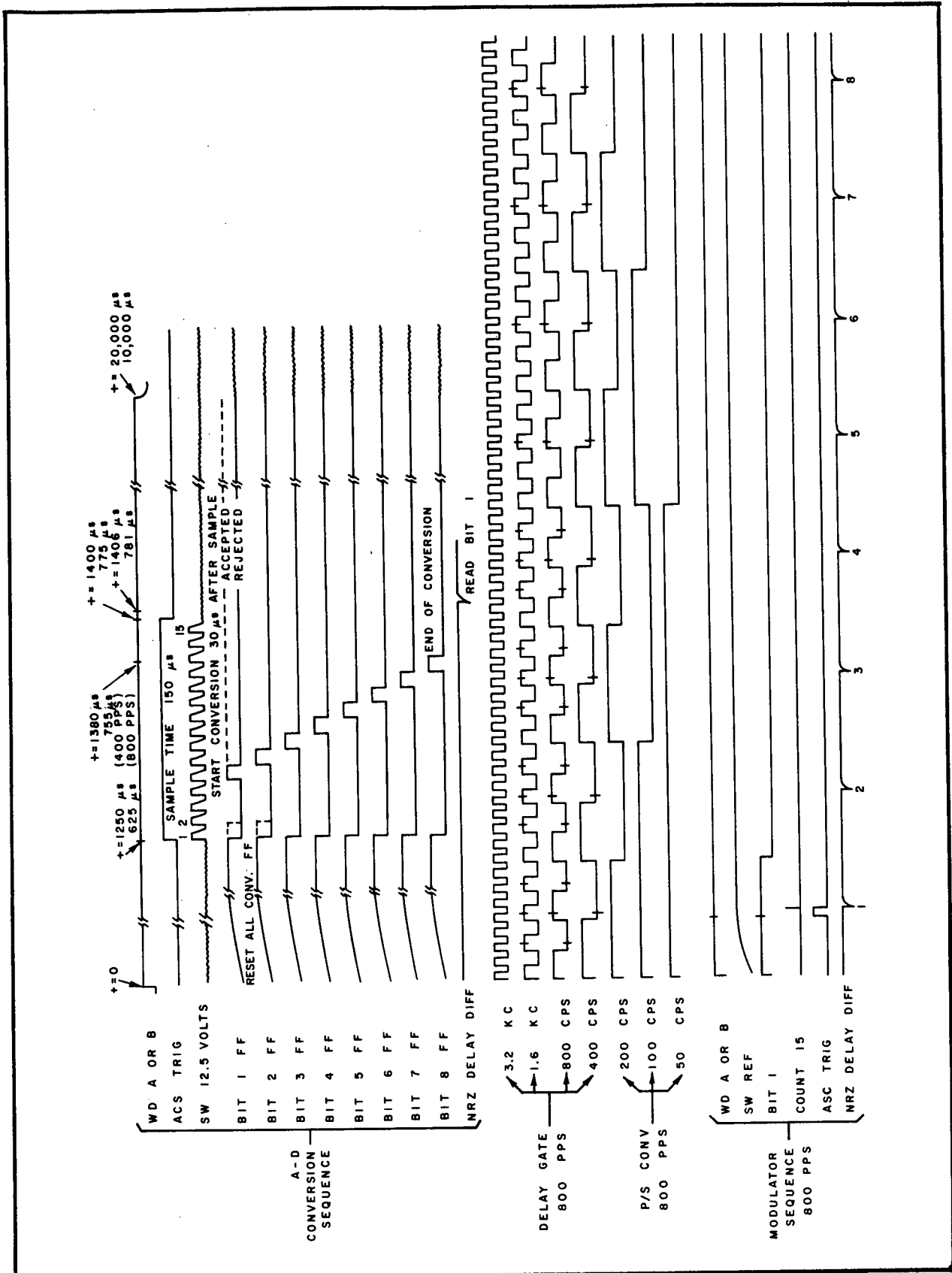


Fig. 9-5 DME Timing Chart



The result of the second comparison is then set into the second storage flip-flop. This process continues through eight successive comparisons, whereby the reference voltage is changed by one-half of its previous incremental change. During the last comparison the reference voltage will have a difference from the input voltage within one part in 256 of the full-scale voltage and a binary code equivalent of the analog input will thus be stored in the eight AND gates. The complete encoding process takes place during each sample interval of the analog subcommutator which is approximately 156 μ sec.

The output of each of the flip-flop storage units is applied to the eight AND gates. These AND gates are then sequentially enabled at the 800-Hz bit rate, and the output is a serial pulse train of eight bits which represents the coded analog signal for that particular ASC channel. These serial data are then applied through OR logic where it is time-multiplexed with the digital data from the experiments and DSM. The complete data train is then applied to the Manchester encoding circuitry which develops the biphase (Manchester) coded output signal.

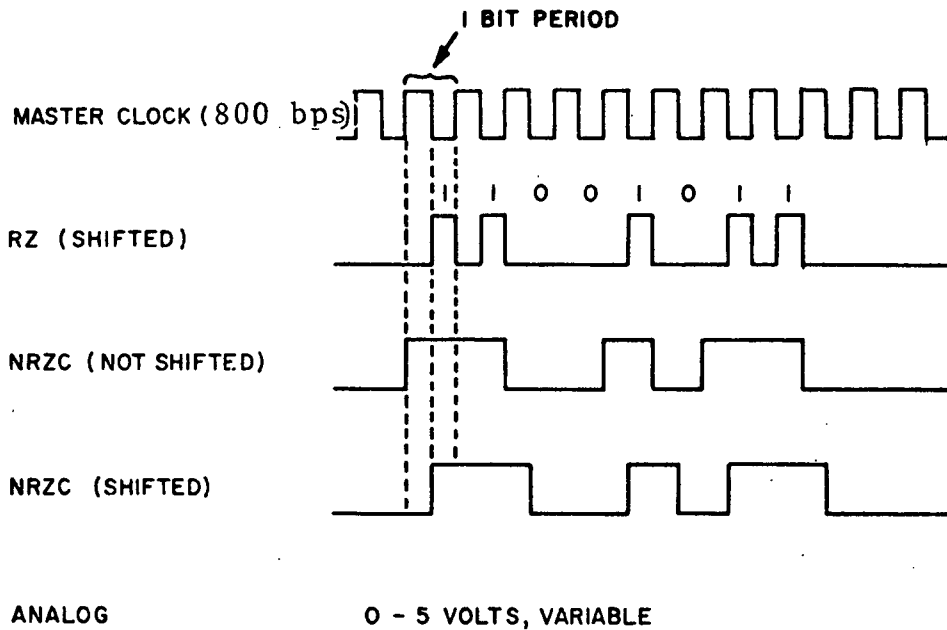
Input and Output Data Formats. The OSO data handling subsystem will accept four types of data formats:

- (1) 0 to 5 V analog
- (2) RZ (shifted)
- (3) NRZC (not shifted), and
- (4) NRZC (shifted).

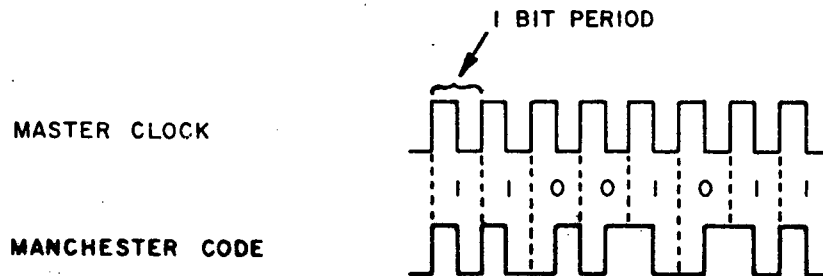
The RZ (return-to-zero) format is where the presence of a bit signifies a binary "one" and the absence of a bit signifies a



zero. The NRZC (non-return-to-zero, change) format is where the data train changes state for every change in binary value. The timing relationships of these formats are illustrated below:



The DME output is biphas (Manchester) format, illustrated below:





ASC Sync-Code Generation. When the input from the sail or wheel ASC is a positive-going pulse (ASC channel 48 only), rather than the normal negative-going pulse, it is detected by the frame sync amplifier in the DME. The normal action of the ADC is then inhibited and a "one" is set into every other storage flip-flop. This alternate "one-zero" code is the synchronization code for the subcommutator, and is read out as encoded data with a count value of 085. The value 085 is unique in that all other ASC channels are inhibited from having this count.

Data Handling Subsystem Synchronization. Main frame synchronization is determined by ensuring that the proper number of main frame words exist between the main frame sync words. As previously stated, these words consist of words 31 and 32 into which a 16 bit pseudo-random code of 30/178 is inserted.

The main-frame sync code is generated by applying pulses to the appropriate AND gates that are used for sampling the encoder storage units. This process of sequentially enabling these AND gates during main-frame words 31 and 32 generates the synchronization (or ID) code.

The wheel and sail ASCs are mutually synchronized within the 32-word main frame by using the unique sync code contained in the 48th word of each ASC. This synchronization is accomplished automatically by circuitry in the DME in the following manner:

- (1) The sync circuits in the DME expect to see both of the ASC sync words at their assigned times within the ASC subframe. The sail ASC sync word is used as the synchronization reference, or "master", and the wheel ASC is "slaved" to this reference.



- (2) The presence of the sail sync word and the absence of the wheel sync word in the same main frame results in a synchronization error decision by the sync circuits in the DME. The sync circuits then generate trigger pulses at 1,024 times the normal ASC trigger rate. These trigger pulses are used to advance the wheel ASC during main-frame words 31 and 32 until the wheel ASC sync word appears. The wheel ASC is then mutually synchronized with the sail ASC again. Since the ASC sync words are assigned to channel 48, the next time the ASC's are read out, channel one will be present because the ASC's will have been recycled.

The DSM subframe channels are identified by using the sync word that appears in the first channel. This sync word (or ID word) is a unique code (085) just as that used for the ASC's. Unlike the ASC, the DSM sync word is generated internally, whereas the ASC sync word is generated in the DME.

External Digital Multiplexing. External digital signals (experiment prime data) are time-multiplexed in the PCM J-Box and are fed to the DME's in serial form. These data are then multiplexed with the converted analog data by OR logic circuits, and signal conditioning is accomplished simultaneously with conversion to Manchester code form.

System Characteristics. With the exception of some of the logic in the analog-to-digital converter, all circuitry within the DME is quad-redundant. That is, each logic function is both series and parallel redundant and multiple component failures must occur before the logic function fails. Assembly failures caused by component failures are greatly reduced by this design, but at the sacrifice of some simplicity in fabrication.



9.2.3 Analog Subcommutator

The purpose of the wheel and sail analog subcommutators (ASC-1 and ASC-2) is to time-multiplex 47 wheel and sail analog input signals varying in amplitude from zero to +5V and to provide an ID synchronization signal to facilitate data reduction. A block diagram of the ASC is shown in Fig. 9-6 and a logic diagram in Fig. 9-7.

The input timing signal consists of the ASC trigger pulse (word A or word B) from the DME. This trigger is applied to a divide-by-48 counter that recycles at the end of 48 counts. The counter consists of binary stages two through seven on the logic diagram. A seventh binary (number one on the logic diagram) is triggered "on" by the leading edge of the trigger pulse and "off" by the trailing edge of the trigger pulse. (See Fig. 9-8 for ASC timing chart.)

The outputs of each stage of the binary counter are applied to decoding gates that are interconnected to form two matrices. One matrix has an eight-line output and the other has a six-line output. Each line of the eight-line matrix is connected to six analog gates, which are referred to as first tier gates, and each line of the six-line matrix is connected to a single analog gate which is referred to as a second tier gate.

The type of analog gate used is characterized by high input impedance in the "off" condition and very low impedance in the "on" condition. The input impedance in the "on" condition is essentially the input impedance (100 k ohm) of the buffer amplifier which provides impedance matching. As shown in the logic diagram, there are six groups of eight analog gates where the outputs of each group are connected. The six common lines are then connected

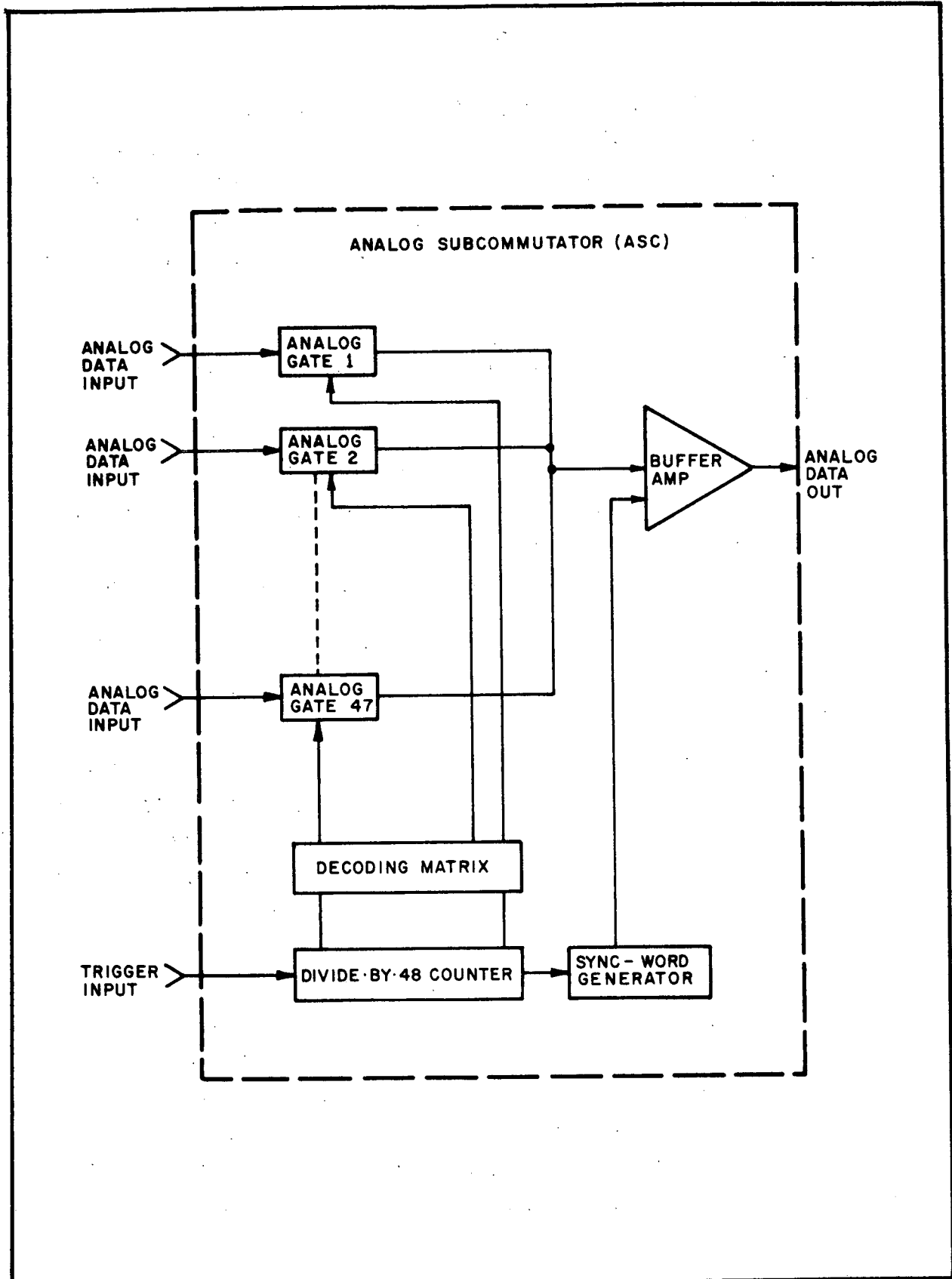


Fig. 9-6 Analog Subcommutator (ASC) Functional Block Diagram

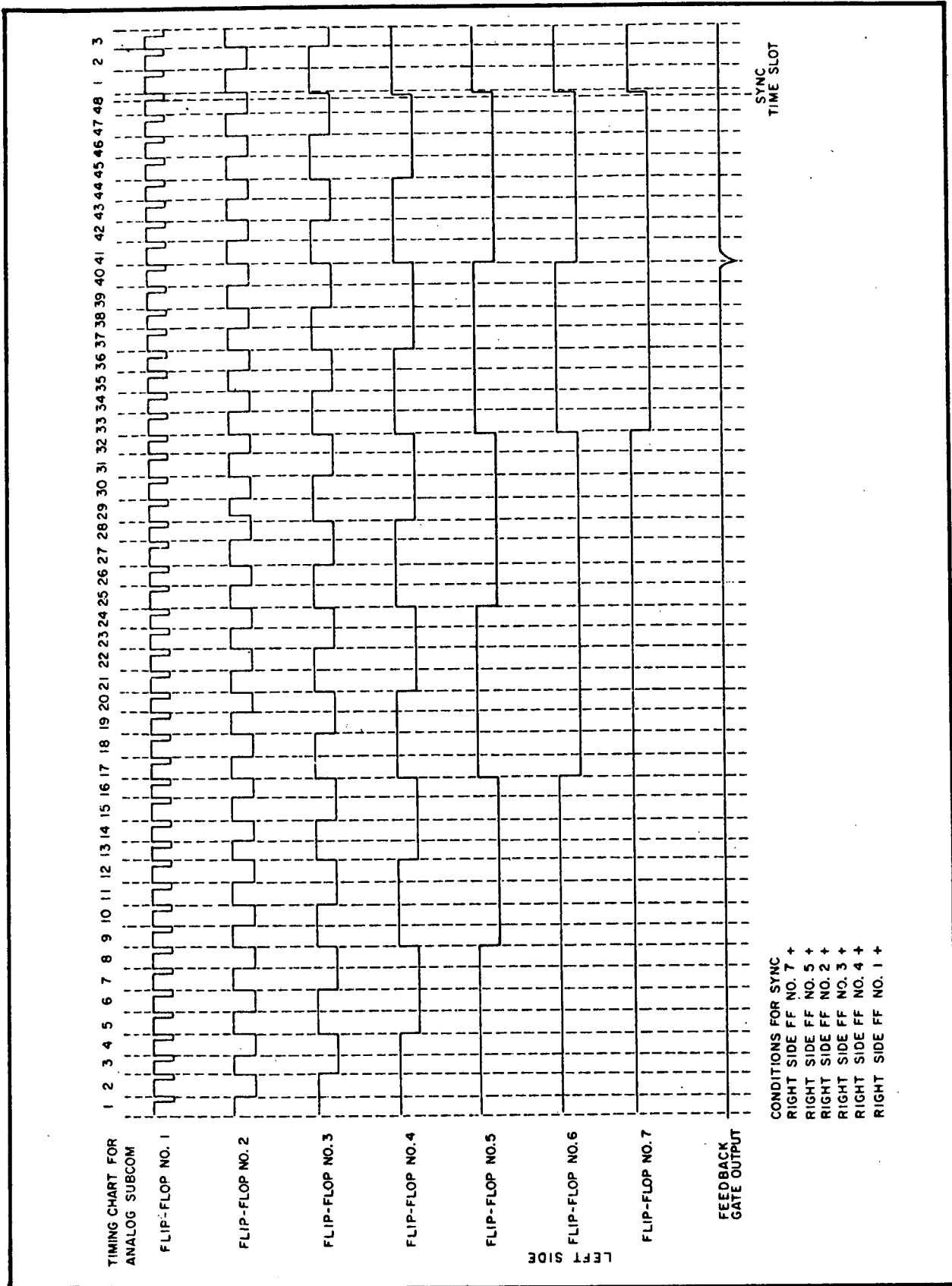


Fig. 9-8 ASC Timing Chart



through the second tier analog gates. The second tier gates sequence at one-eighth the rate of the first tier gates and, therefore, only one input is connected to the output at any one time.

The common connection of the second tier gates is connected to a buffer amplifier. The purpose of the buffer amplifier is to provide a constant input impedance for all channels and provide a low output impedance for the signal going to the encoder in the DME. The buffer also inverts the input signal and inserts a dc reference of +8 v.

Since the analog gates are turned on for only 156 μ sec (the width of the trigger pulse), the output signal is a negative-going pulse that is amplitude modulated over a range of five volts, and has a zero reference of +8 v.

When the binary counter reaches the forty-eighth count, it activates logic circuits which apply a negative voltage to the input of the buffer. Since the buffer inverts, this results in a positive-going pulse being generated for the forty-eighth channel as a sync pulse.

As in the DME, the ASC uses quad-redundant circuits except for the analog gates. The packaging technique is much the same as the DME except that the printed circuit cards are smaller.

9.2.4 Analog Sub-Subcommutator

The analog sub-subcommutator (ASSC) is a commutator capable of time multiplexing 24 analog signals onto a common output line and its purpose is to increase telemetry channel capacity of the sail ASC. The output of the ASSC is fed into channel 40 of the sail ASC. The ASSC is advanced one channel per ASC subframe.



The ASSC consists of a buffer amplifier, five flip-flops, a diode matrix, and 24 analog switches (Fig. 9-9). The subframe rate pulse from the sail ASC is fed into the buffer amplifier, which provides isolation between the internal flip-flops and the external data handling system. The output of the buffer amplifier drives the first flip-flop in the countdown circuit. The five flip-flops are connected in a conventional ripple-through counter arrangement with feedback from the fifth to fourth stage that causes the counter to recycle at the count of 24. The outputs from the flip-flops sequentially turn-on the analog switches via the diode matrix. The analog switch that is turned-on couples the input signal to the common output line with a minimum of signal loss. The input of each switch has an overvoltage protection circuit to prevent an overvoltage condition on any input channel from interfering with the operation of the remaining channels. The ASSC is synchronized by applying 0 to 5 volt signals to the inputs of channels 23 and 24.

The analog switches use field effect transistors (FET's) and have the advantages of: (1) simple control circuits, (2) no offset voltage, and (3) excellent long term stability since small changes in the FET parameters are not critical to the switch operation.

9.2.5 PCM Junction Box

The purpose of the PCM J-box is to: (1) provide interconnection and distribution of all data-handling timing signals (gates), (2) provide buffering and conditioning of these signals for proper interface with other data handling equipment and (3) provide buffering and gating of main frame data. A functional diagram of the PCM J-box is shown in Fig. 9-10.

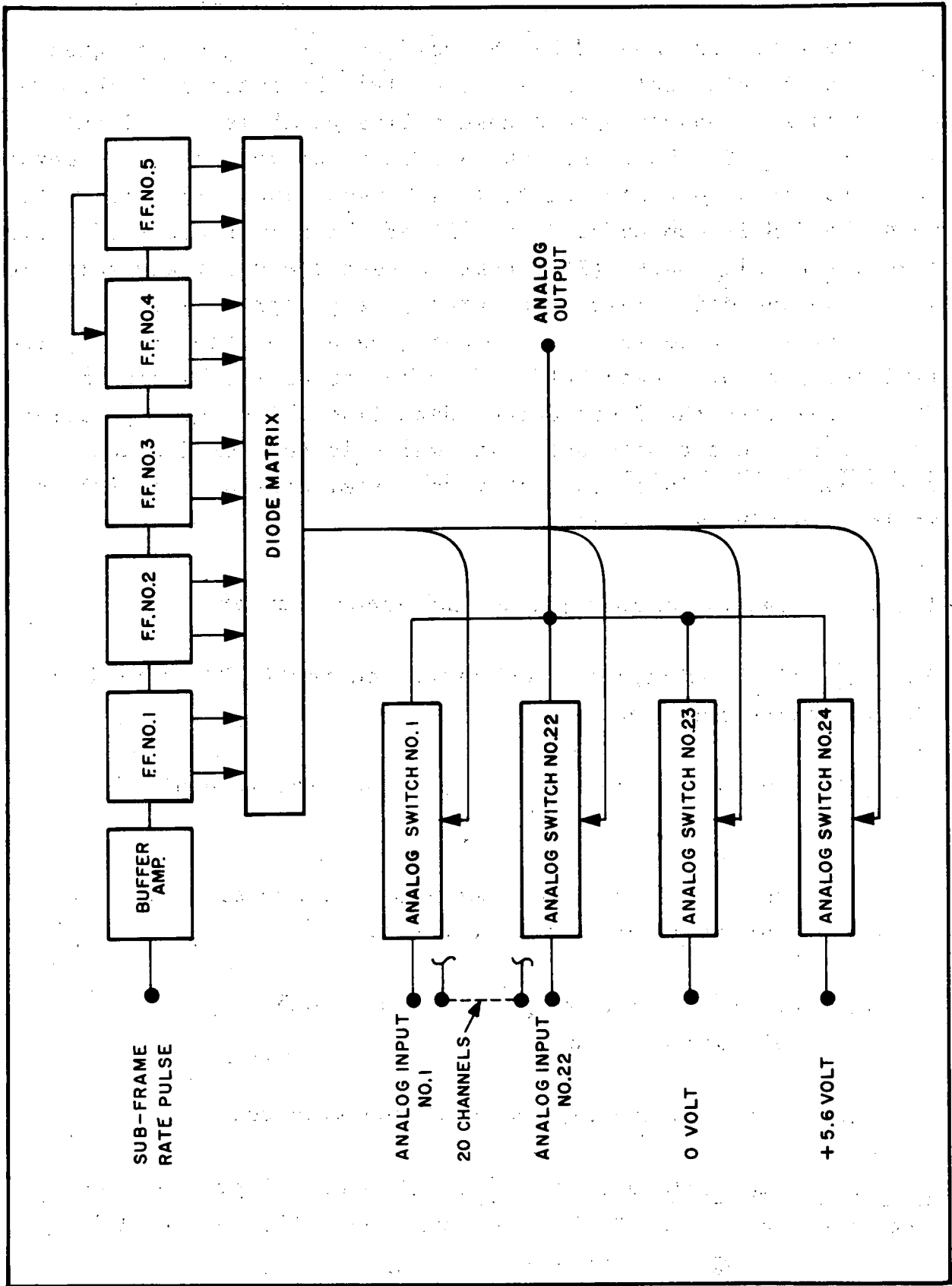


Fig. 9-9 Analog Sub-Subcommutator Block Diagram

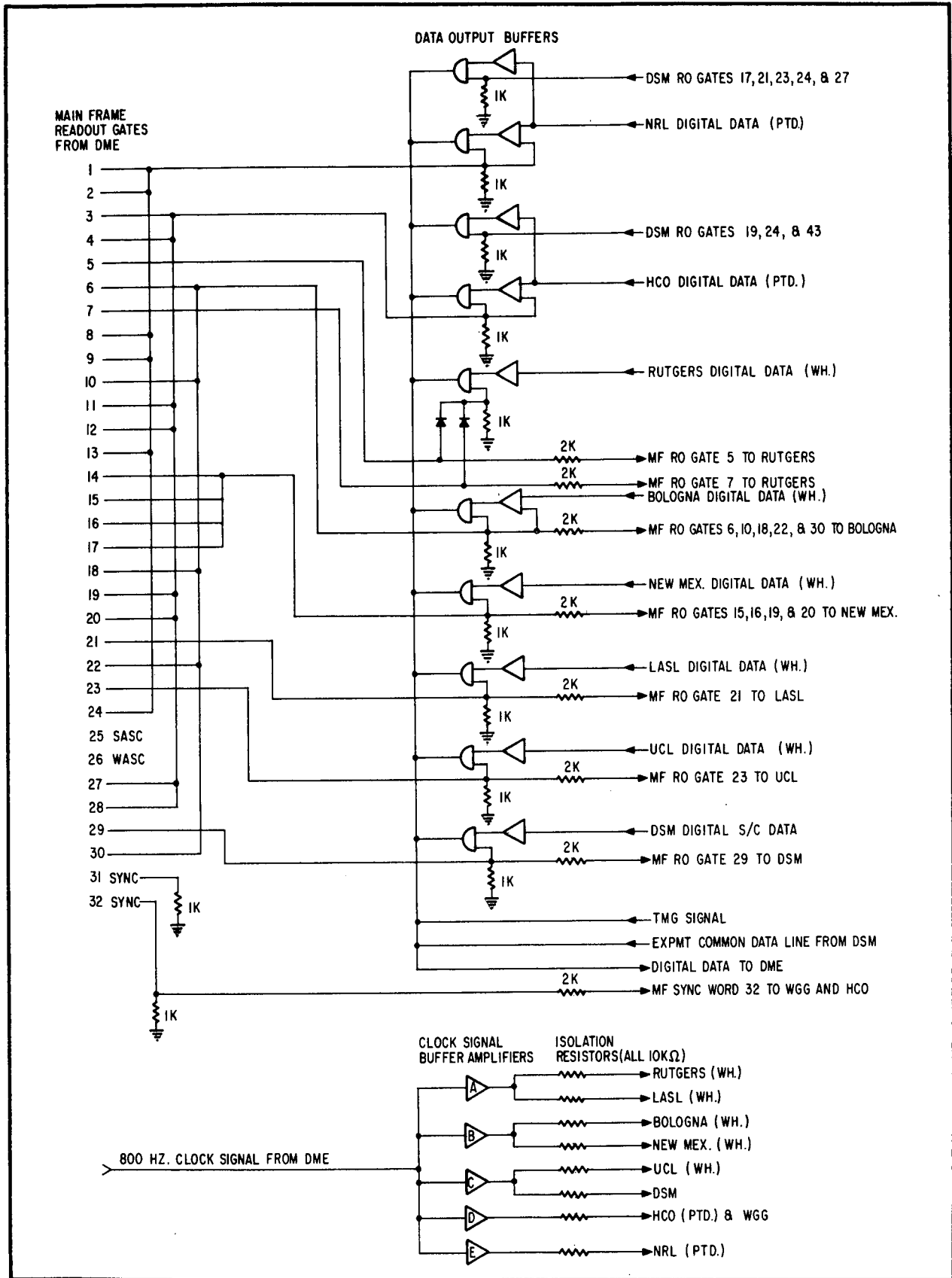


Fig. 9-10. PCM J-Box Functional Diagram



All of the word gate signals (generated by the DME) are routed into the J-box where they are interconnected according to the channel assignments. To prevent excessive loading of the DME output circuits, each word gate is applied across a 1 k ohm load resistor and isolation is provided by a 2 k ohm series resistor.

Master Clock Buffer Amplifiers. The 800 Hz master clock is routed from the DME to the J-box where it is distributed to all experiments and other spacecraft assemblies requiring this signal. To prevent loading by one user affecting the signal characteristics, and to improve overall reliability, the clock signal is routed through five parallel buffer amplifiers. Each of these buffer amplifiers is capable of supplying signals to four separate users in such a way that a short circuit can occur on the external signal line without affecting the signal characteristics for the other users. This is accomplished by providing a low output impedance at the amplifier and inserting series isolation resistors in each line.

Data Output Buffers. It would be possible to directly interconnect the experiment digital data outputs into a common line to the DME if all the experiments had high impedance outputs and if there was no chance of the experiment registers being gated at an improper time. However, due to the possibility of a circuit failure in one experiment affecting another, all digital data signals are buffered and isolated in the PCM J-box before they are multiplexed.

Buffering between the data sources and the data handling equipment is accomplished by connecting each digital data line to a simple buffer amplifier which also provides a compatible interface (e.g., impedance matching, gain etc.) for each data source. The output of each of these amplifiers is connected to a diode



AND gate which is enabled by the word gate(s) signal assigned to the particular data source. Finally, the outputs of the AND gates are connected to a common line which is the signal line to the DME. Note that the 5 volt input from the time-marker generator is also connected to this common line. This means that when the TMG is commanded "on", all of the main frame words will read out as all "ones" (255 count) except the wheel and sail ASC words and the main frame sync words (see paragraph 9.2.8). Also, note that the spacecraft housekeeping data from the DSM is gated (multiplexed) by a data buffer (the bottom buffering amp in Fig. 9-10) onto the J-box output data line while the experiment data is fed on a common data line which is connected directly to the J-box line. This means that the experiment data is multiplexed inside the DSM by gate 29.

9.2.6 Digital Submultiplexer and Frame Counter

The digital submultiplexer and frame counter (DSM/FC) performs the following functions:

- (1) Generates sequential gate pulses for readout of digital data
- (2) Stores and updates a count of the number of digital subframes for a time reference.
- (3) Provides a readout of the frame count into the main multiplexer, and
- (4) Generates the digital subframe sync code.

Digital Submultiplexer. A functional block diagram of the DSM is shown in Fig. 9-11. The synchronization of the DSM

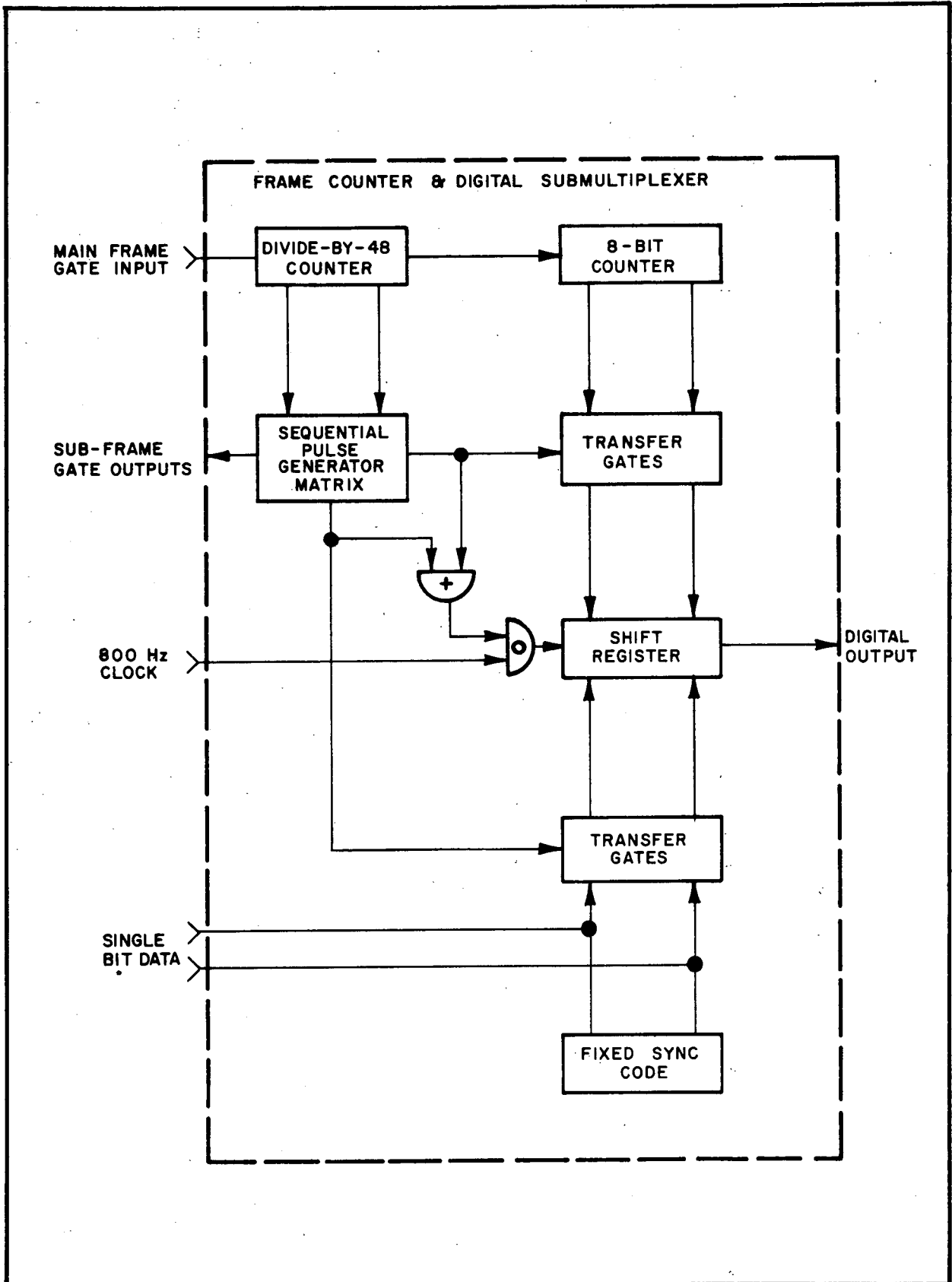


Fig. 9-11 Frame Counter and Digital Submultiplexer Functional Block Diagram



is provided by a gate signal from the DME which occurs once per main frame. This signal drives a divide-by-48 counter which establishes the subframe length. A diode matrix then generates 48 sequential gate pulses that are displaced in time from each other by one main frame. These gate signals can be used in the same manner as gate signals from the DME to readout data from external shift registers. Some of these gates are connected internally for readout of the internal shift register.

The 800-Hz master clock is used to transfer the data into the DME in serial form. Another set of transfer gates is used to transfer a fixed sync code word (085) into the shift register at the beginning of the subframe. The sync code is then shifted into the main multiplex by the 800 Hz clock. There are several other sets of transfer gates built into the DSM for transferring parallel digital data from external sources such as aspect data from the Spin Orientation and Rate Electronics (SORE).

Frame Counter. A signal from the divide-by-48 counter goes into an eight-stage counter which accumulates a count of the subframes. Transfer gates connected between the eight-stage counter and a shift register are actuated by a selected gate signal to transfer the accumulated frame count into the shift register for readout into the main multiplex. This frame count provides a means of determining time correlation of the playback data.

9.2.7 Tape Recorder/Reproducer

Data that are collected when the satellite is out of range of ground receiving stations are stored with two redundant magnetic tape recorders. The tape recorders then play back the stored data, upon command, when the satellite is within range of ground stations. The placement of ground stations used for OSO establishes the



nominal requirement that, at a maximum, data must be stored for a complete orbit, or about 96 minutes. The nominal time required for playback over a ground station is about 5-1/2 minutes. This allows ample time on either side of the playback to avoid the marginal conditions when the satellite is near either horizon.

The OSO magnetic tape recorder uses a continuous loop of magnetic tape to record the biphase signal from the DME. Data are recorded at a rate of 800 bps and are played back at a rate of 14,400 bps. The tape capacity of the recorder is about 300 feet which results in a bit packing density of about 1,333 bits per inch to store 100 minutes of data. The OSO-6 tape recorders, like the OSO-5 recorders, use single track recording techniques and are belt driven. The playback timer and the drive electronics are driven by an internally contained clock and the tape is erased during playback. The recording tape used in the OSO-6 recorders is different from the lot used in the OSO-5 recorders.

Operation. A functional block diagram of the tape recorder/reproducer is shown in Fig. 9-12. The Manchester-coded data from the DME is amplified and differentiated to produce positive and negative spikes. These spikes are fed to a flip-flop that serves as the record-head driver. The negative pulses are fed to one winding of the record head while the positive pulses are fed to the other winding. The pulses drive the record windings in push-pull so that the tape is driven into saturation in both directions.

In the playback mode, the two windings of the playback head develop a pulse that is rounded off and is not a good reproduction of the recorded signal. The playback signal is therefore amplified and clipped by two amplifiers and a level detector. The playback signal is thus conditioned to look more like the recorded signal. The two squared pulses are then differentiated and are applied to

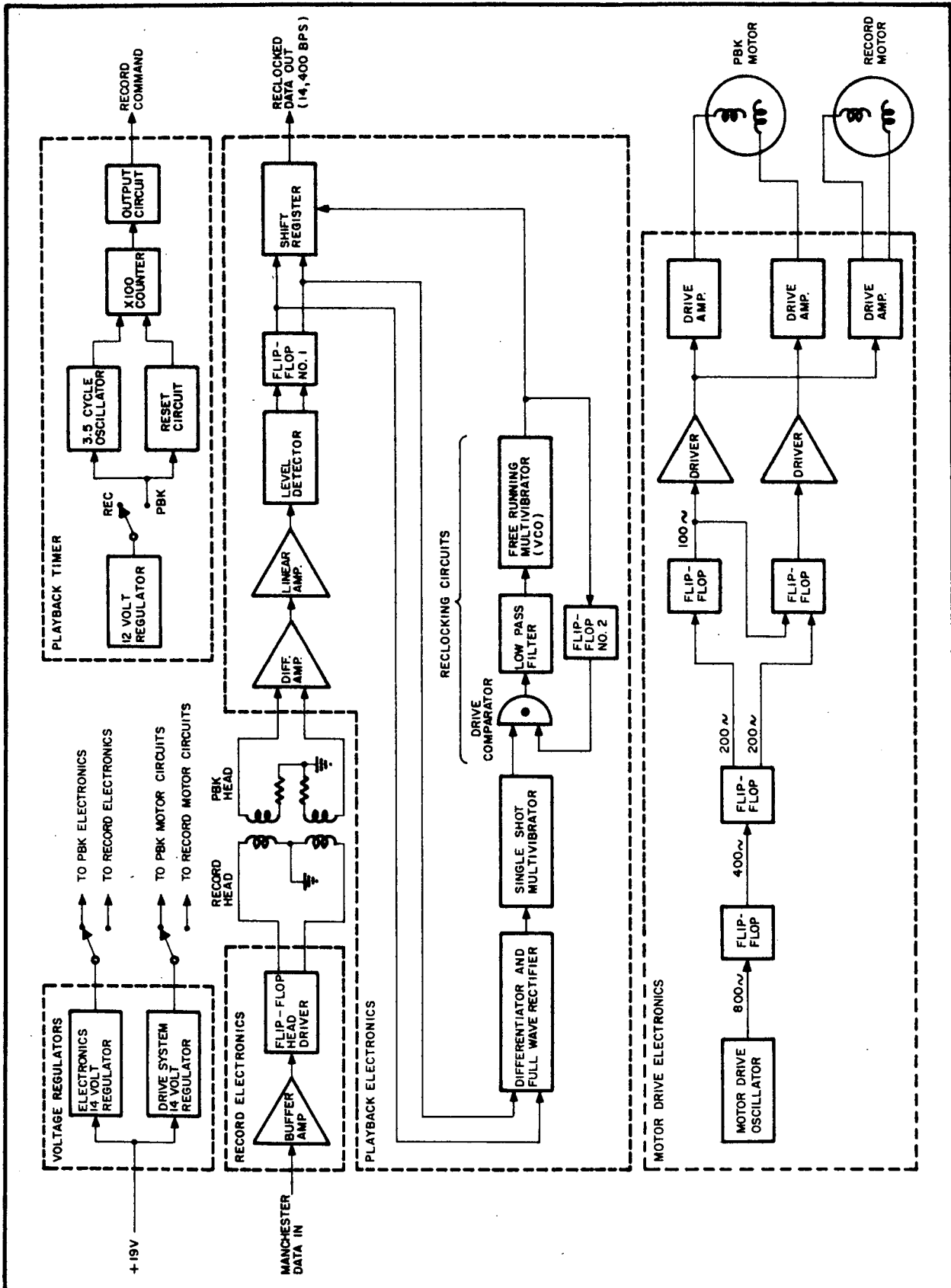


Fig. 9-12 Tape Recorder Block Diagram



the input of the flip-flop No. 1. The output of flip-flop No. 1 is the same as the input signal to the recorder, but is increased in frequency by the 18-to-1 ratio (reproduce/record speed), is modulated by wow and flutter, and has minor distortion caused by the detection electronics. The signal distortion manifests itself in phase and frequency modulation of the signal and is referred to as jitter.

To correct for some of the jitter components, the playback signal is reconditioned by the phase-lock loop circuits. In essence these circuits compare the phase of the flip-flop output with a reference signal obtained from a voltage-controlled oscillator (VCO). The phase difference is then detected and this error signal is filtered and applied to the VCO. The error signal then changes the reference frequency until no error is detected. The filter does not allow high-frequency changes to reach the VCO. Thus, the reference signal is controlled by the average frequency out of flip-flop No. 2. The ac signal from the VCO is used to clock the flip-flop No. 1 output into a one-stage shift register. The output of the shift register has then the same frequency as the flip-flop No. 1 output, with high-frequency jitter components reduced.

Low-frequency changes (wow) in the playback signal are affected substantially by the stability of the motors that drive the tape. Synchronous motors are used and are controlled by the 800-Hz telemetry clock to assure stable operating speed. The 800-Hz clock is divided down to 100 Hz in binaries, and applied to the motor-driver amplifiers. Both motors run at the same speed and drive power is applied to the capstan by a system of pulleys and Mylar belts. Only one motor has power applied to it at any one time. The playback drive mechanism produces a tape speed that is 18 times the record speed.



Tape Recorder Timer. The playback time of the tape recorders is governed by a playback timer contained in each tape recorder. This timer generates a control pulse at the end of a preset time period (337.5 sec) and switches the tape recorders back to the record mode.

When a playback command is received, a latching relay is actuated, applying power to the oscillator. The oscillator consists of a unijunction transistor and an RC timing network which establishes the oscillator period of approximately 3.375 seconds per cycle. The oscillator output is connected to a magnetic counter with a capacity of 100 counts. When power is first applied to the oscillator, the counter receives a reset pulse to assure that it starts at a zero state.

After the counter receives 100 counts, it produces an output pulse which triggers a capacitor discharge in the output circuit. The capacitor discharge is the timer output which switches the recorder back to the record mode of operation. At the same time that the tape recorder is switched, the timer relay disconnects power from the oscillator.

The timer is set for a nominal 337.5 seconds and this varies little over the environmental extremes, thereby assuring that the full tape will be reproduced under all temperature conditions.

Power Switching Change. The OSO-6 tape recorders differ from the OSO-5 recorder in that the OSO-6 recorders have individual on/off commands while the OSO-5 recorders had common power on and individual power-off commands.

Recorder/Transmitter Interface Change. When the spacecraft digital data bit rate was increased from 400 to 800 beginning



with OSO-5, problems were encountered in obtaining the proper modulation characteristics from the transmitter during playback. Analysis of the problem showed that the modulation characteristics are dependent on the amplitude, frequency, rise and fall times and symmetry of the input signal. On OSO-5, the problem was handled by adjusting the output interface network. The range of adjustment, however, was limited by the output circuit of the tape recorder. For OSO-6, the output circuit of the tape recorder was modified to allow a lower impedance interface network to be used and thus improve the rise and fall times of the transmitter input signal. The new interface circuit provided the proper impedance levels to make the best use of the tape recorder output and used diode arrays to provide isolation between the outputs of the two tape recorders.

9.2.8 Time-Marker Generator

The Time-Marker Generator (TMG) is a secondary means by which a time-reference signal may be incorporated into the OSO telemetry signal. It changes the data by applying a positive dc voltage to the digital input line of the DME, thus causing the digital data to appear as all "ones". This feature is used as a backup to the frame counter which provides the primary time reference. The "TMG-On" command function simply applies a dc signal to the DME input line (this is done in the PCM J-box, see Fig. 9-10). This signal is subsequently removed by the "Playback On" command.

9.2.9 Word Gate Generator

The word gate generator (WGG) is a new feature on OSO-6. Its purpose is to generate up to 16 main frame and 12 subframe



word gates for use by the pointed instruments while using only 6 slip ring circuits and thus conserve the use of slip rings. The WGG also provides a data expansion capability for future OSO missions.

Background of Development. The main frame and subframe digital multiplexing requirements of the OSO-6 pointed experiments required the availability of 18 parallel circuits for instrument gating functions. Since, in the current OSO configuration, gating requirements were met by multiplexing equipment (i.e., the PCM J-box and DME) located in the wheel, the pointed instrument gating requirements dictated the need for 18 slip ring circuits. These requirements, when coupled with other sail slip ring circuit requirements, resulted in the need for a minimum of 40 slip ring circuits. The currently qualified slip ring design available for OSO use was for only 22 circuits. These considerations justified the need for adding the WGG to the data handling system.

Operation. The functional purpose of the WGG is to deliver to the pointed instruments, over parallel lines, a set of properly positioned word gates. These word gates sequentially "trigger" the transmittal of data from the pointed instruments. The WGG is located in the sail and operates in synchronism with the DME and DSM located in the wheel.

The word gate generator consists basically of a *main frame generator* and a *subframe generator* which have the capability of being prewired to supply any 16 of the 32 main-frame gates and any 12 of the 48 subframe gates (Fig. 9-13). The main-frame output gates use quad redundancy and both the main-frame and subframe generators have a backup unit. The backup unit can be selected by the command system. Fig. 9-13 shows how the WGG interfaces with the data handling and command systems.



A functional block diagram of the *main-frame gate generator* is shown at the top of Fig. 9-14. The clock signal and word gate 32 are obtained from the DME and used to generate and synchronize the 32 sail gate pulses with the spacecraft data handling system. The clock signal is first applied to a buffer amplifier (B_1) for signal isolation and conditioning and then to the synchronous counter. The synchronous counter divides the 800 cps clock signal down to 3.125 cps and thus provides the timing signals that control the output gate drivers. The counter is connected for synchronous operation to eliminate the propagation delay that is inherent in a normal ripple-through counter. The gate drivers provide the 32 sequential drive pulses that control the output gates. Any 16 gate drivers can be selected to drive the 16 output gates. Word gate 32 is fed through an isolation amplifier where it is differentiated. The trailing edge of word gate 32 resets all counter stages to the main-frame gate 1 state which synchronizes the counter with the DME main-frame gate 1.

A functional block diagram of the *subframe gate generator* is shown at the bottom of Fig. 9-14. The first sync pulse (SASC-48) from the sail ASC is fed through a buffer amplifier which isolates the subframe gate generator from other users of this pulse (e.g., the DME) and provides the necessary drive to reset the ripple counter flip-flops to count 48. The re-setting of the counter to 48 synchronizes the subframe generator with channel 48 in the DSM. Main-frame word gate 29 is supplied by the main-frame gate generator (discussed above). This gate enables the diode matrix and also advances the counter at the DSM rate. At the end of 48 DSM word periods, the ripple counter resets itself and thus becomes independent of the sail ASC sync pulse.

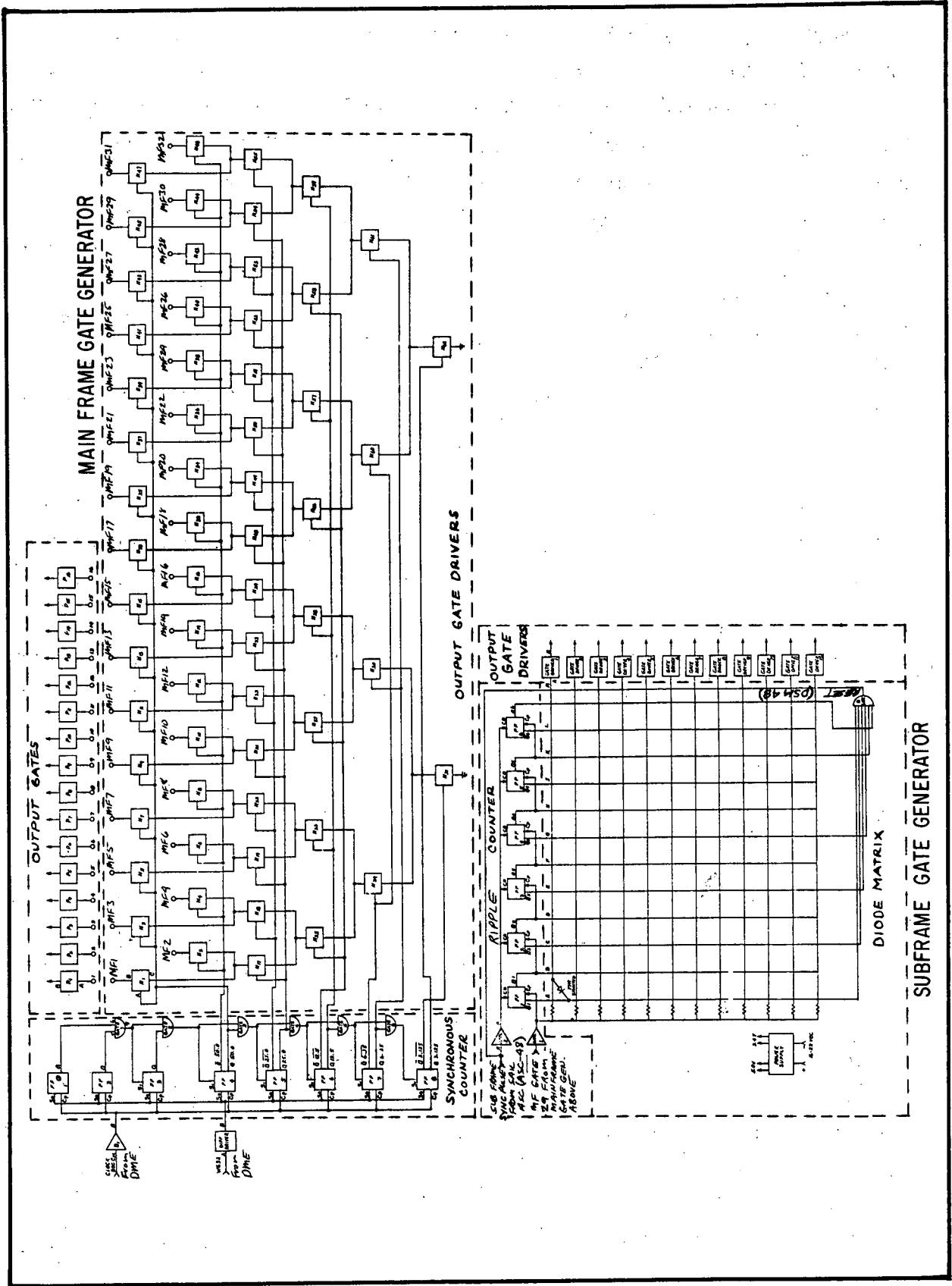


Fig. 9-14 Word Gate Generator Functional Diagram



The WGG is powered by its own internal power supply. This power supply furnishes regulated 5 ± 0.1 vdc and consists basically of a series regulator, an inverter, and two output rectifiers. The 19 ± 3 vdc input is first filtered to suppress high frequency spikes that might damage the regulator transistors and to prevent high frequency noise from the inverter being reflected back onto the 19 vdc bus line. The series regulator then regulates the 19 volt input to about 13.7 volts which is fed to the inverter. The inverter chops this voltage into a 3 Khz signal which is then rectified to provide the 5 volt output. Since regulation is not critical and because the major load is fixed, output regulation is not used.

The WGG uses circuitry essentially identical to that portion of the DME which generates data gates for the pointed instruments. The WGG only results in another series element for the overall spacecraft. The present spacecraft probability of success is $R_T = 0.824$ (from BBRC TR66-64). Thus the spacecraft reliability with redundant WGG's added is:

$$R_T = (0.824)(0.99909) = 0.82325$$

9.2.10 Sail Junction Box

The sail J-box differs from the PCM J-box in the wheel in that it serves only to distribute the various power, command, and telemetry signals used by the various sail electronic components and the pointed instruments. It does not, however, perform any multiplexing chores as does the PCM J-box. The sail J-box also houses the pointed instruments' power control relays, the pitch backup arming relay, and the offset pointing control relays. Finally, it serves as the attach point for the "flex cables" that carry the various signals to and from the pointed instruments.



Sail J-Box Changes. The OSO-5 sail J-box was sheet metal construction with two solder terminal boards hardwired into the box, one in the top and one across the rear, inside the box. The box was hard-wired into the sail harness. It had Bendix pygmy connectors on either end for mating with boxes in the sail and 37 pin connectors for mating with the flex cables.

The arrangement of the two terminal boards made rework extremely difficult and all J-box rework had to be performed with the box on the spacecraft.

The OSO-6 sail J-box is fabricated from standard sheet metal and terminal board stock. It has five solder-terminal type plug-in boards which insert vertically from the top. Each plug-in board mates with the central distribution terminal board in the bottom of the J-box by means of double density connectors. On top of the plug-in boards are double density connectors for mating with the flex cables. On each end of the plug-in boards are connectors for mating the harness on either side of the sail.

Each plug-in board can be removed and replaced by a spare while it is being reworked on the bench. The central distribution board in the bottom of the box can be reworked on the bench by simply unplugging the harness connectors and unbolting the box from the sail.

In addition, the OSO-6 sail J-box uses Teledyne TO-5 size relays which are potted and wired directly to the plug-in boards. They are smaller and have considerably less mass than the Potter Brumfield relays used on OSO-5.



9.3 RF SUBSYSTEM

9.3.1 General

The RF subsystem consists of two redundant telemetry transmitters, a coaxial relay, an RF filter, a diplexer, a hybrid circulator and an antenna array. A block diagram of this subsystem is presented as part of Fig. 9-1.

The telemetry transmitters provide phase-shift keyed (PSK) modulation using the Manchester-coded input data. Power to the redundant transmitters, both of which operate on the same frequency, is controlled by ground commands. The coaxial relay, which is used to connect the desired transmitter to the diplexer, is also operated by these commands.

The diplexer provides a low-attenuation path between the selected transmitter and antenna at the transmitter carrier frequency while providing high attenuation at the command receiver frequency. Thus, any high-power RF signals originating from the transmitter, that are at the command receiver frequency, do not reach the command receivers and cause possible damage. Conversely, the diplexer provides low attenuation between the antenna and the receiver when commands are sent to the spacecraft.

The hybrid circulator is used as a power divider for the two command receivers while providing high isolation between the two receivers. A common antenna array is used for transmitting telemetry signals and receiving command signals.



9.3.2 Transmitters

OSO-6 used the same type transmitter (BBRC-PSK-600A) that was used in OSO-5. The only difference was the addition of a modulation filter that was used to decrease the bandwidth during playback. This modification is described below. A block diagram of the PSK-600A is shown in Fig. 9-15. The electrical and mechanical characteristics of the PSK-600A transmitter are given in Table 9-1.

Operation. The modulator driver conditions the Manchester-coded input data from the tape recorders or DME's and establishes a fixed voltage level and thus the phase shift of the reference signal for a "zero" or a "one" input on the information line. The output of the modulator driver is fed to the phase modulator.

A 34 MHz crystal oscillator is used to establish a stable reference for the transmitter. The output level for this oscillator is -3 dbm. The crystal oscillator is followed by a phase modulator that changes the phase of the reference signal in response to the input data supplied by the modulator driver. Some loss is experienced in the phase modulator, and the output signal level becomes approximately -10 dbm.

A buffer amplifier follows the phase modulator and provides isolation between the modulator and the subsequent multipliers, and raises the signal level to +10 dbm. This level is required to overcome the 0.7 v base-to-emitter drop of the subsequent multiplier stage and drive this stage in to class C operation. Class C operation is necessary for the multiplier to establish a nonlinear waveform on the output of the multiplier so that the second harmonic can be extracted by a bandpass filter.

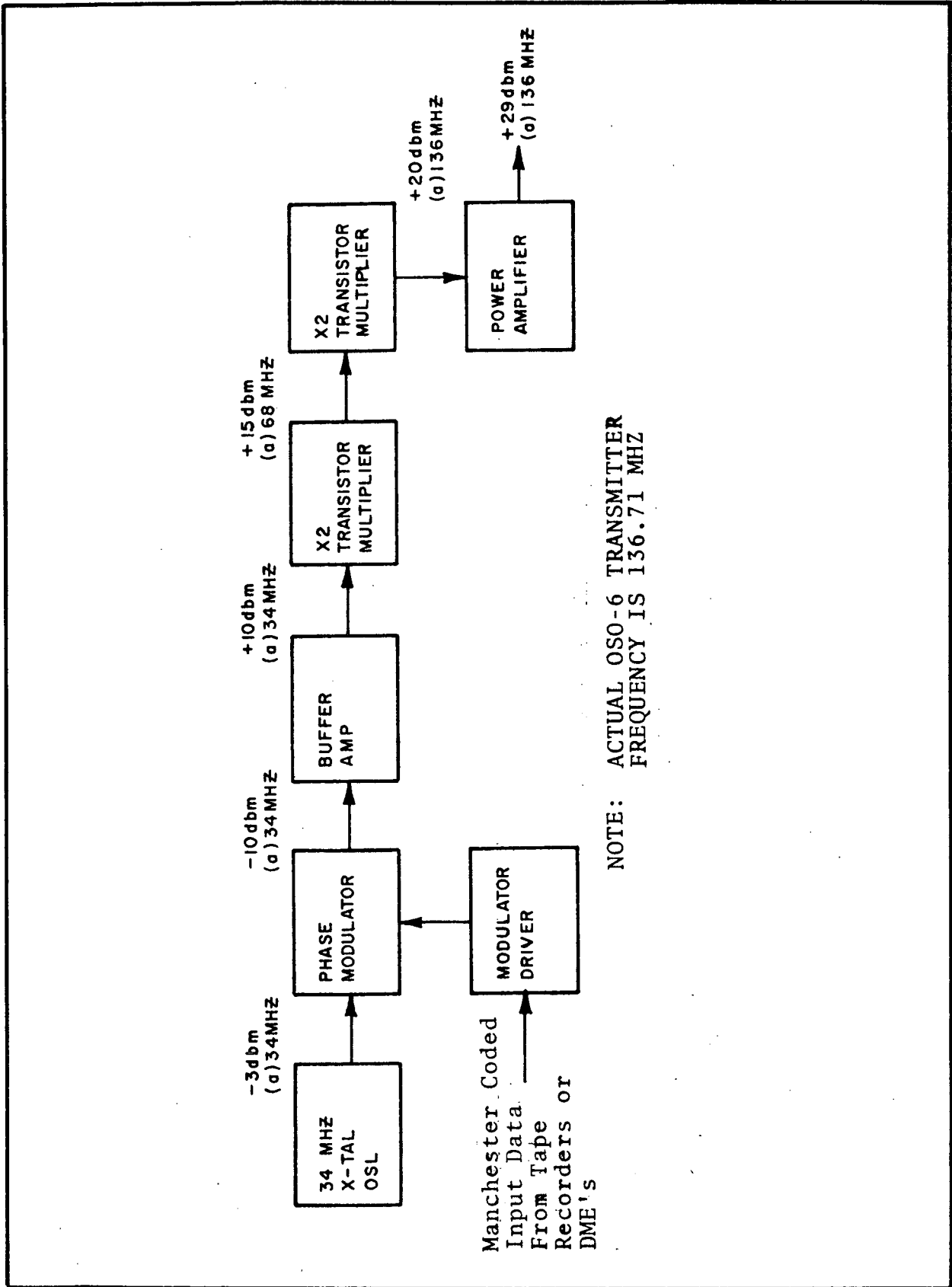


Fig. 9-15 Telemetry Transmitter (PSK-600A) Block Diagram



Table 9-1

SPECIFICATIONS FOR THE PSK-600A TELEMETRY TRANSMITTER

ELECTRICAL CHARACTERISTICS

- (1) Frequency: 136 to 137 MHz (fixed tuned at 136.71 MHz)
- (2) Frequency Stability: ± 0.0037 percent
- (3) Power Output: 700 mw (minimum, PSK-600A)
- (4) DC/RF Efficiency: 25 percent (minimum)
- (5) Modulation: Phase shift keyed
- (6) Frequency Response: 400 to 15,000 bps
- (7) Modulation Sensitivity: 1.75 to 6 v P-P to cause the specified phase deviation
- (8) Deviation: Selectable from 50 to 90 deg. peak ± 5 deg. (nominally 60 deg. on OSO-6)
- (9) Input Impedance: 10,000 ohms
- (10) Coherent Spurious Radiation: All harmonics in the range from 30 to 500 MHz are at least 40 db below the carrier
- (11) VSWR: The transmitter can operate into a 2:1 all-phase load with no spurious outputs greater than 60 db below the carrier and with a maximum power variation of 4 db. The transmitter can also survive a 5:1 all-phase load without damage.
- (12) Power Supply: 16 to 22 v (19 v nominal)
- (13) Incidental AM: 5 percent maximum
- (14) Incidental FM: ± 5 deg. for pulse period at 1/Bit Rate

MECHANICAL CHARACTERISTICS

- (1) Size: 3.125 by 1.75 by 3.25 in.
- (2) Weight: 1 lb. maximum



The output of the first times-2 multiplier is at a +15 dbm level and at a frequency of 68 MHz. This signal drives a second times-2 multiplier that is identical to the first multiplier, with the exception that the output stage is tuned to the second harmonic or about 136 MHz (136.71 MHz on OSO-6). The signal level at this point in the transmitter is about +20 dbm. The final times-2 multiplier is followed by a power amplifier which raises the 136 MHz signal to about +29 dbm (750 mw) at 19.0 volts supply input, a level suitable for transmission.

Modulation Filter Modification. Previous measurements of the PSK-600A transmitter spectrum indicated that the spectrum was not in conformance with NASA Aerospace Data Systems Standards (X560-63-2). To minimize this nonconformance, the technique of pre-modulation filtering was used. This technique limits the bandwidth of the data signal which in turn limits the bandwidth of the transmitted signal to about 90 MHz during playback.

The pre-modulation filter is an active filter with a cut-off frequency of approximately 35 KHz. Functionally, the filter module consists of a shaping circuit followed by a five pole active filter. The supply voltages for these circuits are derived from zener-diode supplies. An EMI filter was added to minimize the amount of conducted 136 MHz on the spacecraft power lines.

Physically, the filter module is contained in an aluminum case 4.25 inches by 3.50 inches by 1.00 inch. The case is mounted on the inside of the rim panel in compartment eight and is wired directly to transmitter 1.



9.3.3 Coaxial Relay

The coaxial relay is a single-pole double-throw magnetic latching relay that requires a +19-volt pulse of 30-millisecond duration to operate. This relay closes in the position corresponding to which transmitter is selected. This relay is extremely small with a volume of approximately one cubic inch not including connectors.

9.3.4 Diplexer

As was mentioned earlier, the purpose of the VHF diplexer is to permit simultaneous operation of the telemetry transmitters and command receivers from a common antenna array. The diplexer and RF filter are incorporated into the same assembly.

An M-derived high-pass type filter using lumped constants is used to provide a minimum of 20 db of attenuation of any signal from the transmitter which is at the receiver frequency. At the same time, this filter allows the transmitter frequency to pass with a maximum attenuation of 0.25 db.

Two low-pass filters, used between the antenna and receiver terminals, provide a minimum of 50 db of attenuation at the transmitter frequency while allowing the receiver frequency to pass with less than 0.7 db loss.

9.3.5 Hybrid Circulator

The hybrid circulator permits simultaneous operation of two command receivers on the same frequency. A lumped-constant bridge circuit is used to provide isolation between the two receiver terminals in excess of 40 db. The input signal is divided equally between the two receiver terminals within ± 0.2 db with an insertion loss of less than 0.5 db.



9.3.6 Antenna Array

Since the OSO is not stabilized with respect to the earth, nearly-isotropic radiation patterns are required. This nearly-isotropic radiation is accomplished with a three-element array. When the radiation pattern is measured by two orthogonally-polarized receiving antennas, the field sensed by the vector sum of the antennas is greater than -6 db for 95 percent of the aspect angles. Field plots of these two components, E_{θ} and E_{ϕ} , are shown in Figs. 9-16 and 9-17, respectively. The figures are equal-power-contour plots reflecting the antenna gain with reference to a linear isotropic source. Refer to Figs. 9-18 and 9-19 for the coordinate definition for all radiation patterns.

The same three-element array is used for command reception at approximately 150 MHz; however, the performance characteristics are somewhat different because command transmission is right circularly polarized. Therefore, radiation field measurements must be sensed with a right circularly polarized antenna. For command reception, the measured gain is greater than -18 db with respect to a linear isotropic source for 95 percent of the aspect angles. Figure 9-20 is an equal-power contour plot of the antenna at the receiver frequency of approximately 150 MHz. Again, the plot reflects the gain with reference to a linear isotropic source.

Figure 9-21 is a view showing one antenna element. Each of the arms on OSO is identical which results in a three-element array. Each antenna element consists of an arm support bracket and a stub. The support bracket also serves its primary function of supporting the arm. Each stub is electrically connected to its respective support bracket to form an element having an electrical length of one-half wavelength. Excitation is applied at the point where the support bracket connects the OSO arm.



BALL BROTHERS RESEARCH CORPORATION

DATE 11-27-68

VEHICLE TYPE OSO-G MODEL SCALE 1

MODEL FREQUENCY 136.5 MHz

POLARIZATION E θ

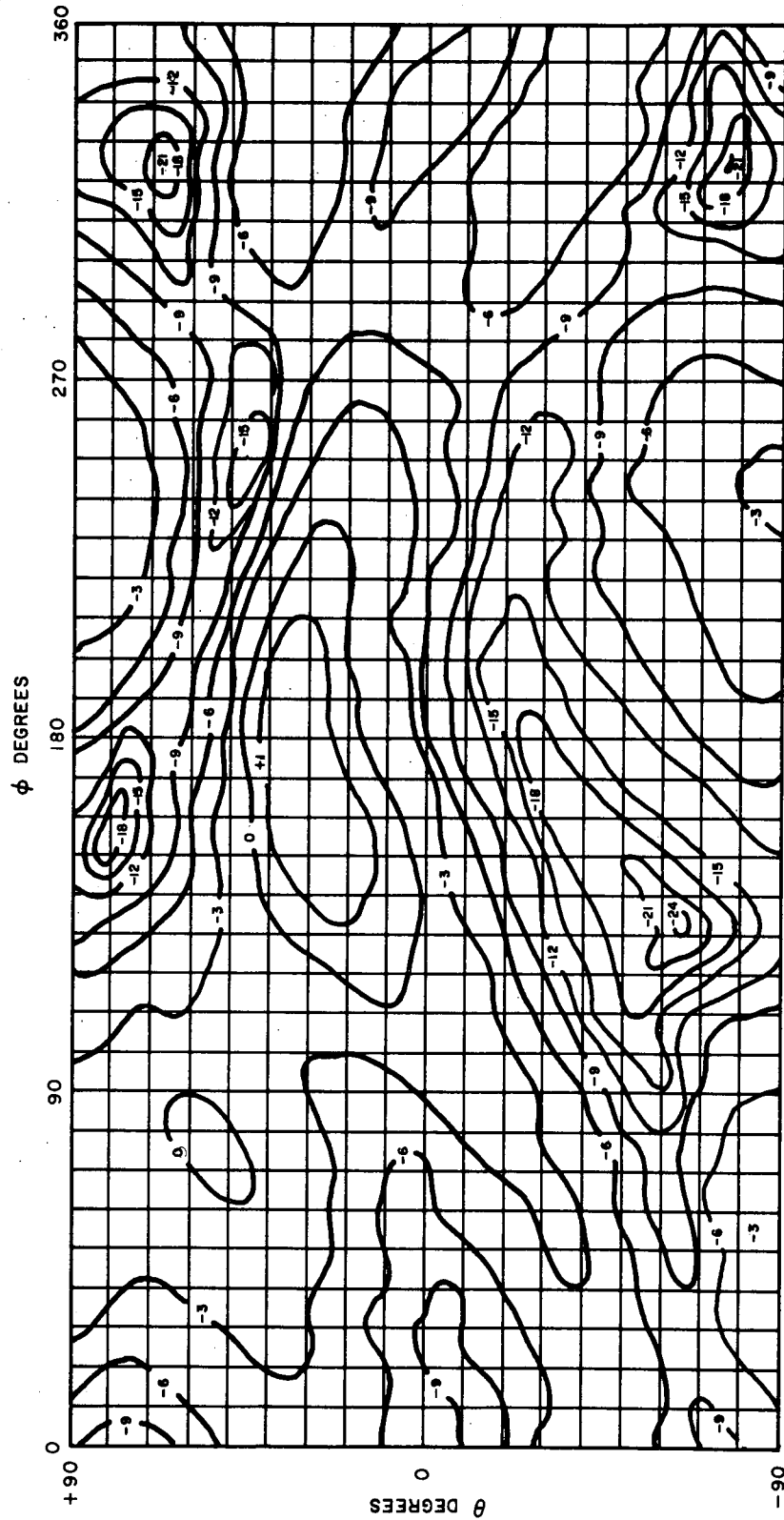


Fig. 9-16 OSO-6 Transmitter Antenna Pattern (E θ Polarization)



BALL BROTHERS RESEARCH CORPORATION

DATE 11-27-68

VEHICLE TYPE OSO-G MODEL SCALE 1

MODEL FREQUENCY 136.5 MHz

POLARIZATION E ϕ

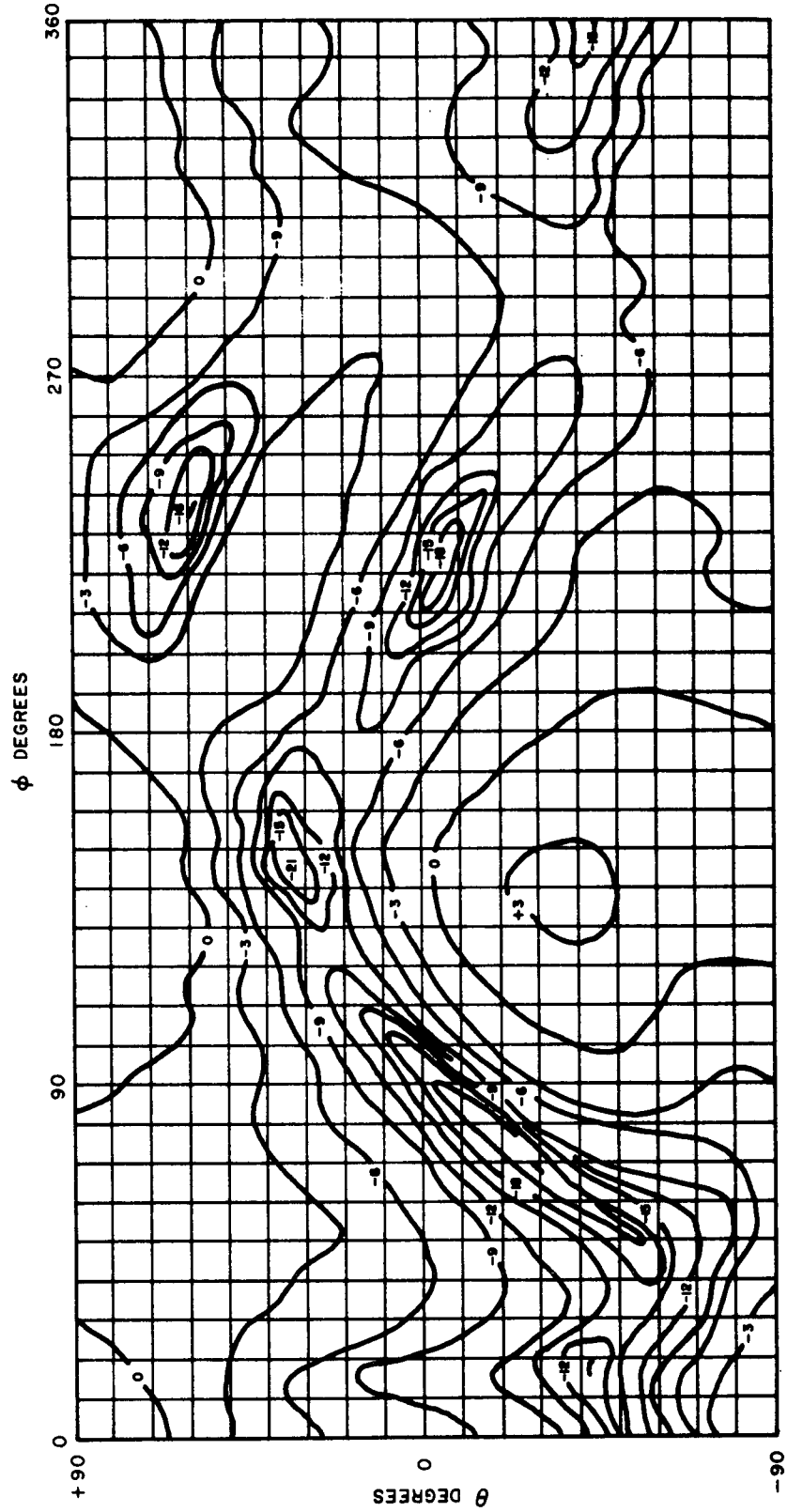


Fig. 9-17 OSO-6 Transmitter Antenna Pattern (E ϕ Polarization)

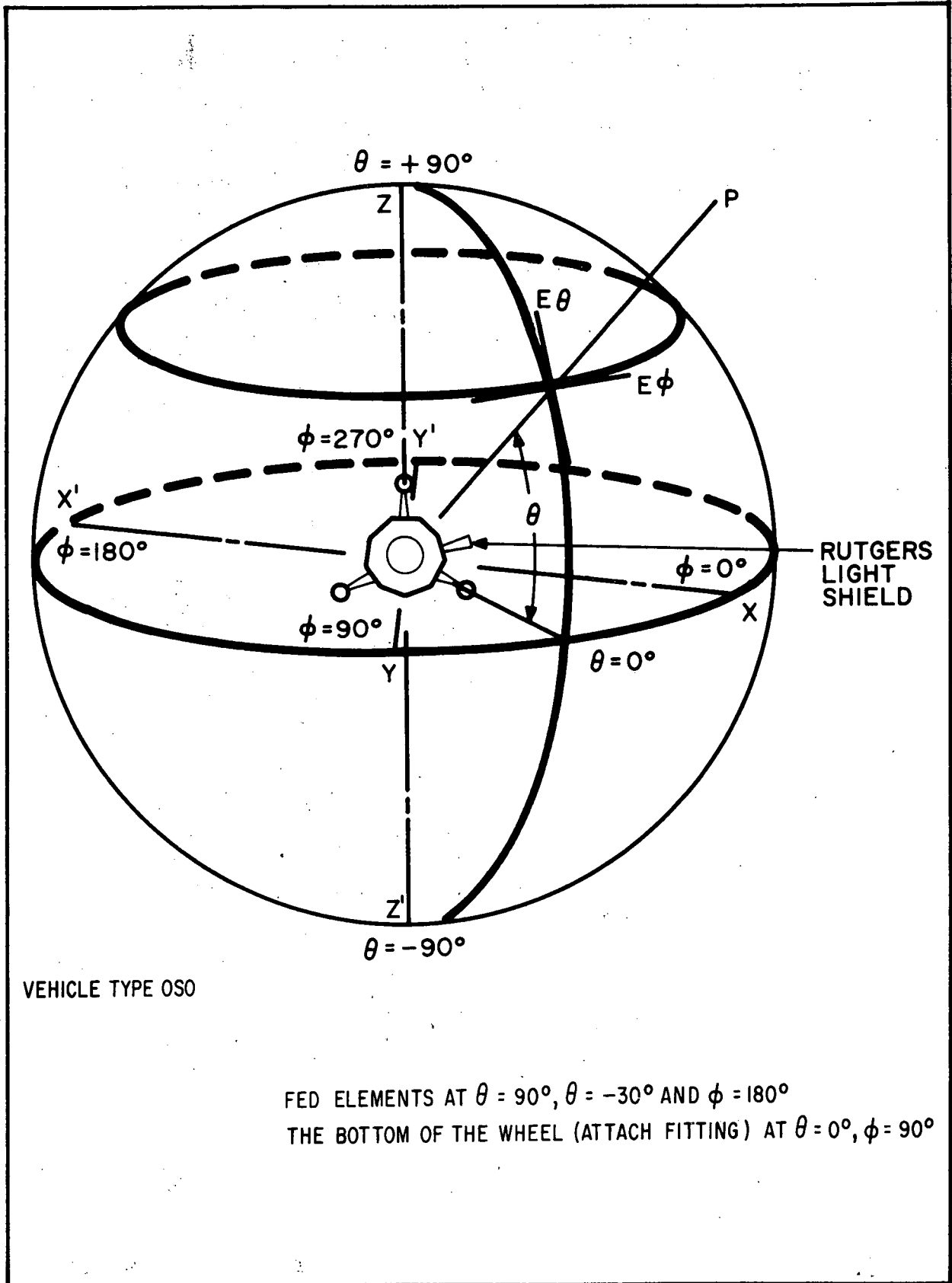


Fig. 9-18 Coordinate System for Radiation Pattern

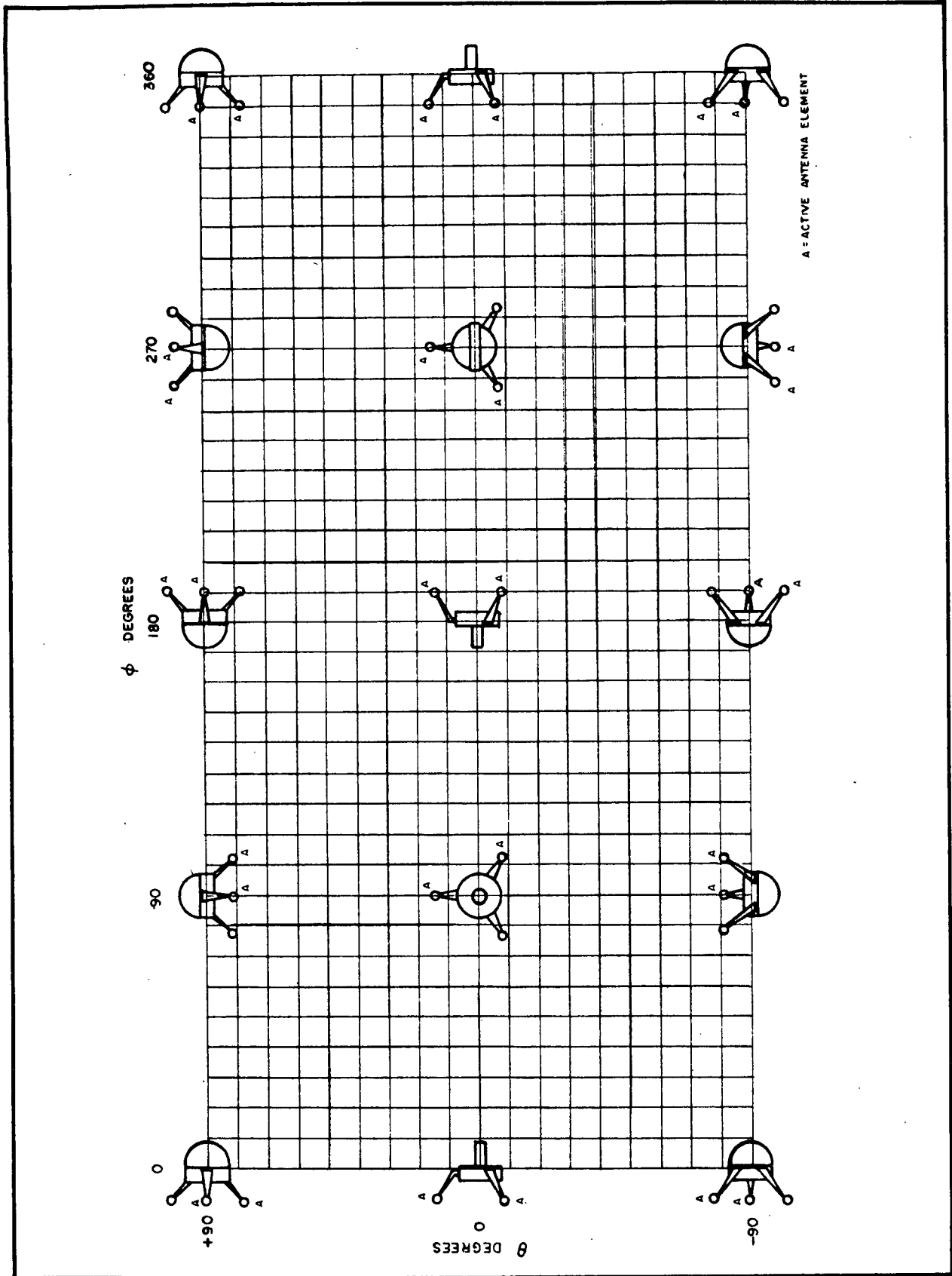


Fig. 9-19 Orientation of OSO Relative to Contour Plots



BALL BROTHERS RESEARCH CORPORATION

DATE 11-27-68

VEHICLE TYPE 050-G MODEL SCALE 1

MODEL FREQUENCY 149.52 MHz

POLARIZATION RT CIRCULAR

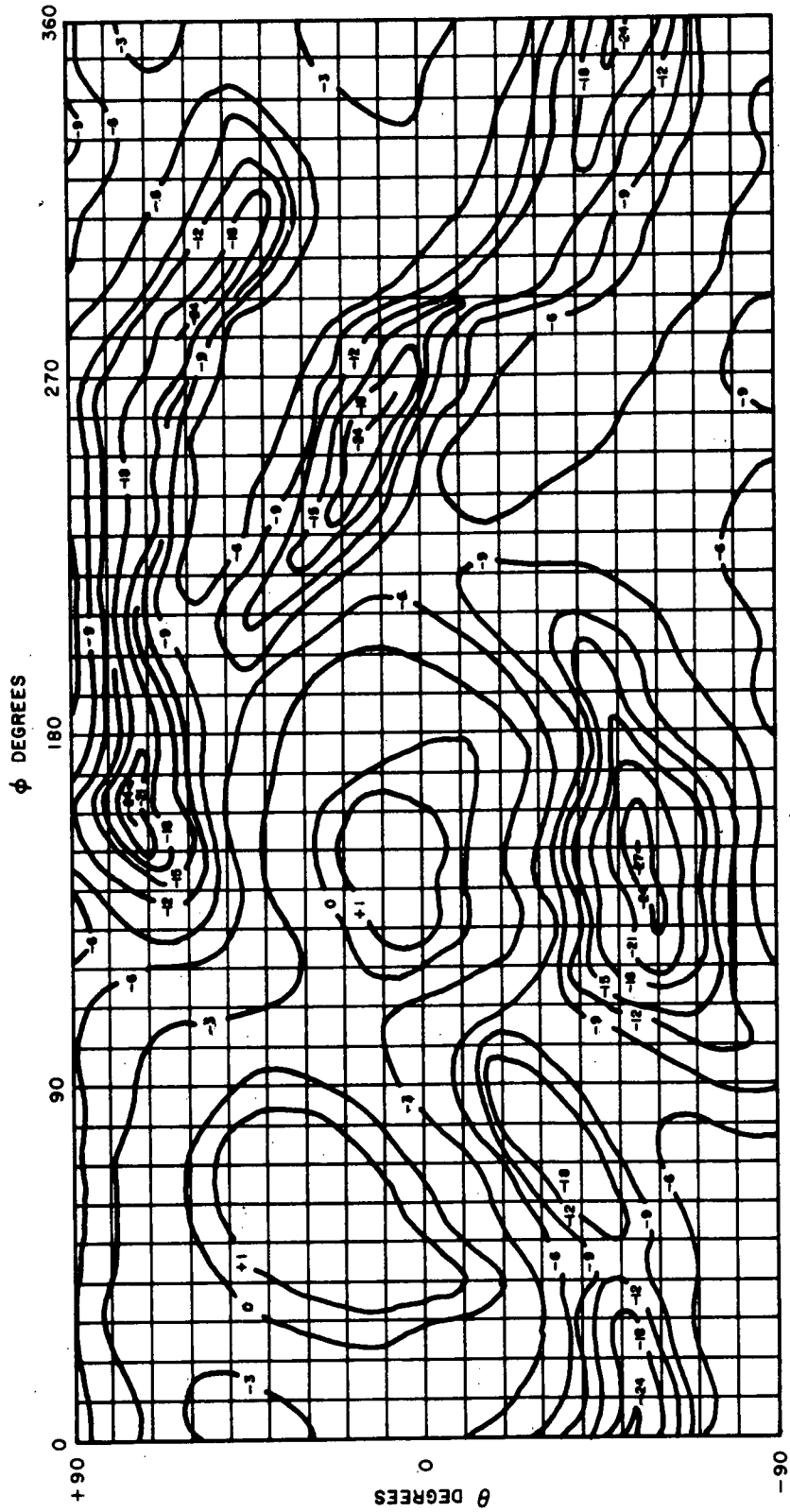


Fig. 9-20 Receiver Antenna Pattern, Right-Circular Polarization

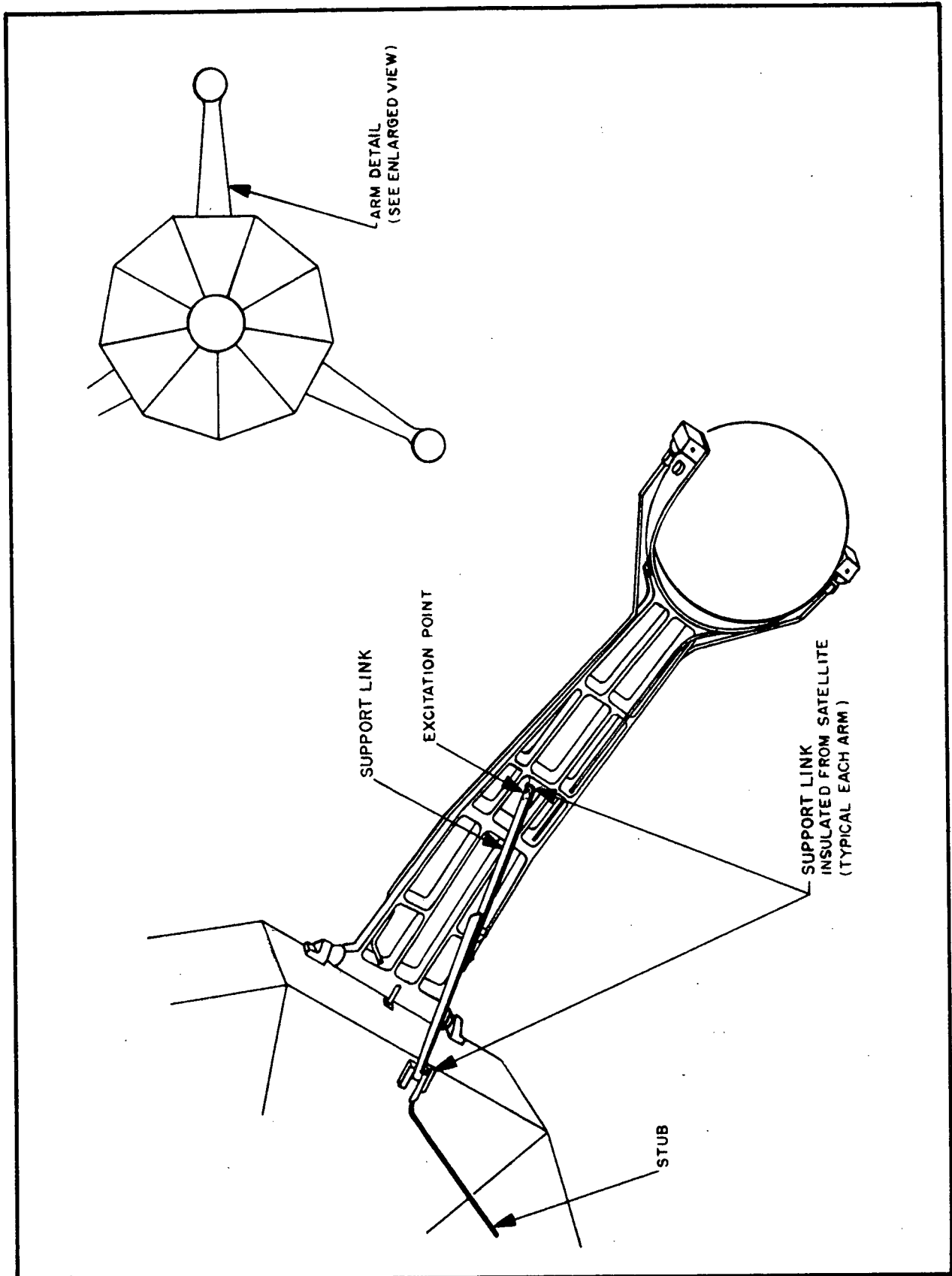


Fig. 9-21 Antenna and Support Bracket Details



The three antenna elements are insulated from the structure by the use of dielectric materials such as fiber glass and nylon.

When the arms are erected, two elements are directly excited and the third element is parasitic. When the arms are stowed, all three elements are driven.

9.4 SPACECRAFT HOUSEKEEPING DATA ACQUISITION

Spacecraft housekeeping data, including performance monitors and status monitors, are read out through the DSM, the two analog subcommutators, and the analog sub-subcommutator.

The input voltages to the analog subcommutators range from zero to +5 v. These monitors include temperatures, voltages, current levels, and others which are not readily converted to digital form in the sensing subassemblies. Conversion is done in the DME's.

The concept of single-bit status monitoring is used in the digital subframe to provide a means by which up to eight status points can be read through a single subframe word. This technique allows more analog channels for experimenter use and provides for simpler machine interpretation of status-monitor data.

Other spacecraft data read through the digital subframe include the aspect (SORE) data and the frame count.



9.5 TELEMETRY SYSTEM PERFORMANCE REQUIREMENTS

The performance of the communications link between the OSO and the GSFC Satellite Tracking and Data Acquisition Network (STADAN) is dependent upon both the airborne and the ground equipment. Table 9-2 shows the gain margin of the communications link for playback transmission of 14400 bps at a range of 1150 statute miles. This table also lists the equipment parameters used to establish the gain margin. The gain margin for real-time transmission at 800 bps is not included in the table.

The post-detection bandwidth for real-time transmission can be much narrower than for playback transmission. Therefore, the output signal-to-noise ratio can be expected to be higher resulting in a gain margin which exceeds the margin established for playback transmission.

Computation of Path Loss:

$$\begin{aligned}
 \text{Path Loss} &= \frac{1}{\left(\frac{4\pi f_{mc} d}{300}\right)^2} = \frac{300^2}{[(4\pi)(136.71)(1150 \text{ stat. mi.} \times 1609 \text{ m/mi})]^2} \\
 &= \frac{300^2}{(3180 \times 10^6)^2} = \frac{300^2}{(3.18 \times 10^9)^2} = \frac{9 \times 10^4}{9.96 \times 10^{18}} = 0.904 \times 10^{-14} \\
 &= -150 + 9.04 = -140.95 \text{ db}
 \end{aligned}$$



Table 9-2
OSO-6 Telemetry Link Gain Margin at 14400 BPS

	<u>Power Ratios</u>
Radiated Power (at antenna terminals) 500 milliwatts	+27 dbm
Receiver Noise Level 1. Mod. 1 receiver with I.F. bandwidth of 100 kHz and noise figure of 2 including preamp 2. Antenna noise temperature: 1400°K	-116.3 dbm
Required signal-to-noise ratio (CNR)*	10.6 db
Miscellaneous losses allowed for tracking errors, transmission line losses and other miscellaneous losses	-4 db
Path Loss 1. Range: 1150** statute miles 2. Frequency: 136.71 MHz	-141 db
Receiver Antenna Gain 1. Nine Yagi array 2. Polarization: horizontal, vertical, right, and left circular	+19.2 db
Transmitter Antenna Gain Polarization: linear	-6 db
Margin of Safety (worst predicted case) = S/N ratio threshold + gains - losses = (116.3 - 10.6) + (27 + 19.2) - (141 + 4 + 6) = 0.9 db	

* The CNR has been increased about 3 db to allow for the 14400 bps bit rate.

** This is worst case since 1150 miles is an unlikely range for playback. 975 mi. is more reasonable and this decreases the path loss about 1.5 db.



Section 10 COMMAND SYSTEM DESCRIPTION

10.1 INTRODUCTION

The OSO-6 command system consists of two redundant VHF-AM command receivers, two redundant wheel decoders, two sail decoders, and the necessary wiring and control relays (Fig. 10-1). The command system provides a total complement of 206 command functions (67 for the spacecraft, 108 for the experiments, and 31 spares). Each wheel decoder is driven from one command receiver while either sail decoder can be connected to either of the two receivers by ground command. The RF input is identical for each receiver, since the RF input power is divided equally by a hybrid circulator. All receivers and decoders have dc power applied continuously.

The spacecraft uses a STADAN compatible tone-digital command system. The command RF signal (149.52 MHz) is 80 percent amplitude modulated by a 7 kHz audio tone. The tone is keyed by the coded digital-command signal.

The main differences between the OSO-5 and OSO-6 command systems is the addition of a sail command decoder and the desensitizing of the command receivers.

10.2 COMMAND FORMAT

The minitrack ground operator transmits commands to the OSO by either a punched paper tape mode or a manual mode. The paper-tape mode, which is normally used, allows the transmission of as many commands as desired in sequence, and the format consists of: address, execute, 1/2-second delay. As a standard procedure, the command frame is transmitted twice.

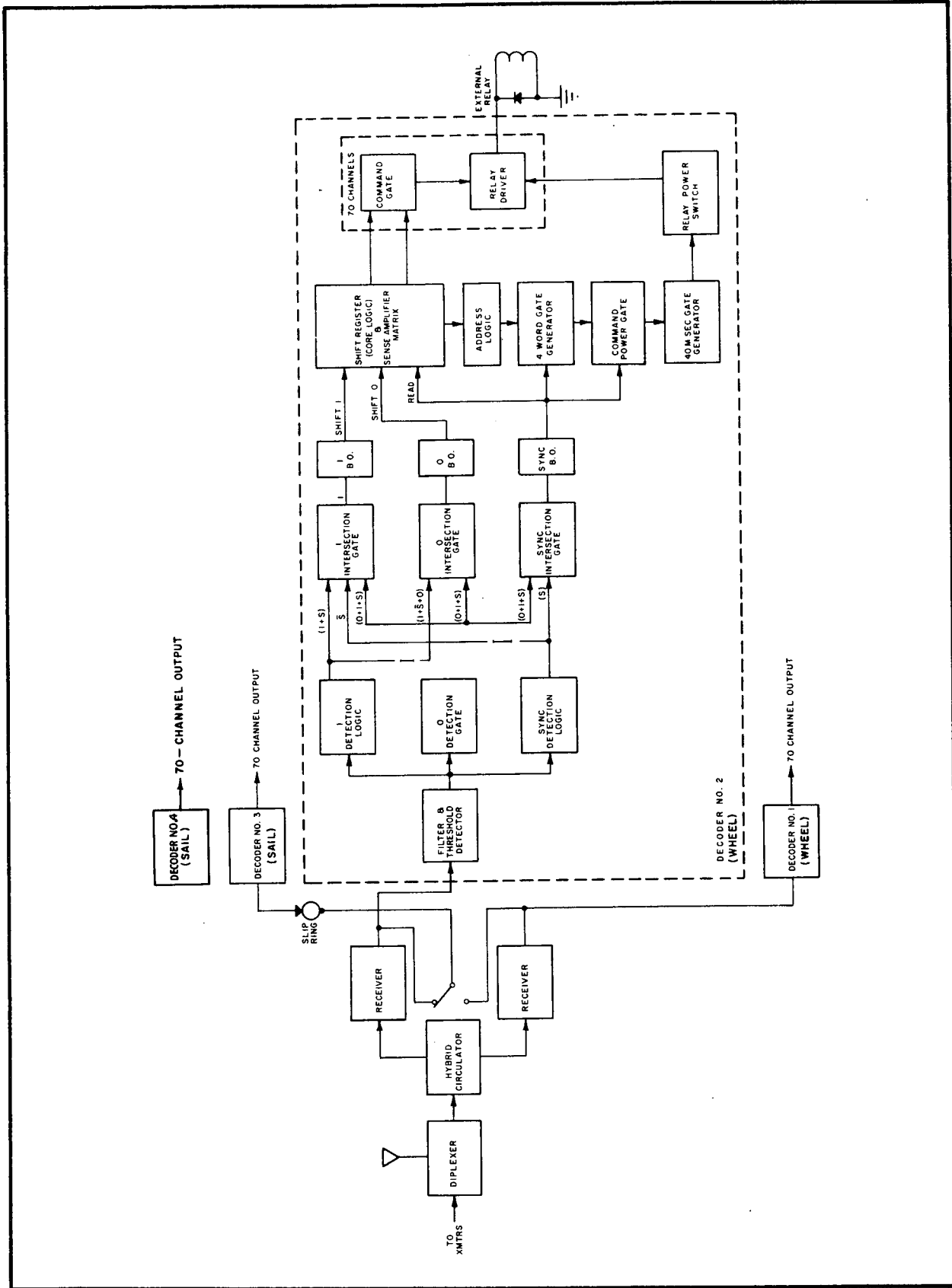


Fig. 10-1 Command System Block Diagram



In emergency situations, the manual mode can be used. This format consists of: address, address, execute, execute, execute.

As the name tone-digital implies, digital information is contained in the pulse duration of the 7 kHz tone (Fig. 10-2). This tone is pulse-duration modulated (PDM) such that three distinct tone bursts occur: 54, 36, and 18 cycles.

A bit period is defined as a time duration equal to 72 cycles of the carrier tone. A sync pulse is defined as a tone burst of 54 cycles in length. Tone bursts of 36 and 18 cycles in length define a "one" and "zero", respectively. A word consists of 10-bit periods in the following order: eight information bits of "ones" and "zeros" followed by a blank bit and a sync pulse. Address words and command words have the same format. They differ only in the combinations of "ones" and "zeros". The arrangement of information bits in an address word is either six "ones" and two "zeros", or six "zeros" and two "ones". The arrangement of information bits in a command word is four "ones" and four "zeros". The period of each 10-bit command or address word is about 0.103 seconds.

Therefore, the output of the minitrack command encoder is a serial train of tone bursts that amplitude-modulate the command transmitter. The OSO command receivers detect this serial train of tone bursts and deliver it to the command decoders. The decoder that is addressed is gated "on", decodes the command word, and outputs a pulse on one of its 70 output lines. The commands used on OSO-6 are listed in Table 10-1.

In Table 10-1, note that there are six different series used in numbering the OSO-6 commands:

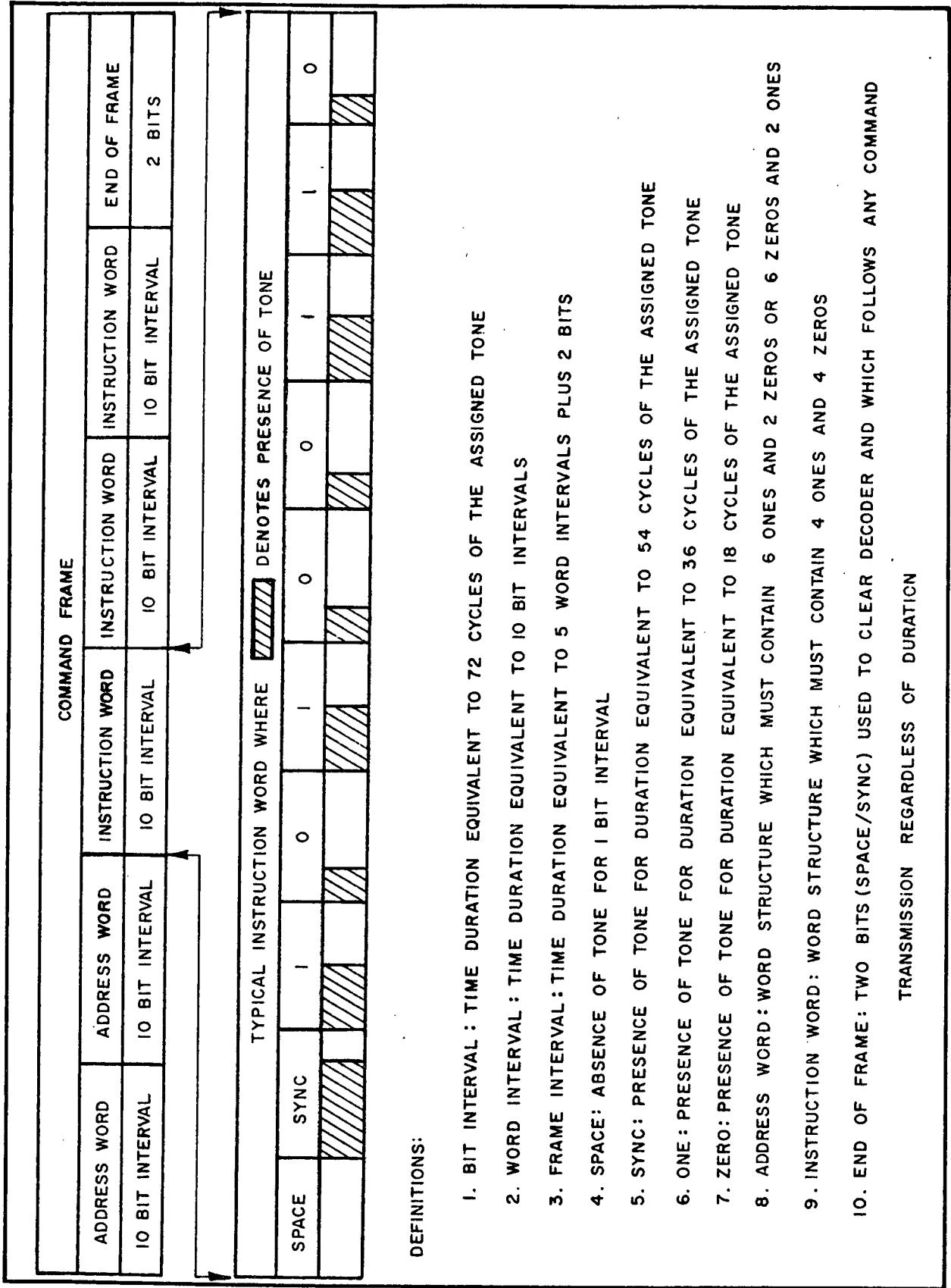


Fig. 10-2 OSO Command Format



Table 10-1
OSO-6 COMMAND ALLOCATIONS

Table with 3 columns: CMMD NO., COMMAND FUNCTIONS, CODE FORMAT. Contains 70 rows of wheel command allocations.

Table with 3 columns: CMMD NO., COMMAND FUNCTIONS, CODE FORMAT. Contains 50 rows of sail command allocations for decoder no. 3.

Table with 3 columns: CMMD NO., COMMAND FUNCTIONS, CODE FORMAT. Contains 50 rows of sail command allocations for decoder no. 4.

- LEGEND:
AGC = AUTOMATIC GAIN CONTROL
APL = AUTOMATIC PITCH LIMITER
ASL = AUTOMATIC SPIN LIMITER
ASBC = ANALOG SUB-SUBCOMMUTATOR
AUTO = AUTOMATIC
AZ = AZIMUTH
BOLOGNA = UNIVERSITY OF BOLOGNA
BYP = BYPASS (EO)
CALIB = CALIBRATE
CKT = CIRCUIT
CMMD = COMMAND
C/W = CONDITIONAL WITH
DCDR = DECODER
DET = DETONATE
DISAB = DISABLE
DL = DUMMY LOAD
DME = DIGITAL MULTIPLEXER ENCODER
D-N = DAY-NIGHT
EL = ELEVATION
ENAB = ENABLE
EXCT = EXECUTE
GEN = GENERATOR
HCO = HARVARD COLLEGE OBSERVATORY
HV = HIGH VOLTAGE
ID = IDENTIFICATION
INT = INTERNAL
LA = LYMAN ALPHA
LASL = LOS ALAMOS SCIENTIFIC LABORATORY

- LNCH = LAUNCH
LG = LARGE
LSB = LEAST SIGNIFICANT BIT
LSBU = LAUNCH SEQUENCE BACKUP
LST = LAUNCH SEQUENCE TIMER
LV = LOW VOLTAGE
LWR = LOWER
MSB = MOST SIGNIFICANT BIT
MTR = MOTOR
NEG = NEGATIVE
NRL = NAVAL RESEARCH LABORATORY
NUT = NUTATION
OPST = OFFSET
OP = OVERLOAD PROTECTION
ORB = ORBIT
PBK = PLAYBACK
POS = POSITIVE
PM = PHOTOMULTIPLIER
PROP = PROPORTIONAL
PWM = PULSE WIDTH MODULATION
PWR = POWER

- R(RUTGERS) = RUTGERS STATE UNIVERSITY
RCVR = RECEIVER
REDT = REDUNDANT
REL = RELEASE
RF = RADIO FREQUENCY
RST = RESET
RSTR = RASTER
RT = RIGHT
SASC = SAIL ANALOG SUBCOMMUTATOR
SORE = SPIN ORIENTATION & RATE ELECTRONICS
SQ = SQUID
S/SW = SEPARATION SWITCH
TEMP = TEMPERATURE
TMG = TIME MARKER GENERATOR
TR = TAPE RECORDER
UCL = UNIVERSITY COLLEGE LONDON
UNM = UNIVERSITY OF NEW MEXICO
UVS = UNDERVOLTAGE SWITCH
V = VOLT
WASC = WHEEL ANALOG SUBCOMMUTATOR
WG = WORD GATE
XMTR = TRANSMITTER



- (1) The 10 series (1 through 70) commands can be executed via either of the two wheel command decoders.
- (2) The 100 series (100 through 170) through decoder No. 1 (wheel) only.
- (3) The 200 series (201 through 270) through decoder No. 2 (wheel) only.
- (4) The 300 series (301 through 370) through decoder No. 3 (sail) only.
- (5) The 400 series (401 through 470) through decoder No. 4 (sail) only.
- (6) The 500 series (501 through 570) through either decoder Nos. 3 or 4.

10.3 COMMAND RECEIVERS

The OSO command receivers use single conversion superheterodyning, and are fix-tuned to the NASA specified frequency of 149.52 MHz. The receivers are solid state, and some of their circuits are connected in series across the power supply to reduce power consumption.

The OSO command receivers are manufactured by AVCO Corporation, Cincinnati, Ohio. A block diagram of the command receiver is shown in Fig. 10-3. A list of electrical characteristics is given in Table 10-2.

The two redundant command receivers are fed from a common antenna system through a diplexer and a hybrid circulator. The diplexer

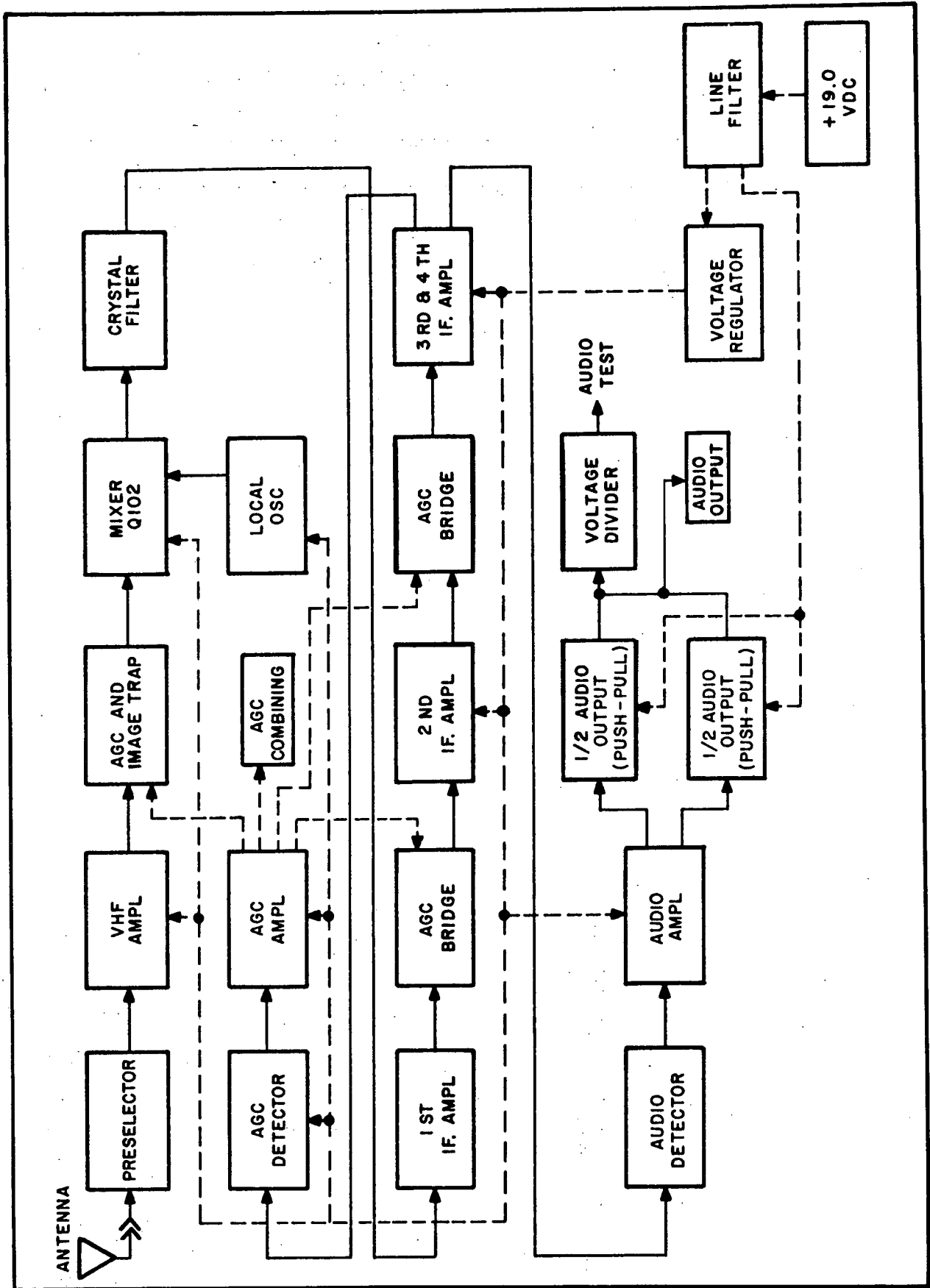


Fig. 10-3 VHF Command Receiver Block Diagram



Table 10-2
RECEIVER ELECTRICAL CHARACTERISTICS

Characteristic	Specification
Type	Superheterodyne, single conversion fixed tuned
Modulation received	Amplitude (am.)
Frequency	149.52 MHz
Minimum Sensitivity	1.5 μ v
Audio response within 1.5 db	5000 to 9000 Hz
Dynamic Range	1.5 μ v to 1 mv
Bandwidth:	
At 6 db points	35 to 40 kHz
At 60 db points	100 kHz maximum
Receiver local oscillator stability	<u>+2</u> kHz
Undesired response rejection:	
Image frequency	80 db
Other spurious signals	60 db
Power Requirements:	
Input voltage	16 to 22 vdc
Standby mode	250 mw maximum
Interrogate mode	330 mw maximum

isolates the OSO telemetry transmitters from the command receivers and permits a common antenna system to be used for both transmitting and receiving. The hybrid circulator provides 40 db isolation between the command receivers to permit independent operation in case one of the receivers fails.



Each receiver has a single conversion 10.2 MHz IF stage with a bandwidth of 36 kHz. The audio frequency response is +1 db from 1.5 to 7.5 kHz. Each receiver has an independent Automatic Gain Control (AGC) circuit that uses varicap diodes in the interstage coupling circuits. This AGC loop holds the audio output power between 50 and 90 milliwatts into a 500-ohm load for input voltage levels of 2 microvolts to 2 millivolts (75 percent modulated).

VHF selectivity is obtained by using a triple-tuned preselector followed by a RF amplifier stage and a single-tuned coupling transformer. An image trap is designed into the coupling transformer. Image frequencies are attenuated 50 db by the preselector and 30 db by the image trap, resulting in an overall image rejection of 80 db.

A high degree of rejection to spurious signals is obtained by use of a crystal-controlled local oscillator and a crystal filter ahead of the IF amplifier stage.

- *Receiver Sensitivity Change*

In an effort to decrease the sensitivity of the command system to any given RF environment, the sensitivity of the receivers was reduced. The measured command threshold using these receivers was on the order of -103 dbm. This is an approximate 10 db increase in system threshold when compared to the -110 to -113 dbm measured on previous command receivers.

10.4 COMMAND DECODERS

A block diagram of the decoder is shown in Fig. 10-4. The incoming serial train of tone bursts from the command receivers are fed to the command decoders. The PWM tone bursts are then passed through a bandpass filter and on to a demodulator where



the envelope of the tone bursts is detected and shaped. The width of the pulses from the demodulator correspond to the width of the tone pulses, i.e., a "one" or a "zero." The three distinct pulses are then separated, and the "ones" are shifted into the "one's" register and "zeros" are shifted into the "zero's" register. A sync pulse is then used to clear the registers and to apply power to the output relay drivers. However, before power is applied to the relay drivers, the proper address word must have been sensed during the preceding 550 milliseconds.

As the registers are being cleared by the sync pulse, the command word is decoded by the sense amplifiers. The sense amplifiers then output a low-level pulse to the appropriate relay driver. The relay driver amplifies this pulse and supplies a 15-volt, 40-millisecond pulse to the corresponding relay coil.

An address word is treated in the same manner as a command word. However, instead of the decoder outputting a control pulse to a relay, a 550-millisecond gate pulse is generated within the decoder. During the gate period, the decoder will accept and decode the command words. Each decoder is prewired to generate the 550-millisecond gate pulse for only one unique address code.

The interfacing circuits between the decoder outputs and spacecraft subsystems are shown in Fig. 10-5.

10.5 SYSTEM PERFORMANCE REQUIREMENTS

The performance requirements of the command system are to provide reliable command control of OSO from earth-located stations. The OSO command system design is based on a maximum

Page intentionally left blank



range of 1750 kilometers and within the constraints of the existing ground equipment. The ground station equipment consists of a 200 watt AM transmitter, a right-circularly polarized transmitting antenna having a gain of +12.5 db, and a command encoder. An RF transmission line loss of three db is assumed for the ground equipment.

The OSO command transmission gain margin calculation is presented in Table 10-3. The characteristics of the OSO command link, which determine the performance of the command system, are given in the table.

Table 10-3
COMMAND LINK GAIN MARGINS

Transmitting power (200 watts) (dbm)	+53
Transmitting antenna gain (db)	+12.5
Cable loss (ground) (db)	-3
Path loss (1750 kilometers) (db)	-138.3
Receiving antenna gain (db)	-18
Miscellaneous losses (OSO) (db)	-4
Command receiver sensitivity (dbm)	-103
Margin of gain (db)	+5.2
Margin of Gain = Gains - Losses	
= (53 + 12.5 + 103) - (3 + 138.3 + 18 + 4)	
= 166.5 - 163.3 = +5.2 db	

The system gain margin is somewhat misleading since the worst case receiving antenna gain was used. As shown in the receiving antenna pattern of Section 9, it can be seen that the antenna gain of -18 db or less occurs only for brief periods of time as the OSO spins. Normal operating procedure at the ground station is to



transmit each command at least twice. This procedure assures that commanding of the OSO will be executed reliably.



Section 11

STRUCTURES, THERMAL CONTROL, PNEUMATICS, AND HYDRAULICS

11.1 SPACECRAFT STRUCTURES

The structural design of the OSO-6 observatory is basically the same as that of earlier OSO's. For completeness, however, a brief description of the structures is repeated here.

The OSO spacecraft consists of two main structural sections: the wheel section and the sail section. The main structural features of these sections are shown in Fig. 1-14. In flight, the wheel section rotates about the spin axis; ideally, the azimuth shaft. During the daylight portion of the orbit, the azimuth servo stops sail rotation, pointing the solar-cell array and the pointed instruments at the sun (in azimuth). The elevation servo aligns the instruments with the sun line in elevation.

11.1.1 The Wheel Structure

The wheel structure provides the interface (attach fitting) for mounting the spacecraft to the two-stage Delta launch vehicle. The attach fitting is located at the base of the central hub assembly. The wheel, so named because of its similarity to a wheel, is a nine-sided polygon varying in depth from about 10 inches at its rim to about 12 inches at the hub. Three places, 120 degrees apart, are provided at the rim for attachment of a lifting assembly used in ground handling.

The spokes of the wheel are radial ribs which separate the wheel into nine compartments. Structural pie-shaped panels, or decks, form the link between the ribs and provide the primary equipment support in the compartments. The compartments house



equipment and scientific payload instruments, and are closed by the rim panels, and top and bottom non-structural aluminum honeycomb thermal shields. Three arms are attached to the rim of the wheel. These are folded along the spin axis for launch and extended radially during the launch sequence. They are arranged symmetrically about the wheel. Each arm supports a spherical pressure vessel containing nitrogen gas for spin-rate control.

The inside of the hub provides the bearing supports for the azimuth shaft and the sail structure. It also provides space for a spherical pressure vessel containing the pitch-control gas supply. The compartment side walls and decks have a hydroformed rib pattern to control flexing.

All primary structural elements except the pressure vessels are aluminum alloy. Sheet-metal elements are 6061-T6 and 2024-T4 aluminum. All castings are A356-T6 aluminum alloy. The azimuth shaft is 7075-T6 aluminum alloy.

11.1.2 The Sail Structure

The sail is a fan-shaped structure that supports the solar-cell array, the pointed instruments, and other equipment. The sail is mounted to an azimuth shaft which provides the mounting interface between the sail and wheel structures. The sail structure is not directly attached to the booster or to any pre-flight lifting equipment.

The pitch-gas vessel is mounted to the azimuth shaft, and rotates with the sail. Two azimuth ball bearings (type CEVM 440C stainless steel) provide the supports between sail and wheel. A torque motor near the thrust bearing provides control of the relative rotations between the sail and wheel. Thus the sail may be fixed to the solar direction while the wheel rotates.



Two castings support the pointed instruments in the sail structure. The instruments mount to the elevation casting, which is trunnion-mounted to the azimuth casting. The azimuth casting is mounted to the azimuth shaft. The trunnion axis is called the spacecraft elevation axis. A torque motor mounted to the azimuth casting provides controlled motion of the elevation casting about the elevation axis of +5 degrees.

The remainder of the sail structure is an open framework which mounts to the azimuth casting. Electrical connection between the sail and wheel is provided by slip rings at the base of the azimuth shaft assembly (see Fig. 1-16).

11.1.3 Structural Analysis

Prior to the launch of the OSO-6, a detailed analysis of the spacecraft structures was performed. The purpose of this analysis was to verify that the structure could withstand the loads imposed by ground handling and flight.

Method: The method used for determining internal structural loads for the sail and wheel structures is called the "Stiffness Method" of structural analysis. With this method, the structure is idealized into realistic structural elements; such as beams, bars, and panels. A sufficient number of degree-of-freedom vectors are then established on the total structure so that a realistic stiffness, or spring matrix, may be determined. External loadings are then applied along these degree-of-freedom vectors.

The flight loadings used in the analysis resulted from a study of a two-mass and a three-mass model of the OSO observatory, separately coupled analytically to a flexible Delta N two-stage booster. For X-axis loading, the observatory was idealized into three masses, namely the sail mass, the pointed instrument



assembly mass, and the wheel mass. For X-axis loads, the pointed instruments are free to pitch relative to the basic sail, thus accounting for treating the pointed instrument assembly as a separate mass. For Y-axis loading, the sail and pointed instruments are essentially rigidly attached and, therefore, were lumped into one mass.

First, the primary structure of the OSO-6 was idealized into many beam, bar, and plate elements to represent a realistic model of the observatory. The mass of the observatory was then distributed at discrete points on the idealized model so that the actual mass and center-of-gravity for the total observatory were unchanged. Load factors resulting from flight conditions and ground handling conditions were then applied to the idealized masses of the observatory so that the product of mass times acceleration resulted in applied loadings on the structure.

Finally, the internal loads for the most critical primary structure elements for both the flight loading conditions and the ground handling conditions were compared to internal loads for the same critical primary structure in the OSO-5 observatory. From this comparison, it was found that the loads on the most critical structure in the OSO-6 observatory were equivalent to or less than the loads for the same elements of primary structure that were most critical on the OSO-5 observatory. Since the internal loads on the critical structural elements of OSO-6 were found equivalent to or less than those of OSO-5, the structural analysis of OSO-6 was then made by a simple comparison of the loads that acted upon the primary structure of the two observatories.

Design Loading Conditions: The design loading conditions for the OSO-6 observatory consisted of five flight conditions and three



ground handling conditions. The five flight conditions were selected from analytically derived load factors and modal forces. From the coupled configuration, load factors were determined at the observatory mass points for the first four natural vibration modes. Steady-state load factors of the observatory-booster combination were also supplied for the following phases of flight.

- Liftoff
- Transonic
- POGO
- MECO

Selection of the analysis design conditions from the predicted flight conditions resulted in choosing design conditions that satisfied the following constraints:

- (1) Flight conditions exhibiting maximum sail load factors at sail center-of-gravity.
- (2) Flight conditions that produced maximum moments on the azimuth shaft.
- (3) Flight conditions that resulted in maximum combination of thrust and lateral load at wheel center-of-gravity.
- (4) Flight conditions that produced maximum loading on the observatory during acceptance vibration testing.
- (5) Flight conditions that caused maximum loads at booster/observatory interface.



Items 1 and 3 involved no more than a search for maximums in a table of flight loads.

Items 2 and 4 involved a calculation of the moments induced into the azimuth shaft due to the sail load factors and a calculation of the moments at the booster/observatory interface.

For Item 5, the equivalent axial loads at the booster interface were calculated for all flight conditions and the maximums were then chosen as analysis design conditions.

Ground handling of the observatory in this analysis was considered as the phase in which the observatory is suspended at three points for shipping purposes. The observatory is expected to withstand load factors of 3.0g in any direction in combination with 1.0g in a mutually perpendicular direction during this phase.

Stress Analysis: A complete detail stress analysis of the OSO-6 observatory primary structure was not performed. Instead, a comparison of the loads for each critical structural element within the OSO-6 observatory was made to the loads in the identical structural element within the OSO-5 observatory. It was found that the internal critical structural loads for the OSO-6 observatory are less than or equivalent to the same internal critical load within the OSO-5 observatory. Therefore, it was concluded that the stresses produced within the OSO-6 critical structural elements were equivalent to or less than those within the OSO-5 observatory.

Summary of Structural Analysis: The detailed structural analysis of the OSO-6 observatory was performed using the OSO-5 structural idealization with OSO-6 mass properties and applying predicted external loads; however, a detailed stress analysis of the OSO-6 structure was not performed because the internal loads upon the



primary structural elements were found to be less than or equivalent to the loads for the same structural elements in the OSO-5 observatory. This being the case the results of the analysis indicated that the OSO-6 observatory was capable of withstanding all flight and ground handling loads imposed upon it.

It was found, in all cases, that the maximum loads acting upon the critical primary structural elements within the OSO-6 observatory were less than the maximum loads acting upon the same primary structural elements within the OSO-5 observatory. Thus, it was confirmed that the OSO-6 observatory possessed sufficient structural integrity to withstand the flight and ground handling environment imposed upon it.

11.1.4 Acceptance Vibration Test Notch Calculations

The acceptance vibration test levels of the OSO-6 observatory were limited in the lateral X-axis and the lateral Y-axis so that the stresses in the most critical primary structural elements during these tests would not exceed the stress levels these structural elements would experience during the actual launch phase.

11.2 THERMAL CONTROL

11.2.1 Why Thermal Control is Needed

For OSO to perform properly, its temperature must be kept within specified limits in those sections of the spacecraft housing temperature-sensitive equipment. Two examples of such equipment are: (1) the solar cells, whose output decreases with rising temperature, and (2) the main storage batteries, which perform most efficiently between -10 and 35°C. Generally, most OSO equipment is designed for the -10 to 35°C temperature range.



Without such temperature restrictions, OSO could be designed as a perfect heat absorber and emitter ("blackbody"). It would then reach an equilibrium temperature (probably very hot) where the amount of solar energy absorbed would equal the amount of infrared energy emitted. Because of the restrictions, however, OSO must have thermal properties somewhere between a perfect "blackbody" and a perfect reflector (which would gain no heat at all). This is done by selecting the proper absorptivities and emittances of the component surfaces where:

absorption (α) = the ratio of the energy absorbed by an object to that absorbed by a "blackbody".

emittance (ϵ) = the ratio of the energy emitted by an object to that emitted by a "blackbody".

11.2.2 Surface Finishes

Special paints and surface finishes and carefully designed heat-conduction paths within the structure are used to provide OSO's passive thermal control.

The surface finishes are selected on the basis of their thermal characteristics. Those having a low α/ϵ ratio are used where it is desired to reduce temperature, and those with a high α/ϵ ratio used to increase temperature. The distribution of the most-used finishes is shown in Fig. 11-1, along with the α/ϵ ratio of each.

Except for the analog sub-subcommutator, the surfaces of OSO-6's sail components are essentially the same as OSO-5's. The surface finishes on the wheel are identical to the OSO-3 finishes.

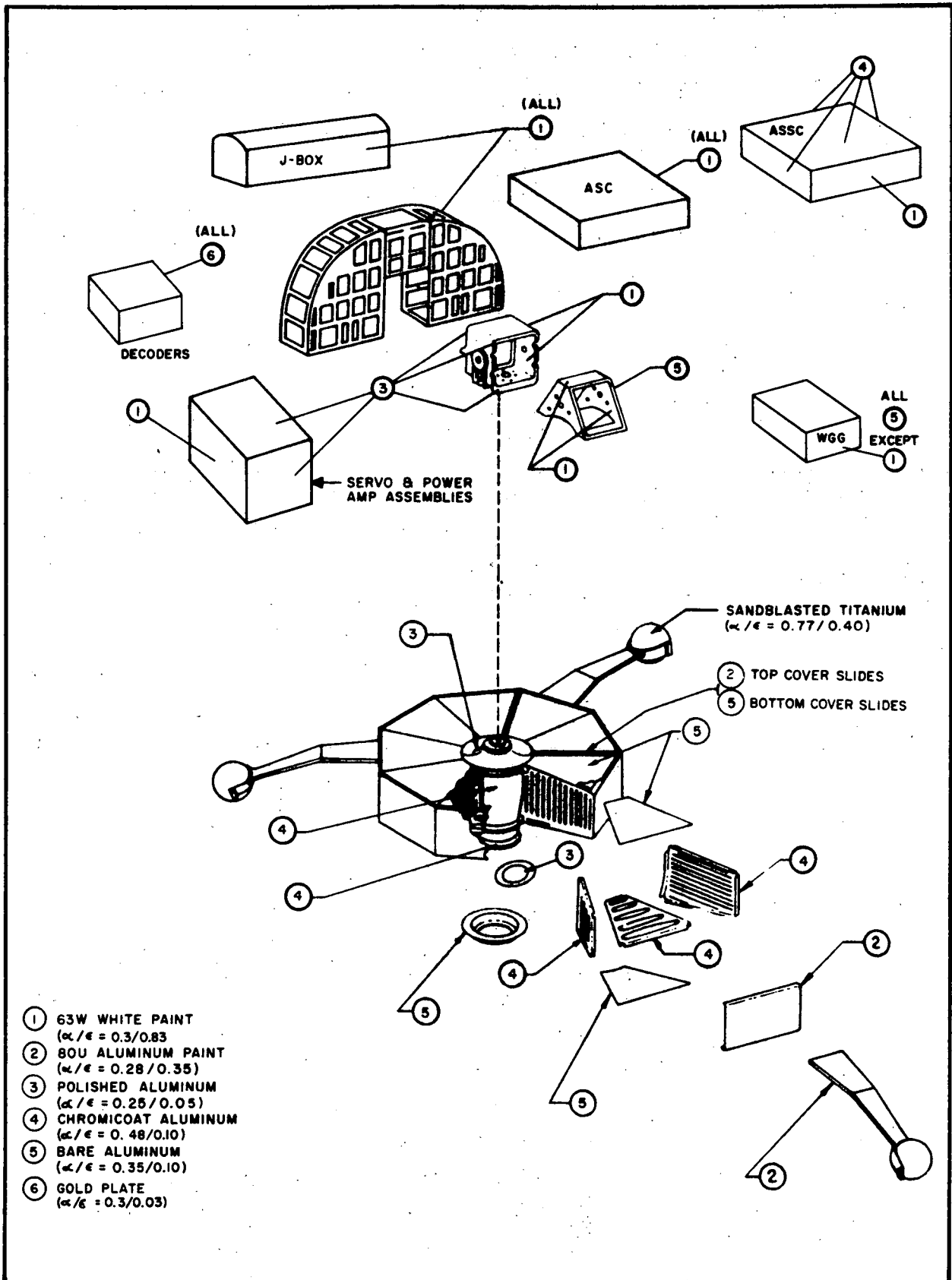


Fig. 11-1 OSO-6 Surface Finishes



Two specially-formulated paints were used for passive thermal control: 63W satellite white and 80U satellite aluminum. The 63W paint is pigmented with titanium dioxide and is used to decrease temperature, since it is an excellent infrared emitter and a poor solar absorber. It is used in the sail, where there is a tendency for components to overheat. The 80U paint is pigmented with a "leafing" aluminum flake and is used in the wheel section to increase the equilibrium temperature. In addition, gold plating, polished aluminum, and bare aluminum are used to provide other α/ϵ ratios where required.

11.2.3 Thermal Analysis

In support of the OSO program, a mathematical system was developed for thermal analysis of the OSO spacecraft. This system was developed for the OSO-3 and is used for predicting the operating temperatures of various components and surfaces and make changes when necessary.

Analysis Method: Because a closed form solution for a complex structure treated as a continuous system is impractical--if not impossible--a mathematical model of OSO, composed of thermally-coupled discrete elements, was constructed and used for the thermal analysis. The elements (or nodes) were assumed to have uniform temperature discontinuously different from adjacent elements.

The original mathematical model 138 nodes, each of which represented a component, part of a component, or group of components. The nodes are designated on the basis of the apparent validity of an assumption of uniform temperature. The heat balance for each node involves the heat capacity of the node, the thermal-radiation interchange between the node and all others, the conduction between the node and all others, the external heat fluxes impinging upon that node, the electrical dissipation within the node, and the heat loss by radiation.



OSO-6 Thermal Analysis: The OSO-6 spacecraft differs from earlier OSO's due to the installation of a word-gate generator and a second decoder on the sail egg-crate structure. We were therefore requested to perform a thermal analysis of the OSO-6 sail to predict the operating temperatures of these components. This analysis is documented in BBRC Document F68-11, OSO-G Sail Thermal Analysis Final Report, dated 27 December 1968.

Although a thermal analysis previously had been performed on the OSO spacecraft, including the egg-crate structure, we decided that satisfactory results would not be produced by attempting to add the two electronic boxes to the OSO mathematical thermal model. The main reasons for this decision were:

- (1) The additional components required that the geometrical model of the egg-crate portion of the OSO sail be taken through the entire computing procedure to obtain radiation exchange factors.
- (2) The egg-crate structure of the OSO-5 sail was crudely modeled because computing programs were not available to solve the heat balance equation for the complex structure. Since then the thermal analysis computer programs have been improved in accuracy and in capacity to handle larger numbers of components simultaneously.
- (3) The junction between the OSO sail substrate and the egg-crate structure was found to be discontinuous. Thus, only a small part of the possible thermal conduction between the substrate and the egg-crate actually took place. Therefore, to predict realistic temperatures, the substrate-to-egg-crate conductances had to be modified to more closely represent the actual conditions.



From the above considerations, we decided that the most practical procedure would be to construct a new mathematical thermal model of the OSO sail egg-crate structure and the components mounted on the aft portion of the sail. This new model would then be used with the other previously modeled sections of the spacecraft to produce a new set of predicted temperatures.

The mathematical thermal model used in OSO-6 analysis is the same as that used for the thermal analysis of earlier OSO's, with the following exceptions:

- (1) The thermal model of the egg-crate structure of the sail is more detailed and thus more closely represents the actual structure.
- (2) Consideration of the word-gate generator and a decoder which are mounted on the egg-crate structure.
- (3) White paint and chromacoat surface finish emissivities and absorptivities were assigned new values in accordance with recent data obtained from tests.
- (4) The junction between the sail substrate and the egg-crate structure was assumed to be in tight physical contact only in the regions of the attachment screws. This area of contact was estimated to be 10 percent of the possible contact area.
- (5) The aft sections of both pointing instruments were assigned gold plated surface finishes in place of one gold and one bare beryllium instrument as used in previous analyses. This was done only to improve



the reflecting view factors and the reflecting external fluxes on the aft section of the sail.

- (6) The surface finish of the sub-subcommutator was changed from totally white to white on the side next to the sail substrate and light chromacoat on the other five sides. This was done to raise the components' operating temperature.
- (7) The nutation damper base was remodeled by replacing the six-sided box representation with a three-legged pedestal shape. This was done to improve the radiation interchange calculations.
- (8) The total number of nodes used in the OSO-6 mathematical thermal model is 206 as compared with 138 nodes used in previous models.

Summary and Conclusions: A mathematical thermal model consisting of 206 nodes now exists for the OSO spacecraft. The complete system of nodes has not been investigated using the surface finishes of a single spacecraft. The present analysis is for OSO-3 surface finishes on the wheel and pointing instruments and OSO-6 surface finishes on the sail.

Transient temperatures were computed for the word-gate generator and decoder, which are new additions to the OSO sail. Improved computing techniques and thermal modeling of the sail structure and components have resulted in predicted temperatures that compare more closely with the measured temperature data from OSO-2 and OSO-3 than did the previous thermal analysis. This is largely because the egg-crate structure has been more closely modeled and because the computation methods have been greatly improved. The improved modeling includes the use of



many more nodes to represent the complex egg-crate structure and the application of the more accurate values of paint emissivity and absorptivity recently measured by the materials and processes laboratory.

11.2.4 Temperature Monitors

The temperature of the spacecraft is monitored in several places by sensors cemented to components, experiments, and the structure. The sensors use the thermal properties of a transistor to develop a 0 to 5 volt signal input to the analog subcommutator. The voltage is representative of the local temperature.

The sensors in the sail are powered by a single 15-volt regulator located in the servo amplifier assembly. Those in the wheel are powered by a single 15-volt regulated supply located in the spin-control assembly.

11.3 HYDRAULIC SYSTEMS

The OSO uses only one hydraulic system: the arm damper system. The arm damper subsystem controls the rate at which the arms deploy during the launch phase. The system consists of three hydraulic cylinders with piston rods connected to each arm (Fig. 11-2). Denatured alcohol is used as the hydraulic fluid and piston travel rate is controlled by forcing this fluid through three 0.020 inch orifices, one in each cylinder.

The three hydraulic cylinders are interconnected by plumbing to ensure that the arms deploy in unison.

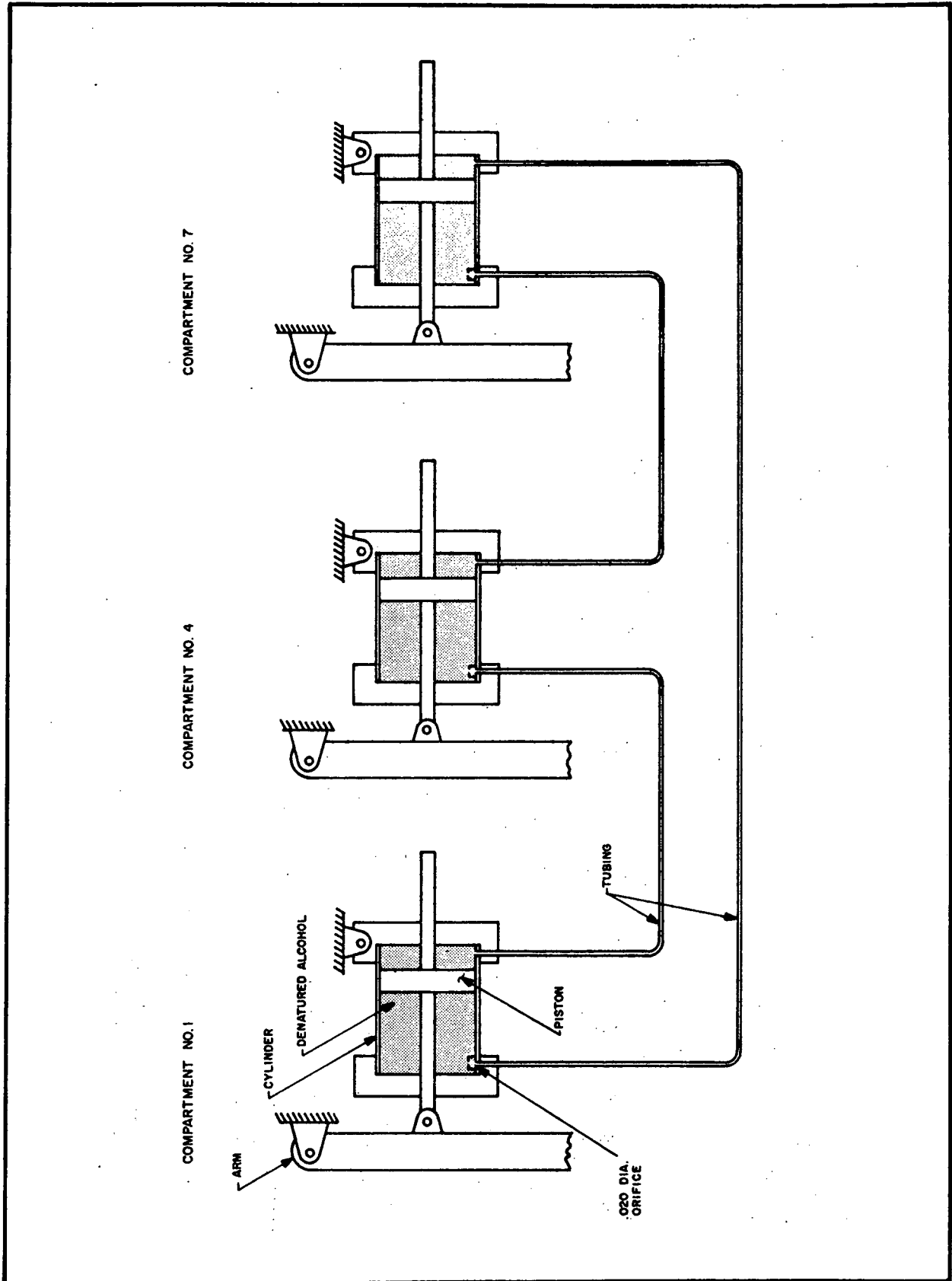


Fig. 11-2 Arm Damper System



11.4 PNEUMATIC SYSTEMS

OSO uses two pneumatic systems: one for pitch control and one for spin-rate control (see Figs. 1-19 and 11-3). Each system produces the required torques by exhausting nitrogen gas through small nozzles (thrusters).

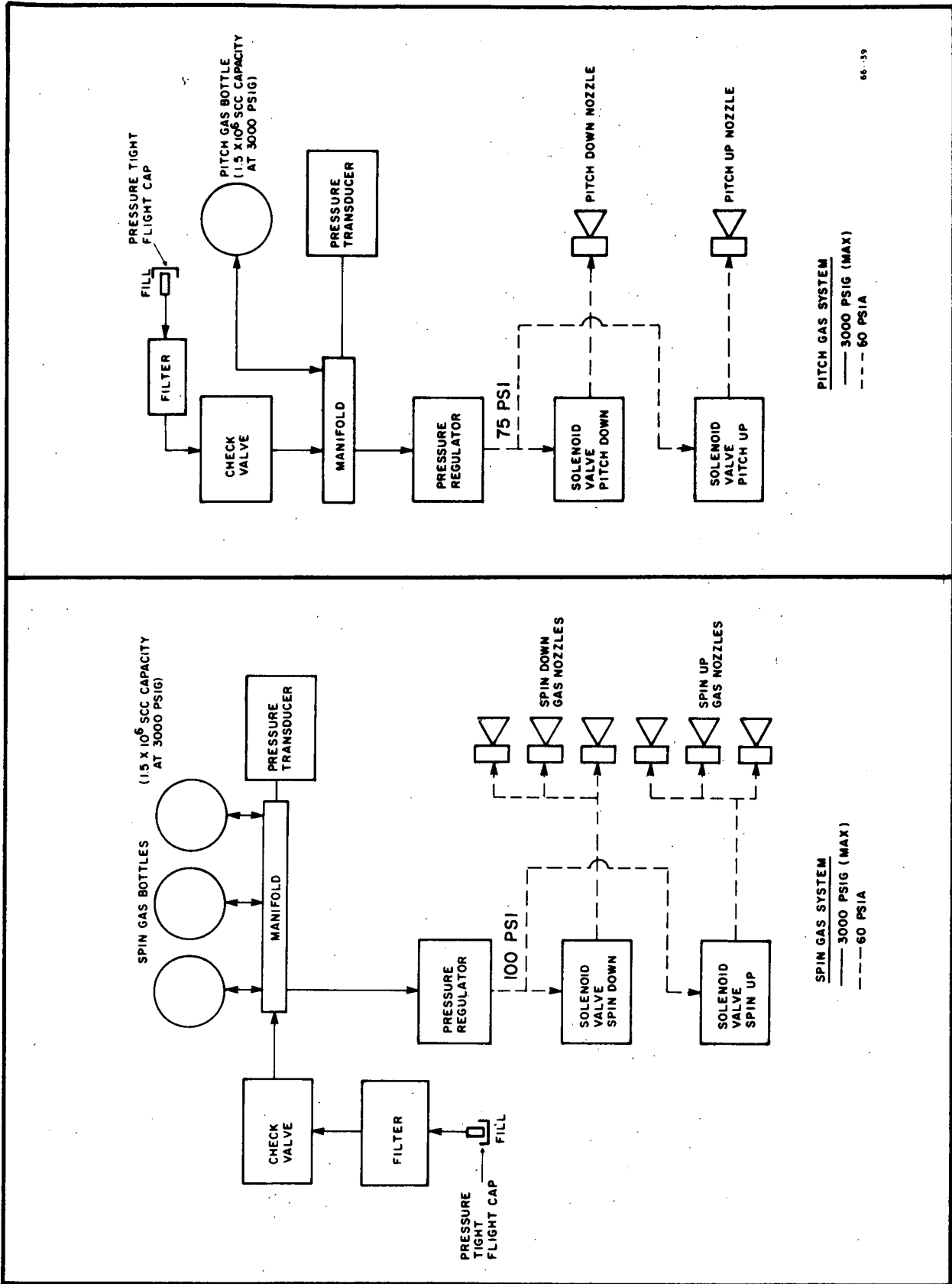
11.4.1 Spin Pneumatics

The spin pneumatic system provides the mechanism through which the spin-control circuits, (described in Section 7) apply accelerating or retarding torques to the spacecraft wheel.

The gas is stored in three titanium bottles at the ends of the spacecraft arms. The initial storage pressure is about 3000 psi. The gas flows from the storage bottles to a manifold block, joining the three bottles into a single gas supply and equalizing the pressures in the bottles. At this point, a pressure transducer senses the pressure and produces a voltage proportional to the pressure. The transducer output is sampled once per wheel ASC subframe and is telemetered to receiving ground stations.

From the manifold block, the gas flows through a filter to a pressure regulator, which reduces from the storage pressure to about 100 psi (static). Fluid friction reduces this pressure to provide a gas-flowing pressure of about 60 psig at the spin nozzles. From the regulator, the gas flows to the spinup and the spindown solenoid valves, which are actuated by the spin control circuits. The spinup valve feeds three nozzles, and the spindown valve feeds three nozzles at the ends of the three arms.

Each nozzle produces a thrust of about 0.10 lb for a total of 0.3 lb for either the three spinup or the three spindown nozzles. This thrust acts through a lever arm of 3.97 ft to produce about 1.19 ft-lb of torque. This torque changes the



66-39

Fig. 11-3 Gas System Block Diagram



wheel spin rate at the rate of about 0.0076 rps every second. The nozzle thrust efficiency in vacuum is about 94 percent. Effective specific impulse is about 66 lb/lb/sec., and the gas consumption rate is about 2,150 std cc/sec. At 3,000 psi storage pressure, the gas stored is equivalent to about 1.5×10^6 standard cc which provides a spin correction capability of about 5.5 rps.

11.4.2 Pitch Pneumatics

The pitch pneumatic system, operated by the pitch control circuits (described in Section 7) provides pitch attitude control of the entire observatory by applying correction torques of either sense about the roll axis. The thrusters that apply these torques are located on either side of the sail and are activated only when the sail is stationary (pointed). The observatory precesses about the pitch axis, thereby providing pitch control, because the torques act upon the stationary sail and because of the gyroscopic properties of the spinning wheel (these properties are discussed in Section 6).

Nitrogen gas, at an initial storage pressure of about 3,000 psi, is stored in a single titanium bottle housed within the hub assembly. A pressure transducer provides information to receiving ground stations, through the spacecraft telemetry system, about the pitch-gas storage pressure. A pressure regulator provides about 75 psig in its static condition, and about 60 psig with gas flowing.

The gas is controlled by the pitch-up and pitch-down solenoid valves. These are actuated by the pitch-control circuits and supply gas to the appropriate nozzles. The pitch-up nozzle is on the left side of the sail (as viewed from the rear) and is aimed upward. The pitch-down nozzle is on the right side, likewise aimed upward.



Each nozzle produces about 0.1 lb. of thrust which acts on a lever arm of 1.93 ft. to produce a torque of 0.193 ft-lb. This torque produces a correction rate of 0.0645 deg.-rps/sec. in pitch angle. The nozzle thrust efficiency in vacuum is about 94 percent. Effective specific impulse is about 66 lb/lb/sec., and the gas consumption rate is about 716 std cc/sec. At 3,000 psi, the gas stored is equivalent to about 1.5×10^6 standard cc which provides about 169° rps of pitch correction.



Appendix A
ABBREVIATIONS USED IN THIS REPORT

(This list excludes many abbreviations which may be found in any standard dictionary or which are extremely common in technical usage. Also excluded are some of those which are defined in the text whenever they are used.)



Table A-1
ABBREVIATIONS USED IN THIS REPORT

A	ampere	cont	continuous
Å	angstrom	CPIF	cost plus incentive fee
AC/ac	alternating current	cps	cycles per second (Hertz)
A/D	analog-to-digital	c/w	conditional with
AGC	automatic gain control	D	DSF or DSM (short form)
alloc	allocated	db	decibels
amp	ampere, amplifier	dbm	decibels (ref 1 mw)
ANG	Air National Guard	DC/dc	direct current
APL	automatic-pitch limiter	dcd	decoder
ASC	analog subcommutator	deg	degrees
ASL	automatic-spin limiter	disab	disab, disabled, disabling
ASSC	analog sub-sub- commutator	DL	dummy load
ass'y	assembly	DME	digital multiplex- encoder
auto	automatic	D-N, D/N	day-night
az/azim	azimuth	doc	document
batt	battery	DS	design specification (BBRC doc)
BBRC	Ball Brothers Research Corporation	DSF	digital subframe
Bev	billion electron volts	DSM	digital submultiplexer
bps	bits per second	dwg	drawing
BU	backup	EDT	Eastern Daylight Savings Time
byp	bypass	el/elev	elevation
C	Celsius (Centigrade) temperature scale	EMI	electro-magnetic interference
calib	calibration	enab	enable, enabled, enabling
cc	cubic centimeter	EST	Eastern Standard Time
CG	center of gravity	ETR	Eastern Test Range
ckt	circuit	ev	electron volt
cm	centimeter	exct	execute
cmd/cmmd	command	expmt	experiment
comp	comprehensive test		
compt	compartment		



Table A-1 (continuation)

ext	external	k	prefix kilo (one thousand)
FC	frame count/counter	k	kilocycles per second
FET	field-effect transistor	KE	kinetic energy
FF	flip flop	KSC	Kennedy Space Center
fig.	figure	LA	Lyman-alpha
FM	frequency modulation	LASL	Los Alamos Scientific Laboratory
freq	frequency	lch	launch
ft	foot	LSB	least-significant bit
g	acceleration due to gravity	LSBU	launch-sequence backup
gen	generator	LST	launch-sequence timer
GFE	government-furnished equipment	LV	low voltage
gnd	ground	M	prefix mega (one million)
GSFC	Goddard Space Flight Center	m	meter, prefix milli (one one-thousandth)
HCO	Harvard College Observatory	ma	milliamperes
hr	hour	mag	magnetometer
HV	high voltage	man	manual
hz	hertz (cps)	max	maximum
I	electrical current in amperes	MDAC	McDonnell-Douglas Astronautics Company
I and T	Integration and Test	MDC	Mission Director's Center
ID	sync identification	meas	measured
IF	intermediate frequency	MF	main frame
in.	inch	min	minutes, minimum
int	internal	mod	modulation
IR	infra-red	MOI	moment of inertia
J-box	junction box	mon	monitor
		MS	model specification (BBRC doc)
		MSB	most-significant bit



Table A-1 (continuation)

MSFC	Marshall Space Flight Center	psi/psia	pounds per square inch (absolute pressure)
		psig	pounds per square inch (gage pressure)
NASA	National Aeronautics and Space Administration	ptd	pointed
		PWM	pulse-width modulator
neg	negative	pwr	power
NM/N.Mex	New Mexico		
nm/nmi	nautical mile	QP	qualification plan (BBRC doc)
No.	number		
NRL	Naval Research Laboratory	rcvr	receiver
nut.	nutations/nutation damper	red't	redundant
N2	nitrogen gas	ref	reference
		rel	release
OATS	Observatory Automatic Test System	RF	radio frequency
		RFI	RF interference
ofst	offset	rms	root mean square
OP	overload protection	RO	readout
orb	orbit	rpm	revolutions per minute
OSO	Orbiting Solar Observatory	rps	revolutions per second
		rst	reset
ov	overvoltage	rstr	raster
PAC	packaged attitude control	S/SASC	Sail Analog Subcom
para	paragraph	SC	sail command
pbk	playback	S/C	spacecraft
PCM	pulse-code modulation	sec	seconds
PERT	Program Evaluation and Review Technique	sel	select
		sep	separation
PM	photomultiplier	seq	sequence
pos	positive, position	S/N	serial number
P-P	peak-to-peak	SOL	start of line
press.	pressure	SOR	start of raster
prop	proportional, proposal	SORE	spin orientation and rate electronics



Table A-1 (continuation)

sq	squib	V/volt	volts, voltage
SS	ASSC (short form)	vhf	very high frequency
STADAN	Satellite Tracking and Data Acquisition Network	VSWR	voltage-standing-wave ratio
std	standard	w	watts (power)
subcom	subcommutator	W/WASC	Wheel Analog Subcom
sw	switch	WC	wheel command
sync	synchronization signal	WG	word gate
sys	system	WGG	word gate generator
S3	Decoder 3 (sail)	wh	wheel
S4	Decoder 4 (sail)	W1	Decoder 1 (wheel)
		W2	Decoder 2 (wheel)
temp	temperature		
tlm	telemetry	xmtr	transmitter
TMG	time-mark generator		
TN	technical note (BBRC doc)		
TP	test point or test procedure (BBRC doc)		
TR	tape recorder or technical report (BBRC doc)		
TS	test specification (BBRC doc)		
T-V	thermal vacuum		
TWX	Teletypewriter Exchange Service		
U/Univ	University		
UCL	University College of London		
UNM	University of N. Mex		
UT	universal time		
UV	ultraviolet, under- voltage		
UVS	undervoltage switch		



Appendix B
BIBLIOGRAPHY



Table B-1
BIBLIOGRAPHY

Document	Title
	<u>SPACECRAFT TEST AND HANDLING DOCUMENTATION</u>
TN65-258-A1	OSO Mass Balance Procedures (29 Apr 69)
TN65-286	Operating Procedure for 10-Foot Diameter NASA-4 Thermal-Vacuum Chamber (9 Sep 65)
TN66-31-B1	Procedures for OSO Weight, Center of Gravity, and Moments-of-Inertia Measurements (12 Nov 68)
TN66-49-A2	OSO Demagnetization and Magnetic Balance Procedure (4 Dec 68)
TN67-104-A	OSO Handling Procedures (18 May 68)
TN68-04-A1	OSO-G Operations Plan (13 May 69)
TN68-05-A3	OSO-G Supplementary Test Procedures (10 Jul 69)
TN68-06	OSO-G Upper Structure Test Procedure (15 May 68)
TN68-14-B	OSO-G Comprehensive Test Procedure (8 Jul 69)
TN68-17	OSO-G Spacecraft Thermal-Vacuum Test Procedure (2 Dec 68)
TN68-18-B	OSO-G Test Data Summary (15 Jul 69)
TN68-20-1	OSO-G Observatory Vibration Test Procedure (19 May 69)
TN68-21-B	OSO-G Observatory Thermal-Vacuum Test Procedure (14 Jul 69)
TN68-23-1	OSO-G ETR Handling and Special Checkout Procedures (10 Jun 69)
TN68-24-3	OSO-G ETR Operations Plan (11 Jul 69)
TN68-27	OSO-G Launch Tower/Payload Countdown Procedures (10 Jun 69)
TN68-53	OSO Battery Conditioning Procedure (17 May 68)
TN68-57-A	OSO-G Spacecraft Acceptance Plan (19 Nov 68)
TN68-167-A	OSO-G Failure and Problem Summary (22 Jul 69)
TN69-63	OSO-G Observatory Acceptance Plan (9 May 69)
TR69-43	OSO Shock Test Qualification Report (12 Jun 69)
16704	OSO Pneumatic System Leak Rate Procedure (13 Sep 65)
20366-B	OSO Pneumatic Pressurization Procedure (2 May 69)
21854-C	OSO-G Observatory Painting Procedure (2 May 67)
26493-D	Model Specification -- OSO-G Spacecraft (19 Mar 69)
26494-G	Test Specification -- OSO-G Spacecraft (14 Mar 69)



Table B-1 (continuation)

Document	Title
<u>ANALYSIS DOCUMENTATION</u>	
F66-06	OSO Dynamics Analysis (15 Nov 66)
F67-12	A Mathematical Thermal Model of the OSO Spacecraft (17 Nov 67)
F68-01	Evaluation of Present OSO Antenna Patterns (15 Mar 68)
F68-11	OSO-G Sail Thermal Analysis Final Report (27 Dec 68)
TN65-304	OSO Roll Attitude Study (18 Oct 65)
TN66-01	OSO Dynamic Analysis (3 Feb 66)
TN66-37	The Effect of Various Orbital Conditions on Observatory Shadow Time (1 Mar 66)
TN66-114	OSO Magnetic Control Study -- Theoretical Investigation (28 Apr 66)
TN68-158	Torque Effect Graphs Showing Pitch, Roll, and Spin Rate Drift and How They Can Be Used for OSO Attitude Control (12 Dec 68)
TN68-161	OSO-G Reliability Analysis (21 Jan 69)
TN68-162	Reliability Analysis of OSO-G Offset Point and Scan System (19 Dec 68)
TN68-166	An Analysis of the OSO-G Roll Coil Efficiency (20 Dec 68)
TN69-79	OSO-G Structural Analysis (27 Jun 69)
TN69-81	OSO-G Flight Readiness Review (2 Jul 69)
TN69-111	OSO-G Roll Coil Error Analysis (27 Oct 69)
TR67-74-E	OSO-G Mass Properties (Report) (3 Jan 69)
TR68-55	Optimum Tape Recorder/Transmitter Interface Evaluation (16 Sep 68)
<u>COMPONENT/SYSTEM TEST DOCUMENTATION</u> (These documents are listed in addition to the specifications, procedures, and reports shown in Table 3-1)	
TN68-55-A	OSO-G Component Qualification Status List (24 Nov 69)
TN68-159-A	OSO-G Certification Log Manual (15 Oct 69)
TN69-49	Calibration Procedure for Offset Point Module Test Fixture (26 Mar 69)
TR69-01	Technical Report -- OSO-G Antenna (24 Jan 69)
TR69-03	OSO Command and RF Systems Susceptibility Report (3 Feb 69)



Table B-1 (continuation)

Document	Title
	<u>MISCELLANEOUS DOCUMENTATION</u>
F63-3	OSO-1 Final Report (30 Oct 64)
F65-9	OSO-C Final Report
F66-03	OSO-2 Final Report (15 Sep 66)
F67-14	OSO-3 Final Report (12 Dec 69)
F68-07	OSO-4 Final Report (14 Aug 70)
F70-02	OSO-5 Final Report (6 Apr 71)
TM65-01	OSO Aspect System Manual (15 Jul 65)
TN65-145-D	Manual of Safety Practice--OSO Integration and Test (18 Mar 66)
	BBRC Specifications for the Integration and Test Laminar Flow Clean Rooms (Revision A, 23 Jan 68)
TN65-175	Ephemeris Equations for Predicting Locations of OSO Earth Coordinates (Apr 66)
TN65-205	Magnetotropometer (8 Jul 66)
TN65-310	OSO Technical Documentation Procedures (1 Sep 65)
TN66-48-A	Observatory Demagnetizer (20 Dec 66)
TN66-169	Aspect Data Reduction Program for an OSO Wheel Experiment (16 Dec 66)
TN67-10	Magnetics for OSO Designers (15 Mar 67)
TN68-16-B1	OSO-G Telemetry Data Conversion Tables (16 Jul 69)
TN68-22	OSO-G Post-Launch Data Reduction Procedure
TN68-25-A	OSO-G In-Orbit Operation Procedures (16 Jul 69)
TN68-26	OSO-G Post-Launch Data Requirements (10 Jul 69)
TN68-61	Preferred Parts Handbook (12 Jul 68)
TN68-80-A	OSO-G Characteristics Data and Launch Requirements (21 Jul 69)
TN69-07	Contamination Tolerance for OSO-G and H Experiments (11 Feb 69)
TN69-47	Preferred Parts List for Space Systems (1 Apr 69)
TN69-56	Preparing OSO Test Procedures for Computerization (23 Apr 69)
TN69-66	Soldering Certification and Recertification Procedure (6 Jun 69)
TN69-91-A	OSO-G Contingency Plan (6 Aug 69)



Table B-1 (continuation)

Document	Title
TR69-08	Category and Contamination Ranking Lists for OSO Materials (1 Mar 69)
TR69-64	OSO New Technology Report (28 Oct 69)
23732B	Installation Control Drawing, OSO-G/DELTA Interface (11 Jul 69)
<u>NON-BBRC PUBLICATIONS</u>	
DAC SM-48897	Improved DELTA Spacecraft Design Restraints (Jan 66)
NASA SP57	Orbiting Solar Observatory 1 (1965)
NASA TR-985	DELTA-72 Orbiting Solar Observatory-G (OSO-G) Operations Summary (5 Aug 69)
NASA TR-987	DELTA-72 Orbiting Solar Observatory-G (OSO-G) Flash Flight Report
NASA X-513-69-274	NASA-GSFC Operations Plan 10-69 Orbiting Solar Observatory OSO-G (Jul 69)
NPC-200-2	Quality Program Provision for Space System Contractors
NPC-250-1	NASA Reliability Publication

EXPERIMENT DOCUMENTATION (Experiments BBRC documents are listed on Table 3-3)



Appendix C
OSO-6 SYSTEMS AND COMPONENTS
DESCRIPTION



Table C-1
FUNCTIONAL DESCRIPTION OF OSO-6 SPACECRAFT SYSTEMS

System	Functional Description
Pitch control system	<p>Provides pitch control of spacecraft by two means: (1) exhausting nitrogen gas through pitch up and pitch down nozzles and (2) torquing the spacecraft with a pitch coil; pneumatic system has two modes of operation:</p> <ol style="list-style-type: none"> (1) Automatic pitch control (2) Manual pitch control <p>Automatic mode maintains spin axis normal to solar vector within ± 4 deg by action of automatic pitch control electronics. Manual mode provides backup in event of automatic mode failure; manual control is accomplished by ground station commands. The pitch coil is controlled solely by ground station commands.</p>
Roll control system	<p>Provides roll attitude control of the spacecraft by means of two magnetic roll coils mounted on the sail. Control is by ground command only.</p>
Spin control system	<p>Provides spin rate control of wheel by exhausting nitrogen gas through spin and despin nozzles; has two modes of operation:</p> <ol style="list-style-type: none"> (1) Automatic spin control (2) Manual spin control <p>Automatic mode maintains spin rate between 0.45 and 0.67 rps by action of automatic spin control electronics; automatic spin control circuits are disabled and the manual mode automatically selected if spin rate goes outside the range of 0.39 to 0.70 rps. Manual mode provides backup in event of automatic mode failure; manual spin-up and spin-down control is accomplished by ground station commands.</p>
Pointing control system	<p>Provides initial solar acquisition and accurate pointing of solar oriented scientific experiments by driving sail opposite to wheel spin direction (azimuth pointing) and rotating the experiments in elevation (elevation pointing); has four modes of operation:</p> <ol style="list-style-type: none"> (1) Normal pointing (experiments point within ± 1 arc minute of solar disk center) (2) Large raster scan (experiments scan the solar disk with a centered 64 line raster pattern of 46 by 46 arc minutes) (3) Offset pointing (experiments can be pointed at any of 16384 points within the large raster pattern) (4) Small raster (experiments can be rastered about any of the 16384 offset points with a 16-line raster 7 1/2 arc minutes high and 7 arc minutes wide. <p>Pointing is accomplished automatically every orbit-morning by the coarse and fine pointing control electronics; raster scanning and offset pointing is enacted by ground station command; pointing accuracy is better than ± 1 arc minute.</p>
Nutation damping system	<p>Damps nutational movement (coning) of the spacecraft spin axis; consists of a passive nutation damper which absorbs nutational energy and dissipates it in the form of heat.</p>
Launch sequence system	<p>Controls the occurrence of observatory events during launch phase and changes observatory from launch configuration to orbit configuration; consists of four separation switches (that sense OSO separation from booster) which start motor-driven timers that directly or indirectly perform the following functions:</p> <ol style="list-style-type: none"> (1) Activates squib pin pullers to release arms, nutation damper, and pointed instruments. (2) Applies orbit-power to observatory and enables the ASL and APL at proper time.
Telemetry system	<p>Provides means by which spacecraft and experiment data are sampled and transmitted to ground stations; consists of PCM data handling subsystem and RF subsystem. Performs the following basic operations:</p> <ol style="list-style-type: none"> (1) Data sampling (2) Data encoding (3) Time multiplexing (4) Data storage (magnetic tape) (5) Transmitting of data
Aspect measuring system	<p>Provides aspect data from which the roll attitude, wheel angular position, and wheel spin rate can be computed; consists of a flux-gate magnetometer and the Spin Orientation and Rate Electronics (SORE box).</p>
Power system	<p>Provides electrical power for spacecraft and experiment consumption by converting sunlight into electrical energy; consists basically of a solar cell array, storage batteries, and a power distribution system.</p>
Command System	<p>Provides means by which the operation mode of the spacecraft and its experiments can be changed by commands sent from ground stations located on earth; consists of spacecraft command receivers, command decoders, and control relays.</p>



Table C-2
 FUNCTIONAL DESCRIPTION OF OSO-6 MAJOR SPACECRAFT COMPONENTS

Component	Functional Description
WHEEL STRUCTURE: <u>Wheel Mechanical Components</u>	Consists basically of nine wedge-shaped compartments arranged around a central hub; houses wheel electronics, wheel experiments, and spin pneumatics; supports sail structure and three extendible arms; provides stable platform for scientific instruments because of gyroscopic properties.
(1) Wheel hub assembly (1) ^(a)	Serves as central connecting hub for wheel equipment compartments; houses the following components:
a. Azimuth shaft (1)	Connects to sail azimuth casting and supports sail structure.
b. Azimuth torque motor (1)	Provides azimuth torque for sail despinning and pointing control; powered by pointing control system.
c. Slip ring assy. (1)	Consists of 22 slip ring contacts that transmit electrical signals and power between wheel and sail.
d. Azimuth bearings (2)	Supports azimuth shaft and provides low friction rotational drag between wheel and sail.
e. Pitch gas bottle (1)	Stores high pressure (3000 psi) nitrogen gas for Pitch Control System.
(2) Equipment compartments (9)	Houses wheel electronics and unoriented experiments; consists of nine wedge-shaped compartments; provides thermal control of electronic equipment by means of thermal shields, passive radiation control, and thermal conduction schemes.
(3) Extendible arms (3)	Extends during launch phase to increase the axial moment-of-inertia of the wheel; includes the following components:
a. Spin gas bottles (3)	Stores high pressure (3000 psi) nitrogen gas for spin control system.
b. Support brackets (3)	Forms part of three RF antennas; stabilizes arms.
(4) Arm damper hydraulics	Reduces arm velocity during deployment to prevent damage to arms and components; consists of three hydraulic cylinders, flow restricting orifices, and interconnecting plumbing.
(5) Spin pneumatics	Provides distribution and control of spin correction gas; actuated by spin control circuits. Consists of the following components:
a. Spin gas bottles (3)	Stores high pressure (3000 psi) nitrogen gas for spin control system.
b. Pressure regulator (1)	Reduces spin gas pressure from 3000 psi initial storage pressure to approximately 100 psi; this pressure is further reduced to approximately 60 psi at the spin nozzles because of fluid friction in the plumbing.
c. Manifold block (1)	Distributes spin gas to system plumbing; maintains pressure balance in spin gas bottles.
d. Spin-up solenoid valve (1)	Controls gas flow to spin-up nozzles; actuated by spin control circuits.
e. Pressure transducer (1)	Provides monitoring of spin gas pressure by telemetry.
f. Spin-down solenoid valve (1)	Controls gas flow to despin nozzles; actuated by spin control circuits.
g. Spin-up nozzles (3)	Provide spin-up thrust.
h. Despin nozzles (3)	Provide spin-down thrust.
i. Check valve (1)	Serves as filling port.

(a) Number in parentheses indicates total number of components.



Table C-2 (continuation)

Component	Functional Description														
<u>Wheel Electrical Components</u>															
(1) Spin control box (1)	Contains spin control electronics, undervoltage switch circuits, day turn-on circuits, and two 15 v DC regulators; provides spin rate control (auto and man.), day turn-on, and battery undervoltage protection.														
(2) Command receivers (2) (redundant)	Detects and amplifies PWM coded RF command signals from ground stations at 149.52 Mhz, the two receivers have common inputs but the outputs drive separate wheel decoders; output selection for sail decoder is accomplished by ground station command; receivers operate continuously.														
(3) Command decoders (2) (redundant)	Accept PWM command tones from command receivers and provide 77 wheel command functions; inputs are provided by separate command receivers; 63 command outputs are redundant; decoder selection is accomplished by unique decoder addresses from ground stations; decoders operate continuously; command functions are executed by the activation of appropriate control relays and circuits.														
(4) Launch sequence timers (2) (redundant)	Controls the occurrence of spacecraft operational events during launch phase; consists of redundant, motor-driven, cam operated, rotary switches; activation is by separation switches during separation from booster. Provides the following launch sequence functions:														
Legend: T_L = Liftoff T_T = Timer start	<table border="1"> <thead> <tr> <th data-bbox="683 932 812 961">Nominal Time (sec)</th> <th data-bbox="812 932 966 961">Function</th> </tr> </thead> <tbody> <tr> <td data-bbox="683 961 812 1012">$T_L + 721$</td> <td data-bbox="812 961 966 1012">$T_T + 0$ OSO separation; OSO timers started; arms released</td> </tr> <tr> <td data-bbox="683 1012 812 1125">$T_L + 1051$</td> <td data-bbox="812 1012 966 1125">$T_T + 330$ Turns on orbit power; selects auto-spin mode. (These functions initiate azimuth acquisition, wheel despin, and pitch error correction.)</td> </tr> <tr> <td data-bbox="683 1125 812 1155">$T_L + 1321$</td> <td data-bbox="812 1125 966 1155">$T_T + 600$ Uncages nutation damper</td> </tr> <tr> <td data-bbox="683 1155 812 1251">$T_L + 1521$</td> <td data-bbox="812 1155 966 1251">$T_T + 800$ Releases elevation frame; enables ASL and APL circuits for spin rate and pitch attitude runaway protection.</td> </tr> <tr> <td data-bbox="683 1251 812 1302">$T_L + 1971$</td> <td data-bbox="812 1251 966 1302">$T_T + 1250$ Repeats all of the above functions to insure operation.</td> </tr> <tr> <td data-bbox="683 1302 812 1333">$T_L + 2051$</td> <td data-bbox="812 1302 966 1333">$T_T + 1330$ Power removed from timers.</td> </tr> </tbody> </table>	Nominal Time (sec)	Function	$T_L + 721$	$T_T + 0$ OSO separation; OSO timers started; arms released	$T_L + 1051$	$T_T + 330$ Turns on orbit power; selects auto-spin mode. (These functions initiate azimuth acquisition, wheel despin, and pitch error correction.)	$T_L + 1321$	$T_T + 600$ Uncages nutation damper	$T_L + 1521$	$T_T + 800$ Releases elevation frame; enables ASL and APL circuits for spin rate and pitch attitude runaway protection.	$T_L + 1971$	$T_T + 1250$ Repeats all of the above functions to insure operation.	$T_L + 2051$	$T_T + 1330$ Power removed from timers.
Nominal Time (sec)	Function														
$T_L + 721$	$T_T + 0$ OSO separation; OSO timers started; arms released														
$T_L + 1051$	$T_T + 330$ Turns on orbit power; selects auto-spin mode. (These functions initiate azimuth acquisition, wheel despin, and pitch error correction.)														
$T_L + 1321$	$T_T + 600$ Uncages nutation damper														
$T_L + 1521$	$T_T + 800$ Releases elevation frame; enables ASL and APL circuits for spin rate and pitch attitude runaway protection.														
$T_L + 1971$	$T_T + 1250$ Repeats all of the above functions to insure operation.														
$T_L + 2051$	$T_T + 1330$ Power removed from timers.														
(5) Separation switches (4) (redundant)	Consists of four individual switches in series-parallel arrangement mounted on the bottom of the OSO attach fitting; detects separation of spacecraft from booster and activates launch sequence timers.														
(6) Hybrid circulator (1)	Isolates the inputs of the two redundant command receivers to allow independent operation in case of receiver malfunction.														
(7) Antennas (3)	Radiate RF telemetry signals and receive RF command signals; consist of three support brackets and three antenna stubs; two dipoles are end-driven and one is parasitic.														
(8) Diplexer (1)	Provides transmitting and receiving with a common antenna array.														



Table C-2 (continuation)

Component	Functional Description
(9) Transmitters (2) (redundant)	Generates a RF signal modulated by Manchester coded data; uses PM (phase - modulation) techniques in which a digital "1" or "0" is denoted by a 57 deg phase shift of the RF carrier; operates at 136.71 Mhz with an output power of 600 mw; transmitter selection is accomplished by ground commands.
(10) Coax switch (1)	Connects appropriate transmitter to antenna array; operates simultaneously with transmitter select commands.
(11) Spin eye assembly (1)	Produces a "sun" pulse each time the wheel sweeps the sun; triggers the spin control circuits to maintain auto-spin control; provides day/night control of observatory; provides ground station monitoring of spin rate by telemetry.
(12) Tape recorders (2) (redundant)	Continuously records telemetry data on magnetic tape during each orbit (approx. 103 min. capacity); plays back recorded data at 18 times record rate (approx. 5.6 min.) upon ground command; automatically reverts to record mode after playback completion; selection is accomplished by ground commands.
(13) Analog subcommutator (1) (WASC)	Commutes wheel and experiment housekeeping data into a 48 word subcom frame; gating and timing is provided by the digital multiplexer-encoders (DME's).
(14) Digital submultiplexer and frame counter (1) (DSM & FC)	Multiplexes digital spacecraft aspect data, frame count, single-bit status monitors, and experiment data into 48 word frame; gating and timing is provided by the DME's.
(15) Main battery assembly (1)	Stores electrical energy for observatory night consumption and peak demands; consists of 42 ni-cad cells arranged in series-parallel; capable of producing more than 12 amp-hr before going into undervoltage state (16.2 volts).
(16) Digital multiplexers and encoders (2) (redundant) (DME No. 1 and No. 2)	Generates telemetry clock and data readout gates that control the commutating and multiplexing of telemetry data; provides analog to digital encoding of analog data; multiplexes all telemetry data (RZ or NRZ) into Manchester Code.
(17) PCM junction box (1)	Provides interconnections within the PCM data handling subsystem; contains isolation circuits for digital data outputs from various experiments and for the telemetry clock; contains TMG gate circuits which, when energized convert all main frame data to "ones" except WASC and SASC words, and the main frame sync words, (used as backup to frame counter).
(18) Pressure cartridges (squibs)	Provides mechanical uncaging of various wheel components during launch phase; are detonated by the wheel squib batteries in conjunction with the launch sequence timers. Consists of 6 armlock squibs (2 for each arm) which release arms at $T_T + 0$ sec.
(19) Squib battery packs (2) (redundant)	Provides electrical power for detonating wheel pressure cartridges; each pack consists of 7 ni-cad cells connected in series; capable of supplying 20 amps into 1/4 ohm load for 2 seconds.



Table C-2 (continuation)

Component	Functional Description
(20) Magnetometer and Electronics (1)	Measures the direction of the earth's magnetic field by detecting when the magnetic component is a positive going zero; the magnetometer is mounted on arm No. 4 (corresponds to compartment 4) with its sensitive axis parallel to the wheel plane; power is obtained from the magnetometer electronics and its output is coupled to the SORE box.
(21) SORE Box (1)	Provides a binary count of the clock pulses that occur between a "rising zero crossing" (from magnetometer electronics) and the first sun pulse after the zero field signal (from this count the angle between the roll axis and field vector can be computed); also provides a binary count of the clock pulses that occur between DSM word No. 3 and the sun pulse or DSM word No. 3 and the magnetometer pulse (from this count the wheel spin rate can be computed).
(22) Pitch Coil (1)	Augments the pneumatic pitch control system by interacting with the earth's magnetic field which produces torques that causes OSO to rotate in the pitch plane; consists of a large inductor placed parallel to the wheel plane around the wheel hub; can be commanded on, off, full pwr, 1/2 pwr, positive or negative to satisfy operation requirements.
SAIL STRUCTURE:	Consists basically of a semicircular framework attached to the wheel by the azimuth shaft; the front surface is covered by solar cells behind which are housed the sail electronics, pitch pneumatics, and nutation damper; provides accurate azimuth and elevation pointing of the solar-oriented instruments by action of pointing control system.
<u>Sail mechanical components</u>	
(1) Azimuth casting (1)	Forms the base of the sail structure at which point the sail is connected to the wheel azimuth shaft; supports the elevation casting and "pointed" instruments.
a. Elevation torque motor (1)	Provides elevation torque for pointing of oriented instruments; actuated by pointing control system.
b. Elevation bearings (2)	Supports elevation stub shafts and assures low-friction drag between azimuth casting and elevation casting.
(2) Elevation Casting (1)	Supports pointed instruments; rotates in elevation within the azimuth casting by action of the elevation torque motor and pointing control system.
a. Elevation shaft (2)	Supports elevation casting by means of elevation bearings; consists of two stub shafts.
(3) Nutation damper (1)	Damps nutational motion of observatory by converting kinetic nutation energy into heat energy; consists of a pendulum that moves in a bath of silicone oil.
(4) Pitch pneumatics	Provides distribution and control of pitch precession gas; is actuated by pitch control circuits; consists of the following components:
a. Pitch gas bottle (1)	Stores high-pressure (3000 psi) nitrogen gas for pitch control system.
NOTE: This component is mounted around the azimuth shaft inside the wheel hub assembly.	



Table C-2 (continuation)

Component	Functional Description
b. Pressure regulator (1)	Reduces pitch gas pressure from 3000 psi initial storage pressure to approximately 72 psi; this pressure is further reduced to approximately 60 psi because of fluid friction in the plumbing.
c. Pressure transducer (1)	Provides monitoring of pitch gas pressure by telemetry.
d. Filter (1)	Prevents foreign material from entering pneumatics during filling operations.
e. Pitch up nozzle (1)	Provides pitch up thrust.
f. Pitch down nozzle (1)	Provides pitch down thrust.
g. Check valve (1)	Serves as filling port.
<u>Sail Electrical Components</u>	
(1) Command decoders (2)	Accept pulse width modulated (PWM) command tones from the command receivers and provides 98 sail command functions; the command functions are executed by the activation of appropriate control relays and circuits.
(2) Servo amplifier box (1)	Amplifies and conditions the azimuth and elevation control signals from the azimuth and elevation control eye assembly before application to the power amplifier; amplifies target eye output and switches from coarse azimuth to fine azimuth control when coarse alignment (± 3 deg) has been achieved; provides target eye, az. and elev. preamp., az. and elev. error signal, and servo box 15 v DC regulator monitoring by telemetry.
(3) Power amplifier box (1)	Amplifies and conditions the azimuth and elevation control signals from the servo amplifier before application to the az. and elev. power switches and torque motors; generates az. and elev. raster scan and offset point signals; generates auto. and manual pitch correction signals from pitch control error signals and ground-station commands, respectively; provides telemetry monitoring of the az. and elev. raster signals, offset point generator status, az. and elev. torque motor currents.
(4) Sail Junction Box (1)	Provides distribution of electrical signals in the sail; houses on-off relays for the pointed instruments and various other control relays.
(5) Analog subcommutator (1) (SASC)	Commutates sail and oriented experiment housekeeping data into a 48 word subcom frame; gating and timing is provided by the digital multiplexer-encoders located in the wheel.
(6) Analog sub-subcommutator (1) (ASSC)	Subcommutates spacecraft analog housekeeping data into a 24-word subframe before inputting to sail ASC; gating and timing is provided by sail ASC.
(7) Word Gate Generators (2) (Redundant)	Regenerate the 32-word main frame for use as read-out gates for the NRL and HCO pointed instruments; selectable by ground command.
(8) Flex cables (2)	Provides electrical connection between right and left pointed instruments and the sail junction box.
(9) Azimuth coarse eye assemblies (4)	Provides azimuth drive signals for initially despinning and pointing the sail; inputs to the pointing control system.
(10) Azimuth and elevation fine control eye assembly (1)	Provides fine azimuth and elevation error and drive signals for fine pointing control of sail and pointed instruments; inputs to the pointing control system.



Table C-2 (continuation)

Component	Functional Description
(11) Pitch control eye assembly (1)	Provides pitch error signals for maintaining the sail within ± 4 deg of normal to the solar vector; inputs to the pitch control system.
(12) Pitch readout eye and amplifier assembly (1)	Provides monitoring of the pitch angle by telemetry.
(13) Pressure cartridges (Squibs) a. Nutation damper squibs (2) (redundant) b. Elevation lock squibs (2) (redundant)	Provide mechanical uncaging of various sail components during launch phase; are detonated by the sail squib batteries in conjunction with the launch sequence timers. Consists of the following components: Uncage nutation damper bob at $T_T + 600$ sec Unlatch elevation frame at $T_T + 800$ sec
(14) Squib battery packs (2) (redundant)	Provide electrical power for detonating sail pressure cartridges; each pack consists of 3 ni-cad cells arranged in series; capable of supplying 6 amps into 1/2 ohm load for two seconds.
(15) Solar cell array (1)	Converts solar energy into electrical energy for observatory consumption; produces approximately 40 watts at about 2 amps and 20 volts; consists of 960 silicon solar cells with an overall area of about 4.2 ft ² .
(16) Target eye assembly (part of fine control eye assembly, item #10)	Detects solar intensity for the purpose of determining when the pointed instruments are within approx. ± 3 deg of stationary azimuth pointing; inputs to the pointing control system and causes switching from coarse to fine control when solar intensity is approx. 10 percent of maximum.
(17) Readout Eye Assembly (1)	Provides monitoring of the azimuth and elevation pointing error by telemetry.
(18) Roll coils (2)	Provides roll attitude control of spacecraft by interacting with the geomagnetic field; consists of two inductors mounted at the top of the sail, one on either side of the spin axis; either coil can be commanded on or off, positive or negative to satisfy operation requirements.



Appendix D

OSO-G

Model Specification

(Retyped from BBRC Doc. 26493
Revision D dated 19 Mar 69)



1.0 SCOPE

This specification describes the physical and functional characteristics of the Orbiting Solar Observatory spacecraft. The spacecraft shall be designed to carry scientific experiments in a 300 nautical mile earth orbit.

Definitions of terms used in this specification are given in paragraph 5.1.

2.0 APPLICABLE DOCUMENTS

The following documents, of exact issue shown, or the latest revision where issue is not specified form a part of this specification as described herein:

<u>Document</u>	<u>Title</u>
BBRC 19541-505 23732	Spacecraft Assembly Installation Control Dwg., OSO-G/Delta Interface
BBRC 29800	OSO-G Experiment/Spacecraft Interface Specification
BBRC 26494	Test Specifications for the OSO-G Spacecraft
BBRC 21883	Environmental Test Specification for Subassemblies of the F, G and H Orbiting Solar Observatory
BBRC 19540-505	Observatory Assembly Drawing
Douglas SM-48897	Improved Delta Spacecraft Design Restraints Dated January 1966

3.0 REQUIREMENTS

3.1 Physical Requirements



3.1.1 Size and Configuration

The maximum overall dimensions of the spacecraft are shown in Ball Brothers Research Corporation (BBRC) Drawing No. 23732.

The spacecraft assembly shall be as defined in BBRC Drawing 19541-505.

3.1.2 Weight

The maximum weight of the spacecraft shall be 375 pounds.

3.1.3 Interface Requirements

3.1.3.1 Spacecraft and Launch Vehicle Interface

3.1.3.1.1 The spacecraft mechanical interface with the Improved Delta launch vehicle shall be compatible with Douglas Aircraft Company Report SM-48897, except that spacecraft rotational alignment shall be in accordance with BBRC Drawing 19540-505.

3.1.3.1.2 The following shall occur as part of the launch sequence:

- (a) The spacecraft shall be spun about the rocket thrust axis in a clockwise direction as viewed from the launch vehicle.
- (b) The spin rate, after spin-up, shall be between 70 and 134 rpm. The spin rate will be determined based on the wheel moment of inertia only.
- (c) At the instant after release from the booster stage, the average spacecraft angular momentum vector shall be pointed perpendicular to the solar direction within ± 8 degrees.



This error includes vehicle attitude errors at injection, tip off errors, and launch window errors. Nutation at this time shall be less than 1.5 degrees half angle.

3.1.3.2 Experiment Interface

The experiment interface with the spacecraft shall be defined in BBRC 29800, OSO-G Experiment/Spacecraft Interface Specification.

3.1.3.3 Experiment Payload Capability

The spacecraft shall be capable of carrying two solar oriented scientific experiments each weighing a maximum of 45 pounds. Maximum single experiment envelope shall be approximately 4 inches by 8 inches and 38 inches long. The spacecraft shall be capable of carrying 150 pounds of nonsolar oriented scientific experiments in five separate pie-shaped compartments. The maximum weight of any one experiment shall be 45 pounds and the maximum experiment envelope shall be approximately 13 inches wide at the front by 4 inches at the back by 13 inches deep and 8-1/2 inches high.

3.1.4 Thermal Characteristics

3.1.4.1 General

Thermal control of the spacecraft shall be accomplished passively by using spacecraft surfaces with known thermodynamic properties.

3.1.4.2 Rotating section compartment temperature excursion over an orbit shall be equal to or less than 5° C. The mean temperature shall be 15 ±5° C.



3.2 Functional Characteristics

3.2.1 Launch Conditions

3.2.1.1 The following equipment will have power applied and be operable during launch.

- (a) Command Decoders
- (b) Command Receivers
- (c) Charge Rate Monitor Circuit
- (d) Undervoltage Monitor Circuit
- (e) Tape Recorders
- (f) Transmitter
- (g) PCM Junction Box
- (h) Digital Multiplexer and Encoder
- (i) Analog Subcommutators
- (j) Digital Submultiplexer and Frame Counter
- (k) Analog Sub-Subcommutator

3.2.1.2 The spacecraft shall be capable of remaining in the launch condition for six hours before the batteries must be recharged.

3.2.1.3 The spacecraft shall perform in accordance with the orbital performance characteristics of paragraph 3.2.2 within 1400 seconds following spin-up.

3.2.2 Orbital Performance

The orbital performance characteristics are defined in terms of spacecraft operation in a 300 ± 50 nautical mile, circular earth orbit inclined 33 ± 3 degrees to the equator.



3.2.2.1 Power Subsystem Characteristics

3.2.2.1.1 General

The power source for the spacecraft shall be an array of solar cells. Energy storage shall be provided by batteries to supply peak loads and power during the spacecraft night. During spacecraft day, the solar array shall furnish power for spacecraft operation and for charging the batteries. The solar array (mounted on the oriented section) shall be maintained perpendicular to the solar direction within 2 degrees around the spin axis and 5 degrees around the pitch axis.

During the first six months of orbit, the solar array shall provide an energy of 1.87 ampere hours per orbit with the spacecraft continuous bus voltage at 19 ± 3 volts. The spacecraft shall withstand a current surge of 8 amps for 5 milliseconds with the spacecraft continuous bus voltage at 19 volts.

3.2.2.1.2 The maximum D.C. power source resistance measured at the spin box launch bus for a 5 ± 3 second duration load of 2.0 ± 0.5 amps, shall be less than 0.3 ohms. The maximum resistance between the launch and the other busses are tabulated below when fuses are jumpered as required for flight.

Wheel exp. day bus	0.13 ohms
Wheel exp. nite bus	0.18 ohms
Sail launch bus	0.30 ohms
Sail day bus	0.20 ohms

Resistance between the above listed busses and associated experiment interface connectors shall not exceed 0.6 ohms for a 5 ± 3 second load of $.2 \pm .02$ amps. If there is an RF choke in series with the power line to the instrument, the resistance shall not exceed 2.4 ohms.



The power busses exhibit increased impedance characteristics to high-frequency signals and pulses. The exact nature of these impedances is not known well enough at this time to be included as a part of this specification.

3.2.2.1.3 Power shall be automatically removed from all experiments and spacecraft electronics, except those listed below, if the voltage at the under voltage sensor drops below 16.2 ± 0.2 VDC. Power shall be reapplied when the batteries have been recharged to 19.0 ± 0.2 VDC.

- a. Rotating Section Command Decoders
- b. Command Receivers
- c. Array Current Monitor Circuit
- d. Undervoltage Switch

3.2.2.1.4 The day-night turn on control circuit shall switch on the power to the pointing control electronics, and the pointed experiments when the spacecraft enters the sunlight.

3.2.2.2 Spacecraft Attitude Control

3.2.2.2.1 General

The attitude control and stabilization system of the spacecraft shall be designed to orient the spacecraft spin axis and oriented section to the sun. This system shall utilize the gyroscopic properties of the rotating section. Solar error sensors shall be used to determine alignment errors with respect to the solar direction. The spin rate of the rotating section and the spin axis orientation with respect to the solar direction shall be maintained within specified limits by attitude correcting gas jet controls. The gas jet controls shall be actuated by sun sensing error detectors. The gas jets shall be supplied with



dry nitrogen gas from storage bottles pressurized to 3000 psig at launch.

3.2.2.2.2 The spin axis of the spacecraft shall be maintained perpendicular to the solar direction within 4.0 degrees.

3.2.2.2.3 The rotating section spin rate shall be maintained between 0.44 rps and 0.68 rps by the automatic system. The spin rate change per correction shall be 0.028 ± 0.01 rps. The "switch to manual" set points shall be 0.39 ± 0.012 rps and 0.70 ± 0.015 rps.

3.2.2.2.4 Roll control of the spacecraft during orbit day shall be achieved by generating a magnetic dipole parallel to the spacecraft X-axis. The dipole will be produced by current flowing through coils mounted in the sail. The amount and direction of current may be altered by command to produce dipole moments of 0, ± 2500 , or ± 5000 dyne-cm. gauss⁻¹. These values will vary in direct proportion to the spacecraft supply voltage. The tolerance for these values with a supply voltage of 19.0 volts shall be $\pm 10\%$.

The system will require less than one watt to produce a moment of 5000 dyne-cm. gauss⁻¹.

The spacecraft roll position measurement shall be accurate to ± 3 degrees with the roll-coil assembly turned off, and ± 6 degrees with the roll-coil assembly turned on. The solar referenced roll rate shall be less than 2 degrees per terrestrial day with the roll-coil assembly turned off.



3.2.2.3 Fixed Pointing Accuracy

3.2.2.3.1 General

The control and readout sensor assemblies shall be mounted to the end of the pointed experiments which face the sun. The surfaces on which the solar sensors are mounted shall be the reference plane from which the pointing accuracies are determined. Zero pointing error shall be when the reference surface is perpendicular to the solar direction. The experiment control and readout sensor assembly interface shall be defined in BBRC 29800, OSO-G Experiment/Spacecraft Interface Specification.

3.2.2.3.2 The spacecraft pointing controls shall orient the pointed experiments to the sun at the beginning of each spacecraft day (the oriented section shall spin with the rotating section during the spacecraft night). The pointed experiments shall be oriented, as specified below, within 90 seconds after the spacecraft enters full sunlight.

3.2.2.3.3 The pointed experiments shall be controlled about the elevation axis. The pointed experiment elevation position shall be maintained within 1 arc minute of the solar direction during the spacecraft day.

3.2.2.3.4 The pointed experiments shall be controlled in azimuth about the spacecraft spin axis. The azimuth position shall be maintained within 1 arc minute of the solar direction during the spacecraft day.

3.2.2.3.5 The pointed instrument package will have an angular motion about the average pointing direction, henceforth called jitter.



The jitter will be less than 5 arc seconds peak (clipped sinusoid) in elevation and less than 3 arc seconds rms random motion in a band between 0.5 and 5 cps in azimuth. It is doubtful that this low a jitter can be demonstrated directly on the ground because atmospheric shimmer is normally of the order of 5 to 10 arc seconds peak-to-peak.

This jitter will be present and unchanged whether in the point or raster mode.

3.2.2.4 Offset Mode

3.2.2.4.1 General

In addition to the basic sun centered pointing as described above, the spacecraft is capable of causing the pointed instrument package to:

1. Generate a large raster centered on and covering the entire solar disc.
2. Generate a small raster that will cover approximately 1/30 to 1/40 of the large raster area and have the capability of being centered on any one of the offset points mentioned below.
3. Provide offset point to any position in a 128 x 128 (16,384) point grid pattern centered on and covering the entire solar disc.

3.2.2.4.2 Characteristics

The characteristics of this mode are given in Table D-1 and the following paragraphs.



Table D-1
OFFSET MODE CHARACTERISTICS

Parameter	Large Raster	Small Raster	Offset Grid
Size	46 x 46 ± 2 arc min.	7 Az x 7.5 El ± 0.5 arc min.	46 x 46 ± 2 arc min.
Resolution	64 lines	16 lines	128 x 128 points
Frame Period	491.5 sec. (24 MF/line)	30.72 sec. (6 MF/line)	-----

(a) Size Variations

The size stated is set up prior to launch for the estimated mean solar intensity, i.e., the solar intensity in orbit at an equinox.

Additional size variations can be expected from the following three sources. In orbit, the absolute size must be computed periodically using preflight calibration data and target intensity because of the following variations:

- (1) A ± 1.5 percent size uncertainty at launch results from a like uncertainty in the mean solar intensity.
- (2) Size will vary ± 3.3 percent due to the annual solar intensity variation.
- (3) Size will increase on the order of 6 percent per year due to sensor degradation.



(b) Scan Velocity

The line scan velocity is determined by the pattern size and frame time as stated in Table I. The nominal velocities are 360 arc sec/sec and 218 arc sec/sec for the large and small raster respectively.

(c) Pattern Synchronization

The start of each line occurs at the instant of the rise of every 24th MF word gate 32 for the large raster and every 6th MF word gate 32 for the small raster.

(d) Servo Lags

The electronic generators instantaneously reverse in azimuth and jump to the next line in elevation. However, the pointed instrument package momentarily lags behind the generators. The angle required for the servo to "catch up" is less than one arc minute from the start of line, i.e., about 0.6 main frames (MF). During "catch up", deviations from the ideal may amount to as much as 0.5 arc minutes.

When changing mode, the servo will "catch up" to the electronics within 16 MF after the mode change command if the servo has been in the fine point mode immediately prior to the command.

After each raster reset occurrence, the servo "catches up" to the electronics in 16 and 6 MF for the large and small rasters respectively.



"Catch up" following acquisition at dawn will be completed within 30 MF following the "on target" indication.

(e) Retrace and Reset

Retrace will always be from lower left to upper left, i.e., the raster will start in the upper left hand corner when facing the sun. When the offset generators are reset, the upper left corner of the pattern will be achieved.

(f) Raster Reconstruction Signals

Recreation of the raster on the ground is accomplished by use of start of line (SOL) and start of raster (SOR) signals plus a status monitor to indicate whether the large or small raster has been selected. Pulses indicating these events are available in the spacecraft. The various experimenters will be responsible for telemetering those signals to the ground. The characteristics of these pulses are listed below:

SOL and SOR Pulses

Width	20 ±4 msec
Rise (SOR)	<10µs
Fall	<100µs
Height	10 ±2V
Source Z	ON 1.2 K 20%
(excluding	OFF SOL 52 KΩ ±10%
5-Ω fan-on	SOR 10 KΩ ±10%
resistors)	
Rise (SOL)	<50µs



Raster Status

Small Raster	<0.5 V
Large Raster	9 ±1 V
Source Z	<400 K

(g) Generator Startup

When either raster generator is commanded on, there is a certain settling time required before the generator is within specification. This settling time is 160 main frames for large raster and 55 main frames for the small raster. The detailed position equivalent output of the generators is given below.

The large raster starts at the center of the first line within 2 seconds after the initiating command.

The small raster starts at the center of the first line within 2 seconds after the initiating command. However, this is an out-of-synchronization condition and motion should be considered to have started in the upper left hand corner. The actual output goes from center to 1/2 line past the right hand edge. The motion starts back at the sixth word 32. Each succeeding line ends nearer the right hand edge and at the seventh line, the system is within specification.

3.2.2.4.3 Performance Specifications

Table D-2 and the following paragraphs list the specifications for the performance of the operations stated in 3.2.2.4.1.

These specifications are for in orbit operation.

C. 8



Table D-2
OFFSET MODE PERFORMANCE

Parameter	Large Raster	Small Raster	Offset Grid
Repeatability ¹	$\pm 1.5\% \pm 0.1$ minute	$\pm 1.5\% \pm 0.1$ arc minute	$\pm 1.5\% \pm 0.1$ arc minute
Relative Size Uncertainty	$\pm 0.7\%$	$\pm 2.0\%$	Ref.
Absolute Size Uncertainty	$\pm 2\%$	$\pm 3\%$	$\pm 2\%$
Pattern Error ²	± 0.4 arc min.	± 0.5 arc min.	± 0.4 arc min.
Pattern Center Offset	± 0.1 arc min.	± 0.1 arc min.	± 0.2 arc min.

1. Repeatability is medium term (1 week) and assumes an eyeblock temperature variation of less than $\pm 5^{\circ}\text{C}$ and an electronic temperature anywhere between $+10$ and $+35^{\circ}\text{C}$. It will not be possible to demonstrate this as a system directly with presently planned test equipment.
2. The primary source of error is the sensor response. Generator errors are about 0.1 arc minute. The error specification does not apply on the first line nor outside of a 40 x 40 arc minute square for the large raster nor outside of 5 x 5 arc minute square for the small raster. The small raster error specification does not apply for parts of the small raster extending beyond a 40 x 40 arc minute square centered on the solar disc.

3.2.2.4.4 Definitions

The following is a list of definitions used in describing the offset mode characteristics and performance.



- (a) Pattern Size - is the size of the ideal pattern when adjusted for minimum errors with an actual pattern. Error adjustment shall be made in the region specified under pattern error.
- (b) Ideal Raster Pattern - is one in which line spacing in elevation is uniform and in which the line sweep rate in azimuth is constant.
- (c) Ideal Offset Point Grid - is one in which all points are uniformly spaced.
- (d) Resolution - is the number of elevation lines in a total raster frame or the number of grid points in an offset point grid.
- (e) Offset Point Grid - is the grid comprised of all the points that the control sensor optical axis can point to when in the offset point mode of operation.
- (f) Frame Period - is the time required to complete one frame of a raster pattern.
- (g) Repeatability - is accuracy to which the spacecraft can return to a given previous position. In the case of raster, the given position is defined in spacecraft time from the start of the raster frame, and in the case of offset point the given position is defined by the offset lines commanded. The accuracy is specified as a percent of the distance of the given position from the center of the solar disc plus an uncertainty angle.



- (h) Relative Size Uncertainty - is the uncertainty in the ratio of the size between patterns. The size ratio is important in selecting the proper point in the offset point grid. The offset point grid is used as the size reference.
- (i) Absolute Size Uncertainty - is the size uncertainty in absolute angle. To obtain the absolute size estimate, preflight calibration and actual target intensity must be taken into account.
- (j) Pattern Error - is the deviation in the average position of each point in the actual pattern from that of an ideal pattern. The size of the ideal pattern is adjusted to minimize errors.
- (k) Pattern Center Offset - is the offset of the center of the best fit ideal pattern from the reference.
 - (1) Large raster offset is referenced to the offset point grid center.
 - (2) Small raster offset is referenced to the offset point about which the raster is generated.
 - (3) The offset point grid is referenced to the normal "on point" position.

The center of the pattern is defined as the geometric center of an ideal pattern that is a best fit for the actual pattern within the 34 x 34 arc minute region in the pattern center.



3.2.2.5 Data Handling and Data Transmission Characteristics

3.2.2.5.1 General

Experiment and spacecraft data shall be continuously time-multiplexed. The data rate shall be 100 words per second. This information shall be stored and continuously transmitted. Upon command from a ground station, the stored information shall be transmitted instead of the "real time" information. The continuous transmission shall be called "real time" transmission, and the stored information transmission shall be called "playback" transmission. No information shall be recorded during "playback" transmission. The experiment and spacecraft information shall be pulse-coded. The code format shall be Manchester (also called biphase or split-phase).

3.2.2.5.2 A data word shall consist of eight binary bits.

3.2.2.5.3 A data main frame shall consist of 32 data words.

3.2.2.5.4 One data word of the main frame shall be for data from a 48-channel digital submultiplexer. One word of the digital submultiplexer shall indicate the main frame count to permit correlation between spacecraft real time and Greenwich mean time. The last word of each submultiplexer frame shall be a subframe synchronization word.

3.2.2.5.5 One data word of the main frame shall be for data from a 48-channel analog subcommutator in the rotating section.



3.2.2.5.6 One data word of the main frame shall be for data from a 48-channel analog subcommutator in the oriented section. The last word period of each subcommutator frame shall consist of a subframe synchronization word. The three subcommutators shall be synchronized to provide data channel correlation.

3.2.2.5.6.1 One data word of the oriented section analog subcommutator shall be for data from a 24 channel analog sub-subcommutator in the oriented section. The last two word periods of each sub-subcommutator frame shall be a sub-subframe synchronization word.

3.2.2.5.7 The last two word periods in each main frame shall consist of a frame synchronization word.

3.2.2.5.8 The remaining 27 word period of the main frame shall be assigned to the experimenters.

3.2.2.5.9 The transmitted carrier shall be within ± 5 kc of a fixed frequency between 136 mc and 137 mc. The exact frequency shall be assigned by NASA for each spacecraft.

3.2.2.5.10 The carrier shall be angle-modulated by a pulse code signal. The peak deviation shall be 57 ± 5 degrees for both playback and real-time transmission.

3.2.2.5.11 The transmitted bit rate during playback transmission shall be 14400 ± 288 bits per second.

3.2.2.5.12 The transmitted bit rate during real-time transmission shall be 800 ± 0.4 bits per second.



3.2.2.5.13 The spacecraft shall be capable of storing pulse-coded data at 800 bits per second for 98 minutes minimum, 101 minutes maximum. This data shall be transmitted within 338 ± 5 seconds after execution of a command from the ground station.

3.2.2.5.14 The transmitter output power referenced to the antenna connectors shall be +27 dbm nominal, and +25 dbm minimum.

3.2.2.5.15 Antenna polarization at the transmitter frequency shall be linear when considering the vector sum of two orthogonal components (see paragraph 5.2).

3.2.2.5.16 The transmitting antenna gain shall be greater than -6db over a minimum surface area of 3.8π steradians with reference to a linear isotropic source.

3.2.2.5.17 The following housekeeping data shall be available as part of the calibrated telemetered data from the spacecraft.

1. Temperatures shall be monitored at 18 spacecraft locations.
2. Spacecraft voltage shall be monitored at the launch bus.
3. A magnetometer pulse shall be provided once each wheel revolution.
4. A sun pulse shall be provided once each wheel revolution during orbit day.
5. Pointing and raster signals shall be provided to indicate pointing direction relative to the solar vector axis.



3.2.2.6 Command Characteristics

3.2.2.6.1 General

The command subsystem shall enable the ground controllers to command the spacecraft and experiments into different modes of operation. Each decoder shall be capable of executing a set of 70 discrete instruction commands. There are two decoders in the rotating section and two decoders in the oriented section each of which will execute any one of its 70 discrete instruction commands only upon receipt of its unique address command. Thus there are a maximum of 280 (4 x 70) address/instruction command functions. To avoid loss of critical command functions due to the loss of a single decoder, the outputs of two decoders are combined to operate a common load. Spacecraft functions of a non-critical nature are operated by single decoder outputs. Thus there are a total of 74 redundant commands. The command subsystem shall receive and decode a serial train of tone bursts which are amplitude-modulated on the command carrier frequency. The information shall be contained in three distinct tone burst widths. Separate and distinct address codes shall be used for actuating the desired decoder.

3.2.2.6.2 The command receiver shall be fixed tuned to 149.52 ± 2 kHz.

3.2.2.6.3 The command carrier shall be amplitude modulated by a 7 kc duration-modulated tone. The carrier shall be modulated a minimum to 75 percent and a maximum of 100 percent.



3.2.2.6.4 A command word shall consist of 10 pulse duration modulated bits. The command word format shall be as follows:

- a. Bit Period: A time duration equivalent to 72 cycles of the assigned audio frequency.
- b. The first bit period in each word shall be a blank. (No modulation for a period of 72 cycles.)
- c. The second bit shall be a "sync" bit having a time duration of 54 cycles of the assigned audio frequency.
- d. The remaining 8 bit periods shall contain "ones" and "zeros".
- e. A "one" shall have a time duration of 36 cycles of the assigned audio frequency.
- f. A "zero" shall have a time duration of 18 cycles of the assigned audio frequency.
- g. The 8 information bits of a command word shall be combinations of 4 "ones" and 4 "zeros".

3.2.2.6.5 An address word shall have the same format as the command word with the exception of the number of "ones" and "zeros" in the message. An address word shall contain a combination of 6 "ones" and 2 "zeros" or 6 "zeros" and 2 "ones". The exact address codes shall be assigned by NASA for each spacecraft.

3.2.2.6.6 A blank bit followed by a sync bit shall appear at the end of any command transmission.

3.2.2.6.7 These channels shall be assigned either to BBRC or the experiments as negotiated by BBRC, the experimenters, and the NASA Project Office.

3.2.2.6.8 The minimum threshold of the command subsystem shall be -95 dbm at the spacecraft antenna terminal when the carrier is 75 percent modulated.



3.2.2.6.9 Antenna polarization at the receiver frequency shall be right circular (see paragraph 5.2).

3.2.2.6.10 The antenna gain at the command frequency shall be greater than -18 db over a minimum surface area of 3.8π steradians with reference to a linear isotropic source.

3.3 Life and Reliability

The design objective shall be for a minimum operating life of six months in a 300 ± 50 nautical mile circular earth orbit inclined 33 ± 3 degrees to the equator.

3.4 Environmental Conditions

The spacecraft shall perform as required during and after exposure to the following environmental conditions. The conditions stated shall be the extreme environmental conditions expected for the OSO.

3.4.1 Temperature - Pressure

The following temperatures with an ambient pressure of 10^{-5} mmHg shall be the design requirements for components located in the indicated area.

-10°C to 35°C	Internal Rotating Section
-10°C to 40°C	External Rotating Section
-10°C to 50°C	Back of Oriented Section
-30°C to 75°C	Front of Oriented Section
-10°C to 40°C	Azimuth Casting

4.0 QUALITY ASSURANCE

4.1 The Quality Assurance Department shall verify compliance with the following requirements.



4.1.1 The spacecraft shall be tested and accepted in accordance with BBRC 26494, Test Specification for the OSO-G Spacecraft.

4.1.2 Spacecraft assemblies and subassemblies environmental tests shall be in accordance with BBRC 21883, Environmental Test Specification for Subassemblies of the Orbiting Solar Observatory.

4.1.3 Two categories of tests which shall be performed on the spacecraft and spacecraft equipment are given below:

- a. Qualification Test
- b. Acceptance Test

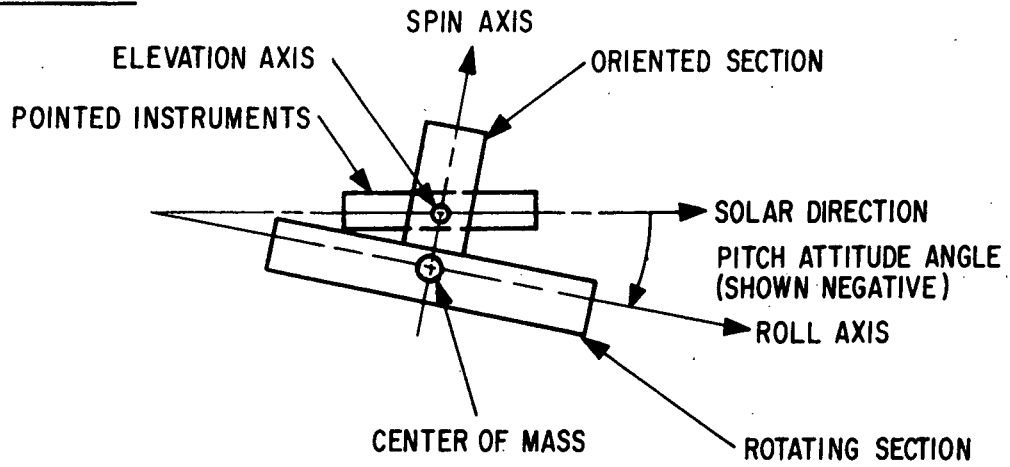
5.0 NOTES

5.1 Definitions

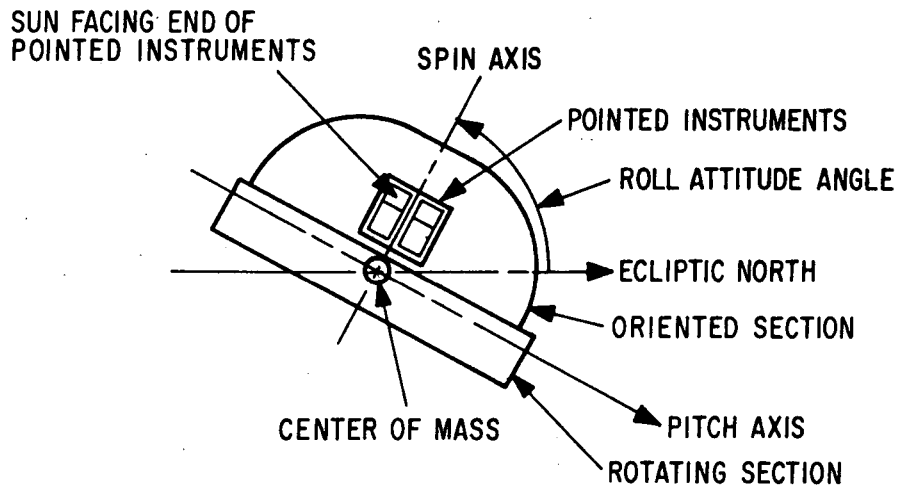
- a. Solar Direction: The line-of-sight between the spacecraft and the center of the sun.
- b. Roll Axis (Fig. D-1): An axis through the center of mass of the spacecraft which is perpendicular to the spin axis and is in the plane formed by the solar direction and the spin axis.
- c. Spin Axis (Fig. D-1): The axis about which the spacecraft is rotating.
- d. Pitch Axis (Fig. D-1): An axis through the center of mass of the spacecraft which is perpendicular to the spin axis and to the roll axis.



SPIN-ROLL PLANE-A



SPIN-PITCH PLANE-B



PITCH-ROLL PLANE-C

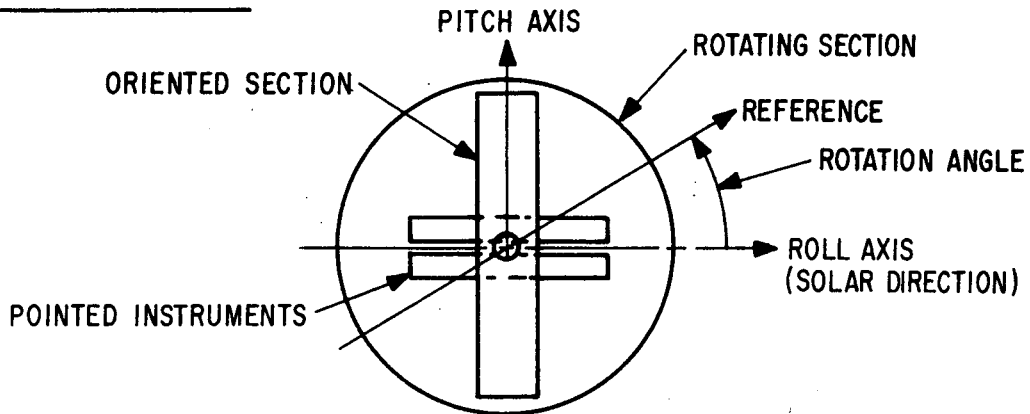
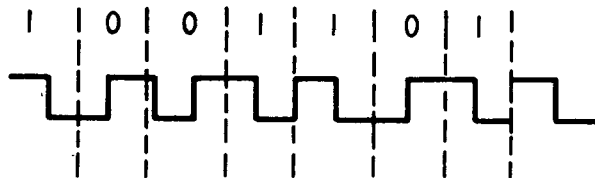


Figure D-1
OSO Coordinate System



- e. Elevation Axis (Fig. D-1): The axis on which the pointed experiments are mounted. The elevation axis is perpendicular to the solar direction and the spin axis.
- f. Spacecraft: The spacecraft is an Orbiting Solar Observatory less the experiments and ballast.
- g. Spacecraft Day: That portion of the orbit in which the spacecraft is in full sunlight.
- h. Spacecraft Night: That portion of the orbit in which the spacecraft is in the earth's shadow.
- i. Oriented Section: The portion of the observatory which is stationary in azimuth with respect to the sun when the pointing controls have oriented the pointed experiments to look at the sun.
- j. Rotating Section: The portion of the observatory which is rotating in azimuth with respect to the sun.
- k. Manchester Code: The Manchester Code is defined by the figure below:





5.2 Antenna Polarization

The Orbiting Solar Observatory is a complex geometric structure which, for antenna considerations, contains two driven elements and one parasitic element with the structure serving as the ground plane. Studies have shown that the polarization of this system is neither linear nor circular, but some combination of these depending on the look angle to the observatory. Since the observatory is constantly spinning and moving through space, the look angle is constantly changing. This implies that the optimum telemetry link is achieved by diversity combining at the ground station; thus the antenna polarization at the transmitter frequency is specified to be linear when diversity combining techniques are used. The observatory antenna does not use diversity combining. To optimize the command link, it is necessary to transmit to the observatory via a right-circularly polarized antenna. Thus the antenna is specified to be right-circularly polarized at the observatory receiver frequency.